NASA CONTRACTOR REPORT

A REVIEW OF CONFINED VORTEX FLOWS

by W. S. Lewellen

Prepared by
MASSACHUSETTS INSTITUTE OF TECHNOLOGY
Cambridge, Mass. 02139
for

NATIONAL AERONAUTICS AND SPACE ADMINISTRATION • WASHINGTON, D. C. • JULY 1971

1. Report No.	2. Government Accession No.	3. Recipient's Catalog No.
NASA CR-1772		

4. Title and Subtitle	5. Report Date
A REVIEW OF CONFINED VORTEX FLOWS	July 1971
	6. Performing Organization Code

7. Author(s)	8. Performing Organization Report No.
W. S. Lewellen	
	10. Work Unit No.

9. Performing Organization Name and Address	11. Contract or Grant No.
Space Propulsion Laboratory Department of Aeronautics & Astronautics Massachusetts Institute of Technology Cambridge, Massachusetts 02139	NSR-22-009-288
	13. Type of Report and Period Covered Contractor Report

12. Sponsoring Agency Name and Address	14. Sponsoring Agency Code
National Aeronautics and Space Administration Washington, D. C. 20546	

15. Supplementary Notes

6. Abstract

This report is an extensive review of the state of knowledge of confined vortex flows and their applications, with particular attention on the possibility of fluid dynamic containment for a gaseous-core nuclear reactor. Various possible exact and approximate solutions of the axisymmetric Navier-Stokes Equations related to confined vortex flows are derived and discussed. Comparisons with available experimental data are made. The influence of compressibility on both potential and laminar viscous flow is discussed. Theory and experiments relating to transition to turbulence is reviewed and some new empirical correlations for turbulent vortices are given. Application of the vortex tube as a fluidic device; as a cyclone separator and as an energy separator are considered in some detail with simple design formulae given. An assessment of the various modes of using a vortex for fluid dynamic containment for a gaseous core nuclear reactor is made, with the problems which remain to be solved dilineated. A bibliography with over 400 references is included.

17. Key Words (Suggested by Author(s))	18. Distribution Statement
Vortex Flow Gaseous-Core Nuclear Reactor Fluidic Vortex Valve Cyclone Separator	Unclassified - Unlimited

19. Security Classif. (of this report)	20. Security Classif. (of this page)	21. No. of Pages	22. Price*
Unclassified	Unclassified	225	$3.00

*For sale by the National Technical Information Service, Springfield, Virginia 22151

FOREWORD

This review is motivated by the possible application of vortices to advanced nuclear rockets. It has also served as the basis for a special 16.60 course on confined vortex flows. I wish to thank my students in this class for their support of this endeavor. Particular thanks are due Mr. R. N. Kumar for his help in preparing the final manuscript, to Mr. H. Lakshmikantha for help with Section 5.6 supported by NASA Grant NGR-22-009-303, and to Mrs. J. Estey for her patient typing.

TABLE OF CONTENTS

Symbols

a	velocity of sound
A	area
A_c	control port area
A_e	exhaust area (also A_o)
A_i	injection area
B	boundary layer interaction parameter
C_f	coefficient of friction
$\mathfrak{D}$	dimensionless operator defined in Eq. 3.1-12
E	Ekman number
f	similarity variable for stream function dependence on y
g	similarity variable for circulation function dependence on y
h	enthalpy
H	total enthalpy
K	circulation distribution parameter defined in Eq. (4.3-4)
ℓ	characteristic axial length
L	dimensionless angular momentum flux; or chamber length
$\dot{m}$	mass flow
M	Mach number
$\tilde{M}$	molecular weight
n	boundary-layer coordinate normal to the wall
N	radial Reynolds number, $\dot{m}/2\pi\rho\nu\ell$ (also Re_r)
N_H	number of exhaust holes
p	pressure
p_o	total pressure
Pr	Prandtl number
$\vec{q}$	velocity vector
Q	volume flow rate
$\tilde{Q}$	boundary-layer volume flow rate
r	radius
r_e	exhaust radius
r_o	characteristic radius
r_w	cylindrical wall radius
$\hat{r}$	stagnation radius

r^* radius of maximum tangential velocity

R radius of the wall surface

Re Reynolds number

s coordinate along the wall meridian

S swirl parameter defined in Eq. 3.1-15

t time

T temperature

$\mathcal{T}$ dimensionless time parameter defined in Eq. 3.1-13

u radial velocity component

v tangential velocity component

w axial velocity component

W dimensionless vortex valve flow

x dimensionless radius, r/r_e

y similarity variable

z axial coordinate

α swirl parameter defined in Eq. 2.2-8 or 2.3-4

Γ circulation (vr)

Γ^* dimensionless circulation Γ/Γ_o

Γ_o characteristic value of circulation

δ boundary-layer thickness

ε_T eddy viscosity

ζ dimensionless boundary-layer coordinate, n/δ

η dimensionless radius squared, $(r/r_o)^2$

Θ diffusion parameter defined in Eq. 8.3-1

μ viscosity

ν kinematic viscosity

ξ dimensionless axial coordinate

ρ density

τ shear stress tensor; or dimensionless time

ϕ similarity variable for stream function dependence on ξ

ψ dimensionless stream function defined in Eq. 3.1-8

Ψ stream function defined in Eq. 2.1-6

$\vec{\omega}$ vorticity vector

Ω angular rotation rate

Other symbols which are only used in one section are defined in that section.

I. INTRODUCTION

1.1 Examples of Confined Vortices

Vortex motions have long been recognized as an important part of fluid dynamics. As early as the 15th century, Leonardo da Vinci sketched and described various vortex motions he had observed. Since the late 19th century, theoretical treatments of vortices have been intimately connected with the search for particular solutions of the general equations of motions. Experimental research has been motivated more frequently by particular applications where vortex flows are desired or where they occur as an essential feature of the flow. Studies concerning wing theory, turbines and compressors, meteorology, cyclone separators and others have each developed a considerable literature on vortex flows as related to that particular application.

Rather than try to give a complete review of all types of vortex flow, that would necessarily cover much of the field of fluid dynamics, this review is restricted primarily to confined vortices of the type sketched in Figure (1.1), where the fluid enters tangentially, spirals radially inward and exits axially at some smaller radius. The most common example of this type flow is the "bath-tub vortex".

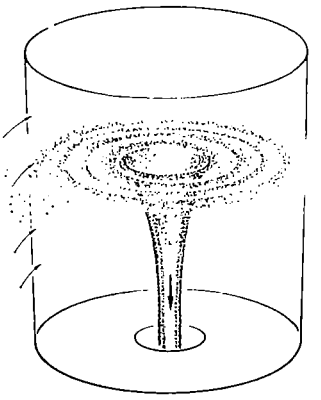

Fig. 1.1 Vortex flow in which fluid enters tangentially, spirals radially inward, and exits axially at some smaller radius.

As a bath-tub drains, any resident angular momentum in the tub causes the fluid to spiral. In an attempt to conserve angular momentum the tangential velocity of a fluid particle increases as its radius decreases, producing the familiar vortex located over the drain. The characteristic funnel shape is a manifestation of the pressure gradient resulting from the centrifugal force field of the swirling flow. For a given depth of fluid in the tub, the mass

flow through the drain is reduced by the vortex, since much of the pressure head available to drive the flow has gone into the swirl motion. This effect is the basis for the fluidic vortex valve which, although invented by Thoma (1928), has only in the last few years become the subject of considerable interest. The flow through the tub drain could be controlled by using a small "control" flow to introduce angular momentum at the outer edge of the tub. This provides all of the elements needed for a valve controlled by purely fluid motion, i.e., a fluidic valve, Figure (1.2). Details of design and methods of predicting performance will be discussed in Chapter VII, after the fundamental fluid dynamics affecting this flow have been reviewed in some detail in the earlier chapters.

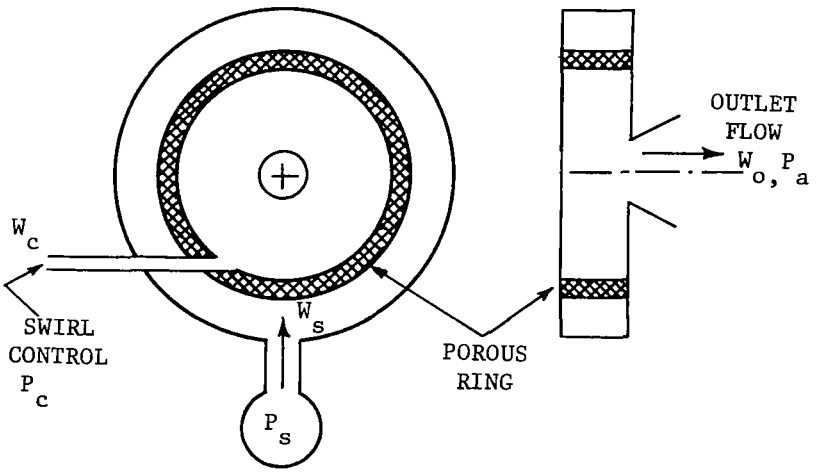

Fig. 1.2 Schematic view of typical vortex valve

Some of the first intensive studies of confined vortices were motivated by the observations of Ranque (1934) and Hilsch (1947) that by blowing tangentially into a cylindrical tube one can obtain separate supplies of hot and cold gas. A typical arrangement for a Ranque-Hilsch tube is shown in Figure (1.3). Westley (1954) has surveyed work done investigating the Ranque-Hilsch effect. Although no one has been able to come up with a completely satisfying theory that checks with experiment quantitatively, it is now generally accepted that the energy separation is caused by the combined effects of centrifugal force, diffusion and dissipation (Hall, 1966). As the gas expands toward the axis through the pressure drop set up by the centrifugal force, it is cooled and its tangential

velocity is increased. But the tangential velocity must go to zero on the axis. This is accomplished by transporting angular momentum radially outward by laminar or turbulent diffusion. Since the cooled gas loses part of its

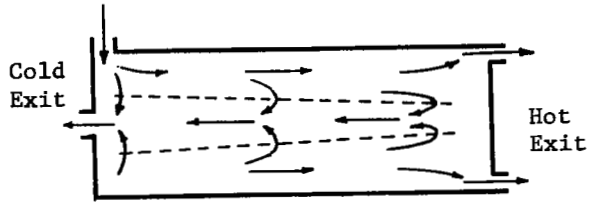

Fig. 1.3 Flow Pattern in Ranque-Hilsch Tube

kinetic energy in the process of momentum diffusion, it must exit the tube with a lower total temperature than that with which it entered the tube. The diffusion of the angular momentum to larger radii produces dissipative heating that can raise the total temperature in this region. The Ranque-Hilsch effect will be discussed in more detail in Chapter IX.

Chapter IX also considers what has been the most useful application of a confined vortex flow, that of a cyclone separator. Particles larger than a few microns diameter (Rietema and Verver, 1961), can be separated from a gas by forcing the mixture to flow through a vortex tube. A popular arrangement for the tube is given in Figure (1.4).

The shape of the tube is selected to take advantage of the secondary flows generated by the wall boundary layers. The fluid in the wall boundary layers feels a lower centrifugal force than the fluid outside the boundary layers, since the tangential velocity must go to zero at the surface of the wall. If the radial pressure gradient remains constant across the boundary layer, this means that a radial flow is necessarily induced in the boundary layer to account for the difference in pressure gradient and centrifugal force there. The secondary flow induced in this way is clearly evident in Von Karman's (1921) solution for the boundary layer on a rotating disk. In the present configuration the secondary flow of principal interest is radially inward along the conical wall. This serves to carry the particles, that have been centrifugally thrown out of the core vortex to the wall, along the wall to the reservoir at the tip of the cone.

The secondary flows, which play an important role in the cyclone separator

are a common feature of almost all confined vortices. The first recognition

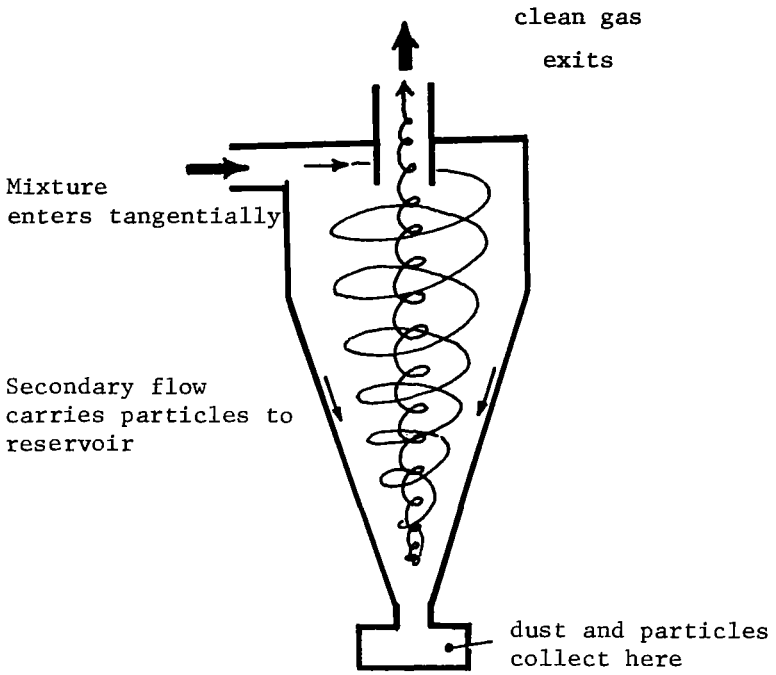

Fig. 1.4 Sketch of typical cyclone separator.

of the way in which a rotating boundary layer can generate a radial flow when the flow outside the boundary layer is purely tangential appears to have been by Ekman (1905) in his studies of ocean currents. The Ekman spiral describes how the velocity vector changes direction in a boundary layer dominated by rotation. The Ekman boundary layer is described by linear equations since the flow is a small perturbation about the state of uniform rotation. The first corresponding, complete nonlinear solution was provided by Bodewadt (1940). A great deal of effort will be devoted in Chapter III to describing subsequent attempts to obtain other solutions to the rotating boundary-layer problem. The radial flow generated by the boundary layer, i.e., the so-called secondary flow, has long been recognized, (see, for example, the movie on "Secondary Flows" by E. S. Taylor, produced by the National Committee for Fluid Mechanics Films) but until recently little attention had been given to the strong effect it may have on the primary rotating flow external to the boundary layer. Although the flow induced into the boundary layer is very small (of the order of the square root

of the product of viscosity times rotation rate), it may be sufficiently large to have a dominant role in the conservation of angular momentum balance in the external flow (Rott and Lewellen, 1966).

This review is supported by the promise of perhaps achieving an advanced space propulsion system utilizing a nuclear fuel in the gaseous state. Kerrebrock and Meghreblian (1961) proposed the use of a vortex tube to suspend an annulus of gaseous nuclear fuel while hydrogen flows through the tube and is heated by the fuel, Fig. (1.5). McLafferty (1968 and 1969) has reviewed the evolution of vortex containment concepts for a gaseous nuclear rocket. Proper assessment of the various schemes requires a thorough knowledge of confined vortex flows. Assessment of these schemes will be discussed in Chapter VIII.

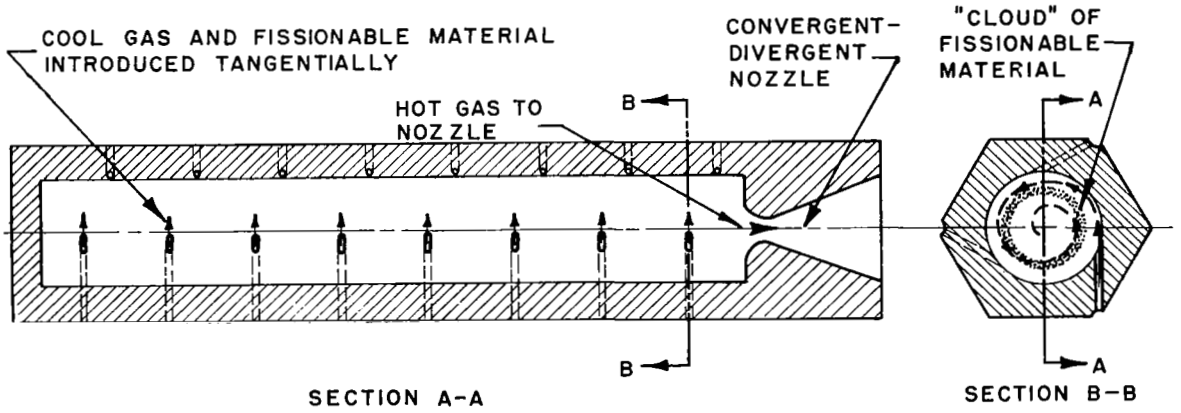

Fig. 1.5 Gas core nuclear rocket as proposed by Kerrebrock and Meghreblian (1961)

1.2 Some Experimental Observations

Before getting enmeshed in solving for various mathematical models of the flow, let us seek some physical insight into the flow by looking at some experimental observations. A typical pressure distribution taken radially along the chamber end wall opposite the exhaust is shown in Fig. (1.6a). Notice the sharp drop in pressure due to the centrifugal force field of the vortex. The pressure on the centerline is often less than the ambient pressure to which the flow is exhausting. Tangential velocity distributions derived from the pressure distributions are shown in Fig. (1.6b). Typically, the velocity distirbution shows that circulation is nearly constant (corresponding to $v \propto 1/r$) at large radii and transitions to nearly uniform angular velocity (corresponding to $v \propto r$)

near the axis. The maximum tangential velocity occurs in the transition region, the radial position of which may be expected to be determined by a balance between convection and dissipation.

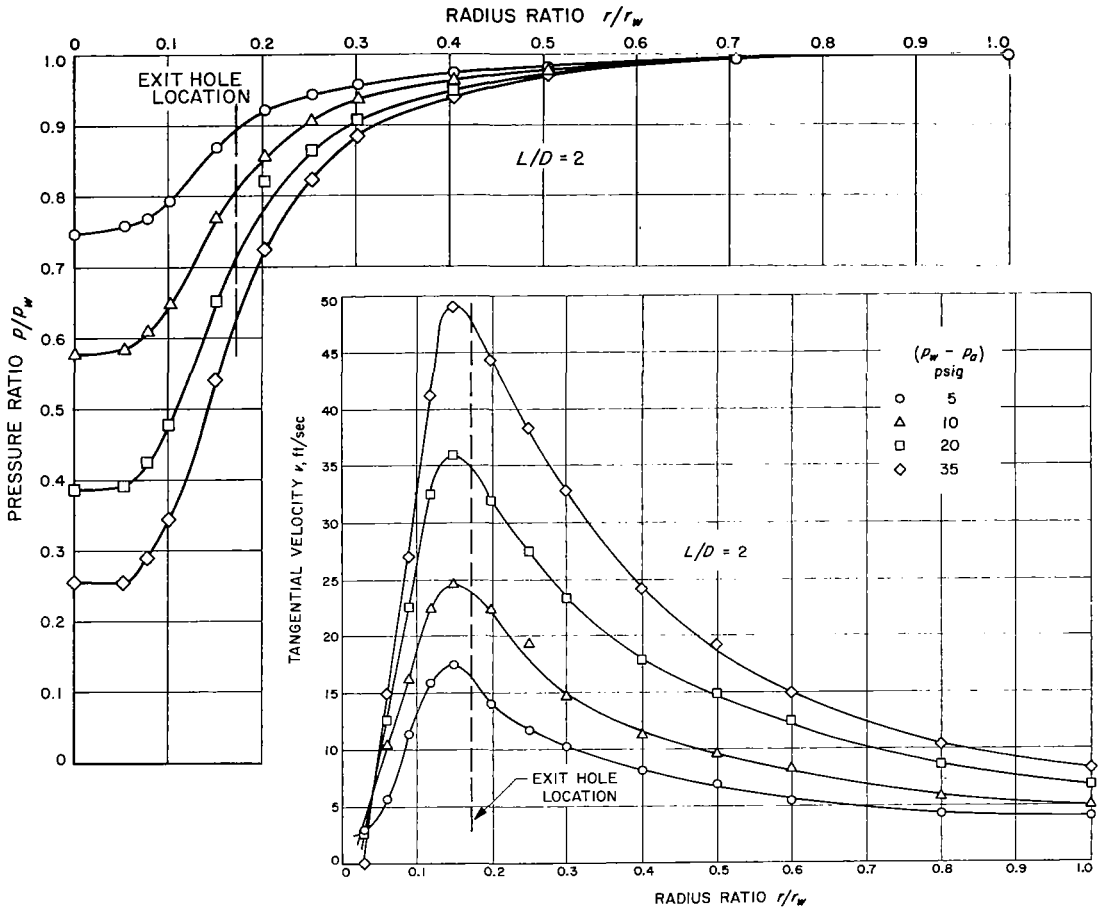

Fig. 1.6 (a) Typical pressure distributions on the end wall of a vortex chamber.

(b) Tangential velocity distributions obtained by differentiating the pressure distributions. (Roschke, 1966).

The pressure drop across a vortex reduces the mass flow out the exhaust for a given pressure differential. This may be illustrated by a typical plot of the mass flow through a vortex valve as a function of control flow (Fig. 1.7).

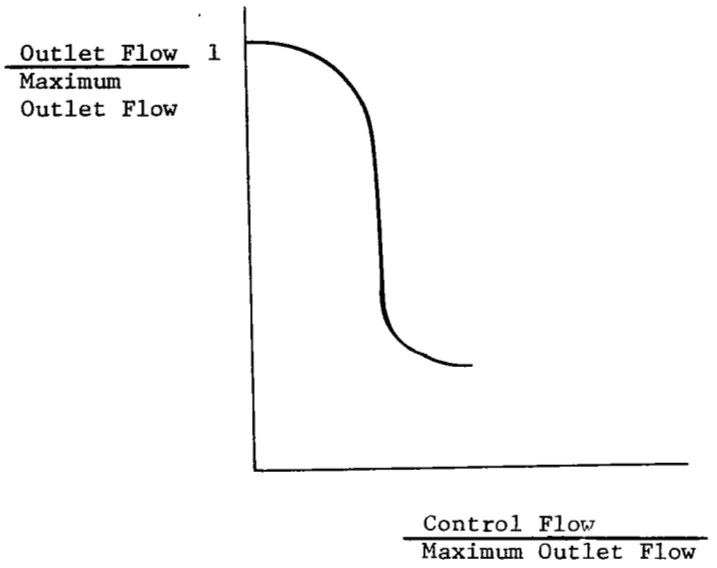

Fig. 1.7 Typical Vortex Valve Performance Curve.

To obtain this performance curve the pressure drop across the valve (the difference between supply pressure and outlet pressure) is held constant while the control flow is increased by increasing control pressure. As more of the potential energy available for driving the flow through the valve is diverted into swirling kinetic energy, flow through the valve is sharply reduced. The curve is terminated at the point where the supply flow is shut off and the output flow is just equal to the control flow. The quantity of control flow required to shut off the supply flow depends on the geometry of the valve. It might be expected that the higher the angular momentum introduced per unit control flow, the lower the flow through the valve at supply flow shutoff. However, this is not always true. For instance, if the angular momentum is increased by increasing the radius ratio between the injection of the control flow and the valve outlet, minimum flow is found

to occur at some moderate value of radius ratio (from 5 to 10). The end-wall boundary layers play a dominant role in determining this optimum value of radius ratio.

It may not be too surprising that flow in such a narrow "pancake" vortex tube as that normally used for a valve can be dominated by the boundary layers, but it is more striking to observe that even flow in chambers with large ratios of length-to-diameter (L/D) are dominated in a similar way. Figure (1.8) shows

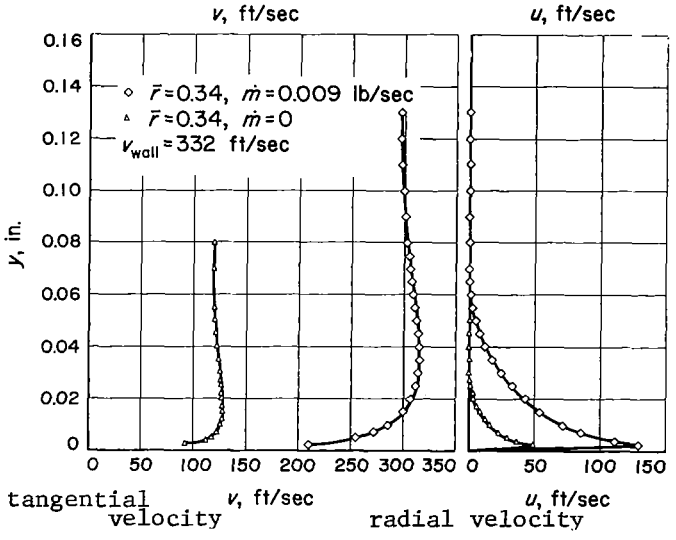

Fig. 1.8 Velocity Profiles in the End-Wall Boundary Layer of a Vortex Chamber. (Kendall, 1962)

velocity profiles in the end-wall boundary layer for a chamber with L/D = 1 (Kendall, 1962). Note that within the accuracy of his measurements there appears to be no radial flow outside of a thin boundary layer that occupies only 1% of the chamber length. Apparently all of the radial mass flow is passing through the chamber by way of the end-wall boundary layers. Another important feature of the boundary-layer profile is that the tangential velocity appears to overshoot its external value. How can this apparent contradiction happen? Since the radial flow in the boundary layer is much larger than that in the external main flow, it is possible for the circulation (vr) of a fluid particle to be more nearly conserved as it moves radially inward in the outer regions of the boundary layer than it is in the external main flow.

The strong boundary-layer flows can also lead to large axial flows. Figure (1.9) shows the sketch of a three-dimensional flow pattern observed in a typical vortex tube (Rosenzweig, Ross, and Lewellen, 1962). This pattern was visualized by injecting dye through a hypodermic probe into the flow at various positions. Figure (1.10) shows the observed dye pattern for the probe in two different positions.

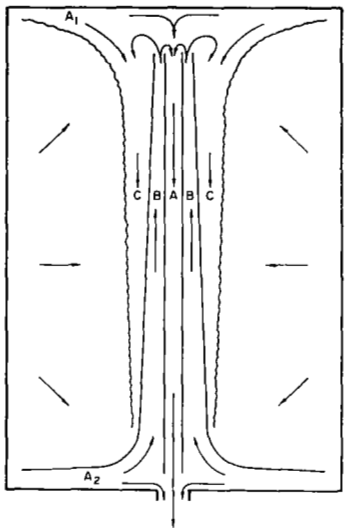

Fig. 1.9 Sketch of three-dimensional flow in jet-driven vortex tube. (Rosenzweig, Ross, and Lewellen, 1962)

In Fig. (1.10a) the probe tip is positioned near the outer edge of the region identified as region B in Figure (1.9) and in the upper portion of the lower boundary layer. Dye is being convected upward as indicated by the arrows. Within this annulus of upward flow, there is a core of flow directed down toward the exhaust where the flow exits the chamber. This downward core of flow is approximately the same diameter as the exhaust diameter. In Figure (1.10b) three axial flow regions are visible. For this picture, the probe is positioned at mid-radius in the upper boundary layer. Now region A and part of region C appear dark while region B is relatively clear since it is supplied with clear fluid from the lower end-wall boundary layer.

Figures (1.9) and (1.10), of course, show only the radial and axial flow

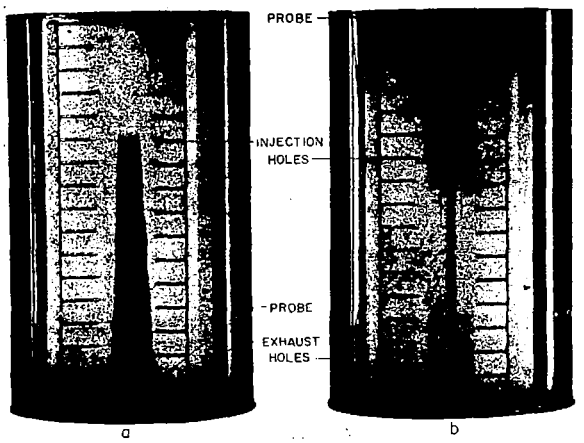

Fig. 1.10 Photos of three-dimensional flow patterns (Rosenzweig, Ross and Lewellen, 1962)

pattern. The actual flow consists of a strong tangential velocity super-imposed on the indicated flow pattern. A striking feature of the tangential velocity distribution is that it is essentially a function of radius only, outside of the thin boundary layers on the walls, even though there is a three-dimensional character to the flow pattern. This preference for two dimensionality is a common feature of all flows dominated by rotation. It was theoretically predicted by Proudman (1916) and observed experimentally by Taylor (1921) and is now known as the Taylor-Proudman theorem (Greenspan, 1968). This characteristic will be demonstrated mathematically later, but physically it may be viewed as a result of the balance between centrifugal force and the radial pressure gradient. If the flow is dominated by rotation then the pressure field also must be dominated by rotation, resulting in a pressure gradient that is directed perpendicularly to the axis of rotation. Any variation in the tangential velocity parallel to the axis of rotation would imply an imbalance between the centrifugal force and the pressure gradient forcing a flow adjustment. If these adjustments are to be small in comparison with the primary flow (i.e. the flow is dominated by rotation) then the variation in the tangential velocity parallel to the axis of rotation must be small.

1.3 Mathematical Formulation

Let us turn now to a formulation of the mathematical equations that must be solved to make our understanding of confined vortex flows more precise.

The principal conservation equations for a fluid in motion may in general be written as (Lagerstrom,1964):

Conservation of mass

$$\frac{D\rho}{Dt} + \rho \ \text{div} \ \vec{q} = 0 \qquad (1.3\text{-}1)$$

Conservation of momentum

$$\frac{D\vec{q}}{Dt} + \frac{1}{\rho} \ \text{grad} \ p = \vec{f} + \frac{1}{\rho} \ \text{div} \ \tau \qquad (1.3\text{-}2)$$

Conservation of Energy

$$\frac{DH}{Dt} - \frac{1}{\rho} \frac{\partial p}{\partial t} = - \frac{1}{\rho} \ \text{div} \ \vec{q}_H + \vec{f} \ . \ \vec{q} + \frac{1}{\rho} \ \text{div} \ (\tau \vec{q}) + I \qquad (1.3\text{-}3)$$

where ρ is the density, $\vec{q}$ the velocity vector, p the pressure, τ the shear stress tensor, H the total enthalpy, $\vec{q}_H$ the heat flux vector, $\vec{f}$ the volume force vector per unit mass, I the energy source per unit mass and the symbol D/Dt denotes the sum of the local rate of change with respect to time, $\partial/\partial t$, and the convective rate of change, $\vec{q} \ . \ \vec{\nabla}$.

Some equation of state for the fluid, (e.g. for a perfect gas, $H = \frac{\gamma}{\gamma - 1} \frac{p}{\rho} + \frac{q^2}{2}$) and the dependence of τ and $\vec{q}_H$ on the other variables must be specified before Eqs. (1.3-1 - 1.3-3) form a complete set. These auxiliary conditions are specified differently in the various models to follow.

Since we are dealing with vortex motions it is often convenient to deal with the vorticity $\vec{\omega}$ of the flow. The vorticity vector is defined as

$$\vec{\omega} = \vec{\text{curl}} \ \vec{q} \qquad (1.3\text{-}4)$$

and is equal to twice the instantaneous angular velocity of a fluid particle about its own axis. An equation for the change in vorticity can be obtained by taking the curl of Eq. (1.3-2). This leads to

$$\frac{\partial \vec{\omega}}{\partial t} + \vec{q} . \nabla \vec{\omega} - \vec{\omega} . \nabla \vec{q} + \vec{\omega} \ (\nabla \ . \vec{q}) = \vec{\text{curl}} \ \left[\frac{-1}{\rho} \ \vec{\text{grad}} \ p + \vec{f} + \frac{1}{\rho} \ \vec{\text{div}} \ \tau \ \right] \qquad (1.3\text{-}5)$$

When this is combined with Eq. (1.3-1), it may be written as

$$\rho \frac{D}{Dt} (\vec{\omega}/\rho) - \vec{\omega}.\nabla\vec{q} = \vec{\text{curl}} \left[\frac{-1}{\rho} \vec{\text{grad}}\, p + \vec{f} + \frac{1}{\rho} \vec{\text{div}}\, \tau \right] \qquad (1.3\text{-}6)$$

If the body force is conservative (i.e., the force is derivable from a potential field) and the fluid is barotropic (i.e., the density at any point is a function of the pressure only and $\frac{1}{\rho} \vec{\text{grad}}\, p = \vec{\text{grad}} \int \frac{dp}{\rho}$) then Eq. (1.3-6) reduces to

$$\rho \frac{D}{Dt} (\vec{\omega}/\rho) - \vec{\omega}\cdot\nabla\vec{q} = \vec{\text{curl}} \left[\frac{1}{\rho} \vec{\text{div}}\, \tau \right] \qquad (1.3\text{-}7)$$

If the right-hand side, representing dissipation is ignored and ρ is assumed constant, this last equation may be used to prove Helmholtz's theorem that a vortex tube (made up of lines tangent to the local vorticity vector passing through a small closed curve) moves with the fluid and its strength remains constant (see Batchelor, 1967).

Rather than carry on a general discussion of vorticity dynamics (for such a discussion see Truesdell, 1954) let us turn attention to more specific flow models to apply for a confined vortex. The approach taken herein is to treat the same basic flow problem in different flow regions; inviscidly in Chapter II, with laminar viscous flow in Chapters III and IV, and as turbulent flow in Chapter VI. In view of the relatively simple flow problem to which attention is being restricted, it may come as a surprise to the reader that so much work has been done with so many questions still unanswered. The applications considered in the last chapters will use the results of the flow regime that appears most appropriate.

II. STEADY, INVISCID, POTENTIAL FLOW MODEL

2.1 Introduction of the Stream Function

For inviscid flow, the shear stress τ and heat flux vector $\vec{q}_H$ are equal to zero. Equation (1.3-7) for this case becomes a homogeneous equation in $\vec{\omega}$ and if there is no vorticity introduced at the boundaries or as initial conditions, then

$$\vec{\omega} = 0 \tag{2.1-1}$$

The three components of this equation for axisymmetric flow with r, θ, and z components of velocity equal to u, v, and w are

radial component: $$\frac{\partial v}{\partial z} = 0 \tag{2.1-2}$$

axial component: $$\frac{1}{r}\frac{\partial rv}{\partial r} = 0 \tag{2.1-3}$$

tangential component: $$\frac{\partial u}{\partial z} - \frac{\partial w}{\partial r} = 0 \tag{2.1-4}$$

It follows from Eqs. (2.1-2) and (2.1-3) that

$$rv = \text{const.} \equiv \Gamma \tag{2.1-5}$$

The constant Γ is the circulation of the flow divided by 2π. This leaves Eqs. (2.1-4) and 1.3-1) to determine u and w together with the boundary conditions for any particular problem.

A streamfunction, Ψ, can be introduced to satisfy Eq. (1.3-1) for steady flow

$$\frac{\partial \Psi}{\partial z} = -\rho u r, \quad \frac{\partial \Psi}{\partial r} = \rho w r \tag{2.1-6}$$

This definition allows Ψ to be positive for negative u corresponding to radial inflow, the case of most interest in Fig. (1.1). When Eq. (2.1-6) is introduced into the tangential component of the vorticity equation, it may be written after some manipulation as

$$\frac{\partial^2 \Psi}{\partial z^2} - \frac{\partial \Psi}{\partial z}\frac{\partial \ell n \rho}{\partial z} + \frac{\partial^2 \Psi}{\partial r^2} - \frac{1}{r}\frac{\partial \Psi}{\partial r}\left[1 + r\frac{\partial \ell n \rho}{\partial r}\right] = 0 \tag{2.1-7}$$

To determine the flow it is still necessary to specify an equation of state. Two different cases are considered here, incompressible flow and isentropic flow.

2.2 Incompressible Flow

If the density is constant, Eq. (2.1-7) reduces to

$$\frac{\partial^2\Psi}{\partial z^2} + \frac{\partial^2\Psi}{\partial r^2} - \frac{1}{r}\frac{\partial\Psi}{\partial r} = 0 \qquad (2.2\text{-}1)$$

A general solution to this linear equation can be obtained by separation of the variables. This leads to solutions of the form

$$\Psi = e^{\pm kz}\, r\, [J_1(kr) + CY_1(kr)] \qquad (2.2\text{-}2)$$

where k is the separation constant and J_1 and Y_1 are independent solutions of Bessel's Equation of first order.

The problem now is to provide boundary conditions appropriate for a confined vortex. The flow of most concern here is that in which the flow is introduced into a chamber at a large radius with some swirl and exhausts at some smaller radius. For concreteness, consider flow through the container with a rotating, porous, cylindrical wall sketched in Figure (2.1). Assume that

$$\left.\begin{aligned} v &= v_w = \Gamma/r_w \\ u &= u_w = -\dot{m}/2\pi\rho r_w \ell \\ w &= 0 \end{aligned}\right\} \quad \text{at } r = r_w \text{ and } 0 \leq z \leq \ell \qquad (2.2\text{-}3)$$

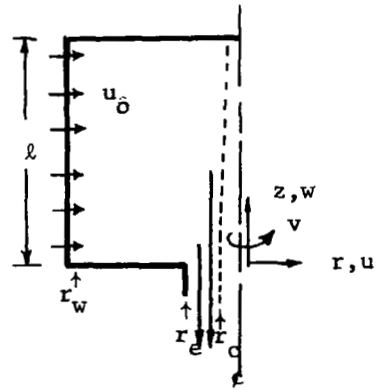

Fig. 2.1 Sketch showing coordinate system for cylindrical vortex chamber.

and $w = 0$ at $z = \ell$ and at $z = 0$ for $r > r_e$. Here the subscript w denotes the value at the surface of the cylindrical wall. The difficulty comes in specifying conditions at $z = 0$ for $r < r_e$. Equation (2.1-5) calls for v to approach infinity at the axis, $r = 0$. Since this singularity cannot exist in nature the region of flow in the immediate neighborhood of the axis must either be excluded or the inviscid model abandoned. In order to preserve the inviscid assumption it is assumed that the flow does not penetrate to the axis, i.e., there is a region $r < r_c(z)$ in which there is no flow with p equal to a constant. The problem now hinges on some valid means of determining r_c.

Binnie and Hookings (1948), in analyzing a series of experiments with swirling water flowing through a nozzle in the presence of an air core, argued that the core size should be determined by the condition that flow through the nozzle be a maximum for the given driving pressure difference across the nozzle. This is equivalent to asking that for a given mass flow the change in pressure (or potential energy) across the nozzle be a minimum. For a small r_c the core pressure is low due to the high swirl velocity, while for a large r_c the core pressure is low due to the high axial velocity required to pass the mass flow through a small annulus. From this tradeoff between w and v it is evident that a particular value of r_c will maximize the core pressure. Smith (1962) applied the same condition for gas flow in a cyclone separator.

Mathematically, the exhaust constraint can be formulated in the following manner. First, the radial velocity may be assumed small in comparison to v and w in the plane of the exhaust. The condition of irrotationality (Eq. 2.1-4) then reduces to $w_e = \text{const}$ for $r_c \leq r \leq r_e$, or in terms of the mass flow through the container, $\dot{m}$,

$$w_e = \dot{m}/\pi\rho(r_e^2 - r_c^2) \tag{2.2-4}$$

Also from Eq. (2.1-5)

$$v_e = \frac{\Gamma}{r_e} \tag{2.2-5}$$

Since the exhaust constraint involves a pressure condition we turn to the momentum equation which for the present flow reduces to Bernoulli's Equation

$$p + \frac{\rho}{2}(v^2 + w^2) = p_o \tag{2.2-6}$$

where p_o is the uniform total pressure of the flow into the chamber. At the radius of the core, r_c, Eq. (2.2-6) with the aid of Eqs. (2.2-4) and (2.2-5) may be written as

$$\frac{\Gamma^2}{r^2} + \frac{\dot{m}^2}{[\rho\pi\,(r_e^2 - r_c^2)]^2} = \frac{2}{\rho}(p_o - p_c) = \frac{2\Delta p}{\rho} \tag{2.2-7}$$

If dimensionless variables are defined as:

$$\alpha^2 \equiv \rho\Gamma^2 / 2 r_e^2 \Delta p \tag{2.2-8}$$

the fraction of the total kinetic energy invested in swirl at the outer edge of the exhaust;

$$\bar{Q} \equiv \frac{\dot{m}}{\pi r_e^2}\left[\frac{1}{2\rho\Delta p}\right]^{1/2} \tag{2.2-9}$$

the volume flow normalized by its maximum possible value; and the dimensionless radius ratio $x_c \equiv r_c/r_e$, then Eq. (2.2-7) may be written

$$\frac{\alpha^2}{x_c^2} + \frac{\bar{Q}^2}{(1-x_c^2)^2} = 1 \tag{2.2-10}$$

When Eq. (2.2-10) is solved for $\bar{Q}$, it yields

$$\bar{Q} = (1-x_c^2)(1-\alpha^2/x_c^2)^{1/2} \tag{2.2-11}$$

The exhaust constraint proposed in the last paragraph calls for determining x_c as a function of α by maximizing $\bar{Q}$ with respect to x_c for any given α, i.e., setting

$$\frac{\partial \bar{Q}}{\partial x_c} = 0 \tag{2.2-12}$$

The relationship between x_c and α determined by Eq. (2.2-12) may be written as

$$\alpha^2 = 2x_c^4/(1 + x_c^2) \tag{2.2=13}$$

and is plotted in Figure (2.2). This gives the size of the stagnate core in the plane of the minimum flow cross-section as a function of the swirl kinetic energy. When there is no swirl, there is no core and the axial

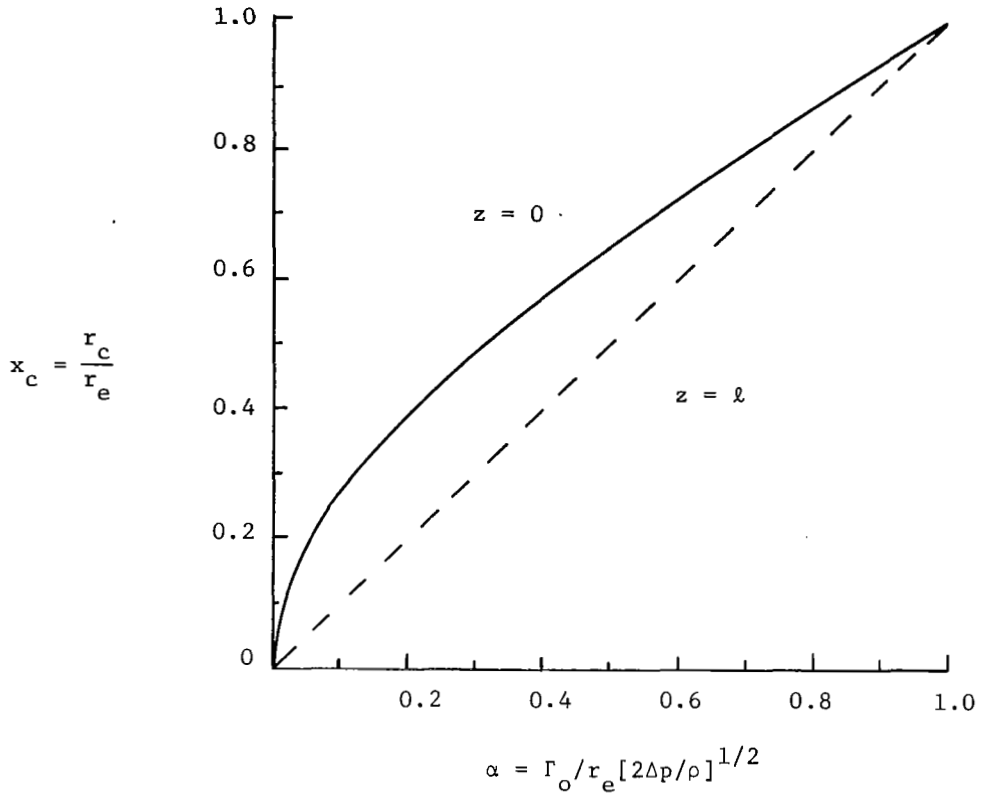

Fig. 2.2 Core radius as a function of swirl for incompressible potential flow.

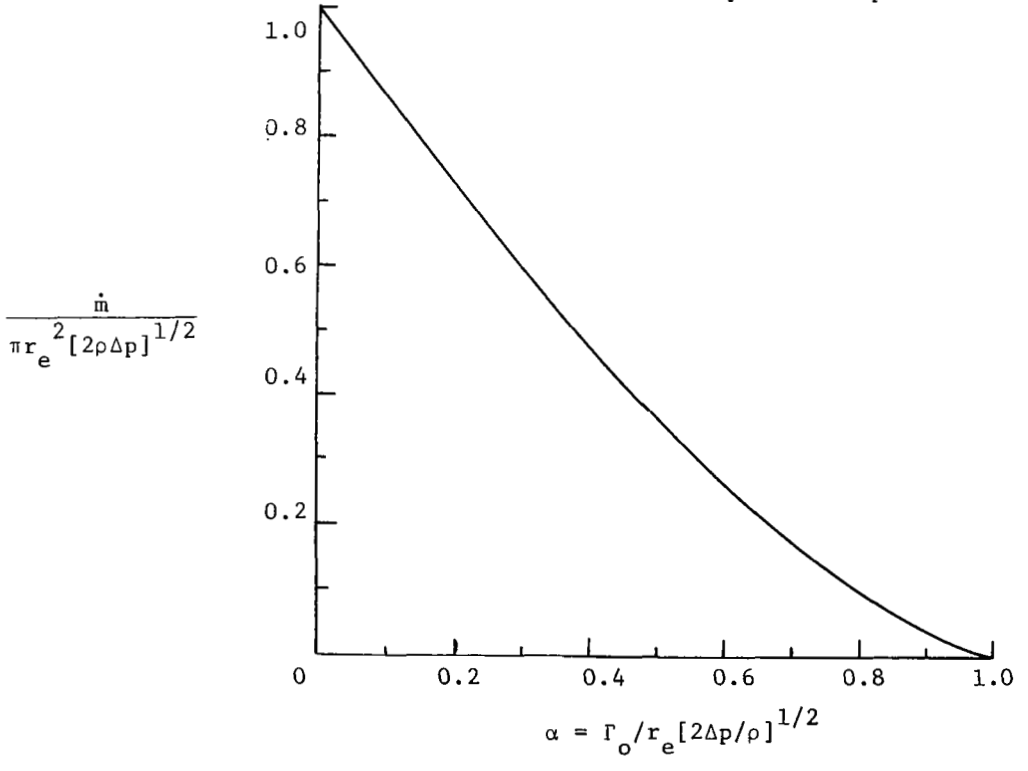

Fig. 2.3 Volume flow as a function of swirl for incompressible potential flow.

velocity is uniform across the total cross-section. In the other limit, if all of the potential energy difference available for driving the flow is converted into swirling kinetic energy, there would be no flow through the cross-section and the core would completely fill the exhaust.

Figure (2.2) also includes a curve of the stagnate core size at the chamber wall opposite to the exhaust. This can be obtained by noting that both w and u are zero there and thus Eq. (2.2-10) would reduce to

$$x_c(z = \ell) = \alpha \tag{2.2-14}$$

this being the radius at which all of the available energy has been converted to swirling kinetic energy.

The total flow through the exhaust is obtained by substituting Eq. (2.2-13) into Eq. (2.2-11) to obtain

$$\bar{Q} = (1-x_c^2)^{3/2} \; / \; (1 + x_c^2)^{1/2} \tag{2.2-15}$$

Equations (2.2-13) and (2.2-15) may be used to plot through flow as a function of swirl. Such a plot is given in Figure (2.3).

With conditions at the exhaust now specified it should be possible to build up a series of solutions of the form given by Eq. (2.2-2) to form a complete solution that satisfies all the boundary conditions. If we ignore the radius of curvature of the exhaust nozzle and specify our exhaust constraint at z = 0, a possible solution appears to be

$$\Psi = \frac{\dot{m}}{2\pi} + \sum_{n=o}^{\infty} A_n r \, J_1(k_n r) \sinh [k_n(z - \ell)]$$
$$+ \sum_{m=o}^{\infty} B_m r \left[I_1\left(\frac{m\pi}{\ell} r\right) + D_m K_1\left(\frac{m\pi}{\ell} r\right)\right] \sin\left(\frac{m\pi}{\ell} z\right) \tag{2.2-16}$$

where the k_n's are determined by

$$J_1(k_n r_w) = 0 \tag{2.2-17}$$

and the coefficients A_n's given by

$$\sum_{n=o}^{\infty} A_n r \, J_1(k_n r) \sinh(-k_n \ell) = \begin{cases} 0 \; ; \; r < r_c(0) \text{ or } r > r_e \\ \dfrac{-\dot{m}}{2\pi} \left[\dfrac{r^2 - r_c^2(0)}{r_e^2 - r_c^2(0)}\right] ; \; r_e \geq r \geq r_c \end{cases} \tag{2.2-18}$$

The determination of the remaining coefficients is complicated by the existence of the stagnate core boundary, along which the solution must satisfy

$$\frac{1}{r}\frac{\partial \Psi}{\partial r}_{r=r_c(z)} = [2\rho\Delta p(1 - \alpha^2 r_e^2/r_c^2)]^{1/2} \qquad (2.2\text{-}19)$$

and

$$\Psi(r_c, z) = \dot{m}/2\pi \qquad (2.2\text{-}20)$$

These conditions together with the condition that $u = -\dot{m}/2\pi\rho r_w \ell$ at $r = r_w$ lead to the following three sets of equations for the determination of the B_m's, D_m's and r_c:

$$\sum_{m=o}^{\infty} B_m r_w \left[I_1\left(\frac{m\pi}{\ell} r_w\right) + D_m K_1\left(\frac{m\pi}{\ell} r_w\right)\right] \sin\frac{m\pi z}{\ell} = \frac{\dot{m}}{2\pi\ell}(z-\ell) \qquad (2.2\text{-}21)$$

$$\sum_{m=o}^{\infty} B_m \left[I_1\left(\frac{m\pi}{\ell} r_c\right) + D_m K_1\left(\frac{m\pi}{\ell} r_c\right)\right] \sin\frac{m\pi z}{\ell} + \sum_{n=o}^{\infty} A_n J_1(k_n r_c) \sinh[k_n (z - \ell)] = 0 \qquad (2.2\text{-}22)$$

and

$$\sum_{n=o}^{\infty} A_n \left[\frac{1}{r}\frac{d}{dr}[r J_1(k_n r)]\right]_{r=r_c} \sinh[k_n(z-\ell)] + \sum_{m=o}^{\infty} B_m \left[\frac{1}{r}\frac{dr}{dr}\left[I_1\left(\frac{m\pi}{\ell} r\right) + D_m K_1\left(\frac{m\pi}{\ell} r\right)\right]\right]_{r=r_c} \sin\left(\frac{m\pi z}{\ell}\right) = [2\rho\Delta p(1 - \alpha^2 r_e^2/r_c^2)]^{1/2} \qquad (2.2\text{-}23)$$

The solution given in Eq. (2.2-16) is not particularly useful due to the difficulty in determining all of the coefficients, but it can be used to show that for a given mass flow through the container, the variation in Ψ with swirl is primarily restricted to the neighborhood of r_c. When $\alpha = 0$, r_c and the D_m coefficients are zero so that the solution is determined by Eqs. (2.2-16), (2.2-17), (2.2-18) and (2.2-21). When α is finite there is a change in higher numbered A_n's due to the introduction of $r_c(o)$ in Eq. (2.2-18). This change will be most evident in the immediate neighborhood of r_c. The other change involves the D_m and B_m terms. Since $K_1 \to \infty$ while J_1 and I_1 both $\to o$ as $r \to o$, Eq. (2.2-22) and (2.2-23) suggests that the D_m's should be small. Thus these terms will be small except near $r = 0$.

In this inviscid, incompressible flow model the largest effect of the swirl is to change the flow rate through the container for a given pressure difference across the container as described in Fig. (2.3). The change in the stream function pattern is primarily limited to the introduction of a stagnate core around the axis when swirl is added.

2.3 Isentropic Model

For isentropic flow of a perfect gas, the density can be related to the velocity through the energy equation. This relation may be written in the following form

$$\rho/\rho_o = \left[1 + \frac{\gamma-1}{2}\frac{q^2}{a^2}\right]^{\frac{-1}{\gamma-1}} \qquad (2.3\text{-}1)$$

where the subscript o denotes the stagnation value and a is the speed of sound. Equation (2.3-1) can be used to eliminate ρ from Eq. (2.1-7) and write it in terms of the component Mach numbers. After some manipulation, the equation for the tangential component of vorticity can be written as, (King, 1967),

$$(1 - \frac{w^2}{a^2})\frac{\partial^2\psi}{\partial z^2} - \frac{2uw}{a^2}\frac{\partial^2\psi}{\partial r\partial z} + (1 - \frac{u^2}{a^2})\frac{\partial^2\psi}{\partial r^2} - \frac{1}{r}\frac{\partial\psi}{\partial r}(1 + \frac{v^2}{a^2}) = 0 \qquad (2.3\text{-}2)$$

The interesting thing to note about Eq. (2.3-2) is that the nature of the equation, i.e., whether it is hyperbolic or elliptic, is unaffected by the tangential Mach number, v/a. The nature of the equation is determined by the coefficients of the highest order derivatives. Thus for axisymmetric flow, we do not expect anything unique to occur when $v/a = 1$, but we can anticipate transonic choking to occur when $(u^2 + w^2)/a^2 = 1$.

Equation (2.3-2) is nonlinear and thus far more difficult to solve than in the incompressible case. Even in the incompressible case, the solution for the stream function pattern does not appear very useful. The most useful information came from the exhaust constraint. Therefore for this isentropic case no attempt will be made to solve for the complete flow; only the exhaust constraint will be considered.

As long as u is neglected in the exhaust, Eqs. (2.1-2) to (2.1-4) lead to constant values for both w and Γ. The energy equation (or the compressible Bernoulli Eq.) may be written as

$$\frac{\gamma-1}{2}\left(\frac{w^2+\Gamma^2/r^2}{a_o^2}\right) + (p/p_o)^{\frac{\gamma-1}{\gamma}} = 1 \qquad (2.3\text{-}3)$$

If the previous definition of α is generalized to

$$\alpha^2 \equiv \frac{\gamma-1}{2}\,\frac{\Gamma^2}{a_o^2 r_e^2[1 - (p_c/p_o)^{\gamma-1/\gamma}]} \qquad (2.3\text{-}4)$$

and the axial velocity is normalized in a similar manner

$$w^2 = \frac{\gamma-1}{2}\,\frac{w^2}{a_o^2\,[1 - (p_c/p_o)^{\gamma-1/\gamma}]} \qquad (2.3\text{-}5)$$

then Eq. (2.3-3) may be written simply as

$$\bar{w}^2 + \alpha^2/x^2 = 1 \qquad (2.3\text{-}6)$$

with $x = r/r_e$. Note that α^2 is still defined as the fraction of available energy invested in the swirl and reduces to the previous definition, Eq. (2.2-8), as $p_c \to p_o$.

The relationship between w and r_c is obtained by evaluating Eq. (2.3-6) at the core

$$\bar{w}^2 = 1 - \alpha^2/x_c^2 \qquad (2.3\text{-}7)$$

The mass flow through the exhaust is given by

$$\dot{m} = 2\pi w \int_{r_c}^{r_e} \rho r dr \qquad (2.3\text{-}8)$$

After considerable algebra, with the aid of Eqs. (2.3-1), (2.3-4), (2.3-5), and (2.3-7), this last equation can be written as

$$\dot{m}/\pi\rho_o a_o r_e^2 \left(\frac{2}{\gamma-1}\right)^{1/2} [1 - (p_c/p_o)^{\frac{\gamma-1}{\gamma}}]^{\frac{\gamma+1}{2(\gamma-1)}} \qquad (2.3\text{-}9)$$

$$= [1 - (\alpha/x_c)^2]^{1/2} (\alpha/x_c)^{2/\gamma-1} \int_{x_c}^{1} \left[\frac{x_c^2/\alpha^2}{(p_o/p_c)^{(\gamma-1)/\gamma} - 1} + 1 - \frac{x_c^2}{x^2}\right]^{1/(\gamma-1)} 2xdx$$

To make the flow unique it is still necessary to fix the core radius. The most satisfying way to do this is to choose x_c to maximize $\dot{m}$ when the other parameters are specified as was done in the incompressible case.

Equation (2.3-9) still yields the incompressible expression, Eq. (2.2-11), as $p_c \to p_o$. The other limiting case of $p_c = 0$ was treated by Mager (1961). For Mager's case the integral in Eq. (2.3-9) reduces to

$$I \equiv \int_{x_c}^{1} \left(1 - \frac{x_c^2}{x^2}\right)^{1/\gamma-1} 2x\,dx \tag{2.3-10}$$

which can be integrated analytically for $\gamma = \frac{n+1}{n-1}$, with n an integer. The extremum condition on $\dot{m}$ with respect to x_c yields

$$\frac{1}{\dot{m}} \frac{\partial \dot{m}}{\partial x_c} = \frac{\alpha^2/x_c^2}{1 - \frac{\alpha^2}{x_c^2}} - \frac{2/(\gamma-1)}{x_c} + \frac{1}{I} \frac{\partial I}{\partial x_c} = 0 \tag{2.3-11}$$

When I is differentiated with respect to x_c and then integrated by parts with respect to x, it is possible to show that

$$\frac{1}{I} \frac{\partial I}{\partial x_c} = \frac{2}{x_c} - \frac{2}{x_c} \frac{(1 - x_c^2)^{1/\gamma-1}}{I} \tag{2.3-12}$$

Equations (2.3-11) and (2.3-12) allow an expression for α as a function x_c to be obtained, after some algebra, i.e.

$$\alpha = x_c \left[1 - \frac{1}{\frac{3-\gamma}{\gamma-1} + 2\frac{[1 - x_c^2]^{1/\gamma-1}}{I}}\right]^{1/2} \tag{2.3-13}$$

This relationship between x_c and α is plotted in Fig. (2.4), for $\gamma = 1.4$ as taken from the results of Mager. We can include on Fig. (2.4) the core size at the chamber wall opposite to the exhaust. From Eq. (2.3-7) with $w = 0$ it may be seen that we still have

$$x_c\,(z = \ell) = \alpha \tag{2.3-14}$$

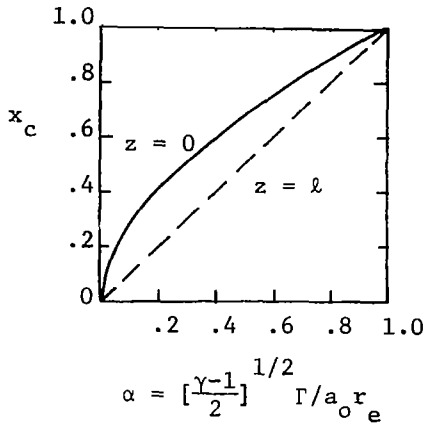

Fig. 2.4 Core radius as a function of swirl for isentropic flow with $\gamma = 1.4$ exhausting to a vacuum. (Mager 1961)

When Eq. (2.3-13) is substituted into Eq. (2.3-9) to obtain the mass flow, it may be shown that

$$\frac{\dot{m}}{\pi \rho_o a_o r_e^2 [\frac{2}{\gamma-1}]^{1/2}} = I \frac{\left[1 - \frac{1}{\frac{3-\gamma}{\gamma-1} + \frac{2(1-x_c^2)}{I}}\right]^{1/(\gamma-1)}}{\left[\frac{3-\gamma}{\gamma-1} + \frac{2(1-x_c^2)}{I}\right]^{1/2}} \tag{2.3-15}$$

Equations (2.3-15) and (2.3-13) permit the mass flow to be plotted as a function of swirl. Figure (2.5) is such a plot for $\gamma = 1.4$.

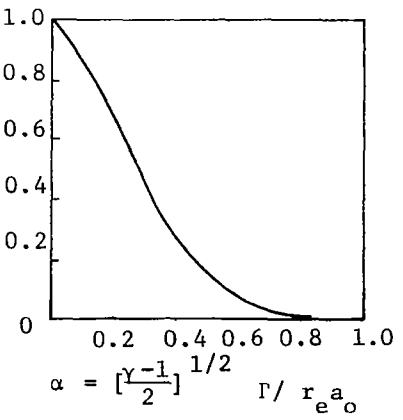

Fig. 2.5 Mass flow as a function of swirl for isentropic flow exhausting to a vacuum with $\gamma = 1.4$ (Mager, 1961).

Both Figs. (2.4) and (2.5) are quite similar to Figs. (2.2) and (2.3). The biggest difference appears to be that the mass flow in the compressible case at the same value of α is always less than it is in the incompressible, while the core radius is smaller than in the incompressible case. The similarity of these two limiting cases leads one to guess that results for intermediate values of p_c will lie between these two cases. Mass flow as a function of swirl for $p_c = 0$ and other values of γ have been computed by Glick and Kilgore (1967). As γ decreases, the mass flow for a given value of α is reduced.

Binnie (1949) determined the critical value of w as a function of swirl for general values of p_c/p_o for $\gamma = 1.4$ and $\gamma = 2$. However, he worked out the problem for a given core size, x_c, and assumed that $\partial x_c/\partial z = 0$ at the throat to obtain his critical conditions. His results for $p_c = 0$ are valid since $\rho(x_c) = 0$ in this case and the coefficient of $\partial x_c/\partial z$ in his critical equation would vanish anyway. In this limiting case, the results of Binnie and the later, more complete results of Mager are in agreement.

It is interesting to note that the axial Mach number, M_a, across this choked cross-section for swirling flow is not equal to one. The centrifugal force of the swirling flow forces a radial pressure gradient which for isentropic flow results in a radial temperature gradient. Thus, even though the axial velocity is constant, a gradient in sound speed produces a radial gradient in axial Mach number. For $p_c = 0$, M_a has a value less than 1 at r_e and increases as r is decreased, reaching ∞ at $r = r_c$. It is reassuring that the proper limit of $M_a = 1$ is reached as $\alpha \to 0$. From Eqs. (2.3-10) and (2.3-13) it may be seen that as $\alpha \to 0$, $I \to 1$, and $\alpha/x_c \to [2/(\gamma + 1)]^{1/2}$, so that $\bar{w} \to [(\gamma - 1)/(\gamma + 1)]^{1/2}$ and

$$M = \left(\frac{2}{\gamma-1}\right)^{1/2} \frac{a_o}{\bar{w}\, a} \to 1 \qquad (2.3\text{-}16)$$

The preceding case of choked axial flow through a minimum cross-section is quite different from the other limiting case when the radial flow chokes at the minimum annular area. This can be seen by considering an ideal two-dimensional, isentropic vortex with

$$\rho u r = \text{const} = \frac{\dot{m}}{2\pi \ell} \qquad (2.3\text{-}17)$$

$$vr = \text{const} = \Gamma \tag{2.3-18}$$

$$\frac{\gamma-1}{2}(u^2 + v^2) + a^2 = \text{const} = a_o^2 \tag{2.3-19}$$

and

$$p/\rho^\gamma = \text{const} = p_o/\rho_o^\gamma \tag{2.3-20}$$

After some algebra these equations can be manipulated to give

$$\frac{\dot{m}}{2\pi r \ell \rho_o a_o} = M_r \left[\frac{1 - \frac{\gamma-1}{2}\frac{\Gamma^2}{a_o^2 r^2}}{1 + \frac{\gamma-1}{2} M_r^2}\right]^{\frac{\gamma+1}{2(\gamma-1)}} \tag{2.3-21}$$

The right-hand-side of Eq. (2.3-21) must be a maximum when r is a minimum and this maximum occurs when $M_r = 1$ regardless of the energy invested in swirl. Thus, for choked radial flow

$$\frac{\dot{m}}{\dot{m}_{\Gamma=o}} = \left[1 - \frac{\gamma-1}{2}\frac{\Gamma^2}{a_o^2 r_e^2}\right]^{\frac{\gamma+1}{2(\gamma-1)}} \tag{2.3-22}$$

When Eq. (2.3-22) is compared with Fig. (2.5) in Fig. (2.6) it can be seen that $\dot{m}$ does not decrease as fast (as swirl is increased) in this case of radial choking as it does in the previous case of axial choking.

In summary, the inviscid model appears to be useful in yielding an approximate relationship between the pressure drop across a vortex chamber and the flow through it. This relationship will be compared with experiment in Chapter VII. This model is not very useful in determining the streamline pattern through the chamber.

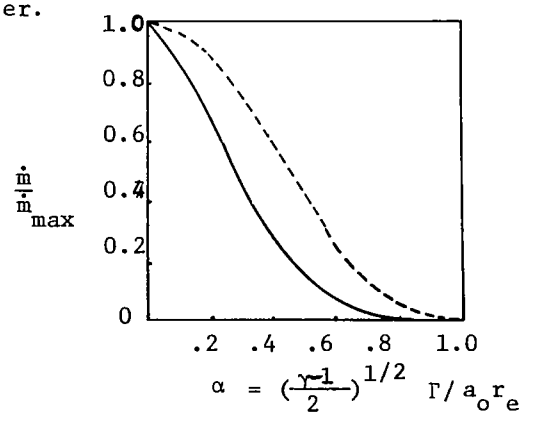

Fig. 2.6 Comparison of reduction in choked mass flow with swirl between radial choking (---) and axial choking (——).

III. INCOMPRESSIBLE, AXISYMMETRIC, LAMINAR FLOW

3.1 Governing Parameters in the Navier-Stokes Equations

For an incompressible fluid with constant viscosity, Eqs. (1.3-1) and (1.3-2) reduce to

$$\text{div } \vec{q} = 0 \tag{3.1-1}$$

$$\frac{D\vec{q}}{Dt} + \frac{1}{\rho} \text{ grad } p = \nu \text{div grad } \vec{q} \tag{3.1-2}$$

when the volume force, $\vec{f}$, is zero. These two equations form a complete set with the energy equation decoupled.

The pressure can be eliminated from the system of equations by using Eq. (1.3-5), the curl of the momentum equation, to replace Eq. (3.1-2)

$$\frac{D\vec{\omega}}{Dt} - \vec{\omega} \cdot \nabla\vec{q} = \nu \nabla^2\vec{\omega} \tag{3.1-3}$$

For axisymmetric flow, the vorticity may be written in terms of the circulation, Γ, and stream function, Ψ, defined in Eqs. (2.1-5) and (2.1-6)

$$\vec{\omega} = \frac{1}{r}\frac{\partial\Gamma}{\partial r}\vec{i}_z - \frac{1}{r}\frac{\partial\Gamma}{\partial z}\vec{i}_r - \frac{1}{\rho r}\hat{\nabla}^2\Psi\,\vec{i}_\theta \tag{3.1-4}$$

with the operator $\hat{\nabla}^2$ defined as

$$\hat{\nabla}^2 = \frac{\partial^2}{\partial z^2} + r\frac{\partial}{\partial r}\left(\frac{1}{r}\frac{\partial}{\partial r}\right) \tag{3.1-5}$$

Equation (3.1-3) could now be written as 3 scalar equations in terms of the two variables Γ and Ψ. However, it can be shown that the radial and axial components of Eq. (3.1-3) contain the same information. In fact, they may conveniently be replaced with the tangential momentum equation which for axisymmetric flow is independent of the pressure. Therefore, we may choose as our system of equations the tangential components of the momentum and the vorticity equations. These two equations may be written in terms of Γ and Ψ as

$$\frac{\partial\Gamma}{\partial t} - \frac{1}{\rho r}\left(\frac{\partial\Psi}{\partial z}\frac{\partial\Gamma}{\partial r} - \frac{\partial\Psi}{\partial r}\frac{\partial\Gamma}{\partial z}\right) = \nu\,\hat{\nabla}^2\Gamma \tag{3.1-6}$$

and

$$\frac{\partial}{\partial t}\hat{\nabla}^2\Psi - \frac{1}{\rho}\frac{\partial\Psi}{\partial z}\frac{\partial}{\partial r}\left(\frac{1}{r}\hat{\nabla}^2\Psi\right) + \frac{1}{\rho r}\frac{\partial\Psi}{\partial r}\frac{\partial\hat{\nabla}^2\Psi}{\partial z} + \frac{\nabla^2\Psi}{\rho r^2}\frac{\partial\Psi}{\partial z} + \frac{2\rho\Gamma}{r^2}\frac{\partial\Gamma}{\partial z} = \nu\,\hat{\nabla}^4\Psi \tag{3.1-7}$$

The dimensionless parameters governing the flow may be determined by normalizing the variables in Eqs. (3.1-6) and (3.1-7) with respect to their characteristic values. The following dimensionless variables are introduced:

$$\psi = \frac{2\pi\Psi}{\dot{m}}, \quad \Gamma^* = \frac{\Gamma}{\Gamma_o}, \quad \xi = \frac{z}{\ell}, \quad \eta = \left(\frac{r}{r_o}\right)^2, \quad \tau = \frac{t}{t_c} \tag{3.1-8}$$

where $\dot{m}$, Γ_o, ℓ, r_o, and t_c are characteristic values of mass flow, circulation, axial length, radius, and time, respectively. It is important to remember that the dimensionless parameters to be obtained when Eqs. (3.1-8) are introduced into Eqs. (3.1-6) and (3.1-7) are the most appropriate governing parameters only when the normalized variables are of order one. The equations could, in fact, be written so that no parameters appeared by taking

$$\ell = r_o, \quad \dot{m} = 2\pi\rho\nu r_o, \quad \Gamma_o = \nu, \quad \text{and} \quad t_c = \frac{r_o^2}{\nu} \tag{3.1-9}$$

but this only hides the governing parameters in the boundary conditions, since in this case, the order of the dimensionless variables, ψ, Γ, ξ and τ are all set by the boundary conditions.

Equations (3.1-6) and (3.1-7) may be written in terms of the variables defined in Eq. (3.1-8) as

$$\frac{1}{\mathcal{T}}\frac{\partial\Gamma^*}{\partial\tau} - 2\,\frac{\partial\psi}{\partial\xi}\frac{\partial\Gamma^*}{\partial\eta} + 2\,\frac{\partial\psi}{\partial\eta}\frac{\partial\Gamma^*}{\partial\xi} = \frac{1}{N}\mathcal{L}\Gamma^* \tag{3.1-10}$$

and

$$\frac{S^2}{\eta}\frac{\partial\Gamma^2}{\partial\xi} = -\frac{1}{\mathcal{T}}\frac{\partial\mathcal{L}\psi}{\partial\tau} + 2\eta\,\frac{\partial\psi}{\partial\xi}\frac{\partial(\frac{1}{\eta}\mathcal{L}\psi)}{\partial\eta} - 2\,\frac{\partial\psi}{\partial\eta}\frac{\partial\mathcal{L}\psi}{\partial\xi} + \frac{1}{N}\mathcal{L}^2\psi \tag{3.1-11}$$

with the dimensionless operator $\mathcal{L}$ defined as

$$\mathcal{L} = r_o^2\hat{\nabla}^2 = 4\eta\,\frac{\partial^2}{\partial\eta^2} + \left(\frac{r_o}{\ell}\right)^2\frac{\partial^2}{\partial\xi^2} \tag{3.1-12}$$

and the dimensionless parameters N, $\mathcal{T}$, and S defined as:

$$\mathcal{T} = \frac{t_c\,\dot{m}}{2\pi\rho r_o^2\ell}, \text{ the reciprocal of a reduced frequency} \tag{3.1-13}$$

$$N = \frac{\dot{m}}{2\pi\rho\nu\ell}, \text{ a Reynolds number based on thru flow} \tag{3.1-14}$$

$$S = \frac{2\pi\rho\Gamma_o r_o}{\dot{m}}, \text{ a swirl parameter measuring the interaction of the circulation and the stream function} \tag{3.1-15}$$

The general problem in this chapter is governed by 4 parameters, including the ratio of characteristic lengths appearing in the operator in Eq. (3.1-12). The parameter most unique to our vortex problems is the swirl parameter. The swirl parameter could be referred to as the reciprocal of a Rossby number. The Rossby number is usually defined as the ratio of the convective acceleration to the Coriolis force present when the equations are written in a rotating frame of reference (Greenspan, 1968). There

is no advantage to using the rotating coordinate system when the swirl distribution departs markedly from that of uniform rotation. Herein the term Rossby number will be reserved for these cases in which a uniform rotation is separated out from the general swirl distribution.

Before looking at particular solutions to Eqs. (3.1-10) and (3.1-11) let us look at the reduced equations in different limits of the governing parameters.

If N and $\gamma \to \infty$, then Eqs. (3.1-10) and (3.1-11) reduce to

$$\frac{\partial \psi}{\partial \xi}\frac{\partial \Gamma^*}{\partial \eta} - \frac{\partial \psi}{\partial \eta}\frac{\partial \Gamma^*}{\partial \xi} = 0 \tag{3.1-16}$$

and

$$\frac{S^2}{\eta}\frac{\partial \Gamma^{*2}}{\partial \xi} = 2\eta \frac{\partial \psi}{\partial \xi}\frac{\partial (\frac{1}{\eta^2}\mathcal{L}\psi)}{\partial \eta} - 2\frac{\partial \psi}{\partial \eta}\frac{\partial \mathcal{L}\psi}{\partial \xi} \tag{3.1-17}$$

Equation (3.1-16) is satisfied if Γ^* is constant along streamlines, i.e,

$$\Gamma^* = \Gamma^*(\psi) \tag{3.1-18}$$

and Eq. (3.1-17) is satisfied if

$$\frac{1}{\eta}\mathcal{L}\psi = F(\psi) - \frac{S^2}{2\eta}\frac{d\Gamma^{*2}}{d\psi} \tag{3.1-19}$$

The function $F(\psi)$ may be related to the derivative of the total pressure with respect to the stream function (Batchelor, 1967). After some manipulation it can be shown that

$$F(\psi) = \left(\frac{2\pi\rho r_o^2}{\dot{m}}\right)^2 \frac{d(\frac{p_o}{\rho})}{d\psi} \tag{3.1-20}$$

When the total pressure and circulation are assumed constant, Eq. (3.1-19) reduces to the normalized form of Eq. (2.2-1)

$$4\eta \frac{\partial^2 \psi}{\partial \eta^2} + \left(\frac{r_o}{\ell}\right)^2 \frac{\partial^2 \psi}{\partial \xi^2} = 0 \tag{3.1-21}$$

which was discussed in Section 2.2. The swirl parameter only affects the equation when the circulation distribution varies from streamline to streamline. However, the swirl can still influence the boundary conditions as seen in Chapter II.

When $S \to 0$, Eqs. (3.1-10) and (3.1-11) decouple and Eq. (3.1-10) becomes a linear equation to solve for Γ^* after the stream function has been determined. An expansion in powers of S may be used to determine the initial influence of swirl on the stream function. It is possible to consider perturbations about any of the known solutions of the axially symmetric

Navier-Stokes equations. The problems most nearly related to confined flows have been considered by Görtler (1954), Talbot (1954), Newman (1959), Lewellen (1965), Fiebig (1966), and Pedley (1969).

The most interesting limit is that of $S \to \infty$. If N, τ, and r_o/ℓ remain finite, then from Eq. (3.1-11) it follows that

$$\Gamma^* = \Gamma^*(\eta,\tau) \tag{3.1-22}$$

and from Eq. (3.1-10) this leads to the further restriction that

$$\psi = \psi_o(\eta,\tau) + \xi\psi_1(\eta,\tau) \tag{3.1-23}$$

That is, the radial and tangential velocities are independent of z and the axial velocity varies at most linearly with z. For the case in which the flow departs only slightly from uniform rotation, i.e. $\Gamma^* = \eta + O(S^{-2})$ this two-dimensional nature of the flow is known as the Taylor (1929) - Proudman (1916) Theorem. The 2-D nature of the flow holds as long as $\Gamma^* \neq$ constant. If Γ^* = constant, then Eq. (3.1-11) for ψ is independent of S and the flow need not be 2-D.

Often in problems with large swirl the boundary conditions do not permit the radial and tangential velocities to be independent of the axial coordinate. The flow must then accommodate in regions in which one or more of the other parameters do not remain finite. For example, in steady flow if $(r_o/\ell)^2 \to \infty$ as $S \to \infty$, then Eqs. (3.1-10) and (3.1-11) reduce to

$$2\frac{\partial\psi}{\partial\xi}\frac{\partial\Gamma^*}{\partial\eta} - 2\frac{\partial\psi}{\partial\eta}\frac{\partial\Gamma^*}{\partial\xi} = -\frac{1}{N}\left(\frac{r_o}{\ell}\right)^2\frac{\partial^2\Gamma^*}{\partial\xi^2} \tag{3.1-24}$$

and

$$\left(\frac{\ell}{r_o}\right)^2\frac{S^2}{\eta}\frac{\partial\Gamma^{*2}}{\partial\xi} = 2\eta\frac{\partial\psi}{\partial\xi}\frac{\partial}{\partial\eta}\left(\frac{1}{\eta}\frac{\partial^2\psi}{\partial\xi^2}\right) - 2\frac{\partial\psi}{\partial\eta}\frac{\partial^3\psi}{\partial\xi^3} + \frac{1}{N}\left(\frac{r_o}{\ell}\right)^2\frac{\partial^4\psi}{\partial\xi^4} \tag{3.1-25}$$

To keep all the remaining terms in the equations of order one it is necessary to set

$$\left(\frac{r_o}{\ell}\right)^2 = O(S^2) = O(N) \tag{3.1-26}$$

Recalling that $N = \dot{m}/2\pi\rho\nu\ell$, we see this requires that

$$\dot{m} = O(2\pi\rho\nu r_o^2/\ell) \tag{3.1-27}$$

and since $S = 2\pi\rho\Gamma_o r_o/\dot{m}$,

$$\left(\frac{r_o}{\ell}\right)^2 = O\left(\frac{\Gamma_o\ell}{\nu r_o}\right)^2 \tag{3.1-28}$$

Therefore

$$\frac{\ell}{r_o} = O\left[\frac{\nu}{\Gamma_o}\right]^{1/2} \tag{3.1-29}$$

and

$$\dot{m} = O[2\pi\rho r_o(\nu\Gamma_o)^{1/2}] \tag{3.1-30}$$

From the preceding argument, we may conclude that when $S^2 >> 1$, all axial adjustments in Γ imposed by the boundary conditions will occur in thin boundary layers that have a thickness of the order of one over the square root of a tangential Reynolds number, $[\nu/\Gamma]^{1/2}$ this is sometimes referred to as a Taylor number (Greenspan, 1968). We also obtain the important result that these thin adjustment layers will have a secondary mass flow associated with them as given in Eq. (3.1-30).

Most of this review will be limited to steady flow, but the time dependence has been retained to this point to give an opportunity for a brief discussion of inertial waves. The possibility for an incompressible swirling fluid to support waves is the consequence of the restoring force supplied by any perturbation of the equilibrium between pressure gradient and centrifugal force in a stable swirling fluid. When S is large and r_o/ℓ of order one the radial component of the momentum equation yields

$$\frac{\partial p}{\partial r} = \frac{\rho\Gamma^2}{r^3} \tag{3.1-31}$$

regardless of the order N. If a fluid element is perturbed from its equilibrium position it tends to conserve its circulation. The forces on the element in its perturbed position consist of the pressure gradient that balances the centrifugal force at that position and the centrifugal force determined by the circulation at its equilibrium position, i.e.,

$$\Delta F = \frac{\rho}{r_2{}^3}(\Gamma_1{}^2 - \Gamma_2{}^2) \tag{3.1-32}$$

where the subscript 1 refers to the equilibrium position of the element and subscript 2 to its perturbed position. As long as $d\Gamma/dr > 0$ (in Chapter IV it can be seen that this is a necessary condition for a stable swirling flow), Eq. (3.1-32) provides a restoring force for the fluid element. If $r_2 > r_1$ then $\Gamma_2 > \Gamma_1$ and $\Delta F < 0$, tending to force the fluid element to decrease its radius back to r_1.

In order to exhibit the inertial waves mathematically, consider the limit of $N \to \infty$, and let τ and S be inversely related as $S \to \infty$. Also let

$$\Gamma^* = \Gamma_o^*(\eta) + \frac{1}{S}\, g(\eta,\xi,\tau) \tag{3.1-33}$$

Equation (3.1-10) and (3.1-11) reduce to

$$\frac{1}{\mathcal{I}S}\frac{\partial g}{\partial \tau} - 2\Gamma_o^{\bullet\prime}\frac{\partial \psi}{\partial \xi} = 0 \tag{3.1-34}$$

$$\frac{2S\Gamma_o^{\bullet}}{\eta}\frac{\partial g}{\partial \xi} = -\frac{1}{\mathcal{I}S}\frac{\partial^2 \psi}{\partial \tau} \tag{3.1-35}$$

Cross differentiation of these last equations leads to

$$\frac{1}{\mathcal{I}^2S^2}\frac{\partial^2 \psi}{\partial \tau^2} + \frac{4\Gamma_o^{\bullet}\Gamma_o^{\bullet\prime}}{\eta}\frac{\partial^2 \psi}{\partial \xi^2} = 0 \tag{3.1-36}$$

From the definition of $\mathcal{I}$ and S, Eqs. (3.1-13) and (3.1-15), we see that

$$\mathcal{I}^2S^2 = \left(\frac{\Gamma_o\, t_c}{r_o \ell}\right)^2 \tag{3.1-37}$$

This can be set equal to one with no further loss in generality. Let us also limit ourselves to the main body of flow outside any shear layers by assuming $r_o = \ell$. Then Eq. (3.1-36) reduces to

$$\frac{\partial^2}{\partial \tau^2}\left[4\eta\frac{\partial^2 \psi}{\partial \eta^2} + \frac{\partial^2 \psi}{\partial \xi^2}\right] + \frac{4\Gamma_o^{\bullet}\Gamma_o^{\bullet\prime}}{\eta}\frac{\partial^2 \psi}{\partial \xi^2} = 0 \tag{3.1-38}$$

The time dependence of ψ may be Fourier analysed since this is a linear equation. For simplicity we will consider only a sinusoidal time variation, i.e. assume

$$\psi = \bar{\psi}(\xi,\eta)\ \sin \lambda\tau \tag{3.1-39}$$

Then

$$4\eta\frac{\partial^2 \bar{\psi}}{\partial \eta^2} + \left[1 - \frac{4\Gamma_o^{\bullet}\Gamma_o^{\bullet\prime}}{\eta\lambda^2}\right]\frac{\partial^2 \bar{\psi}}{\partial \xi^2} = 0 \tag{3.1-40}$$

Equation (3.1-40) is elliptic or hyperbolic depending upon whether λ is $>$ or $< 2\left[\frac{\Gamma_o^{\bullet}\Gamma_o^{\bullet\prime}}{\eta}\right]^{1/2}$. When the frequency is sufficiently low for the equation to be hyperbolic, characteristic surfaces, along which disturbances propagate, will exist in the flow. The waves are dispersive with the slope of these characteristic surfaces given by

$$\frac{d\xi}{d\eta} = \pm\frac{1}{2\lambda\eta^{1/2}}\left[\frac{4\Gamma_o^{\bullet}\Gamma_o^{\bullet\prime}}{\eta} - \lambda^2\right]^{1/2} \tag{3.1-41}$$

In the case of nearly uniform rotation, i.e., when $\Gamma_o^{\bullet} = \eta$ these surfaces are conical. Figure 3.1 from Greenspan (1968) shows these wave propagation patterns and demonstrates that the slope of the characteristics has the frequency dependence predicted by Eq. (3.1-41). Note that as $\lambda \to 0$, the slope of the characteristics approach ∞ and the characteristic cones become cylinders. This is another demonstration of the flow tending toward two-dimensionality. In steady flow these cylindrical surfaces which permit the flow to be 2-D,

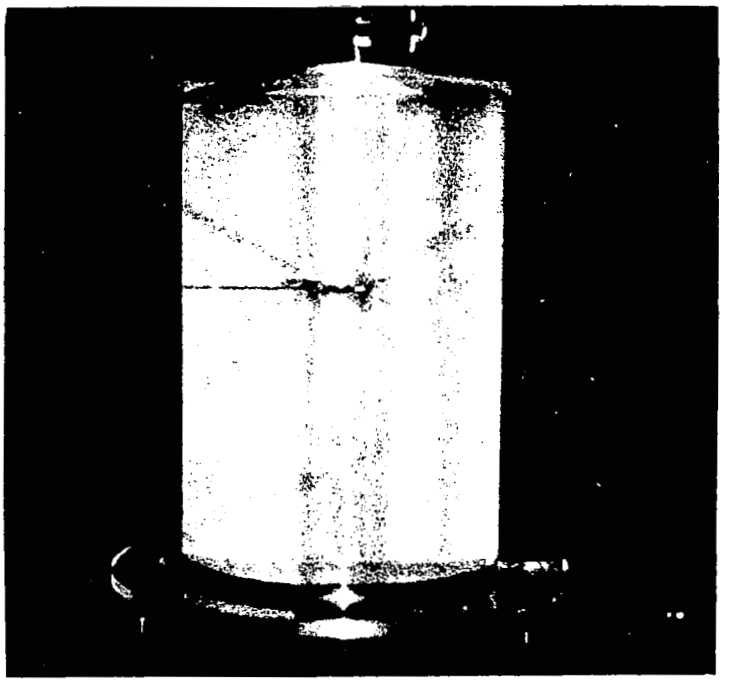

(a)

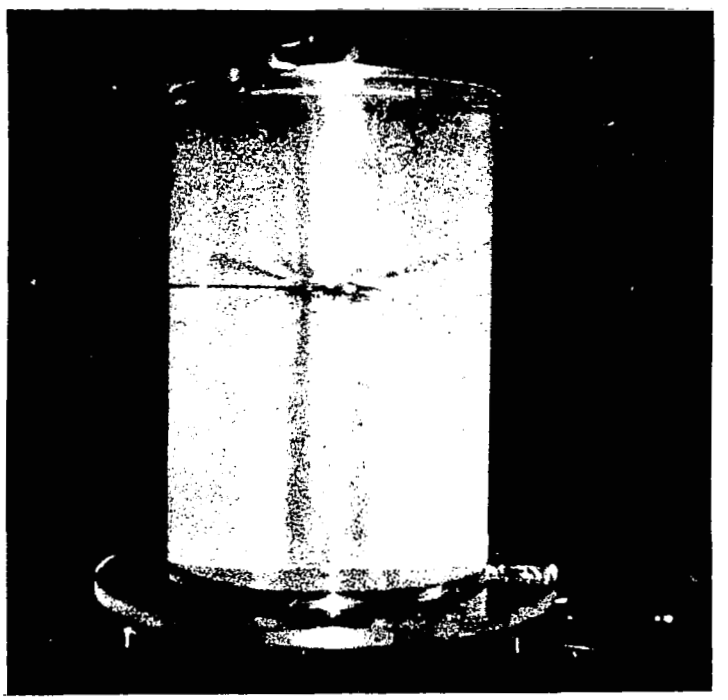

(b)

Fig. 3.1 (a) Waves produced by an oscillating disk with $\lambda = 1.75$. The half apex angle is 59° and the theoretical value is 56°. (b) The apex angle increases for a larger value of λ (Greenspan, 1968).

when the boundary conditions are not, are known as Taylor columns.

3.2 Similarity Solutions

The most common method of obtaining exact solutions to the Navier-Stokes equations is by using a so-called similarity transformation. That is, the variables are transformed to functions of a single elementary function of the coordinates. In this form the unknown variables satisfy ordinary differential equations. The solution of such equations (numerically, if necessary) is considerably simpler than the solution of the original partial-differential equations.

The similarity constraint imposes a strong restriction on the flow. In general, one cannot expect the boundary conditions associated with the complete flow pattern in any container to conform to a similarity solution. At best, one can expect the similarity solution to hold in certain regions of the flow. But often even this is not the case. The most useful purpose served by these solutions is in providing exact solutions which demonstrate the different type flow patterns to be expected.

A. Possible Similarity Transformations for Steady Flow

The type of similarity transformation attempted is in general related to the boundary conditions of the particular problem considered. The present geometry of confined vortices suggests the use of the following rather general similarity transformation:

$$\begin{aligned} \Gamma &= g(y)\ \theta(\xi) \\ \psi &= f(y)\ \phi(\xi) \\ y &= \eta\ \Delta(\xi) \end{aligned} \tag{3.2-1}$$

In terms of the variables of Eqs. (3.2-1), the tangential momentum equation, Eq. (3.1-10), becomes

$$fg'\phi' - f'g\phi\frac{\theta'}{\theta} + \frac{2yg''}{N} + \frac{(r_o/\ell)^2}{2N\Delta}\left[g\frac{\theta''}{\theta} + 2\frac{\theta'}{\theta}g'y\frac{\Delta'}{\Delta} + g''y^2\frac{\Delta'^2}{\Delta^2} + g'y\frac{\Delta''}{\Delta}\right] = 0 \tag{3.2-2}$$

Since the terms of Eq. (3.2-2) are not in general separable into terms which are functions only of one or the other of the variables, y or ξ, it is necessary to find special values of the functions which permit the equations to be only a function of one variable. If Eq. (3.2-2) is to be a function of y only, then from the first and third terms either $\phi' = \text{const.}$ or $g'' = 0$.

Considering $\phi = \xi$ first, the second term, for a nonzero f', requires $\theta = \xi^n$, but this is inconsistent with the fourth and fifth terms unless n = 0, i.e., θ = constant, or n = 1 and $\Delta' = 0$. Then from the last two terms in the equation either $\Delta' = 0$ or $\Delta = \xi^{-2}$. On the other hand, if g" = 0 then Eq. (3.2-2) is an ordinary differential equation with respect to ξ providing f" and ϕ' equal zero.

Thus the following possibilities are found after considering only Eq. (3.1-10):

$$\text{(i)} \quad \theta = 1, \quad \phi = \xi, \quad \Delta = 1 \tag{3.2-3}$$

$$\text{(ii)} \quad \theta = 1, \quad \phi = \xi, \quad \Delta = \xi^{-2} \tag{3.2-4}$$

$$\text{(iii)} \quad \theta = \xi, \quad \phi = \xi, \quad \Delta = 1 \tag{3.2-5}$$

$$\text{(iv)} \quad g = y, \quad f = y, \quad \Delta = 1 \tag{3.2-6}$$

All four of these forms are also found to be consistent with Eq. (3.1-11). It is also found that a combination of (i) and (iii) of the form

$$\text{(v)} \quad \Gamma = \Gamma_o(\eta) + \xi\, \Gamma_1(\eta); \quad \psi = \psi_o(\eta) + \xi\, \psi_1(\eta) \tag{3.2-7}$$

reduces the equations of motion to a set of four ordinary differential equations.

The above similarity transformations which permit exact solutions are quite restrictive. However, if boundary-layer assumptions are used, a more general class of transformations is available. Considering an axial "boundary layer," i.e., a thin region within which the derivatives of the variables with respect to z are very large, the ratio of characteristic lengths, r_o/ℓ, will be very large. Neglecting order $(\ell/r_o)^2$, i.e., order of the boundary-layer thickness squared over the characteristic radius squared, Eqs. (3.1-10) and (3.1-11) reduce to Eqs. (3.1-24) and (3.1-25).

Eqs. (3.1-24) and (3.1-25) can be reduced to ordinary differential equations by any member of the following class of transformations

$$\begin{aligned} \Gamma(\eta,\xi) &= g(y)\, \eta^q \\ \psi(\eta,\xi) &= f(y)\, \eta^{\frac{q+1}{2}} \\ y &= \xi\, \eta^{\frac{q-1}{2}} \end{aligned} \tag{3.2-8}$$

When q = 1, this boundary-layer transformation is the same transformation as given by (iv) for the full equations. Also, when q = 0, the form in Eq. (3.2-8) is equivalent to that of type (ii). The special members of the

transformation in Eq. (3.2-8) represented by q = 1 and q = 0 thus reduce the full equations while any q suffices to reduce the boundary-layer equations.

If a boundary layer is considered in the opposite sense, i.e., as a region of thin radial extent about the axis within which the derivatives with respect to radius are very large, then r_o/ℓ will be small. The equations of motion neglecting $O(r_o/\ell)^2$ then become

$$\frac{\partial\psi}{\partial\xi}\frac{\partial\Gamma^*}{\partial\eta} - \frac{\partial\psi}{\partial\eta}\frac{\partial\Gamma^*}{\partial\xi} = -\frac{2\eta}{N}\frac{\partial^2\Gamma^*}{\partial\eta^2} \tag{3.2-9}$$

$$S^2\Gamma^*\frac{\partial\Gamma^*}{\partial\xi} = 4\eta^2\left[\frac{\partial\psi}{\partial\xi}\frac{\partial^3\psi}{\partial\eta^3} - \frac{\partial\psi}{\partial\eta}\frac{\partial^3\psi}{\partial\xi\,\partial\eta^2} + \frac{2}{N}\left(2\frac{\partial^3\psi}{\partial\eta^3} + \eta\frac{\partial^4\psi}{\partial\eta^4}\right)\right] \tag{3.2-10}$$

Equations (3.2-9) and (3.2-10) are reducible to ordinary differential equations by the transformation

$$\begin{aligned}\Gamma^* &= g(y)\ \xi^m \\ \psi &= f(y)\ \xi \\ y &= \eta\ \xi^{2(m-1)}\end{aligned} \tag{3.2-11}$$

It can again be noted that of the class of transformations represented by Eq. (3.2-11) the two, m = 1 and m = 0, represent transformations for the full equations corresponding respectively to type (iii) and (ii). Type (i) also, of course, reduces Eqs. (3.2-9) and (3.2-10) but is not included in Eq. (3.2-11). Transformation (i) is the special case for which the right and left-hand sides of Eq. (3.2-10) are individually equal to zero.

If the boundary layer of thin radial extent occurs away from the axis at some radius which is large compared to the boundary-layer thickness, then the radial curvature terms in Eq. (3.2-10) and (3.2-9) can be neglected. by setting

$$\eta = 1 + \delta x \tag{3.2-12}$$

Eqs. (3.2-9) and (3.2-10) become to $O(\delta)$

$$\frac{\partial\psi}{\partial\xi}\frac{\partial\Gamma^*}{\partial x} - \frac{\partial\psi}{\partial x}\frac{\partial\Gamma^*}{\partial\xi} = -\frac{2}{N\delta}\frac{\partial^2\Gamma^*}{\partial x^2} \tag{3.2-13}$$

$$S^2\Gamma^*\frac{\partial\Gamma^*}{\partial\xi} = \frac{4}{\delta^3}\left[\frac{\partial\psi}{\partial\xi}\frac{\partial^3\psi}{\partial x^3} - \frac{\partial\psi}{\partial x}\frac{\partial^3\psi}{\partial\xi\,\partial x^2} + \frac{2}{N\delta}\frac{\partial^4\psi}{\delta x^4}\right] \tag{3.2-14}$$

Equations (3.2-13) and (3.2-14) can be reduced to ordinary differential equations by the transformation

$$\begin{aligned}\Gamma^*(x,\xi) &= g(y)\ \xi^{\frac{5p-3}{2}} \\ \psi(x,\xi) &= f(y)\ \xi^p\end{aligned} \tag{3.2-15}$$

$$y = x\,\xi^{p-1}$$

The similarity transformations given in this section, of course, do not exhaust all the possibilities. Some special forms different from Eq. (3.2-1) are possible. A couple of these will be included in the next section.

B. Existing Solutions

Transformation (i) yields a flow with the tangential and radial velocities independent of the axial coordinate. It has been studied most completely by Donaldson and Sullivan (1960). Since the tangential velocity is independent of the axial coordinate in these flows, by Eq. (3.1-11), the stream function is independent of the circulation. It should perhaps be emphasized that the solutions for the stream function found in this class are obtainable in flows without any swirl. The same equations and boundary conditions for the stream function studied by Donaldson and Sullivan was earlier investigated by Yuan and Finkelstein (1956) in the study of laminar flow in a porous tube. The corresponding solutions for the circulation represent those tangential velocity distributions which can be superimposed upon the basic flow without in any way changing the stream function. This complete decoupling of the stream function from the circulation distribution is seldom achieved in real flows except in the limit of small swirl. However, a great deal can be learned about the circulation distribution by investigating how it varies for different stream function distributions of this class.

When transformation (i) is used Eqs. (3.1-10) and (3.1-11) reduce to

$$2\eta g'' + Nfg' = 0 \tag{3.2-16}$$

and

$$N(ff''' - f'f'') + 4f''' + 2\eta f'''' = 0 \tag{3.2-17}$$

The simplest solution of the last equation is f = constant, corresponding to a line sink along the axis. For this case it is appropriate to normalize the mass flow so that f = 1 and Eq. (3.2-16) integrates to

$$g = c_1\,\eta^{1-\frac{N}{2}} + c_2 \tag{3.2-18}$$

This solution was first discussed by Hamel (1916) and may be used to look at the swirl distribution that could occur between two concentric porous cylinders when one or both of them are rotating and a mass flow passes radially through the cylinders. If the larger cylinder of radius r_o is assumed to rotate with an angular velocity Ω_o, and the smaller cylinder of

of radius r_i is stationary, then in dimensional terms

$$v = \frac{\Omega_o r_o}{r} \left[\frac{r^{-N+2} - r_i^{-N+2}}{r_o^{-N+2} - r_i^{-N+2}}\right] \tag{3.2-19}$$

where the radial Reynolds number N is based on the mass flow per unit length passing through the cylinders. Equation (3.2-19) is plotted in Fig. 3.2.

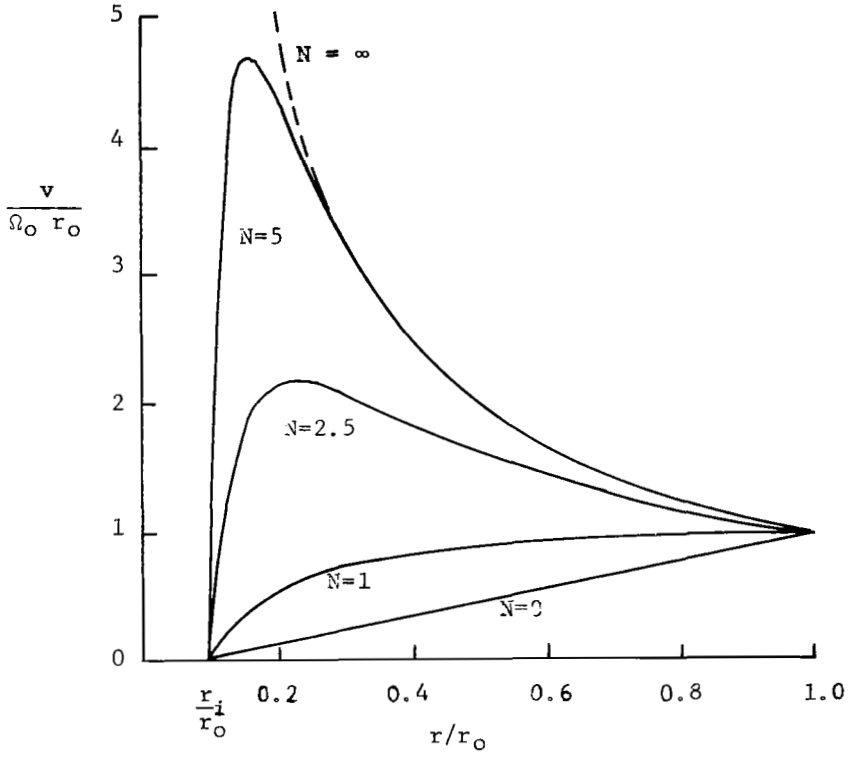

Fig. 3.2 Tangential velocity profile inside a rotating porous cylinder for various values of radial thru flow.

There is a boundary layer formed on the outer cylinder when $N < 0$ corresponding to a radial mass flow passing from the inner cylinder out. A vortex type flow occurs when $N > 2$ corresponding to an inward mass flow. When $N >> 1$ there is a potential vortex between the cylinders with a thin boundary layer on the inner cylinder.

The next solution of Eq. (3.2-17) to be considered is that of $f = \eta$ corresponding to flow with a sink located at $z = +\infty$ and $z = -\infty$. The vortex distributions possible with such sink flows were discussed by Burgers (1948) and Rott (1958). If the boundary conditions that $v = 0$ at $r = 0$ and the circulation is a given finite value Γ_o at large radii, then Eq. (3.2-16) may be

integrated for this case to give

$$\Gamma = \Gamma_o \left(1 - e^{-\frac{N}{2}\eta}\right) \tag{3.2-20}$$

Again, an inflow corresponding to $N > 0$ is necessary to obtain a vortex type flow. One of the most basic features of real vortex flows is evident from this solution. Namely, that at large radii the vortex tends to have a constant circulation since the exponential term can be ignored there, while near the axis the exponential term may be expanded in a series to show that

$$\Gamma \to \Gamma_o \frac{N}{2} \eta \quad \text{as} \quad \eta \to 0 \tag{3.2-21}$$

corresponding to solid-body rotation. The maximum velocities in the vortex occur in the transition region between potential circulation and uniform rotation. The radius at which this occurs is the natural characteristic length for this problem. This corresponds to setting $N = 1$. It is also more convenient to work with a velocity gradient, a, defined so that $u = -ar$, $w = 2az$, then with the mass flow which varies with r^2 , i.e.

$$N = \frac{ar_o^2}{\nu} = 1 \tag{3.2-22}$$

$$r_o = \left(\frac{\nu}{a}\right)^{1/2} \tag{3.2-23}$$

The axial and tangential velocity distributions for this case are given in Fig. 3.3 as the one cell solution.

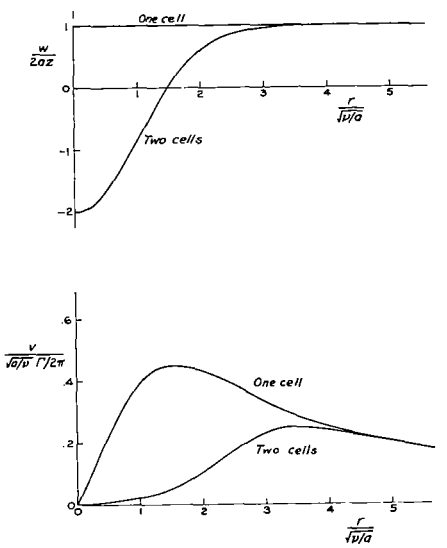

Fig. 3.3 Velocity distributions (a) Top: axial velocity.
(b) Bottom: tangential velocity. (Sullivan, 1959)

Donaldson and Sullivan (1960) have obtained the swirl distribution associated with a wide variety of stream function distributions obtained by solving Eq. (3.2-17) numerically. The solutions for f exhibit a varying number of flow reversals which may be described as nested cells. However, one should not attribute these multiple-celled solutions as being caused by the vortex motion, since Eq. (3.2-17) is completely decoupled from the swirl. An analytic solution of this class was given by Sullivan (1959) corresponding to a two-celled stream function. One can readily check that

$$f = \eta - \frac{6}{N}\left(1 - e^{-\frac{N}{2}\eta}\right) \tag{3.2-24}$$

satisfies Eq. (3.2-17). The axial velocity given by this solution is plotted in Fig. 3.3 as is the tangential velocity obtained by substituting Eq. (3.2-24) into Eq. (3.2-16) and integrating. The velocities obtained for Eq. (3.2-20) are also included for comparison.

When transformation (ii) is used the stream function is coupled to the circulation. The equations for this case may be written as

$$2yg'' + \left(\frac{r_o}{\ell}\right)^2 (3g' + 2y^2 g'') + Nfg' = 0 \tag{3.2-25}$$

and

$$-S^2\frac{gg'}{2y} = ff''' + 3f'f'' + \frac{2}{N}(yf'''' + 2f''') + \frac{1}{2}\left(\frac{r_o}{\ell}\right)^2 [2yff''' + 6f'f'' + ff'' - 3f'^2] + \frac{1}{N}\left(\frac{r_o}{\ell}\right)^2 \{[4y + 2\left(\frac{r_o}{\ell}\right)^2 y^2]\, f'''' + [14y + 12\left(\frac{r_o}{\ell}\right)^2 y^2]f''' + [4 + \frac{21}{2}\left(\frac{r_o}{\ell}\right)^2 y]f'' - 3\left(\frac{r_o}{\ell}\right)^2 f'\} \tag{3.2-26}$$

Long (1961) has considered the problem analogous to Burgers-Rott for this transformation. Actually the solutions presented by Long belong to the family of Eq. (3.2-11) since after obtaining ordinary differential equations for the full equations, they were solved using the boundary-layer approximation $[(r_o/\ell)^2 \to 0]$. Long's flow problem can perhaps be best described as a swirling jet exhausting into an unbounded fluid which has constant circulation. In the limit of zero circulation it reduces to Schlichting's jet problem (Schlichting, 1968). Long's solutions demonstrate that as the ratio of the angular momentum in the jet to the axial momentum in the jet is increased the axial velocity on the axis of the jet is retarded. The parameter used by Long is

$$M = \frac{2\pi}{\Gamma_o^2} \int_o^\infty \left(\frac{p}{\rho} + w^2\right) r \, dr \qquad (3.2\text{-}27)$$

He found that two solutions could exist for each value of $M > 3.65$ and that no solution exists for $M < 3.65$. In each pair of solutions one has a positive axial velocity on the axis and the other a negative axial velocity. The solution with a negative axial velocity corresponds to the jet with the higher ratio of angular momentum to axial momentum.

Equations (3.2-25 and 3.2-26) also were used by Gol'dshtik (1960) to consider the flow produced by a potential vortex over an infinite stationary wall. He was able to show that no solution exists for this problem with a tangential Reynolds number, $SN > 8$. This points out the fact that although a particular transformation may reduce the equations of motion to ordinary differential equations and seemingly physical boundary conditions which do not destroy the similarity are applied, the resulting system of equations and boundary conditions may not permit a real solution. The small Reynolds number solution was recently computed, numerically by Kidd and Farris (1968).

No solutions appear in the literature for transformation (ii). The transformation which has received the most attention in the literature is (iv). This was first used by Von Kármán (1921) and Cochran (1934) to find the flow due to an infinite rotating disk in an unbounded fluid at rest. It was later used by Bodewadt (1940) to solve the opposite problem of a uniformly rotating fluid over and infinite stationary wall.

For transformation (iv), Eqs. (3.1-10 and 3.1-11) reduce to

$$\theta'' - 2N \left(\frac{r_o}{\ell}\right)^{-2} [\phi\theta' - \phi'\theta] = 0 \qquad (3.2\text{-}28)$$

and

$$S^2 \left(\frac{\ell}{r_o}\right)^2 \theta\theta' = - \phi\phi''' + \frac{1}{2N} \left(\frac{r_o}{\ell}\right)^2 \phi'''' \qquad (3.2\text{-}29)$$

As demonstrated in Section 3.1, it is possible to take the characteristic length ratio as

$$\frac{\ell}{r_o} = \left(\frac{\nu}{\Gamma_o}\right)^{1/2} \qquad (3.2\text{-}30)$$

and set $S^2(\ell/r_o)^2 = \frac{1}{N}(r_o/\ell)^2 = 1$ with no loss in generality. The solution then depends only on the boundary conditions. It also is convenient to integrate Eq. (3.2-29) once formally so that the two equations now reduce to

$$\theta'' - 2\phi\theta' + 2\phi'\theta = 0 \qquad (3.2\text{-}31)$$

$$\phi''' - 2\phi\phi'' + \phi'^2 - \theta^2 = \text{const.} \qquad (3.2\text{-}32)$$

Von Karmán's problem of a rotating disk may be solved by numerically integrating Eqs. (3.2-31 and 3.2-32) with the boundary conditions

$$\phi(0) = \phi'(0) = \phi'(\infty) = 0$$
$$\theta(\infty) = 0, \qquad \theta(0) = 1 \qquad (3.2\text{-}33)$$

The velocity distributions obtained in this manner are plotted in dimensional terms in Fig. 3.4.

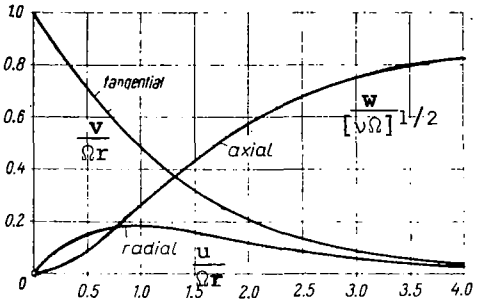

$$\xi = z\sqrt{\frac{\Omega}{\nu}}$$

Fig. 3.4 Velocity distribution near a disk rotating in a fluid at rest.

Bödewadt (1960) considered the opposite problem of a uniformly rotating flow over a stationary disk. The boundary conditions for this problem are

$$\phi(0) = \phi'(0) = \phi'(\infty) = 0$$
$$\theta(0) = 0, \qquad \theta(\infty) = 1 \qquad (3.2\text{-}34)$$

The numerical solutions obtained with these conditions are quite different from the preceding solutions. The velocity distributions are plotted in Fig. 3.5.

The oscillations appearing in the Bödewadt profiles have tempted several authors to discount this solution, but as seen in Section 1.2 the oscillations rest on firm physical ground.

The variety of flows which can possibly be represented by one of the transformations is amply demonstrated by the number of flows considered with transformation (iv) by varying the compatible boundary conditions. Batchelor (1951) not only considered the family of solutions in which the ratio of the fluid rotation to the disk rotation varies from $-\infty$ to $+\infty$, but also considered the two-parameter family of solutions which describes the flow between two parallel infinite disks which are rotating about the same axis with different

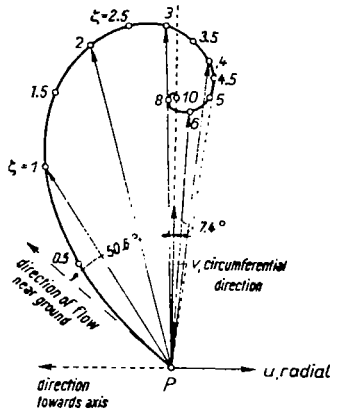

(a)

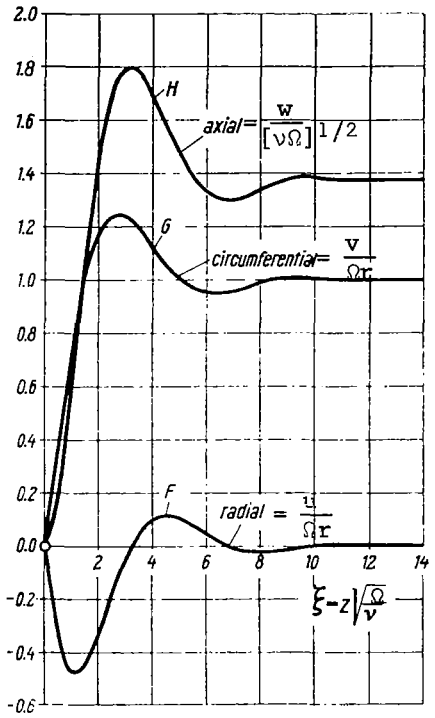

(b)

Fig. 3.5 Rotation near a solid wall, after Bödewadt. (a) Vector representation of the horizontal velocity component. (b) Velocity components as a function of z

angular velocities. This later problem was also discussed by Stewartson (1953). The solutions for some of the flows discussed by Batchelor and Stewartson were obtained numerically by Rogers and Lance (1960, 1962), and by Pearson (1965). Stagnation flow against a rotating disk was studied by Hannah (1952) by including a source on the axis of rotation at infinity. These flows can be given a further degree of freedom by permitting sucking or blowing through the disk (Stuart, 1954 and Nanda, 1961). An analogous variety of boundary conditions could be combined with the other transformations resulting in an enormous number of possible solutions, most of which would be of restricted interest.

These exact solutions (of the Navier-Stokes equations) obtained using transformation (iv) all exhibit a boundary-layer type behavior when the tangential Reynolds number is large. This family of boundary-layer solutions can

be greatly expanded when the less strenuous transformation of boundary-layer similarity as given in Eq. (3.2-8) is used. The boundary-layer equations can then be written as (with $\beta = 2q - 1$).

$$g'' - \frac{1}{2}(3 + \beta) fg' + (\beta + 1) f'g = 0 \qquad (3.2\text{-}35)$$

$$-f''' + \frac{1}{2}(3 + \beta) ff'' - \beta f'^2 + g^2 = g^2(\infty) - \beta f'^2(\infty) \qquad (3.2\text{-}36)$$

These last equations reduce to Eqs. (3.2-31) and (3.2-32) when $\beta = 1$ with $g = \theta$ and $f = \phi$. They were integrated numerically by King and Lewellen (1964) for values of β between -1 and +1 and boundary conditions which correspond to rotating flow over a stationary, solid wall, i.e.

$$f(0) = f'(0) = f'(\infty) = 0$$
$$g(0) = 0, \quad g(\infty) = 1 \qquad (3.2\text{-}37)$$

It was found, as shown in Fig. 3.6, that the oscillations exhibited in the Bödewadt solution for $\beta = 1$ increased in magnitude and wavelength as β decreased; no solution exists for an external potential flow, $\beta = -1$

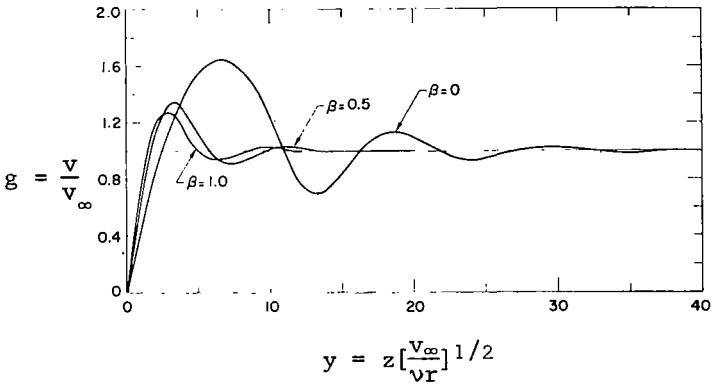

Fig. 3.6 The dimensionless tangential boundary-layer velocity distributions of the terminal similarity solutions for a fluid rotating as $V = Cr^{\beta}$ over a stationary disk. (King and Lewellen, 1964).

Some properties of the solution can be seen by integrating Eq. (3.2-36) twice, formally. This leads to

$$f^2(\infty) = \frac{-2}{3 + \beta} \int_0^\infty dy \int_y^\infty [3 (1 + \beta) f'^2 + 2 (g^2(\infty) - g^2)] \, dy \qquad (3.2\text{-}38)$$

Since the right hand side of this equation must be positive for a real solution, it is clear that g must exceed $g(\infty)$ at some points within the boundary layer. For the case of rotating flow over a stationary wall this can only happen if the tangential velocity profile has some type of overshoot which in turn implies an oscillation.

An asymptotic expansion of the equations for $y \to \infty$ can be used to show that $f(\infty) > 0$. This corresponds to flow out of the boundary layer. These solutions thus correspond to a "terminal" similarity. The boundary layer began with an infinite reservoir of flow which is steadily expelled as the radius decreases and approaches zero as $r \to 0$.

With the terminal nature of the boundary layer in mind the oscillations in the velocity profiles may be explained in the following way. (King and Lewellen 1964). The radial inflow, induced by the retardation of the tangential velocity in the neighborhood of the wall, tends to conserve the angular momentum of the flow and thus to increase the tangential velocity with decreasing radius. For an overshoot, radial convection of angular momentum in the boundary layer must be strong enough to more than balance the dissipation of angular momentum caused by the wall shear. This inward radial convection of surplus angular momentum is possible as long as the distribution of circulation in the outer flow increases with increasing r. However, a local overshoot in the tangential velocity increases the centrifugal force locally which then tends to induce a radial outflow. This radial outflow convects an angular momentum defect to force an undershoot in the tangential velocity, and the whole process is repeated to yield the oscillatory approach to infinity exhibited by the solution.

The requirement of the infinite reservoir at infinite radius leads to the question of whether a terminal similarity solution is ever valid. It can only be valid if the boundary-layer flow can forget about its history, since the initial conditions at large radius can never be exactly fulfilled, and be controlled by local conditions. A laser-Doppler velocimeter has been used by Bien and Penner (1970) to show that the Bödewadt terminal similarity solution is found near the center of a stationary disk in a rotating flow. The flow field investigated was that between a rotating disk and a stationary disk. The comparison between theory and experiment is shown in Fig. 3.7. A profile similar to von Kármán's occurs near the rotating disk and the Bödewadt profile of Fig. 3.5 near the stationary disk. The matching condition between these two determines the core flow as will be discussed in Section 3.5. Numerical integrations of the boundary-layer equations by Rogers and Lance (1964), Anderson (1966), and Cooke(1966) show that the boundary layer created by a uniformly rotating flow over a finite disk of radius r_o approaches the terminal similarity profiles given in Bödewadt's solution when $r/r_o \leq 0.5$. The build

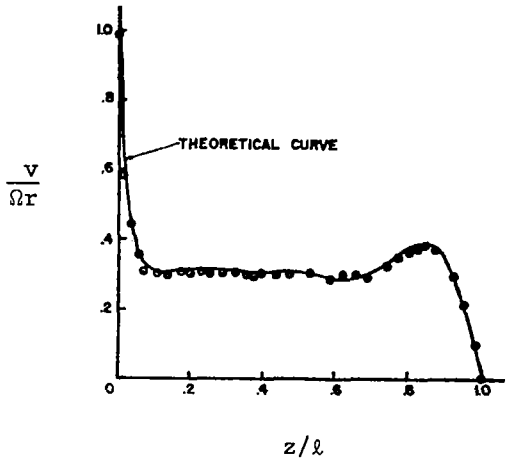

Fig. 3.7 Tangential velocity profile between a rotating disk and a stationary disk at $r/r_o = 0.52$ for $\Omega\ell^2/\nu = 1002$. (Bien and Penner, 1970)

up of the overshoot in circulation within the boundary layer is shown in Fig. 3.8. The overshoot in circulation within the boundary layer is zero at the beginning of the boundary layer at $r = r_o$. As the boundary layer grows in the direction of decreasing radius the maximum rotation rate increases until it reaches the value given by Bodewadt.

These terminal similarity solutions are closely related to the classical Ekman (1905) Spiral obtained in a boundary layer determined by the balance between viscous and Coriolis forces. When the wall rotates at a rate only slightly different from the rotation rate of the fluid the solution for the boundary-layer profiles is the Ekman Spiral. It can be obtained from Eqs. (3.2-35) and (3.2-36) with $\beta = 1$ and the boundary conditions given in Eqs. (3.2-37) modified to $g(0) = 1$ and $g(\infty) = 1 + \varepsilon$. The solution for $\varepsilon << 1$, then is

$$g = 1 + \varepsilon\,[1 - e^{-y} \cos y] \qquad (3.2\text{-}39)$$

$$f = -\frac{\varepsilon}{2}\,[1 - e^{-y}\,(\sin y + \cos y)] \qquad (3.2\text{-}40)$$

This gives a spiral distribution for the horizontal velocity component similar to that given in Fig. 3.5a. In this limit the boundary layer, generally termed Ekman layer (Greenspan, 1968) is completely determined by local conditions. The parameter ε may be a function of r and Eqs. (3.2-39) and (3.2-40) remain valid.

The similarity solution of the boundary layer of thin radial extent that most closely relates to the problem of a confined vortex flow is the solution given by Stewartson (1957, 1958). If the transformation given in

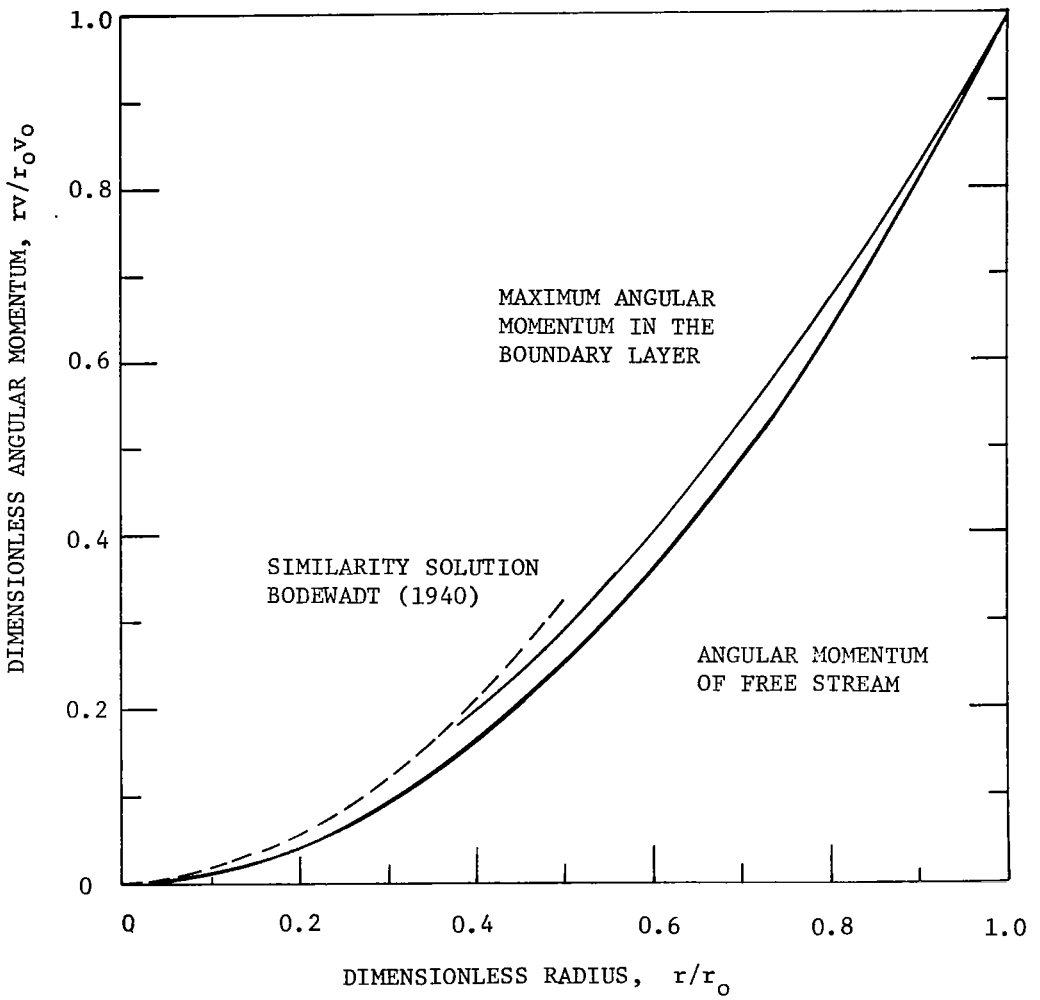

Fig. 3.8 Comparison of the angular momentum in the boundary layer with the angular momentum of the free stream for solid-body rotation (Anderson, 1966).

Eqs. (3.2-15) is to be used to represent a flow which has constant circulation on a cylindrical surface of constant radius, then the parameter p must be restricted to a value of 3/5. For this case Eqs. (3.2-13) and (3.2-14) reduce to

$$\frac{2}{N\delta} g'' + \frac{3}{5} fg' = 0 \qquad (3.2\text{-}41)$$

$$\frac{S^2\delta^3}{2} ygg' = 3ff''' + 4f'f'' + \frac{10}{N\delta} f'''' \qquad (3.2\text{-}42)$$

In order to keep the dimensionless variables and their derivatives as order one quantities it is appropriate to set

$$S^2\delta^3 = 1 \quad \text{and} \quad N\delta = 1$$

It follows directly, with the aid of the definition of N and S^2, that

$$\delta = \left(\frac{\nu}{\Gamma_o}\frac{\ell}{r_o}\right)^{2/5} \tag{3.2-43}$$

The boundary conditions assumed by Stewartson which are appropriate for the boundary layer on a semi-infinite cylinder that rotates about its axis in a fluid otherwise at rest are

$$\begin{aligned} f(0) = f'(0) = f'(\infty) = 0 \\ g(0) = 1, \quad g(\infty) = 0 \end{aligned} \tag{3.2-44}$$

The profiles obtained by integrating Eqs. (3.2-41) and (3.2-42) with the boundary conditions of Eq. (3.2-44) are given in Fig. 3.9 in dimensional terms. The convection within this layer is driven by the pressure gradient across it and consequently has a weaker dependence on Reynolds number than the typical inverse 1/2 power dependence.

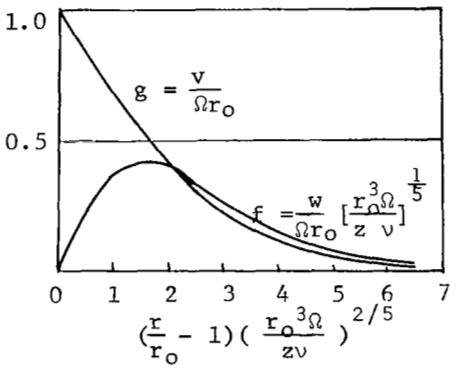

Fig. 3.9 Velocity distributions near a semi-infinite cylinder rotating about the z axis. (Stewartson, 1958).

Before closing this section, let us consider an unsteady, similarity solution that was derived by Oseen (1911) and Hamel (1916). If we assume that the stream function is a constant and that the circulation depends on η and τ only, then Eq. (3.1-11) is identically satisfied and Eq. (3.1-10) reduces to

$$\frac{1}{\tau}\frac{\partial \Gamma^*}{\partial \tau} = \frac{4\eta}{N}\frac{\partial^2 \Gamma^*}{\partial \eta^2} \tag{3.2-45}$$

This can be transformed into an ordinary differential equation in terms of the similarity variable $y = \eta/\tau$

$$\Gamma^{*\prime\prime} + \frac{N}{4\tau}\Gamma^{*\prime} = 0 \tag{3.2-46}$$

which can be easily integrated twice to give

$$\Gamma^* = c_1 + c_2 e^{-\frac{N}{4\tau}y} \tag{3.2-47}$$

When the boundary conditions that $\Gamma^*(0) = 0$ and $\Gamma^*(\infty) = 1$ are applied, Eq. (3.2-47) yields

$$\Gamma^{\flat} = 1 - e^{-\frac{N}{4\tilde{\tau}} y} \tag{3.2-48}$$

or in dimensional terms

$$v = \frac{v_o r_o}{r} \left(1 - e^{-\frac{r^2}{4\nu t}}\right) \tag{3.2-49}$$

Equation (3.2-49) provides the rate of decay of an isolated vortex under the action of viscosity. This solution can also be applied to the asymptotic decay of a trailing vortex far downstream by replacing t with z/w_∞, with w_∞ the constant freestream velocity (Batchelor, 1964, and Newman, 1959). The solution is valid as long as the axial velocity is nearly equal to the freestream velocity throughout the vortex. In terms of our governing parameters, this is true when $S^2 << 1$.

3.3 Steady, Core Solutions for Large Swirl

A standard method for solving the Navier-Stokes equations is to look for combinations of the governing parameters that are small in the problem of interest and to obtain asymptotic solutions to the equations for the limit of this particular combination approaching zero. A vortex solution for small N was considered by Granger (1966), for small $(\ell/r_o)^2$ by Ostrach and Loper (1966) and Kwok (1969), and for small S by several authors as mentioned in Section 3.1. However, as also seen in Section 3.1, the most interesting limit for our problem is that of $S \to \infty$. Asymptotic expansions for this limit were considered by Lewellen (1962, 1964) with the additional restriction that $\tilde{\tau} = \infty$.

Since the swirl parameter enters Eqs. (3.1-10) and (3.1-11) as S^2 only, it is appropriate to let $\varepsilon = S^{-2}$ and consider the two variables expanded in powers of ε, i.e.

$$\Gamma^{\flat} = \sum_{n=o}^{\infty} \varepsilon^n \Gamma_n^{\flat}(\eta, \xi) \tag{3.3-1}$$

and

$$\psi = \sum_{n=o}^{\infty} \varepsilon^n \psi_n(\eta, \xi)$$

When these series are substituted into the equations of motion and terms of equal powers of ε equated, a set of equations for the Γ_n's and ϕ_n's are obtained. Since there is only one term with ε^{-1}, it is necessary to have

$$\frac{\partial \Gamma_o^{\flat 2}}{\partial \xi} = 0 \tag{3.3-3}$$

Terms with coefficients of order one lead to the following two equations;

$$\frac{\partial \psi_o}{\partial \xi}\frac{\partial \Gamma^4_o}{\partial \eta} - \frac{\partial \psi_o}{\partial \eta}\frac{\partial \Gamma^4_o}{\partial \xi} = -\frac{2\eta}{N}\frac{\partial^2 \Gamma^4_o}{\partial \eta^2} \tag{3.3-4}$$

and

$$\frac{\Gamma^4_o}{4\eta^2}\frac{\partial \Gamma^4_1}{\partial \xi} = \frac{\partial \psi_o}{\partial \xi}\frac{\partial^3 \psi_o}{\partial \eta^3} - \frac{\partial \psi_o}{\partial \eta}\frac{\partial^3 \psi_o}{\partial \xi \partial \eta^2} + \frac{2}{N}\frac{\partial^2}{\partial \eta^2}\left(\eta \frac{\partial^2 \psi_o}{\partial \eta^2}\right) \tag{3.3-5}$$

As discussed in Section (3.1), Eqs. (3.3-3) and (3.3-4) lead to the requirements that

$$\Gamma^4_o = g_o(\eta) \tag{3.3-6}$$

and

$$\psi_o = f_\infty(\eta) + \xi\, f_{o1}(\eta) \tag{3.3-7}$$

When Eqs. (3.3-6) and (3.3-7) are used in Eq. (3.3-5) it is clear that Γ_1 will be of the form

$$\Gamma^4_1 = g_{1o}(\eta) + \xi\, g_{11}(\eta) + \xi^2 g_{12}(\eta) \tag{3.3-8}$$

This process can be continued to show that this expansion in ε also leads to and expansion in ξ. The dual subscript notation represents first the exponent of ε and second the exponent of ξ. The ordinary differential equations for the radial functions are; from Eq. (3.3-4)

$$2\eta\, g_o'' + N\, f_{o1}\, g_o' = 0 \tag{3.3-9}$$

and from Eq. (3.3-5)

$$\frac{g_o\, g_{11}'}{4\eta^2} = f_o\, f_{oo}''' - f_{oo}'\, f_{o1}'' + \frac{2}{N}\left(\eta f_{oo}''\right)'' \tag{3.3-10}$$

$$\frac{g_o\, g_{12}'}{2\eta} = f_{o1}\, f_{o1}''' - f_{o1}'\, f_{o1}'' + \frac{2}{N}\left(\eta\, f_{o1}''\right)'' \tag{3.3-11}$$

These 3 equations are not sufficient to determine the 6 unknown variables. The same situation holds if the series is truncated at any higher order value of ε. Truncation of the series at any point leaves more unknowns then equations.

The system of equations can be made determinant at any order of ε if appropriate boundary values are specified to that same order of ε. It is possible to specify the stream function at two axial positions, say at $\xi = 0$ and $\xi = 1$. For example if ψ_o is specified to order one at the two axial positions then

$$f_{oo}(\eta) = \psi_o(\eta, 0) \tag{3.3-12}$$

$$f_{o_1}(\eta) = \psi_o(\eta, 1) - \psi_o(\eta, 0) \tag{3.3-13}$$

This leaves Eq. (3.3-9) to determine g_o. This is the same equation for circulation as Eq. (3.2-16) for the Donaldson family of similarity solutions. However, the requirements on the stream function are quite different now.

Previously, f had to satisfy the vorticity equation (corresponding to setting the right hand side of Eqs. (3.3-10) and (3.3-11) to zero) but now the vorticity equation is satisfied by a higher order axial variation in the circulation so that the radial variation of the stream function is free to be determined by the boundary conditions.

Equation (3.3-9) can be formally integrated twice with the boundary conditions that

$$\lim_{\eta \to \infty} \Gamma^* = 1, \quad \text{and} \quad \Gamma^*(0) = 0 \tag{3.3-14}$$

to give

$$\Gamma^*_o = \frac{\int_o^\eta \left[\exp \int_o^\eta - \frac{N f_{o1}(\eta)}{2\eta} d\eta\right] d\eta}{\int_o^\infty \left[\exp \int_o^\eta - \frac{N f_{o1}(\eta)}{2\eta} d\eta\right] d\eta} \tag{3.3-15}$$

If the boundary layers on the walls of a cylindrically contained vortex are ignored an approximate variation for f_{o1} appropriate for flow in a cylinder as in Fig. 2.1 is

$$\begin{aligned} f_{o1} &= 1, \qquad (\frac{r_e}{r_o})^2 \leq \eta < 1 \\ f_{o1} &= \eta(\frac{r_o}{r_e})^2, \quad \eta \leq (\frac{r_e}{r_o})^2 \end{aligned} \tag{3.3-16}$$

This assumes uniform radial flow when $r > r_e$ and uniform axial flow out the exhaust. Equation (3.3-15) with f_{o1} as given in Eq. (3.3-16) yields (Einstein and Li, 1951)

$$\begin{aligned} \Gamma^*_o &= \frac{\eta_e\, e^{-\frac{N}{2}}}{1 - \frac{N}{2}} \left[(\frac{\eta}{\eta_e})^{-\frac{N}{2}+1} - 1\right] - \frac{2\eta_e}{NK}(e^{-\frac{N}{2}} - 1) ; \qquad \eta > \eta_e \\ &= \frac{2}{N}\frac{\eta_e}{K}(1 - e^{-\frac{N\eta}{2\eta_e}}) ; \qquad \eta \leq \eta_e \end{aligned} \tag{3.3-17}$$

with

$$K = \frac{\eta_e\, e^{-\frac{N}{2}}}{1 - \frac{N}{2}} \left[e^{(\frac{N}{2} - 1)} - 1\right] - \frac{2\eta_e}{N}(e^{-\frac{N}{2}} - 1) \tag{3.3-18}$$

The circulation distributions given by this solution as a function of N are given in Fig. 3.10.

With the discontinuity in f'_{o1} present in Eq. (3.3-16), it is impossible to continue this solution to higher order in ε. If f_{o1} is made properly

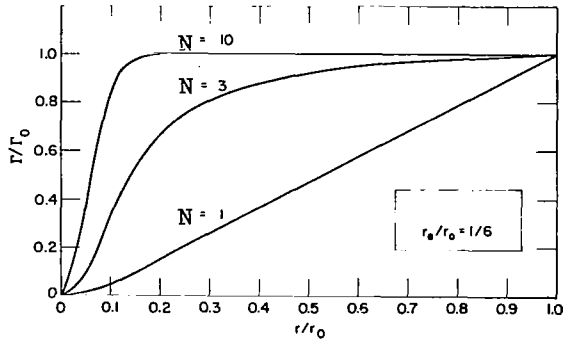

Fig. 3.10 Circulation distribution as a function of radius.

continuous, then the solution can be continued to higher order (Lewellen, 1962). Axial boundary conditions which correspond more nearly to an experimentally obtained axial velocity distribution have been considered by Turner (1965).

It is also possible to extend the expansion procedure to the case in which the axial flow is allowed to be of the same order as the tangential flow (Lewellen, 1964). This can be done by letting

$$\Gamma^{\prime} = \sum_{n=o}^{\infty} \Gamma^{\prime}_n(\eta,\xi)\ S^{-n} \tag{3.3-19}$$

$$\psi = \sum_{n=o}^{\infty} \psi_n(\eta,\xi)\ S^{1-n} \tag{3.3-20}$$

where S is based on the radial mass flow as in the previous case. The lowest order term in the stream function expansion which determines the relative magnitude of the axial velocity must now be independent of ξ. When Eqs. (3.3-19) and (3.3-20) are used in the equations of motion, it is clear ψ_1 and Γ_1 may be linear in ξ providing the boundary conditions are compatible. In this case, without loss in generality, the coordinate system can be chosen so that at $\xi = 0$, $\psi_1 = \Gamma_1 = 0$. It is appropriate then to take

$$\begin{aligned} \psi_1 &= \xi\ f_{o1}(\eta) \\ \Gamma^{\prime}_1 &= \xi\ g_{11}(\eta) \end{aligned} \tag{3.3-21}$$

Then if $g_{11}(\eta)$ is eliminated from the resulting equation, Eq. (3.3-9) may be generalized to

$$2\eta g_o g_o'' + N f_{o1} g_o g_o' - \frac{4N}{S_a^2}\,\eta^2 f_{oo}'\left[f_{oo}''' f_{o1} - f_{oo}' f_{o1}'' + \frac{2}{N}\,(2f_{oo}''' + \eta f_{oo}'''')\right] = 0 \tag{3.3-22}$$

with $S_a = \left(\frac{2\pi\rho\Gamma_o r_o}{\dot{m}_{axial}}\right)$ and $f_{oo}(\eta) = S_a \psi_o(\eta)$.

When $S_a^2 >> 1$, the circulation distribution is determined by the balance between radial convection and diffusion of angular momentum. When $S_a^2 < 1$ the axial convection is more important than the radial convection in balancing the radial diffusion of angular momentum.

Linderstrom-Lang (1970) used Eq. (3.3-22) to investigate the type of vortex flow found in a Ranque-Hilsch tube. This is discussed in Section 3.6.

To use either Eq. (3.3-9) or the more general (3.3-22) to solve for the circulation distribution in a vortex chamber it is necessary to determine the stream function at two axial locations, say the top and the bottom of the chamber. However, as already seen in the last section there are adjustment layers required on the end walls to bring Γ to zero and these adjustment layers induce a secondary flow of the order

$$\dot{m}_{b.l.} \sim 2\pi\rho\,[\Gamma_o\nu]^{1/2}\,r_o \qquad (3.3\text{-}23)$$

Whenever this boundary-layer flow is of the same order as the total mass flow through the chamber, the boundary layer may be expected to play an important role in determining the stream function distribution. This occurs whenever

$$\frac{\dot{m}_{b.l.}}{\dot{m}_{total}} \sim \frac{2\pi\rho\,[\Gamma_o\nu]^{1/2}\,r_o}{\dot{m}_{total}} = S\,\left[\frac{\nu}{\Gamma_o}\right]^{1/2} \sim 1 \qquad (3.3\text{-}24)$$

Thus unless $\Gamma_o/\nu >> S^2$ it is necessary to solve the end wall boundary-layer problem to specify the boundary conditions on the stream function.

Boundary layers in a rotating flow are considered in the next section prior to considering the complete flow in the chamber in the subsequent section.

3.4 Boundary Layers in Rotating Flow

This section is largely a condensed version of the review by Rott and Lewellen (1966). The boundary-layer simplifications (valid if the boundary-layer thickness is much smaller than the radius of curvature of the wall surface in either direction) reduce the axisymmetric Navier-Stokes equations for constant property fluids to the following set of equations, expressed in boundary-layer coordinates, s and n, along and normal to the wall meridian:
Momentum along the wall,

$$u_s \frac{\partial u_s}{\partial s} + u_n \frac{\partial u_s}{\partial n} - \frac{v^2}{R}\frac{dR}{ds} = -\frac{1}{\rho}\frac{\partial p}{\partial s} + \nu\frac{\partial^2 u_s}{\partial n^2} \qquad (3.4\text{-}1)$$

Tangential momentum,

$$\frac{u_s}{R}\frac{\partial vR}{\partial s} + u_n \frac{\partial v}{\partial n} = \nu\frac{\partial^2 v}{\partial n^2}$$

Momentum normal to the wall,

$$- u_s^2 \frac{d^2R}{ds^2} + \frac{v^2}{R}\left[1 - \left(\frac{dR}{ds}\right)^2\right]^{1/2} = \frac{1}{\rho}\frac{\partial p}{\partial n} \tag{3.4-3}$$

Continuity

$$\frac{1}{R}\frac{\partial R u_s}{\partial s} + \frac{\partial u_n}{\partial n} = 0 \tag{3.4-4}$$

Here u_s and u_n are the velocity components along s and n, v is the tangential velocity and R the radius of the wall surface from the axis of rotation.

If R is equal to s then the wall becomes a disk and u_s and u_n are the radial velocity u and the axial velocity w, respectively. In this case Eqs. (3.4-1) to (3.4-4) are equivalent to Eqs. (3.1-24) and (3.1-25). In the other limiting case when R = constant these boundary-layer equations are equivalent to Eqs. (3.2-13) and (3.2-14). Similarity solutions for these two limiting cases have been considered in Section 3.2. A discussion of similarity transformations for a more general variation of R(s) may be found in Rott and Lewellen (1966). Of more primary interest here is an integral method of solution which has sufficient flexibility and simplicity to be used when there is a strong interaction between the boundary-layer flow and the outer core flow.

Momentum integral equations may be obtained by integrating Eqs.(3.4-1) and (3.4-2) with respect to n across the boundary layer. Equation (3.4-3) may be ignored and the pressure assumed constant across the boundary layer as long as $|dR/ds| >> |d\delta/ds|$. If $u_s \to 0$ and $v \to v(\infty)$ as $n \to \infty$ the two momentum integral equations may be written as

$$\frac{d}{ds}\int_0^\delta u_s^2 \, R \, dn - \int_0^\delta \frac{v^2 - v(\infty)^2}{R}\frac{dR}{ds} R \, dn = -R\nu \frac{\partial u_s}{\partial n}\Big|_0 \tag{3.4-5}$$

and

$$\frac{d}{ds}\int_0^\delta u_s \, v \, R^2 \, dn - v(\infty) \, R^2 \, u_n(\delta) = - R^2\nu \frac{\partial v}{\partial n}\Big|_0 \tag{3.4-6}$$

When the continuity equation is used

$$u_n(\delta) \, R = \frac{d}{ds}\int_0^\delta u_s R \, dn \tag{3.4-7}$$

the tangential momentum equation can be written as

$$\frac{d}{ds}\int_0^\delta (v - v(\infty)) \, u_s R^2 \, dn + \frac{dv(\infty)R}{ds}\int_0^\delta u_s R \, dn = -R^2\nu \frac{\partial v}{\partial n}\Big|_0 \tag{3.4-8}$$

Equations (3.4-5) and (3.4-8) can be used to determine 2 variables. Thus

an approximate solution to the boundary layer can be obtained if it is possible to assume shape factors that put all of the integrals and the two wall derivatives in terms of only 2 variables. For this purpose, assume that

$$\frac{v}{v(\infty)} = g(\zeta) \tag{3.4-9}$$

$$\frac{u_s}{u_{s_{max}}} = f'(\zeta) \tag{3.4-10}$$

with $\zeta = n/\delta$, and f and g known functions of ζ. The two momentum equations may then be written in terms of the 2 variables δ and $\tilde{Q} \equiv \int_o^\delta u_s R\, dn$ as

$$\frac{d}{ds}(\tilde{Q}\Gamma) - \lambda_1 \tilde{Q} \frac{d\Gamma}{ds} = \lambda_1 g'(0) \frac{\nu R \Gamma}{\delta} \tag{3.4-11}$$

$$\lambda_2 \frac{d}{ds}\left(\frac{\tilde{Q}}{R\delta}\right) + \lambda_3 \frac{dR}{ds} \frac{\Gamma^2 \delta}{R^2} = -\frac{f''(0)}{f(1)} \frac{\nu \tilde{Q}}{\delta^2} \tag{3.4-12}$$

with $\Gamma = v(\infty)R$ and λ_1, λ_2 and λ_3 known functions of the profile shapes given by

$$\lambda_1 = f(1) / \int_o^1 f'(1 - g)\, d\zeta \tag{3.4-13}$$

$$\lambda_2 = \int_o^1 [f'^2/f(1)^2]\, d\zeta \tag{3.4-14}$$

$$\lambda_3 = \int_o^1 (1 - g^2)\, d\zeta \tag{3.4-15}$$

Of course, the crucial step in this integral formulation is the choice of the profiles f' and g. In general, one would not expect f' and g to be independent of s. In fact, when they are independent of s it is possible to obtain exact similarity solutions to the boundary-layer equations and as seen in Section 3.2 these similarity solutions can only be obtained for quite special flows. The trick then is to choose f' and g as some average functions which make Eqs. (3.4-11) and (3.4-12) approximately valid over a wide range of flows. The profiles chosen by Taylor (1950) appear to be appropriate. Investigation of other profiles may be found in the work of Cooke (1952), Anderson (1961), Mack (1962) and King (1964). Taylor's profiles are given as

$$f' = \frac{27}{4} \zeta (1 - \zeta)^2 \tag{3.4-16}$$

$$g = 2\zeta - \zeta^2 \tag{3.4-17}$$

With this choice of profiles, the numerical values of the profile parameters are found to be

$$\lambda_1 = 2.5, \quad \lambda_2 = 1.375, \quad \lambda_3 = 0.467$$

$$f''(0)/f(1) = 12, \quad g'(0) = 2$$

It is now possible to solve Eqs. (3.4-11) and (3.4-12) numerically when $\Gamma(R)$ and $R(s)$ are given along with boundary conditions at some s for $\tilde{Q}$ and δ. However, in order to couple the boundary-layer solution to the solution of $\Gamma(R)$ it is desirable to obtain an even simpler solution. One way of doing this is to approximate Eq. (3.4-12) as an algebraic relation between δ and $\tilde{Q}$. If $\tilde{Q}$ and δ start from 0 at some R_o where $\Gamma = \Gamma_o$ and $dR/ds = R'(0)$ then a series expansion about this point shows that initially

$$\delta^3 = [g'(0)\frac{5\lambda_1\lambda_2}{3\lambda_3} + \frac{1}{\lambda_3}\frac{f''(0)}{f(1)}]\frac{\nu R_o^2\tilde{Q}}{\Gamma_o^2[-R'(0)]} \tag{3.4-19}$$

In the initial development of the boundary layer, Eq. (3.4-19) can be substituted for Eq. (3.4-12) with very little loss in accuracy. It is also possible to show that if the boundary layer develops to some type of terminal similarity as discussed in Section (3.2), then again

$$\delta^3 \propto \frac{\nu R^2\tilde{Q}}{\Gamma^2(-R')} \tag{3.4-20}$$

This suggests that Eq. (3.4-19) may be a good approximation at all stages of boundary-layer development if local values of R, Γ and R' are used instead of the initial values. With this simplification, Eq. (3.4-11) may be written as

$$\frac{d\tilde{Q}\Gamma}{ds} - \lambda_1 Q\frac{d\Gamma}{ds} = \frac{\lambda_1 g(0)}{[g'(0)\frac{5\lambda_1\lambda_2}{\lambda_3} + \frac{1}{\lambda_3}\frac{f''(0)}{f(1)}]}\frac{\nu^{2/3}R^{1/3}\Gamma^{5/3}(-R')^{1/3}}{\tilde{Q}^{1/3}} \tag{3.4-21}$$

This can be formally integrated with Q assumed 0 at s = 0 to give

$$\tilde{Q} = 1.56\,\nu^{1/2}\Gamma^{\lambda_1-1}\{\int_o^s \Gamma^{2-\frac{4}{3}\lambda_1}[R(-R')]^{1/3}\,ds\}^{3/4} \tag{3.4-22}$$

Perhaps the two most interesting cases to consider are those of potential flow (Γ = constant) and solid body rotation ($\Gamma \propto R^2$) over a flat disk R' = -1. (Note R' is negative because the boundary layer begins at the outer edge of the disk as long as the fluid rotates faster than the disk). In both these limiting cases, Eq. (3.4-22) reduces to

$$\tilde{Q} = 1.26\,[\nu/\Gamma_o]^{1/2}\Gamma[R_o^{4/3} - R^{4/3}]^{3/4} \tag{3.4-23}$$

This approximate solution is compared with a step-by-step numerical integration of the exact boundary-layer equations by Anderson (1966) and Cooke (1966) in Figure (3.10). The comparison is quite favorable. The Bödewadt terminal similarity solution is included on the figure. Shear and boundary-layer profiles do not compare near as favorably, but for the interaction problem to be considered in the next section a correct solution for the boundary-layer mass flow

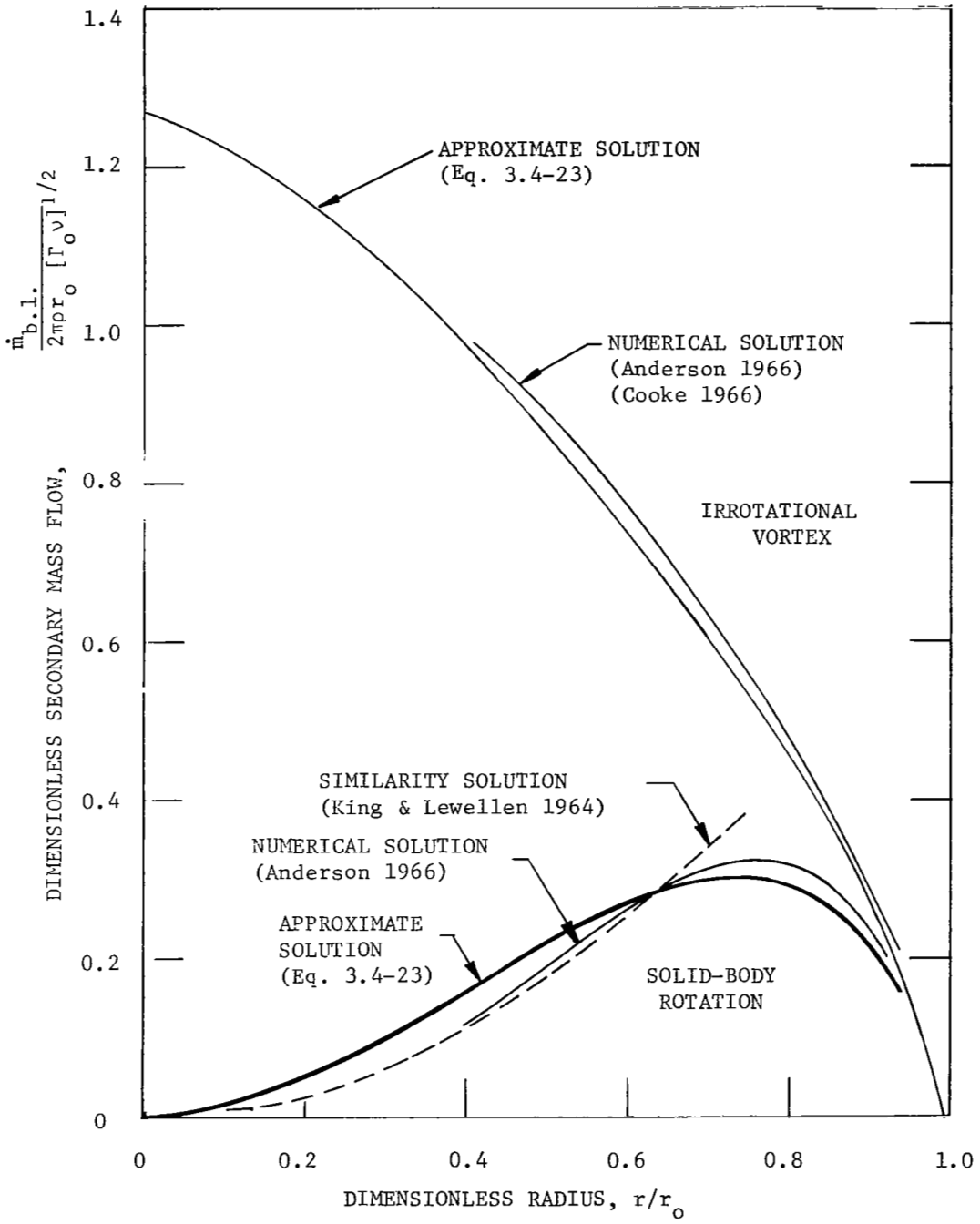

Fig. 3.11 Comparison of solutions for the radial secondary mass flow in the end-wall boundary layer.

is the most important.

Since Eq. (3.4-23) agrees reasonably well with more precise numerical

results in the limiting cases of Γ = constant and $\Gamma = \Omega R^2$, Rott and Lewellen (1966) suggest that it be used for all variations of Γ over a flat stationary wall. It is hard to conceive of a physically possible $\Gamma(R)$ distribution for which Eq. (3.4-23) will differ significantly from Eq. (3.4-22).

The boundary-layer calculations presented in this section have received the benefit of very few comparisons with experiment, since most of the flows of interest referred to in Chapter I are turbulent. Figure 3.7 gives a comparison in one limit. Also, Anderson (1966) made measurements in laminar flow around a bend with different vorticity distributions and found the profiles to be closely related to those he obtained numerically. Maxworthy (1967) compared Eq. (3.4-23) with measurements of boundary-layer mass flow based on u(z) profiles found using vertical, hydrogen-bubble wires. There was a wide discrepancy which Maxworthy attributed to the breakdown of the boundary-layer approximation in the neighborhood of the axis. In his experiment, the boundary-layer appeared to erupt in a jet on the axis as seen in Fig. 3.12. A short distance from the wall, this jet appears to undergo a type of "vortex breakdown" phenomenon. This unusual feature will be discussed in a later chapter.

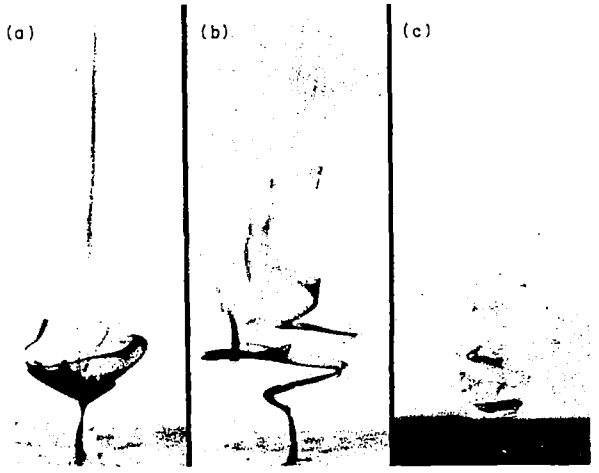

Fig. 3.12 Eruption of the boundary layer flow at the axis of vortex flow over a stationary wall. (Maxworthy 1967).

3.5 Interaction Between Boundary-Layer Flow and Core Flow

The boundary-layer solution derived in the last section may be used as the boundary conditions required to complete the series solution developed

in Section 3.3. The flow through a cylindrical vortex chamber may be divided into three regions shown in Fig. 3.13. The flow in region I is governed by Eq. (3.3-9) to order S^{-2}.

$$2\eta\Gamma_o^{\flat}{}'' + Nf_{o1}\Gamma_o^{\flat}{}' = 0 \tag{3.3-9}$$

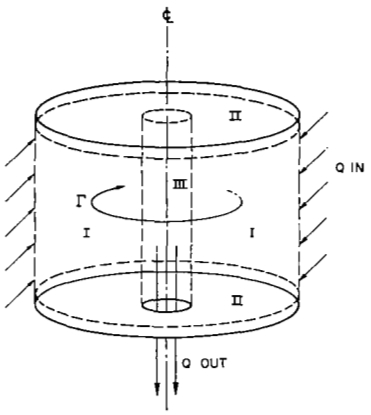

Fig. 3.13 Vortex tube geometry showing division of flow into the three regions described in the paper.

The flow in region II is governed by the boundary-layer equations. The two flows must match along the common boundary of the two regions. The tangential velocity may be matched by identifying the circulation Γ in the boundary-layer equations with the circulation in region I. The radial velocities are matched by setting

$$f_{o1} = 1 - \frac{2\dot{m}_b}{\dot{m}}.1. \tag{3.5-1}$$

in region I and requiring that $u \to 0$ at the outer edge of the boundary layer. As long as $S^2 >> 1$ the radial velocity in the boundary layer will be much larger than it is in the external flow, region I. Thus when dealing with the boundary-layer flow $u \to 0$, to order S^{-2}, as $n \to \infty$. For those familiar with perturbation methods (Van Dyke, 1964), the present problem may be recognized as a singular perturbation problem.

If the approximate relationship between the mass flow in the boundary layer and the circulation distribution given in Eq. (3.4-23) adequately describes the boundary layer, then Eq. (3.5-1) can be written as

$$f_{o1} = 1 - B\Gamma^{\flat}\,(1 - \eta^{2/3})^{3/4} \tag{3.5-2}$$

with the new parameter B defined as

$$B \equiv 2.52 \left(\frac{2\pi\rho\nu\ell}{\dot{m}}\right)\left(\frac{\Gamma\alpha}{\nu}\right)^{1/2} \frac{r_o}{\ell} = 2.52 \frac{S}{Re_t^{1/2}} \qquad (3.5\text{-}3)$$

Since B is equal to the ratio of the maximum possible flow in the 2 boundary layers to the total flow through the chamber, it may appropriately be called a boundary-layer interaction parameter.

The stream function distribution, f_{o1}, may be eliminated between Eqs. (3.3-9) and (3.5-2) to yield a single equation for the circulation.

$$2\eta\Gamma^{4\prime\prime} + N\left[1 - B\Gamma^{4}\left(1 - \eta^{2/3}\right)^{3/4}\right]\Gamma^{4\prime} = 0 \; ; \quad \eta \geq \eta_e \qquad (3.5\text{-}4)$$

Appropriate boundary conditions for this equation are that $\Gamma(1) = 1$ and that Γ match to the flow in region III. The simplest way to satisfy the matching conditions to region III is to assume that the flow remaining in region I at r_e be uniformly distributed across the exhaust so that

$$f_{o1} = \frac{\eta}{\eta_e} f_{o1}(\eta_e) \; ; \quad \eta \leq \eta_e \qquad (3.5\text{-}5)$$

and

$$2\eta_e\Gamma^{4\prime\prime} + N\left[1 - B\Gamma_e^{4}\left(1 - \eta_e^{2/3}\right)^{3/4}\right]\Gamma^{4\prime} = 0 \; ; \quad \eta \leq \eta_e \qquad (3.4\text{-}6)$$

and to add in the boundary condition that $\Gamma^4(0) = 0$. This system may now be solved by numerical integration for general values of N,B, and η_e. Solutions to a problem equivalent to this were first given by Anderson (1961) with a slightly different solution for the boundary layer than that used here. If $B << 1$, the solution to Eqs. (3.5-4) and (3.5-6) reduces to Eqs. (3.3-17).

Although a numerical solution is required in general, an analytic solution may be obtained in the limit of $N >> 1$. This, also, is probably the most interesting limit physically since the Reynolds number is large even for relatively small flow rates. In this limit it is readily seen from Eq. (3.5-4), that if $\Gamma^{4\prime\prime}$ is to remain finite either

$$\Gamma^{4\prime} = 0 \qquad (3.5\text{-}7)$$

or

$$\Gamma^{4} = \frac{1}{B}\left(1 - \eta^{2/3}\right)^{-3/4} \qquad (3.5\text{-}8)$$

If the boundary condition that $\Gamma^4(1) = 1$ is imposed, then the solution in the large Reynolds number limit is

$$\begin{aligned} \Gamma^{4} &= 1 \; ; \quad \eta \geq \left[1 - B^{-4/3}\right]^{3/2} \equiv \hat{\eta} \\ \Gamma^{4} &= \frac{1}{B}\left(1 - \eta^{2/3}\right)^{3/4} ; \quad \eta \leq \hat{\eta} \end{aligned} \qquad (3.5\text{-}9)$$

Because of the $N >> 1$ limit the boundary condition at $\eta = 0$ cannot be satisfied. The stream function variation corresponding to Eq. (3.5-9) is

$$\begin{aligned} f_{o1} &= 1 - B\left(1 - \eta^{2/3}\right)^{3/4} ; \quad \eta > \hat{\eta} \\ f_{o1} &= 0 \qquad\qquad\qquad\qquad ; \quad \eta < \hat{\eta} \end{aligned} \qquad (3.5\text{-}10)$$

Physically, this flow may be described by saying that as the flow enters through the outer rotating cylinder the circulation of the main flow remains constant as the flow in the boundary layers builds up. When a radius is reached at which all of the radial through flow has been diverted to the boundary layers (corresponding to $\hat{\eta}$) then the through flow remains in the boundary layers and the circulation distribution adjusts to whatever is required to drive this flow.

Although $f_{o1} = 0$ for $\eta < \hat{\eta}$, the product Nf_{o1} remains finite so that there is a small but finite radial flow in this region. In fact, by combining Eqs. (3.3-9) and (3.5-8), it may be seen that

$$Nf_{o1} = -\frac{2\eta\Gamma''}{\Gamma'} = -\frac{3\eta^{2/3} - 2/3}{1 - \eta^{2/3}} \qquad (3.5\text{-}11)$$

Since this last expression is negative whenever $\eta > 2\sqrt{2}/27$, it demonstrates that there is a region of small radial outflow whenever $\hat{\eta} > 2\sqrt{2}/27$. A typical streamline pattern is shown in Fig. 3.14.

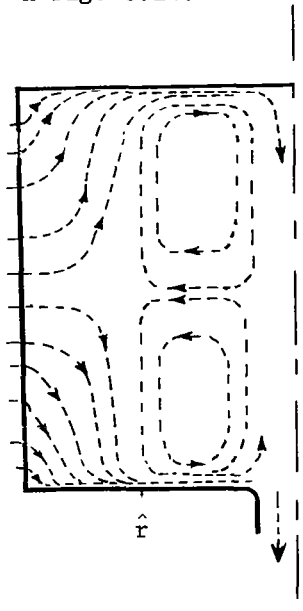

Fig. 3.14 Typical meridional streamline pattern in a vortex chamber with $S^2 >> 1$, $N >> 1$ and $B \geq 1$.

The existence of a radial stagnation surface is demonstrated by the dye front in Fig. 3.15. The chamber shown had a variable length to allow B to vary. In this picture $\ell/D = 1$. A detailed comparison of its position with theory is reserved until Chapter V, after turbulent boundary layers have been discussed.

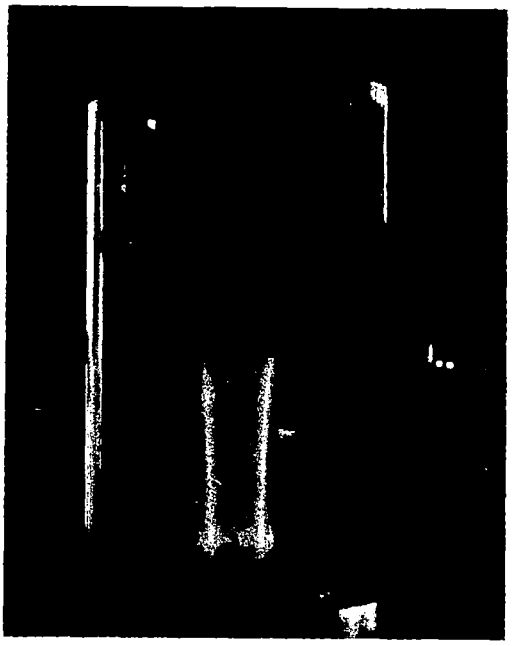

Fig. 3.15 Photograph of the dye pattern observed in a vortex after a pulsed dye injection at a time equal to that required for a few chamber volumes of water to flow through the apparatus. (Lewellen, Ross and Rosenzweig 1966).

The analytic solution, of course, looses its validity in the region of the exhaust hole where the boundary-layer must breakdown. Figures 1.9 and 1.10 show that a significant fraction of the boundary-layer flow erupts into axial jets in the immediate neighborhood of the exhaust. The details of this boundary-layer separation problem has not been solved. In the theoretical treatments in the literature it has either been ignored or treated parametrically (Rosenzweig, Lewellen and Ross 1964).

A comparison of the present interaction theory with experiment was given by Rott and Lewellen (1966) for an experiment by Maxworthy (1964) which did not involve any of the uncertainties associated with the exhaust. The experimental arrangement is shown in Fig. 3.16. Equation (3.4-23) may be used to describe the flow distribution into the boundary layer on the stationary wall but an additional expression must be derived for the boundary layer over the rotating disk. A procedure analogous to that of Section 3.4 may be carried out for the rotating wall (Rott and Lewellen, 1966). The simple approximation proposed for use is that

$$\dot{m}_{b.l.\,(\text{rotating wall})} = 0.55\,(2\pi\rho)\,[\frac{\nu}{\Omega}]^{1/2}(\Omega R^2 - \Gamma) \qquad (3.5\text{-}12)$$

provided the wall rotates faster than the fluid. In this case the boundary layer mass flow is directed toward increasing radius.

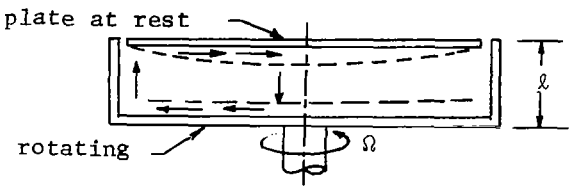

Fig. 3.16 Experimental arrangement to investigate confined flow between a rotating disk and a stationary disk. (Maxworthy 1964).

Since there is no net mass flow through the container in this problem the radial flow in the main flow results from any difference between the flow in the two end wall boundary layers, i.e.,

$$Nf_{o1} = \frac{\dot{m}_{b.l.\,(\text{rotating wall})} - \dot{m}_{b.l.\,(\text{stationary wall})}}{2\pi\mu\ell} \qquad (3.5\text{-}13)$$

thus

$$Nf_{o1} = -(\frac{\Omega}{\nu})^{1/2}\frac{R_o^2}{\ell}\{1.26\,\Gamma^*\,(1 - \eta^{2/3})^{3/4} - 0.55\,(\eta - \Gamma^*)\} \qquad (3.5\text{-}14)$$

The governing equation for the circulation, Eq. (3.3-9), for this problem may be written with the aid of Eq. (3.5-14) as

$$2\eta\Gamma^{*\prime\prime} - (\frac{\Omega}{\nu})^{1/2}\frac{R_o^2}{\ell}\{1.26\,\Gamma^*\,(1 - \eta^{2/3})^{3/4} - 0.55(\eta-\Gamma^*)\}\Gamma^{*\prime} = 0 \qquad (3.5\text{-}15)$$

It is evident from Eq. (3.5-15) that if the rotational Reynolds number (or Taylor number), $\Omega R_o^2/\nu$ is much greater than one, and the boundary conditions on Γ^*, namely $\Gamma^*(1) = 1$ and $\Gamma^*(0) = 0$, do not permit Γ^* to be constant, then the term in the brackets must approach zero. That is, there must be a detailed matching of the flow out of one boundary layer into the other. This occurs when

$$\Gamma^* = \frac{0.55\,\eta}{0.55 + 1.26\,(1 - \eta^{2/3})^{3/4}} \qquad (3.5\text{-}16)$$

This circulation distribution is compared with Maxworthy's experimental distribution obtained by photographing hydrogen bubbles released in the flow in Fig. 3.17. The agreement, even though not perfect, is quite encouraging. Near the center where the influence of the side walls is small this problem can be solved exactly by providing detailed matching of the flow out of a Bödewadt

boundary layer on the stationary disk into the boundary layer on the rotating disk. This gives the profile in Fig. 3.7. The experimental points of Fig. 3.7 were taken with a stationary outer cylinder so that its influence is not felt to as small a radius as it would be for a rotating outer cylinder.

Recently, Pao (1970) has investigated the flow field for the conditions of Fig. 3.16 with a numerical scheme for integrating the full Navier-Stokes equations. For $Re_t < 200$ (his numerical scheme diverges for higher Reynolds numbers), his solutions agree very well with his companion experiments. His results are closer to Eq. 3.5-16 than would be predicted by the finite Reynolds number correction given by Rott and Lewellen (1966). At Reynolds numbers of a few thousand his experiments exhibited boundary-layer eruption at the center of the stationary plate with the subsequent breakdown as observed by Maxworthy (Fig. 3.12). It is interesting to note that this discrepancy in the boundary layer flow near the axis of the stationary wall does not have a large influence on the mid-plane circulation distribution as given in Fig. 3.17.

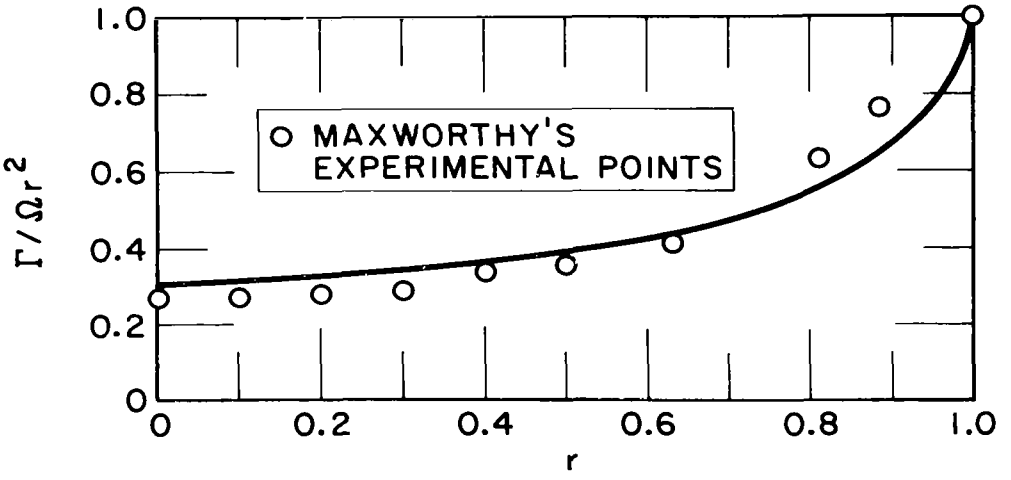

Fig. 3.17 Angular velocity distribution of the main body of fluid between a rotating and a stationary disk when enclosed by a cylinder rotating with the rotating disk. (Rott and Lewellen, 1966)

Another interaction problem which avoids the problems of the exhaust is that of flow through finite, concentric, porous cylinders with the outer cylinder rotating with an angular velocity Ω. This problem has been considered by Farris, et al (1969). Their experimental set up involved rotating one end wall with the rotating outer cylinder and holding the other end wall stationary. They numerically integrated the axisymmetric Navier-Stokes equations

using a finite difference technique. Their limited comparison with numerical and experimental results was favorable. Unfortunately, their numerical integration scheme diverged at tangential Reynolds numbers above a few hundred or at radial Reynolds numbers much above 10.

When there is no net radial flow through the cylinders in the present problem, it is quite similar to the previous problem. The extent to which detatiled matching occurs between the two boundary layers at as low a Reynolds as $\Omega R_o^2/\nu = 200$ is shown in Fig. 3.18.

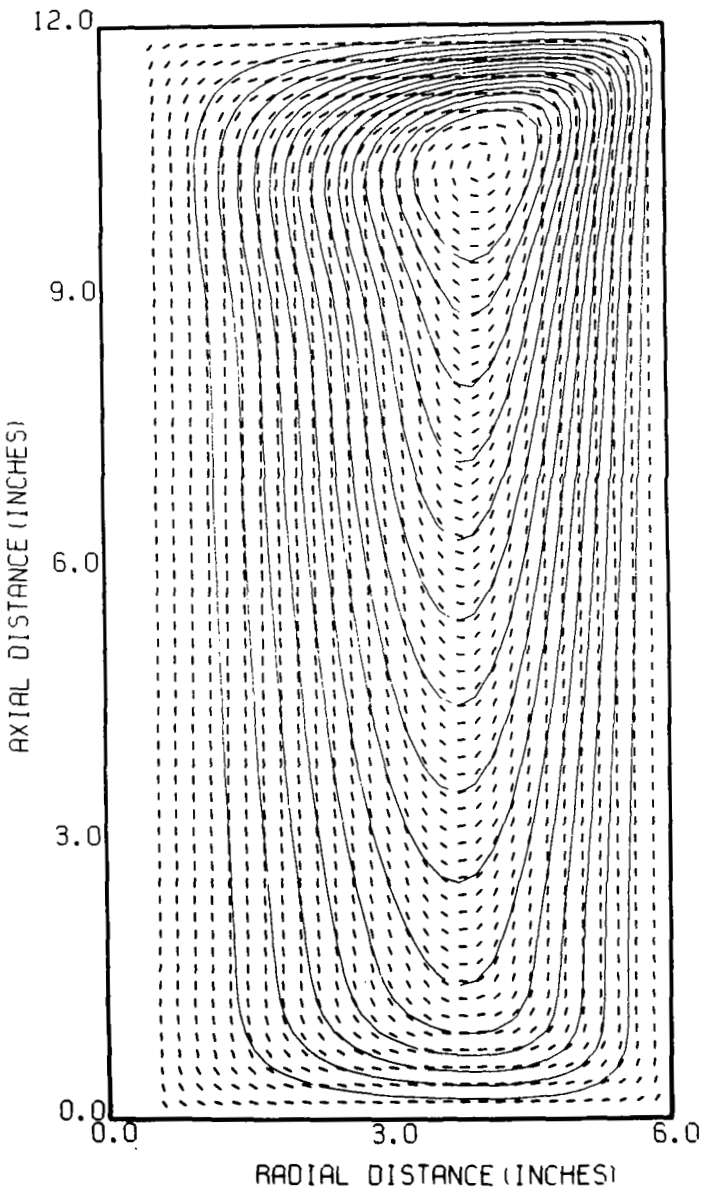

Fig. 3.18 Flow pattern with no net radial flow for flow between a rotating outer cylinder and a stationary inner cylinder (r_i = 3/4 in). Upper end wall is stationary and the lower one rotates with the outer cylinder. Re_t = 200.00, N = 0.0. (Farris, Kidd, Lick and Textor, 1969).

The fact that the lower end wall is rotating prevents a simple comparison of their results for radial through flow with Eq. (3.5-4), but the general features of the flow agree with the analytic model. Contours of constant tangential velocity, from their numerical data, are shown in Fig. 3.19 for a case with S ≈ 13. It is evident that the tangential velocity is independent of the axial coordinate except in thin adjustment layers imposed by the boundary conditions.

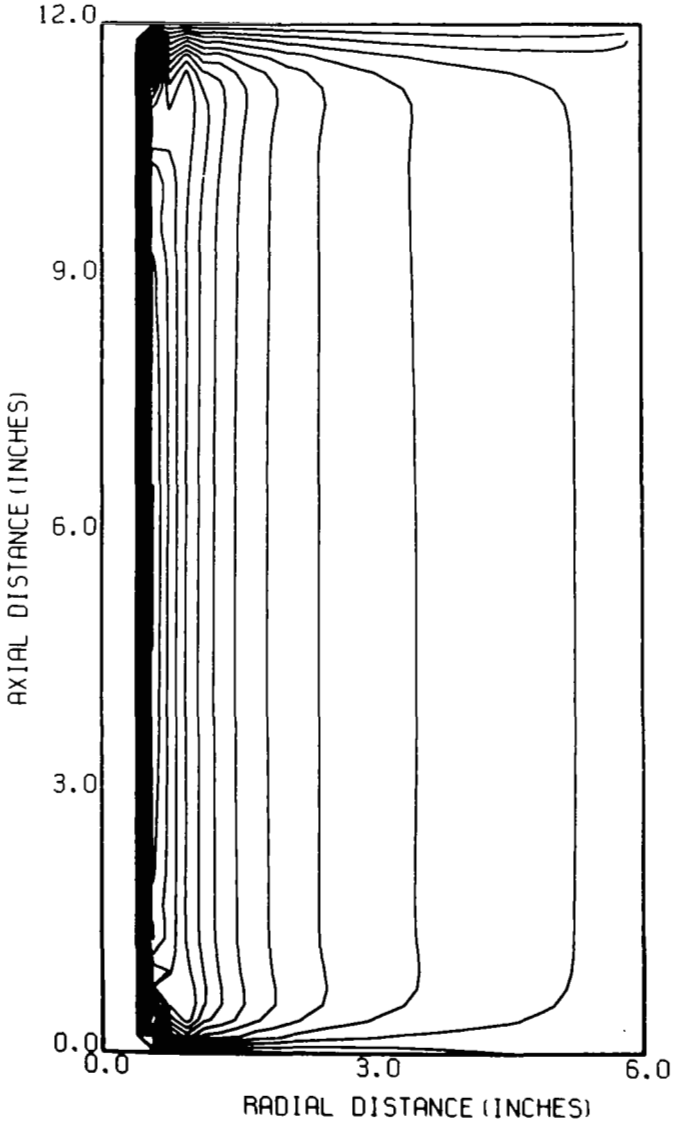

Fig. 3.19 Tangential velocity contours with radial inflow for conditions similar to Fig. 3.19. Re_t = 260.0, N = 9.83, S = 13.2 (Farris, et al, 1969).

The problem which permits the most complete analytic solution to the interaction of the boundary-layer flow with the chamber flow is that of weak flow through a rotating container. As long as the Rossby number, $R_o \equiv \dot{m}/2\pi\rho\Omega r_w^3 = 1/S$, is sufficiently small the flow consists of a linear perturbation about uniform rotation. Greenspan (1968) has given extensive treatment of this type of flow. Figure 3.20 is a sketch of the flow path for flow introduced through one porous cylinder and withdrawn through an inner porous cylinder. With the exception of the regions immediately adjacent to the cylinders the radial flow passes through the end wall boundary layers, now termed Ekman layers, $E \equiv \nu/\Omega r_w^2$. The solutions for the velocity distributions within the Ekman layer are given in Eqs. (3.2-39) and (3.2-40). As long as the no slip condition on the axial velocity at the surface of the porous cylinders is relaxed the solution to the flow can be obtained by coupling Eq. (3.3-9) with the Ekman layer dependence of stream function on circulation perturbation. The perturbation to the circulation is a constant equal to $-\Omega r_o^2 R_o/E^{1/2}$ except in the radial layers adjacent to the cylinders. In these layers

$$v = \Omega r - \frac{\Omega r_w^2}{r} \frac{R_o}{E^{1/2}} [1 - e^{-x}] \tag{3.5-17}$$

with

$$x = \{\frac{N}{2} \pm [\frac{N}{4} + \frac{2}{E^{1/2}} \frac{r_w}{L}]^{1/2}\} | r - r_w | \tag{3.5-18}$$

where the plus sign corresponds to a cylindrical source and the minus sign a cylindrical sink through either the outer cylinder at r_w, or the inner at r_i. Hide (1968) has shown that this model agrees well with experimental results. To include the no slip condition on w at the surfaces of the cylinders a third type boundary layer of order $E^{1/3}$ is required. For the solution in this layer see Greenspan (1968, page 116).

For this limit of complete domination of the flow by rotation, the radial stagnation surface in Fig. 3.14 has essentially moved out to the outer cylinder so that the outer region of potential flow has been eliminated.

To complete the flow problem of primary interest in this review it is necessary to consider the viscous exhaust problem. This is done in the next section.

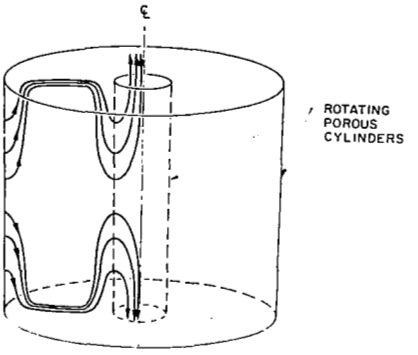

Fig. 3.20 Rotating cylindrical container showing paths of radial flow through it.

3.6 Viscous Exhaust Flow

To complete the solution for imcompressible laminar flow in a vortex chamber it is necessary to consider flow through the exhaust. Flow in region III of Fig. 3.13 may be expected to depend strongly on the exhaust constraint. The inviscid approximation to the constraint on flow through the chamber imposed by the exhaust was discussed in Section 2.2. How is this constraint affected by vixcosity? The effects of viscosity may be separated into two categories: those due to the rotational nature of the flow through the exhaust, and those due to local dissipation within the neighborhood of the exhaust. Probably, the first is the most important of these two and it is certainly the most amenable to direct analysis. Therefore it will be treated first.

Neglect of local dissipation in the flow is equivalent to letting $N \to \infty$ in the governing equations. In Section 3.1 it was shown that in this limit, for steady flow the tangential momentum equation reduces to

$$\Gamma = \Gamma(\psi)$$

and the tangential vorticity equation may be written as

$$\mathfrak{D}(\psi) = \eta F(\psi) - \frac{S^2}{2}(\Gamma^2)' \qquad (3.1\text{-}19)$$

If the local exhaust problem is treated as a quasi-one-dimensional problem, that is axial derivatives are neglected in comparison to radial derivatives, this equation may be reduced to

$$4\eta \frac{\partial^2 \psi}{\partial \eta^2} = \eta F(\psi) - \frac{S^2}{2}(\Gamma^2)' \qquad (3.6\text{-}1)$$

For the exhaust problem it is appropriate to consider $F(\psi)$ and $\Gamma(\Psi)$ as given for the flow upstream of the exhaust. Recall that $F(\psi)$ is related to the total pressure variation thru Eq. 3.1-20. For any given distributions, Eq. (3.6-1) can be solved for $\psi(\eta)$, subject to the exhaust constraint discussed in Chapter 2, that thru flow be a maximum for any given pressure drop across the exhaust. The previously considered potential example may be obtained by setting

$$\Gamma'(\psi) = 0 = F(\psi) \tag{3.6-2}$$

with the boundary conditions that $\psi(\eta_e) = 1$ and $\psi(\eta_c) = 0$ and the constraint that the dynamic pressure be a minimum at η_c.

An example of rotational flow which has received a great deal of attention in the literature (Batchelor, 1968) is that of Γ proportional to ψ which corresponds to uniform rotation when the axial velocity is uniform. Since the ratio of circulation to stream function may be absorbed in the parameter S, there is no loss of generality in setting $\Gamma = \psi$. In this case Eq. (3.6-1) may be written as

$$4\psi'' = F(\psi) - \frac{S^2}{\eta}\psi \tag{3.6-3}$$

A further specification of upstream conditions is necessary to determine the function $F(\psi)$. For example if the axial velocity is constant with radius upstream

$$\text{(i)} \qquad F = \text{constant} = S^2 \tag{3.6-4}$$

while if the total pressure is constant across streamlines

$$\text{(ii)} \qquad F = 0 \tag{3.6-5}$$

In either case (i) or (ii), Eq. (3.6-3) may be reduced to

$$4\eta\bar{\psi}'' + S^2\bar{\psi} = 0 \tag{3.6-6}$$

where $\bar{\psi} = \psi - \eta$ in case (i) and directly equal to ψ in case (ii). The general solution of Eq. (3.6-6) may be determined to be first order Bessel functions

$$\bar{\psi} = A\sqrt{\eta}\, J_1(S\sqrt{\eta}) + B\sqrt{\eta}\, Y_1(S\sqrt{\eta}) \tag{3.6-7}$$

The constants are determined by the boundary conditions

Case (i)	Case (ii)
$\bar{\psi}(\eta_e) = 1 - \eta_e$	$\bar{\psi}(\eta_e) = 1$
$\bar{\psi}(\eta_c) = -\eta_c$	$\bar{\psi}(\eta_c) = 0$

(3.6-8)

and the extremum constraint given by

$$\left|1 + \bar{\psi}'\right|_{\eta = \eta_c} = \text{minimum} \qquad \text{or} \qquad \left|\bar{\psi}'\right|_{\eta = \eta} = \text{minimum} \tag{3.6-9}$$

is used to determine η_c.

Case (i) was worked out by Hawkes (1969) and case (ii) by Strickland (1968). Results for the core size and normalized mass flow are given in Figures (3.21) and (3.22) as a function of the swirl parameter α to facilitate comparison with the potential results of Chapter II. In each case, the value of Δp used to normalize the results is the difference between $p_o(r_e)$ and p_c. In case (i) the swirl parameter is limited to a value of $\sqrt{2}/2$ since a portion of Δp is needed to maintain the difference in total pressure between r_c and r_e imposed by the constraint that the axial velocity be uniform upstream of the exhaust.

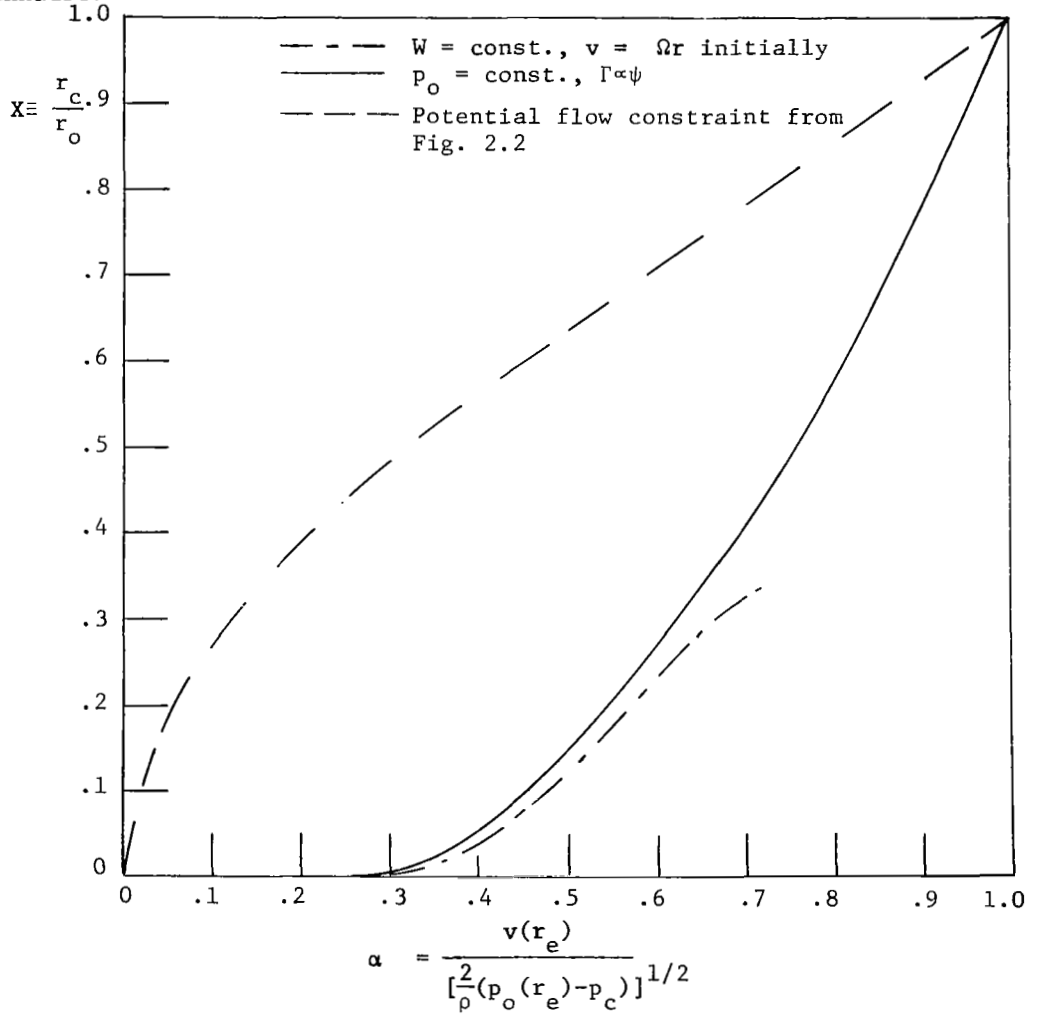

Fig. 3.21 Exhaust core radius as a function of swirl for different initial flow distributions.

It may be concluded from Figure (3.22) that including the effect of vorticity tends to reduce the influence of swirl or mass flow thru the exhaust.

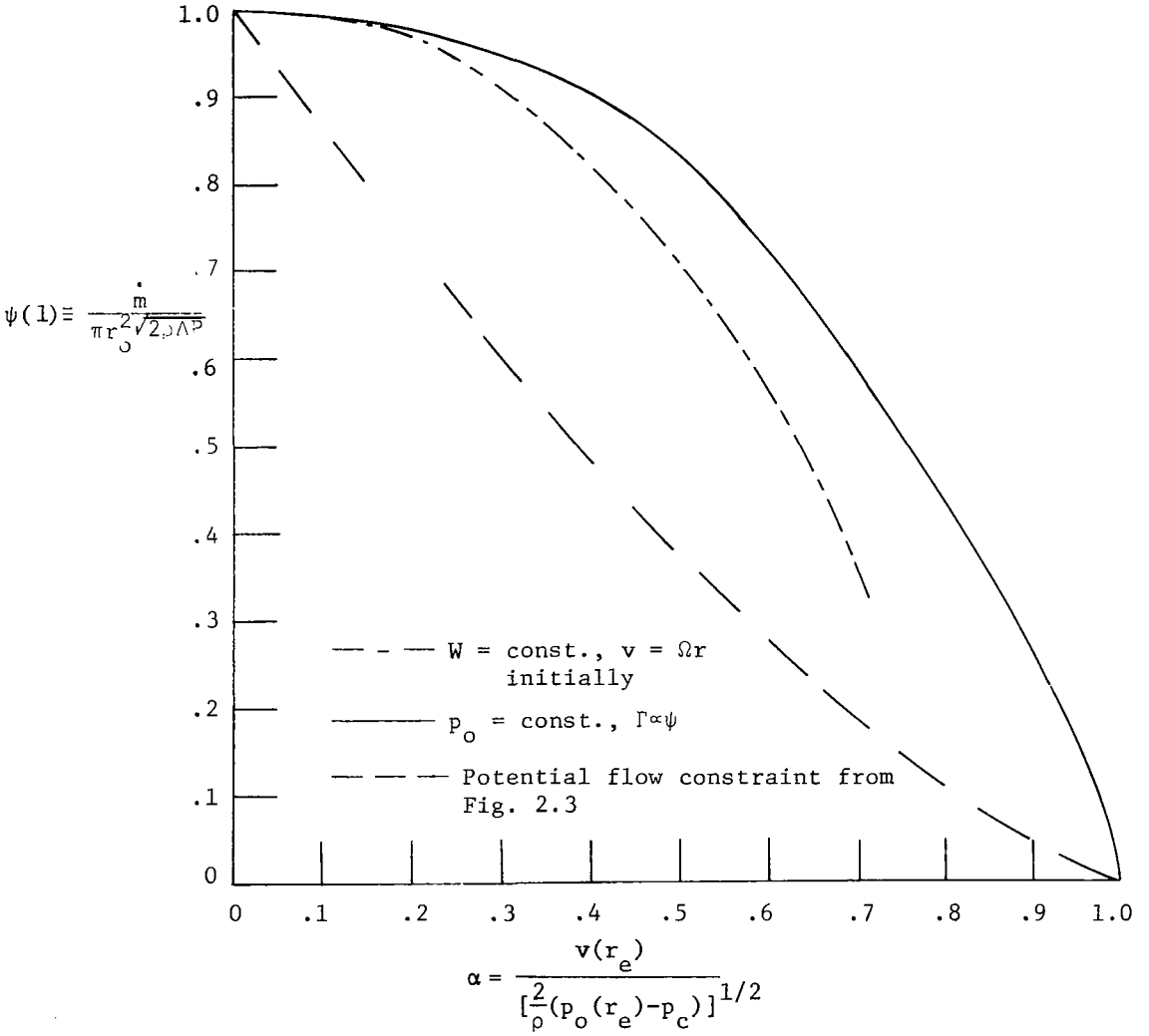

Fig. 3.22 Exhaust mass flow as a function of swirl for different initial flow distributions.

In the present inviscid, rotational model of exhaust flow there is a discontinuity in velocity at r_c. This discontinuity is diffused out in a real viscous flow and results in a recirculating flow within the core of the exhaust. The reversed flow along the axis of a vortex induced by this recirculation is often observed experimentally (e.g. Donaldson and Snedeker 1962). The shear layer between the counter flowing streams is difficult to solve by standard techniques. Three different approaches to this problem merit discussion.

The similarity solution of Long (1961) discussed in Section 3.2 represents one attempt at the solution of this viscous exhaust problem. This solution does successfully exhibit the reversed axial velocity along the axis of the vortex over a range of values of the ratio of angular momentum flux to axial momentum flux. On the other hand, it cannot be used to completely describe the flow in the exhaust of a vortex chamber because of the inflexibility of the similarity solution to match the boundary conditions.

The momentum integral approach to this problem has been used by Mager (1970). He obtained two types of solutions, a mass-flow-dominated core solution and a swirl-dominated core solution. Some of his results are given in Fig. 3.23, plotted in the same way as Fig. 3.22 to facilitate comparison. These results of Mager were carried out for nozzles whose shape is given by

$$R^2 = 5R_t^2 + \frac{4zR_t}{30}\left(\frac{z}{30R_t} - 2\right) \qquad (3.6\text{-}10)$$

and the axial velocity was assumed uniform across the entrance of the nozzle. The initial tangential velocity is specified as

$$\begin{aligned} v &= \frac{\Gamma}{r} \qquad ; \; r > \delta \\ v &= \frac{\Gamma}{\delta}\left[2\,\frac{r}{\delta} - \left(\frac{r}{\delta}\right)^3\right] \; ; \; r < \delta \end{aligned} \qquad (3.6\text{-}11)$$

with δ representing a viscous core. The parameter ΔP_i on Fig. 3.23 represents the ratio of the initial difference in stagnation pressure between the axis and the nozzle wall to the maximum dynamic pressure available thru the nozzle. With α and ΔP_i specified, δ_i is determined. The dashed line on the plot is a limiting case of $\delta_i = R_i$ which bears a close resemblance to the W = const. curve on Fig. 3.22, and is limited to $\alpha \leq 0.42$. This represents all of the dynamic pressure available for conversion into swirl dynamic head, since the rest of the available pressure is needed to maintain the initial pressure difference between the axis and the nozzle wall.

Mager's swirl-dominated solutions are more difficult to interpret. The initial conditions required for these solutions apparently would be unstable and therefore unlikely to occur in an experiment. The reversed flows which occur at the throat for these swirl-dominated solutions should extend to the nozzle entrance. To support this statement it is necessary to borrow from ideas in the future section on vortex breakdown. If the nose of a reversed flow bubble represents a type of vortex breakdown as suggested there, then it cannot occur in an accelerating region of the flow.

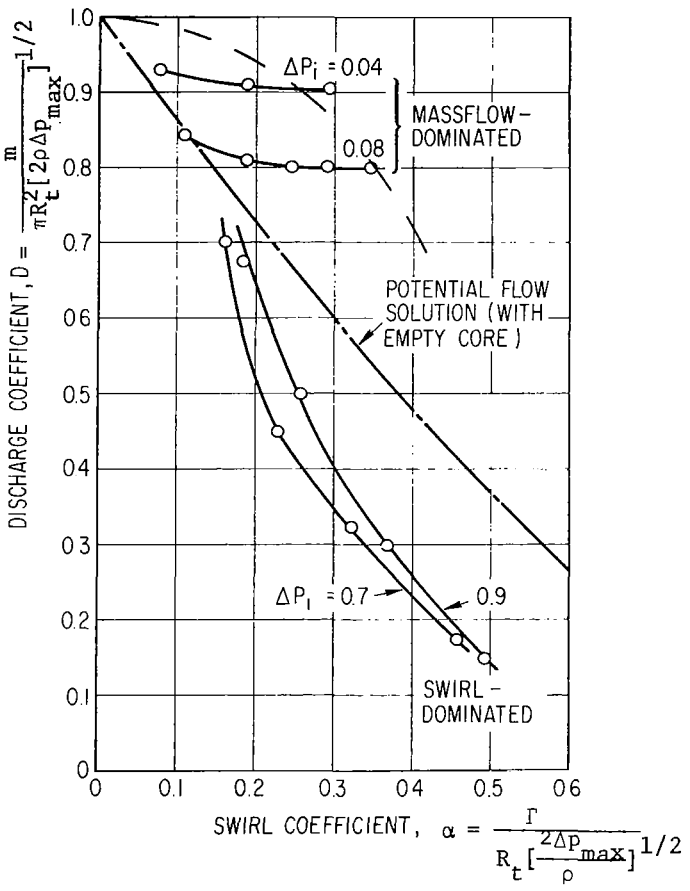

Fig. 3.23 Mass flow thru a converging-diverging nozzle as a function of swirl for different initial conditions after Mager (1970).

Figure 3.23 was obtained for a thru flow Reynolds number of 10^4. Mager demonstrated that in general, for the mass-flow-dominated solution, a decrease in Reynolds number tends to increase mass flow thru the nozzle. However, the degree of variation is relatively small.

A third approach to the problem of viscous shear in the exhaust is to utilize the series expansion of Section 3.3. Linderstrom-Lang (1970) used Eq. (3.3-22) to determine the circulation distribution across the exhaust after determining f_{oo} and f_{o1} by matching two experimentally measured axial velocity distributions. However, the resulting circulation distribution could not be compared directly with experiments since the experiments were for turbulent flow. Instead, comparison leads to an estimation of turbulent diffusivity.

3.7 Complete Flow in a Chamber

The ideas of the last 4 sections may be summarized in terms of an iteration procedure for solving for flow in a cylindrical vortex chamber.

1) Solve the inviscid, potential problem to determine the mass flow, $\dot{m}$, as a function of a specified pressure drop across the chamber, Δp, and input circulation, Γ_o. From this solution (Fig. 2.3) compute the dimensionless parameters

$$N = \frac{\dot{m}}{2\pi\mu L} \tag{3.7-1}$$

$$S = \frac{2\pi\rho\Gamma_o r_w}{\dot{m}} \tag{3.7-2}$$

and

$$B = 2.5 \left(\frac{2\pi\mu L}{\dot{m}}\right) \left(\frac{\rho\Gamma_o}{\mu}\right)^{1/2} \frac{r_w}{L} = 2.5 \left(\frac{S}{N}\frac{r_w}{L}\right)^{1/2} \tag{3.7-3}$$

If $N >> 1$ and $B << 1$, this potential approximation should be reasonably valid and no iteration is required.

2) (a) If $N = O(1)$, $B << 1$, and $S^2 >> 1$, compute the solution as given in Eq. (3.3-17) as the next approximation.

(b) If $N >> 1$, $B \gtrsim O(1)$, and $S^2 >> 1$, compute the solution as given in Eq. (3.5-9) and (3.5-10) as the next approximation.

(c) If both N and S^2 are $O(1)$, the flow must be treated as a fully viscous flow and the approximations considered here cannot be used. If $S^2 << 1$, the swirl may be neglected in the flow.

3) Solutions given in (2a) and (2b) may be used as initial conditions to solve the inviscid, rotational exhaust problem as outlined in Eq. (3.6-1) for a new value of $\dot{m}$. This would permit recomputing N and B and the repetition of step (2) until the iteration (hopefully) converges.

The iteration as outlined here has not been carried out in the literature. The major difficulty is the jump between steps (2) and (3). As discussed in Section 3.5 there is a separation of the end-wall boundary layer in the neighborhood of the exhaust hole. This makes it difficult to specify the initial conditions for the exhaust problem. Perhaps, a better reason for this omission of a rigorous solution to the complete laminar vortex flow thru a chamber, is that vortices of interest are almost invariably turbulent in one part or another of the flow.

The most complete numerical solution for laminar flow in a vortex chamber was obtained by Anderson (1961). He considered $\dot{m}$ as specified and assumed the axial velocity to be uniformly distributed across the exhaust. His solution is equivalent to the numerical integration of Eqs. (3.5-4), (3.5-5) and (3.5-6) with a slightly different solution to the boundary layer as was referred to in Section 3.4. A comparison of Anderson's solution with the approximation of Section 3.5 is given in Fig. 3.24.

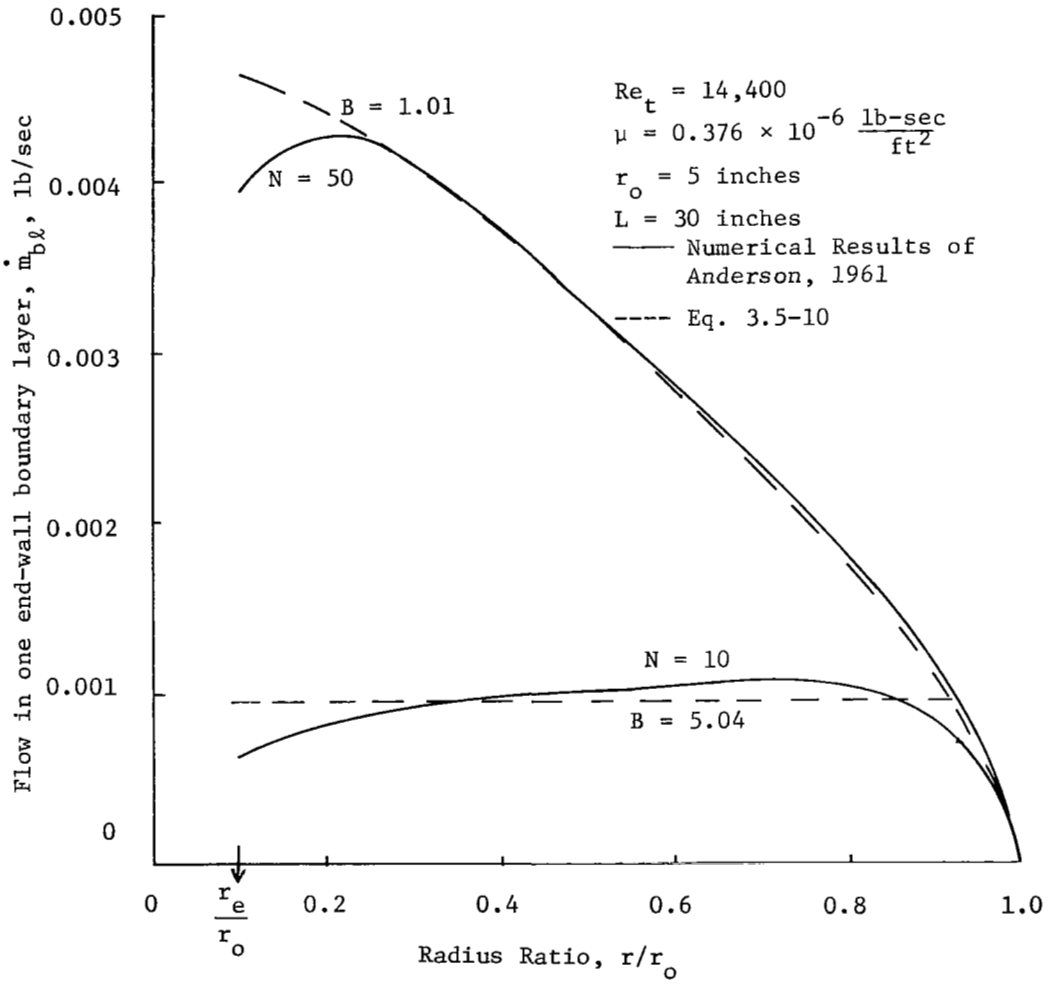

Fig. 3.24 Theoretical variation of mass flow rate in a laminar boundary layer on the end wall of a vortex chamber.

Ostrach and Loper (1966) solved the laminar, vortex chamber problem by using an expansion with $r_w/L \gg 1$. They also limited themselves to radii larger than that for which boundary-layer blockage might occur, i.e. to $r > \hat{r}$. This restricts them to a small portion of the chamber unless $B \leq 1$. Their solution is not valid when the chamber flow is dominated by the end-wall boundary layers, in spite of the fact that the assumption of $r_w/L \gg 1$ would lead to this condition even for moderate values of swirl.

Hornbeck (1969) has used a finite difference technique to numerically integrate the equations considered by Ostrach and Loper. He specified the ratio of v/u at the outer radius from 0 to 50, and the radial Reynolds number based on the radial inlet velocity and chamber height between 20 and 2000 for two values of r_o/L, 25 and 5 with an assumed line sink as the boundary condition on the axis. Figure 3.25 gives a comparison of his numerical values of $\hat{r}$ with the value given in Eq. 3.5-9. The limiting values given by Eq. 3.5-9 should be somewhat larger than those obtained numerically since the effect of a freestream u on the boundary-layer flow is neglected in Section 3.4. Unfortunately, Hornbeck's numerical scheme diverged for $r < \hat{r}$, so there also may be some doubt about the accuracy of the numerical values.

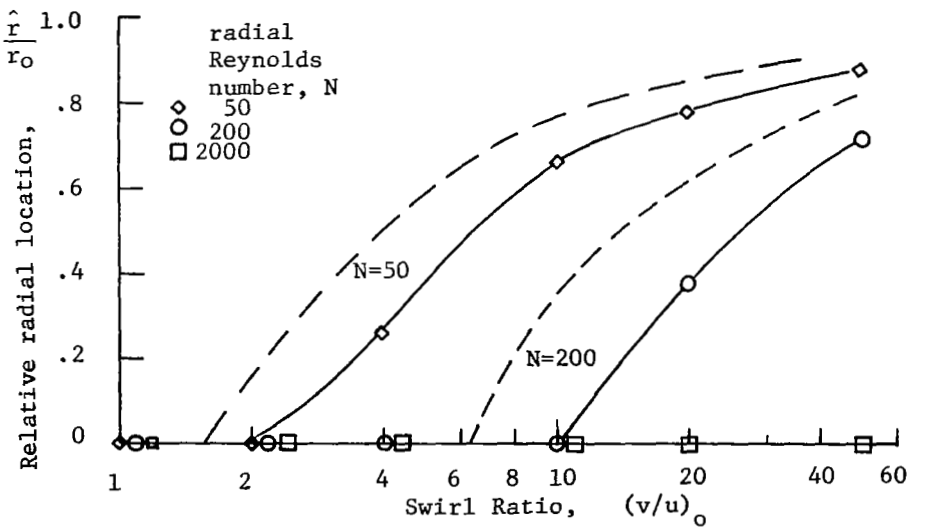

Fig. 3.25 Radial stagnation surface for a chamber with L/D = 0.1. Points calculated by Hornbeck (1969). Dashed curve from Eq. 3.5-9.

Other solutions for the complete flow in a vortex chamber have involved a turbulent boundary layer on the end walls. These solutions by Rosenzweig, Lewellen and Ross (1964), by Wormley (1968), by Bauer (1968) and by Bichara and Orner (1969) will all be discussed in a later section.

3.8 Proper Boundary Condition on Circulation for a Jet-Driven Vortex

Before closing this section on incompressible, steady, laminar flow in a vortex chamber it is necessary to consider further the boundary conditions at the outer cylindrical wall. In an experimental set up, the rotating porous wall is rarely used. It is much more convenient to drive the vortex with tangential injection thru a slit or a number of discrete jets. This raises the question of the relationships between the jet velocity and the outer circulation of the vortex.

This problem was considered by Keyes, Chang, and Sartory (1967). They obtained a finite difference solution to the two-dimensional boundary layer equations with periodic boundary conditions. The flow was assumed to be injected into the vortex thru n number of slits. Their solution for the recovery factor, defined as the ratio of effective circulation at the outer radius of the vortex, to the ideal circulation based on the injection velocity is given in Fig. 3.26. Experimental results confirm the theory. It should be noted that since the cylindrical wall boundary layer is inherently unstable, an electrically conducting fluid with an applied axial magnetic field was used in the experiment to prevent transition to turbulence. Caution was taken to minimize induced radial electric current flow which would interact with the magnetic field to influence the stationary velocity distribution.

A crude approximation to the numerical result of Keyes, Chang, and Sartory can be obtained from a simple angular momentum balance across the boundary layers formed on the cylindrical side walls. This leads to

$$\dot{m}\Gamma_i = \dot{m}\Gamma_o + 2\pi r_o^2 \ell \tau_w - 2\pi r_o \ell \mu \frac{2\Gamma_o}{r_o} \qquad (3.8\text{-}1)$$

The term on the left hand side represents the angular momentum introduced thru the injection ports. The first term on the right hand side represents

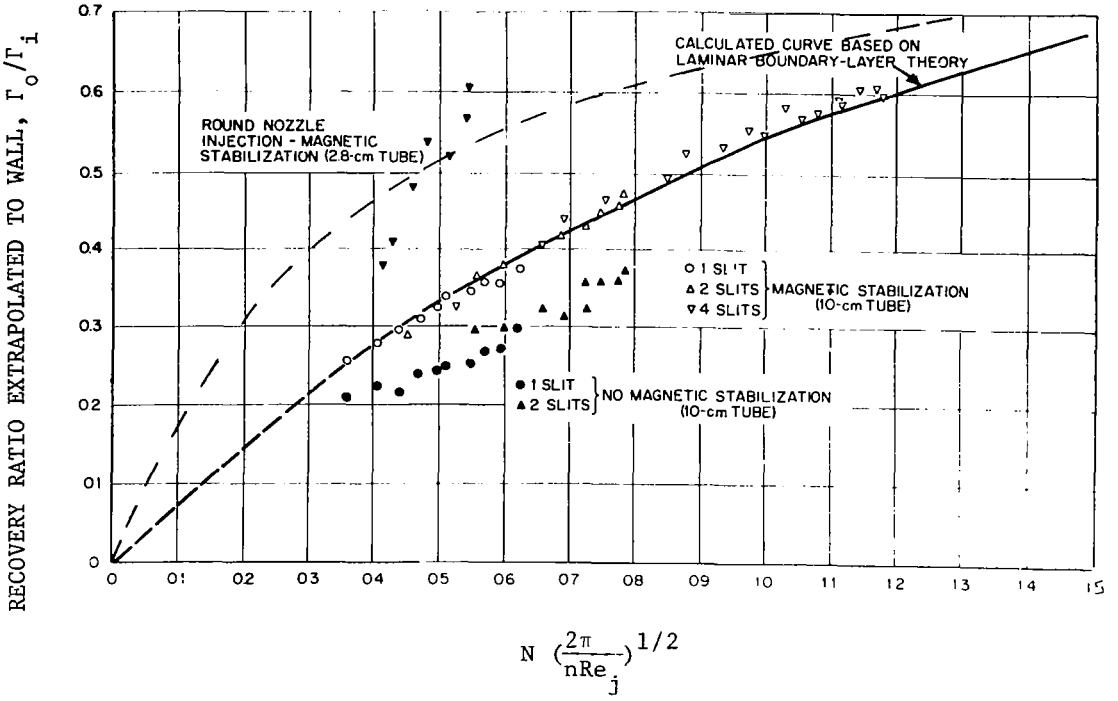

Fig. 3.26 The ratio of effective circulation at the outer radius of the vortex to the ideal circulation based on injection velocity as a function of the radial Reynolds number N, the jet Reynolds Re_j, and the number of injection slits, n. [— — — Eq. (3.8-5)] (Keyes, Chang, and Sartory, 1967).

the angular momentum flowing into the vortex; the second term the torque on the wall; and the final term the torque of the vortex (assuming Γ constant) on the boundary-layer fluid. Equation (3.8-1) can be rearranged to give

$$\frac{\Gamma_i}{\Gamma_o} = 1 + \frac{2\pi r_o^2 \ell\ \tau_w}{\dot{m}\Gamma_o} - \frac{2}{N} \tag{3.8-2}$$

An approximation is necessary to obtain a simple estimate of τ_w. If flat plate skin friction is assumed then

$$\tau_w = \frac{1}{2}\rho\frac{\Gamma_o^2}{r_o^2}\frac{n}{2\pi r_o}\int_o^{\frac{2\pi r_o}{n}} \frac{0.66}{\left[\frac{v_o x}{\nu}\right]^{1/2}}\,dx \tag{3.8-3}$$

i.e.,

$$\tau_w = 0.66\ \rho_o \frac{\Gamma_o^{3/2}}{r_o^2} \left[\frac{n\nu}{2\pi}\right]^{1/2} \tag{3.8-4}$$

When Eq. (3.8-4) is substituted into Eq. (3.8-2), it reduces to

$$\frac{\Gamma_i}{\Gamma_o} = 1 + \frac{0.66}{N} \left(\frac{nRe_j}{2\pi}\right)^{1/2} \left(\frac{\Gamma_o}{\Gamma_i}\right)^{1/2} - \frac{2}{N} \tag{3.8-5}$$

with $Re_j = \Gamma_i/\nu$. This approximation is included in Fig. 3.27 for the case in which the torque of the vortex on the boundary layer can be neglected (as was assumed by Keyes, Chang and Sartory). Since it under estimates the torque on the wall it falls somewhat above the numerical solution. Interestingly, it falls close to the experimental results for discrete jet driven vortex.

IV. COMPRESSIBLE, LAMINAR FLOW

4.1 Core Flow

Whenever the flow Mach number in gases is high enough for compressibility effects to be important, the flow is usually turbulent. In spite of this fact, it appears useful to provide a brief survey of the more important effects of compressibility on laminar vortices that have been predicted in the literature.

For an isotropic, Newtonian fluid the components of the shear stress tensor which appear in the momentum equation (1.3-2) may be written in cylindrical coordinates as

$$\tau_{rr} = \frac{2\mu}{3}\left[\frac{2\partial u}{\partial r} - \frac{u}{r} - \frac{1}{r}\frac{\partial v}{\partial \theta} - \frac{\partial w}{\partial z}\right]$$

$$\tau_{\theta\theta} = \frac{2\mu}{3}\left[2\left(\frac{1}{r}\frac{\partial v}{\partial \theta} + \frac{u}{r}\right) - \frac{\partial u}{\partial r} - \frac{\partial w}{\partial z}\right]$$

$$\tau_{zz} = \frac{2\mu}{3}\left[\frac{2\partial w}{\partial z} - \frac{\partial u}{\partial r} - \frac{u}{r} - \frac{1}{r}\frac{\partial v}{\partial \theta}\right]$$

$$\tau_{r\theta} = \tau_{\theta r} = \mu\left[r\frac{\partial}{\partial r}\left(\frac{v}{r}\right) + \frac{1}{r}\frac{\partial u}{\partial \theta}\right] \qquad (4.1\text{-}1)$$

$$\tau_{rz} = \tau_{zr} = \mu\left[\frac{\partial u}{\partial z} + \frac{\partial w}{\partial r}\right]$$

$$\tau_{z\theta} = \tau_{\theta z} = \mu\left[\frac{1}{r}\frac{\partial w}{\partial \theta} + \frac{\partial v}{\partial z}\right]$$

and the heat flux vector may be written as

$$\vec{q}_H = -k\left[r\frac{\partial T}{\partial r}\vec{i}_r + \frac{1}{r}\frac{\partial T}{\partial \theta}\vec{i}_\theta + \frac{\partial T}{\partial z}\vec{i}_z\right] \qquad (4.1\text{-}2)$$

When these forms for τ and $\vec{q}_H$ are used in Eqs. 1.3-1 to 1.3-3 together with an equation of state and a viscosity law, they provide a formidable set of equations. Rather than proceed with an extension of the general development of the last chapter the outline of the present chapter is to review a few particular cases considered in the literature to see when and in what way it modifies the incompressible results.

For flow dominated by swirl, i.e. $v >> u$ or w, cross differentiation of the radial and axial components of Eq. (1.3-2) leads to

$$\frac{\partial \rho v^2}{\partial z} \simeq 0 \qquad (4.1\text{-}3)$$

Thus if attention is restricted to only radial variations in density, the

tangential velocity is, as in the similar incompressible case, independent of z. The compressible tangential momentum equation can then be written as

$$\rho u r \frac{d(vr)}{dr} = \frac{-\partial \Psi}{\partial z} \frac{d(vr)}{dr} = \frac{d}{dr}\left[\mu r^3 \frac{d(v/r)}{dr}\right] \tag{4.1-4}$$

and the stream function must still be linear in z. The energy equation to the same degree of approximation is given by

$$\rho u r\left(c_p \frac{dT}{dr} + v \frac{dv}{dr}\right) = \frac{d}{dr}\left[kr \frac{dT}{dr} + \mu r^2 v \frac{d(v/r)}{dr}\right] \tag{4.1-5}$$

Mack (1960) has considered the case of an axisymmetric vortex flow with no radial or axial component of velocity, and with v a function of r only. In this case the tangential momentum equation requires that the torque be a constant, i.e.

$$\mu r^3 \frac{d}{dr}(v/r) = \text{const.} \tag{4.1-6}$$

Note that a constant viscosity is required to maintain an irrotational vortex, $v \sim 1/r$. The energy equation requires that the heat transfer differ from a constant only by the viscous dissipation, i.e.

$$-rk \frac{dT}{dr} = r^2 v \mu \frac{d}{dr}(v/r) + \text{const.} \tag{4.1-7}$$

When these two equations are combined for a perfect gas with the radial momentum equation, he shows that even for the familiar irrotational velocity distribution, there is, in general, a gradient in total temperature across the vortex.

$$\frac{T_t}{T_{t\infty}} = \frac{1 + \frac{\gamma-1}{2} M^2}{1 + (\gamma-1) Pr\, M^2} \tag{4.1-8}$$

As long as the Prandtl number, $Pr = C_p \mu/k$, exceeds 1/2, the total temperature decreases with decreasing radius. This observation will play an important role in the discussion of the Ranque-Hilsch Tube in Chapter IX. Since this solution requires the absence of radial velocity, Mack considered it as associated with flow outside of a rotating cylinder. But it is also appropriate for flow in a vortex tube in those regions where the radial velocity is zero. Mack, also integrated Eqs. 4.1-6 and 4.1-7 numerically for the Sutherland viscosity law.

Equation 4.1-4 is decoupled from the energy equation as long as μ is assumed constant and the radial variation of the stream function is specified by boundary conditions. Thus it is interesting to take some of the radial circulation distributions discussed in Section 3.2 and solve for the corresponding temperature distribution thru Eq. 4.1-5. This has been done by

Deissler and Perlmutter (1958) for the 2-D solution in Eq. 3.2-19, by Rott (1959) for the sink flow solution given in Eq. 3.2-20, and by Donaldson and Sullivan (1963) for some of their numerical solutions to Eqs. 3.2-16 and 3.2-17. Figure 4.1 is a plot of Rott's results for infinite Prandtl number. The curves are similar for other values of Pr but with a reduced cooling effect in the middle. For Pr = 1, $C_p[T(0) - T_\infty]/H^* = 0.564$ and for Pr = 1/2, equal to 0.462. In each case the cooling effect at the center is balanced by an increase in stagnation enthalpy outside the radius of maximum velocity.

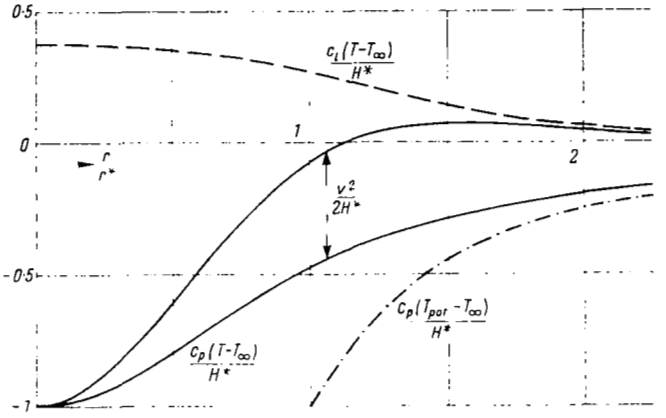

Fig. 4.1 Temperature distributions near the viscous core of a vortex for zero heat conductivity (infinite Prandtl number). The solid curves represent the temperature and stagnation temperature (or enthalpy) for a gas. The broken curve (top) shows the temperature field in a liquid. The dash-dotted curve gives the temperature for an inviscid-isentropic (potential) vortex flow of a gas. Note $H^* = 1.22\ V^2_{max}$ and $r^* = [2\mu r/u]^{1/2}$. (Rott, 1959)

For strong vortices the largest influences of compressibility on the circulation distribution may be expected to be related to the determination of the boundary conditions on $\partial\Psi/\partial z$ thru the end wall boundary layer and the exhaust constraint. These two effects are treated separately in the following two sections.

4.2 Influences on the Boundary Layer

The boundary layer for a compressible vortex perpendicular to a solid boundary has been considered by Anderson (1966), Ohrenberger (1967), and

Rott and Ohrenberger (1968). The flow depends on three new parameters, in addition to those discussed in Section 3.4. These parameters are the Mach number, the Prandtl number and the ratio of wall enthalpy to free stream enthalpy. Anderson's work was restricted to low Mach numbers so that the influence of the energy equation on the velocity distributions could be ignored. His results can be used to predict wall heat transfer in this regime.

Most of Ohrenberger's and Rott's analysis was restricted to Prandtl number equal to 1 with the viscosity proportional to temperature. This permits the influences of wall temperature and Mach number on the boundary layer parameters to be observed. In a generalization of the integral analysis of Section 3.4., Ohrenberger (1967) gives the mass flow in the boundary layer of a potential vortex with a constant total enthalpy over a flat disk as

$$\dot{m}_{b\ell} = 1.56(2\pi)\ (\rho_\infty \mu_\infty \Gamma_\infty)^{1/2}\left[1 - 0.72\left(1 - \frac{H_w}{H_\infty}\right)\right]^{1/4} \times \left[\int_0^s \left(1 + \frac{\gamma-1}{2} M_\infty^2\right)^{-\frac{\gamma+1}{3(\gamma-1)}} r^{1/3}\, ds\right]^{3/4} \tag{4.2-1}$$

with the subscript ∞ denoting the stagnation condition in the free vortex and H_w/H_∞ the ratio of wall enthalpy to free stream total enthalpy. According to this relation, cooling the wall serves to decrease the flow in the boundary layer. The maximum reduction for $H_w/H_\infty = 0$ is only a factor of 0.73. Increasing the Mach number also decreases the flow in the boundary layer. The cooling effect on mass flow may be understood as a result of the increase in shear while the Mach number influence is a result of the reduction in radial pressure gradient.

4.3 Compressible Exhaust Constraint

The region where compressibility may be expected to have the greatest influence on velocity profiles is in the neighborhood of the exhaust. The isentropic, inviscid exhaust flow was considered in Section 2.3. In Section 3.6 it was argued that the effects of viscosity on the exhaust flow could be separated into those due to the introduction of vorticity into the flow entering the exhaust and those due to local viscous shear within the neighborhood of the exhaust, with the first of these the more important. The

generalization of Mager's (1961) analysis of inviscid swirling flow thru a sonic nozzle to include the influence of vorticity has been made by Norton, et al (1969) and Lewellen, et al (1969).

Equations 2.3-3 to 2.3-7 are still valid along streamtubes even when there is a variation of Γ, a_o and p_o across streamlines. In order to ensure radial equilibrium in the general case the radial momentum equation must be added to these equations. (It is automatically satisfied when there is no gradient in stagnation conditions across streamlines). For quasi-cylindrical flow, this is given by

$$\frac{\partial p}{\partial r} = \frac{\rho v^2}{r} \tag{4.3-1}$$

The radial pressure gradient may be related to stagnation conditions thru the compressible Bernoulli equation to write Eq. 4.3-1 as

$$\frac{1}{p_o}\frac{\partial p_o}{\partial r} - \left[\frac{2}{\gamma} - \frac{\gamma-1}{\gamma}\left(\frac{w^2+\Gamma^2/r^2}{a_o^2}\right)\right]^{-1}\frac{\partial}{\partial r}\left(\frac{w^2+\Gamma^2/r^2}{a_o^2}\right) = \frac{\gamma}{a}\frac{\Gamma^2}{r^3} \tag{4.3-2}$$

When $p_o(\psi)$, $a_o(\psi)$ and $\Gamma(\psi)$ are specified, Eq. 4.3-2 may be combined with the definition of the stream function

$$\frac{\partial \Psi}{\partial r} = \rho w r \tag{4.3-3}$$

to give a second order, nonlinear system of differential equations to determine $\Psi(r)$. The boundary conditions may be given as $\Psi(0) = 0$ and $\Psi(r_e) = \dot{m}/2\pi$. As in the incompressible case this is not sufficient to uniquely determine $\Psi(r)$. This is done by invoking the extremum condition at the exhaust that centerline pressure be varied until r_e is a minimum for a given $\dot{m}$, or equivalently, that for a given r_e and $\dot{m}$ the centerline pressure be a maximum. The possibility of a core is included by starting from $\Psi = 0$ at a finite radius.

Norton, et al, integrated Eqs. 4.3-2 and 4.3-3 for some initial conditions appropriate for spinning rockets. Lewellen, et al, integrated them for p_o and a_o assumed constant for a parametric variation of $\Gamma(\Psi)$

$$\Gamma = C\left[1 - e^{-K\Psi/\Psi(r_e)_{\Gamma=o}}\right] \tag{4.3-4}$$

where $2\pi\Psi(r_e)_{\Gamma=o}$ denotes the no-swirl mass flow. The parameter K plays the role of a Reynolds number in determining the transition of Γ from its constant value in the outer potential flow to zero on the axis. It was allowed to vary from 0 to ∞. For $K = \infty$ the flow reduces to the isentropic

flow considered in Section 2.3. Figure 4.2 shows the variation in mass flow with swirl normalized with respect to its no-swirl value for a completely choked nozzle. Figure 4.3 gives the corresponding radial distribution of axial Mach number for a specific swirl condition. The centerline axial Mach numbers can be used to determine the minimum pressure ratio required to completely choke a swirling flow, since the pressure ratio must be large enough to support this Mach number. There is a strong influence of K on both mass flow and M_a. However when the mass flow is plotted against angular momentum flux as in Fig. 4.4 there is only a relatively small influence of K. Thus viscous effects may significantly increase the mass flow thru a nozzle for a given swirl but leaves the relationship between mass flow and angular momentum flux relatively unchanged.

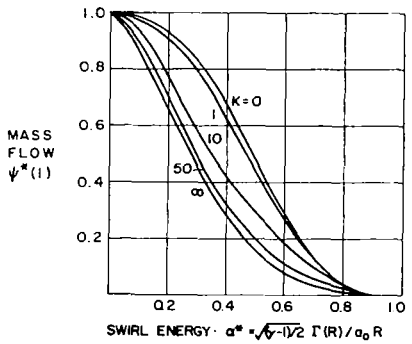

Fig. 4.2 Mass flow through a choked nozzle as a function of swirl with the effective Reynolds number K as a parameter and with the total energy held constant (Lewellen, Burns, and Strickland, 1969)

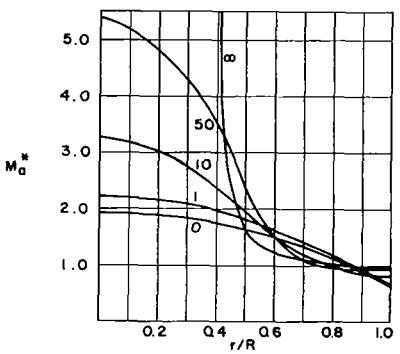

Fig. 4.3 Radial distribution of axial Mach number at the throat for $\alpha^* = 0.4$ with the effective Reynolds number as a parameter

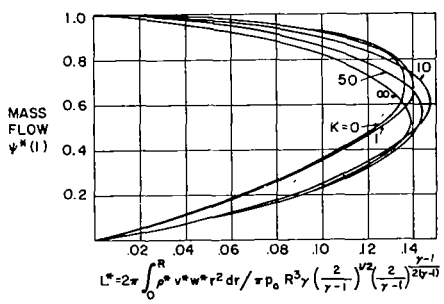

Fig. 4.4 Mass flow through a choked nozzle as a function of angular-momentum flux with K as a parameter

V. TRANSITION FROM LAMINAR TO TURBULENT FLOW

5.1 Introduction

Most of the vortices of interest for the applications in Chapters 7 through 9 involve turbulent flow in at least some region of the flow. Where and under what conditions the transition from smooth laminar flow to turbulent flow takes place, is the central question of the present chapter. This is the question of stability of the flow. The reader is referred to Chandrasekhar (1961) for the theory of hydrodynamic stability. A given motion may be said to be unstable if the effects of any small disturbance lead to the development of either another laminar flow or a state of turbulence. A general review of stability theory for rotating flows, although relevant, is beyond the scope of the present work. Rather, some of the more relevant results, taken principally from Greenspan (1968), are quoted herein without attempting to derive them. The significance of these results for confined vortices is discussed and some comparisons made with experimental investigations of stability in confined vortices.

5.2 Rayleigh's Criterion

In the consideration of inertial waves in Chapter 3, it was pointed out that any axisymmetric disturbance arising in a swirling fluid, where the principal balance of forces is between the centrifugal force and the radial pressure gradient, will set up a force tending to restore equilibrium whenever $\frac{dr^4}{dr} > 0$. By the same argument it follows that if $\frac{dr^4}{dr} < 0$ the departure from equilibrium will tend to grow. This criterion for stability was first discussed by Rayleigh, (1917).

As an indication of the general approach to the question of stability, Rayleigh's criterion will be proved mathematically. Assume that

$$r^4 = r_o^4(\eta) + g(\eta,\xi,\tau) \tag{5.2-1}$$

$$\psi = \psi(\eta,\xi,\tau) \tag{5.2-2}$$

with g and Ψ << 1 while $r^4 = O(1)$. When viscous and higher order terms are dropped the basic, unsteady equation of motion reduces to Eq. 3.1-36.

$$\frac{1}{\mathcal{I}^2 S^2}\frac{\partial^2 \mathcal{D}\psi}{\partial\tau^2} + \frac{4r_o^4 r_o'}{\eta}\frac{\partial^2\psi}{\partial\xi^2} = 0 \tag{5.2-3}$$

Since the equation is linear any general motion can be subdivided into separate wave modes. Therefore, let

$$\psi = f(\eta)\, e^{i(k\xi - \sigma\tau)} \tag{5.2-4}$$

There also is no loss in generality in setting $\mathcal{L}^2 S^2 = 1$ and $(r_o/\ell)^2 = 1$ since these parameters only scale σ and k. Under these conditions, Equation (5.2-3) reduces to

$$\eta f'' - \left[1 - \frac{4\Gamma_o\Gamma_o'}{\eta\sigma^2}\right]\frac{k^2}{4} f = 0 \tag{5.2-5}$$

The question of stability now reduces to the problem of solving this equation with appropriate boundary conditions on f, to determine the permitted eigenvalues of σ for any given k. If any k leads to a positive imaginary value of σ the flow will be unstable for this particular wave mode. However, for the present problem a general condition for all wave modes can be determined.

Equation (5.2-5) can be multiplied by f/η and formally integrated between two radial stations, say $\eta = 1$ and $\eta = \eta_i$ to give

$$ff'\Big]_{\eta_i}^{1} - \int_{\eta_i}^{1} \left(f'^2 + \frac{k^2}{4}\frac{f^2}{\eta}\right) d\eta + \frac{k^2}{\sigma^2}\int_{\eta_i}^{1} \frac{\Gamma_o\Gamma_o'}{\eta^2} f^2\, d\eta = 0 \tag{5.2-6}$$

If the radial velocity is forced to be zero at $\eta = 1$ and η_i, as would be the case for solid walls at these locations, then the first term in Eq. 5.2-6 is zero and it can be rearranged so that

$$\frac{\sigma^2}{k^2} = \frac{\displaystyle\int_{\eta_i}^{1} \frac{\Gamma_o\Gamma_o'}{\eta^2} f^2\, d\eta}{\displaystyle\int_{\eta_i}^{1} \left(f'^2 + \frac{k^2}{4}\frac{f^2}{\eta}\right) d\eta} \tag{5.2-8}$$

For k real the sign of σ^2 depends on the sign of $\Gamma_o\Gamma_o'$, i.e.,

$$\sigma^2 = |C|\ (\Gamma^2)'$$

Therefore when $d\Gamma^2/d\eta < 0$

$$\sigma = \pm i\ [\,|C(\Gamma^2)'|\,]^{1/2} \tag{5.2-9}$$

and a part of the disturbance given in Eq. (5.2-4) can grow with time, i.e. the flow is unstable. A somewhat more involved argument can be used to show that the flow is, at least, locally unstable if $d\Gamma^2/dr < 0$ anywhere.

5.3 Flow between Rotating Cylinders

The simplest stability problem in rotating flow is the problem of motion between concentric cylinders which revolve at different rates. As seen in the previous analysis, Rayleigh's criterion says the flow is unstable whenever $r_i^2\Omega_i^2 > r_o^2\Omega_o^2$. This simple criterion is based on inviscid flow and some modification may be expected at low Reynolds numbers. Figure 5.1 shows the stability boundary as a function of the Reynolds numbers of the two cylinders. This boundary has been obtained both theoretically and experimentally (See Greenspan, 1968) and the agreement is quite good. When the stability boundary is crossed the flow does not become turbulent. Instead, the flow transitions to another laminar flow that consists of toroidal vortex cells periodic in the axial direction, Fig. 5.2a. This pattern of Taylor vortices remains axisymmetric. Even after this singly periodic flow becomes unstable it transitions to a third type of flow that is periodic in θ as well as in z before a transition to general turbulence occurs. Figure 5.1 does not indicate the point of transition to turbulence.

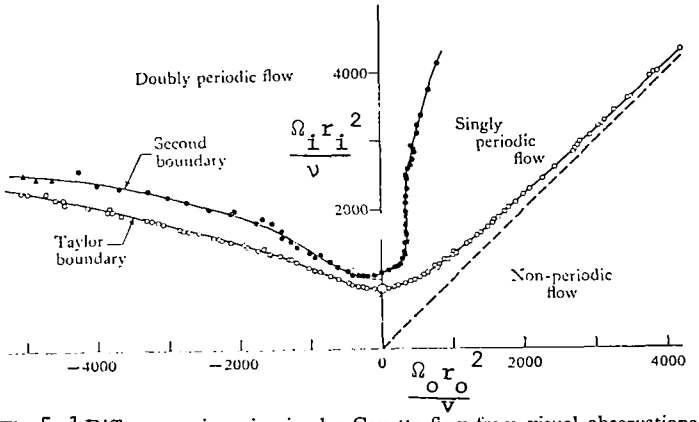

Fig. 5.1 Different regimes in circular Couette flow from visual observations (rough cylinders, $r_o/r_i = 1{\cdot}135$; $\nu = 0{\cdot}11$ cm²/sec). (Coles, 1965)

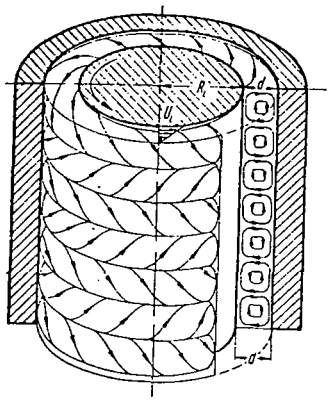

a) Taylor vortices

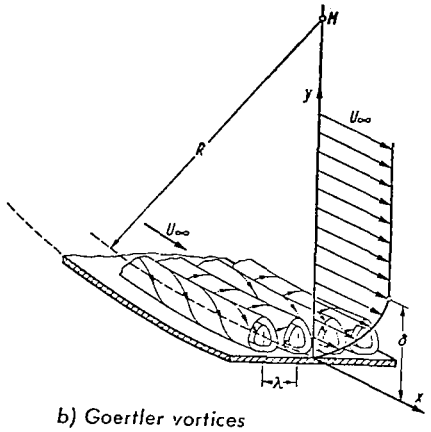

b) Goertler vortices

Fig. 5.2

(a) Taylor vortices between two concentric, rotating cylindersInner cylinder rotating, outer cylinder at rest; *d*-width of annular gap

(b) Goertler vortices in the boundary layer on a concave wall

$U(y)$ — base flow

δ — boundary layer thickness

λ — wavelength of disturbance

For the case of the outer cylinder at rest, Schlichting (1968) says that transition to turbulence is governed by a characteristic parameter known as the Taylor number, i.e., the flow becomes turbulent whenever

$$Ta \equiv \frac{\Omega_i r_i}{\nu}^2 \left[\frac{d}{r_i}\right]^{3/2} \geq 400 \qquad (5.3\text{-}1)$$

with $d = r_o - r_i$.

The opposite case in which the outer cylinder, only, is rotating is much more stable. Transition Reynolds number still depends on the spacing between the cylinders, but in a different way than that implied by the Taylor number dependence. When $d/r_i \ll 1$ the result reduces to that of Couette flow for which the transition Reynolds number $\frac{\Omega_o r_o d}{\nu} \simeq 2{,}000$ independent of d/r_i. This increases as d/r_i increases and according to Dryden (1959) when $\frac{2(r_o - r_i)}{r_o + r_i} = .3$, the transition Reynolds number is 65,000.

Another flow closely associated with that of flow between rotating cylinders with the outer cylinder at rest is that of a boundary layer on a concave wall. Roll vortices of the same type as the Taylor vortices may form in the boundary layer. These are usually called Goertler vortices. A sketch of these vortices is given in Fig. 5.2b. This instability occurs when

$$\frac{U_\infty \delta_2}{\nu} \left[\frac{\delta_2}{r_o}\right]^{1/2} \gtrsim 0.3 \qquad (5.3\text{-}2)$$

and transition when

$$\frac{U_\infty \delta_2}{\nu} \left[\frac{\delta_2}{r_o}\right]^{1/2} \gtrsim 7 \qquad (5.3\text{-}3)$$

with δ_2 equal to the momentum thickness of the boundary layer and r_o the radius of curvature of the wall (Schlichting, 1968). This corresponds to a Taylor number based on δ_2 and r_o. The critical value for transition is nearly two orders of magnitude lower than the corresponding transition Taylor number for flow between rotating cylinders, but this is fairly consistent with theoretical predictions which also predict a much lower stability limit for the onset of Goertler vortices.

Axial velocity gradients may introduce instabilities into the flow between rotating cylinders. Howard and Gupta (1962) have shown that a necessary condition for inviscid stability of axisymmetric disturbance is

$$\frac{d\Gamma^2/dr}{r^3 \left(\frac{dw}{dr}\right)^2} > \frac{1}{4} \qquad (5.3\text{-}4)$$

This criterion is analogous to the condition that the Richardson number, $(g\, d\rho/dx)/\, \rho(dw/dx)^2$ exceed 1/4 for a stratified flow to be stable in the presence of a gravity field. The proper extension to stratified rotating flow is (Leibovich, 1969)

$$\frac{\frac{d(\rho\Gamma^2)}{dr}}{r^3 \rho \left(\frac{dw}{dr}\right)^2} > \frac{1}{4} \qquad (5.3\text{-}5)$$

However, this is not a sufficient condition. The flow may be unstable to nonaxisymmetric disturbances. Solutions for this more general stability condition have only been obtained within the narrow gap approximation, i.e. when $(r_o - r_i)/r_o \ll 1$. Ludwieg (1961, 1964) has obtained the inviscid stability diagram shown in Fig. 5.3 for this case. The experimental points appear to indicate that the major effect of viscosity is to make the case of uniform angular velocity stable for small axial velocity gradient where the inviscid theory says that any finite axial velocity gradient should lead to an instability. Pedley (1969) has shown that this case of uniform angular velocity

remains inviscidly unstable for finite axial velocity gradients even when the inner cylinder is removed, i.e. $r_i \to 0$.

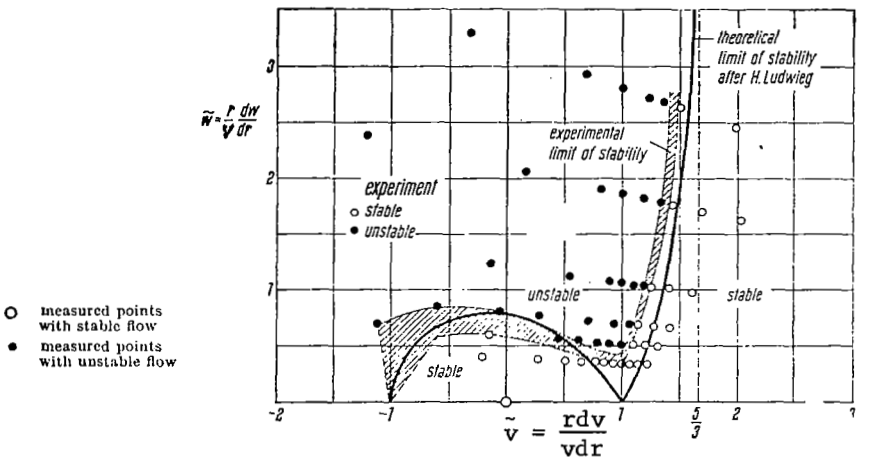

Fig. 5.3 Experimental verification of the stability theory for flow between two concentric, rotating cylinders with axial motion superimposed, after H. Ludwieg(1964)
$R = (R_0 - R_i)^2 \omega_i / \nu = 650$

Shaded area: experimentally determined limit of stability

The extension of Ludwieg's diagram to include the influence of density gradients as done by Kurzweg (1967, 1969) is shown in Fig. 5.4. A positive gradient of density with radius increases stability and a negative gradient decreases the region of stability.

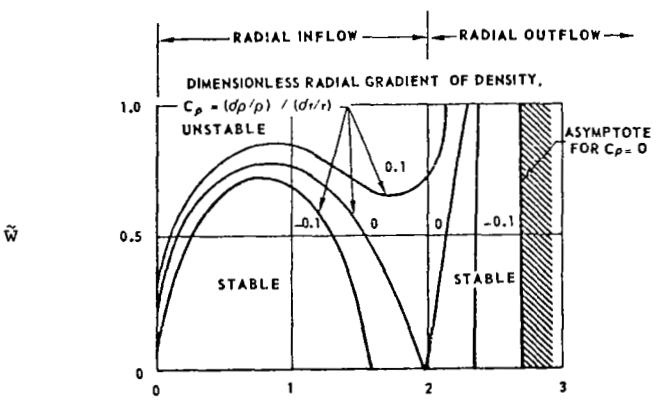

Fig. 5.4 Influence of density gradient on Ludwieg's stability curve, (Kurzweg, 1967)

5.4 Flow in the End-Wall Boundary-Layer

Confined vortex flow is usually considerably more complicated than the flow between rotating cylinders. In particular, the flow is complicated by the end wall boundary layers which have characteristic instabilities of their own. Some ideas on the conditions leading to transition in these boundary layers may be obtained by looking at the results of investigations into the stability of Ekman layers. The boundary layer on the axial end walls of a vortex chamber may be viewed as a nonlinear Ekman layer with the Rossby number of order 1 or larger. Here the Rossby number is defined as

$$R_o \equiv \frac{V_1}{\Omega r} \tag{5.4-1}$$

with V_1 the difference between the tangential velocity outside the boundary layer and that of the wall. The principal results of Ekman-layer stability investigations, as summarized by Greenspan (1968) are given in Fig. 5.5. Two distinct types of instabilities have been detected. The waves of both families form a series of horizontal roll vortices whose spacing is related to the depth of the boundary layer. Transition to general turbulence occurs at a Reynolds number somewhat higher than that for the onset of instabiltiy.

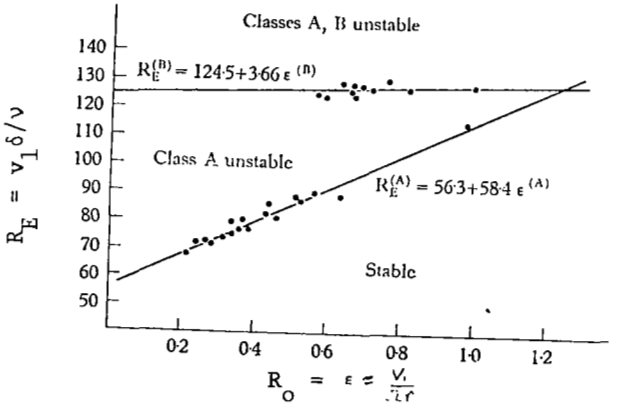

Fig. 5.5 The critical Reynolds number vs. Rossby number for Class A and Class B instabilities in an Ekman boundary layer. (Tatro and Mollo-Christensen, 1967).

The results of Fig. 5.5 can be used to estimate the transition Re_t for flow in the end wall boundary layer of a vortex chamber. For a stationary end wall

$$R_o \gtrsim 1$$

$$V_1 \sim \Gamma/r \tag{5.4-2}$$

$$\delta \sim \left[\frac{\nu}{\Gamma}\right]^{1/2} r$$

Therefore $\frac{V_1 \delta}{\nu} \gtrsim 125$ whenever

$$Re_t \equiv \frac{\Gamma}{\nu} = \left(\frac{V_1 \delta}{\nu}\right)^2 \gtrsim (125)^2 \tag{5.4-3}$$

i.e.

$$Re_{t_{(crit)}} \gtrsim 1.5 \times 10^4 \tag{5.4-4}$$

This suggests that the end wall boundary layer will transition from laminar to turbulent flow where Re_t is much above 10^4.

It is not surprising to find that the oscillating profile distributions of the Ekman layer lead to instabilities at lower Reynolds numbers than do the monotonic profile distributions associated with a rotating disk. The flow field of a rotating disk becomes unstable when (Schlichting, 1968)

$$Re_t \equiv \frac{\Omega r^2}{\nu} \gtrsim 1.9 \times 10^5$$

and transition occurs when

$$Re_t \gtrsim 2.8 \times 10^5$$

In terms of the Reynolds number based on the boundary-layer thickness as in Fig. 5.5 this corresponds to $\delta V_1/\nu = 550$ for the stability limit and 670 for transition. The instability in the rotating disk boundary layer is of the same type as the Class B in Fig. 5.5.

5.5 Stability in a Confined Vortex

The general flow pattern for a strong vortex as represented by Fig. 3.13 is too complicated for the prediction of general stability conditions, but some indication of the expected transition Reynolds numbers can be obtained from the

preceding sections. When the external boundary condition is a rotating, porous cylinder and there is radial inflow, turbulence probably first appears in the end wall boundary layers. According to the last section this should occur when

$$Re_t \gtrsim 10^4 \tag{5.5-1}$$

Also, transition may be expected at a rather low Re_t in the region of $r > \hat{r}$ when the necessary condition on the Richardson Number is violated, i.e. transition should have occurred when

$$r^3 \left(\frac{dw}{dr}\right)^2 > 4 \frac{d\Gamma^2}{dr} \tag{5.5-2}$$

Since the approximate solution discussed in Section 3.5 calls for significant axial velocities in this region of $r > \hat{r}$ while at the same time calling for Γ to be essentially constant, flow in this region may be expected to be unstable.

These speculations are confirmed by Travers' (1965, 1967) experimental investigations. By taking microflash pictures of dye filaments in a water vortex, he was able to observe clear demarcations between regions of turbulence and apparently laminar regions and to identify the dividing line with the radial stagnation surface. An example of these photographs is reproduced in Fig. 5.6. For the conditions of the photograph ($Re_t \simeq 1 \times 10^5$, $N \simeq 30$, and $L/D \simeq 3$) the end wall boundary layer should be turbulent and the $\hat{r}$ based on turbulent boundary-layer calculation (see Chapter 6) falls close to the demarcation line between the laminar and turbulent region. This division of turbulent and laminar regions by the radial stagnation surface was observed for all tangential Reynolds numbers tested ($Re_t = .5$ to 2.5×10^5) whether the vortex was driven by rotating the peripheral wall, by injecting flow tangentially through slots, or by injecting through a large number of discrete jets.

Travers and Clark (1968) also demonstrated that a vortex with radial outflow is more unstable than that for radial inflow. A one inch diameter, porous tube was installed in the center of the vortex discussed in the last paragraph and also provisions made to rotate either the central tube or the end walls. For small amounts of outflow ($-N \lesssim 100$) the flow was turbulent for $r \gtrsim 0.3\, r_o$ and laminar for smaller radii when both the inner tube and the end walls were stationary (Re_t was varied from 1.2×10^4 to 3.2×10^5 for these

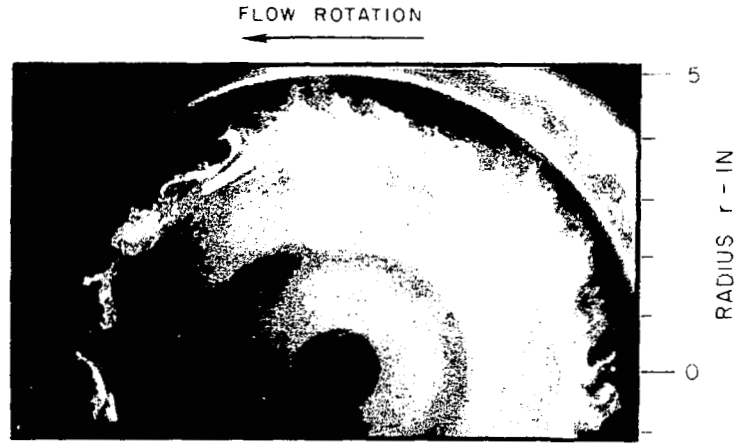

Fig. 5.6 Microflash photographs of dye patterns for a vortex driven by tangential injection thru a single slot with Re_t = 120,000, N = 30, and L/D = 3 (Travers, 1965).

experiments). Rotating the inner tube at an angular rate equal to that of the outer cylinder made the flow turbulent over all the flow. Rotating the end walls had a stabilizing effect for sufficiently low N. A summary of the results for the rotating end wall with the inner tube stationary are given in Fig. 5.7.

The addition of axial velocities to either the basic inflow vortex or the outflow vortex tends to destabilize the flow.

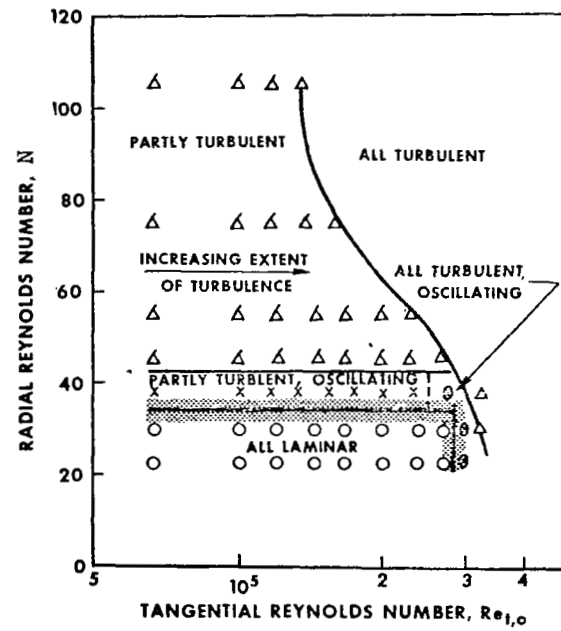

Fig. 5.7 Summary of laminar and turbulent flow conditions observed for radial outflow vortex with rotating end walls and fluid injection through stationary inner porous tube (Travers and Clark, 1968).

In summary, the experimental results are consistent with theoretical results for the basic vortex configuration with radial inflow. However, for radial outflow, where the steeper circulation gradient may have been expected to stabilize the flow, the flow is unstable. It appears that either the radial outflow itself is destabilizing because of the adverse pressure gradient, or the flow pattern forces the turbulence generated in the boundary layers out into the main flow.

5.6 Vortex Breakdown

Vortex breakdown is the name given to the abrupt and rather drastic change in structure which often occurs in a well defined vortex core. The phenomenon first gained attention in connection with delta-wing leading edge vortices. It has since been recognized to occur under certain conditions in many other situations including the core region of confined vortices. A brief review of pertinent experimental observations associated with breakdown and some of the theories that have been given to explain the phenomenon is given in this section. Also, conclusions relevant to confined vortices are made.

A review of experimental observations has been given by Bossel (1967). The broad conclusions to be drawn from these are:

1) The swirl angle of the flow must exceed a certain value before breakdown may occur.
2) Breakdown is always associated with an adverse pressure gradient along the axis.
3) Reynolds number and Mach number effects play a minor role.
4) As swirl is increased in a vortex tube a stage is reached where a bubble of recirculating fluid with a stagnation point appears on the axis. At still larger values of swirl the bubble proceeds upstream until a two-celled vortex is established in the tube.
5) Breakdown may be either an axisymmetric or a spiral character as shown in Fig. 5.8.

Theories offered to explain breakdown approach the problem in three distinctly different ways; as a stability problem, as a large amplitude wave standing in the flow, or as a natural separation of the flow from the axis as it undergoes a transverse pressure gradient.

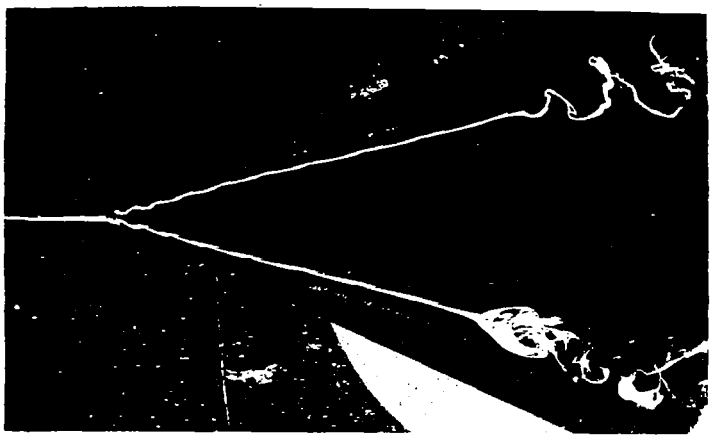

Fig. 5.8 Vortex breakdown over a delta wing, showing both the axisymmetric and the spiral mode of breakdown (From Lambourne and Bryer, 1962)

The stability approach has been pursued by Ludwieg (1960-1964) and Jones (1960). Some of Ludwieg's results are summarized in Fig. 5.3. His basic premise is that when a swirling flow crosses the stability boundary, any disturbance must grow until the flow transforms into a stable pattern or breaks up into turbulence. This theory appears more relevant for the spiral breakdown mode than the axisymmetric since it is the spiral disturbances which the theory predicts should be amplified. Note that the swirl angle $\frac{v}{w}_{max}$ does not affect the stability boundary as much as the velocity gradients do. In fact increasing $\frac{v}{w}_{max}$ for the same velocity profiles would make the flow more likely to be stable. This runs contrary to observations. On the other hand, the strong axial velocity gradients observed immediately upstream of the breakdown stagnation point do tend to make the flow in this region cross the stability boundary (Hummel, 1965). These facts suggest that Ludwieg's instability mechanism is not the primary cause of breakdown, but may play an important role in the subsequent development.

The analysis of breakdown as related to a wave phenomenon was first made by Squire (1960) and improved upon by Benjamin (1962,-65,-66, and -67). These analyses predict a swirl angle at which a standing wave can occur in the flow.

The derivation of this critical angle may be made in the following way beginning with Eq. 3.1-19. In dimensional terms this equation may be written as

$$\Psi_{yy} + \frac{1}{2y}\Psi_{zz} = \frac{dp_o}{d\psi} - \frac{1}{4y}\frac{d\Gamma^2}{d\psi} \tag{5.6-1}$$

with $y = r^2/2$. If a primary flow with $u = 0$, $\Gamma = \Gamma(y)$ and $w = W(y)$ is to support a small amplitude wave, the perturbation stream function, $\hat{\psi}$, must satisfy the equation

$$\hat{\psi}_{yy} + \frac{1}{2y}\hat{\psi}_{zz} - \left[\frac{W_{yy}}{W} - \frac{\Gamma\Gamma_y}{2y^2W^2}\right]\hat{\psi} = 0 \tag{5.6-2}$$

When a wave-like depencence of $\hat{\psi}(z)$ is assumed, i.e.,

$$\hat{\psi}(y,z) = \tilde{\psi}(y)e^{i\lambda z} \tag{5.6-3}$$

then Eq. 5.6-2 transforms to

$$\tilde{\psi}_{yy} - \left(\frac{\lambda^2}{2y} + \frac{W_{yy}}{W} - \frac{\Gamma\Gamma_y}{2y^2w^2}\right)\tilde{\psi} = 0 \tag{5.6-4}$$

and the boundary conditions appropriate for flow in a tube are

$$\tilde{\psi}_{(o)} = 0 \ , \quad \tilde{\psi}\left(\frac{1}{2}r_w^2\right) = 0 \tag{5.6-5}$$

For given primary flow distributions, Eqs. 5.6-4 and 5.6-5 lead to critical values of $(V/W)_{max}$ which will permit a given wave length $(1/\lambda)$ to stand in the flow. The lowest critical value is that associated with the longest possible wave length, $\lambda = 0$, Eqs. 5.6-4 and 5.6-5 may readily be solved for a Rankine vortex primary flow, $v = \Omega r$ $(r \leq r^*)$ and $v = \Omega r^{*2}/r$ $(r \geq r^*)$, with uniform axial flow in terms of Bessel functions. The critical swirl parameter in this case is given by

$$\frac{\Omega r^*}{w}\frac{J_o\left(\frac{2\Omega r^*}{w}\right)}{J_1\left(\frac{2\Omega r^*}{w}\right)} = \frac{(r^*/r_w)^2}{(r^*/r_w)^2 - 1} \tag{5.6-6}$$

This yields values of $\Omega r^*/w$ between 1.2 and 1.9 as r^*/r_w varies from 0 to 1 as seen in Fig. 5.9. A somewhat more realistic circulation distribution is the exponential variation given in Eq. 3.2-20. The critical velocity ratio for this distribution is also plotted in Fig. 5.9 from numerical values given by Leibovich (1970). The radius of maximum tangential velocity is still identi-

fied as r*.

Critical values of swirl predicted by this wave approach are close to the experimentally observed values for breakdown. A swirling flow with a swirl angle less than critical is too fast to support a standing wave, and thus may be termed supercritical. A deceleration of the flow will increase the swirl angle and drive it towards the critical condition eventually reaching the point where a large amplitude wave may stand. In this way, breakdown is viewed as a transition from supercritical to subcritical flow in complete analogy with the hydraulic jump. Benjamin (1966), Pritchard (1970) and Leibovich (1969) have carried out weakly nonlinear wave analyses to predict the breakdown bubble shape. Although their solitary wave analysis is not valid for large amplitude waves which lead to stagnation of the flow on the axis, they do appear adequate to show this approach is completely consistent with the axisymmetric bubble breakdown observed by Harvey (1962), Fig. 5.10. It cannot be readily extended to the spiral mode.

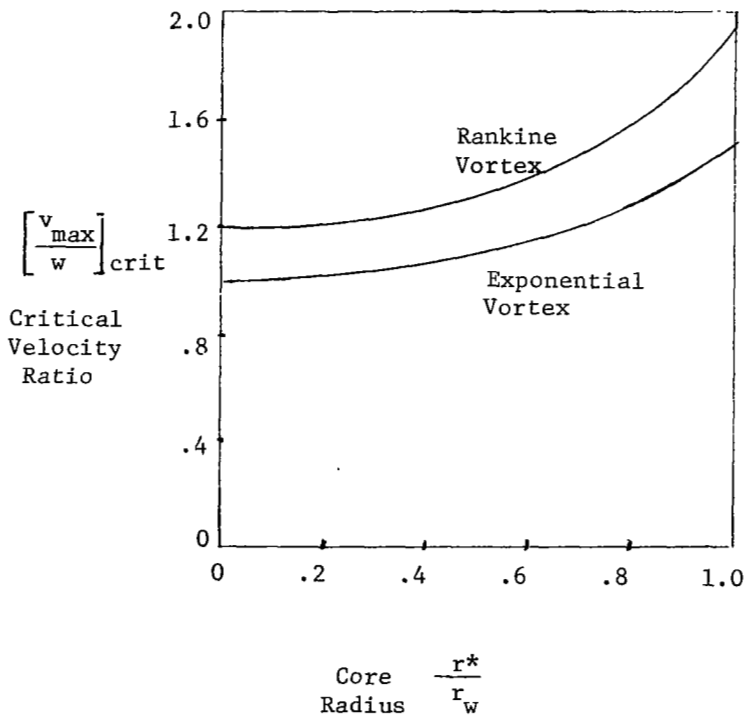

Fig. 5.9 Critical velocity ratio as a function of the core radius for a Rankine vortex (Squire, 1960) and for an exponential tangential velocity distribution (Leibovich, 1970) with w = const.

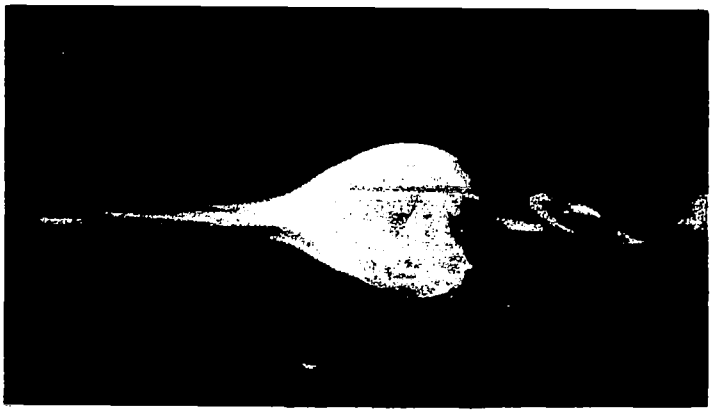

Fig. 5.10 (plate 1). A photograph of vortex breakdown using an electronic flash Harvey (1962)

The breakdown may also be viewed as a natural stagnation of the centerline flow leading to separation of the flow from the axis. As demonstrated in Section 3.1, when the swirl parameter is large, small axial variations in tangential velocity must produce large effects on the axial velocity. If the tangential velocity increases with z as it would in an inviscid contraction of the streamtube, i.e. as in vortex "stretching," the centerline velocity must be greatly increased. Conversely, if the streamtube expands, $\frac{\partial v}{\partial z}$ will be negative leading to a positive $\frac{\partial p}{\partial z}$ along the centerline which retards the flow. For a given radial variation of w and v, there is a critical value of swirl $(v/w)_{max}$ at which an infinitesimal expansion in the streamtube will lead to stagnation on the axis. Hall (1966) shows that for an initial distribution with uniform w and uniform Ω, this critical value is $(v/w)_{max} = 1.9$, the same value as obtained in Eq. 5.6-6. This case can be worked out exactly because the governing equation, Eq. 5.6-1, is linear. Hall (1967) has given a numerical procedure based on finite difference calculations of the quasi-cylindrical equations for determining the critical conditions for more general distributions, and including the effect of viscous diffusion. Due to the quasi-cylindrical approximation, the numerical procedure can not be used through the breakdown, but only to predict the conditions leading to breakdown. In all cases tested the critical conditions are consistent with those obtained from the wave approach discussed previously.

As calculated by Hall (1967), the influence of viscous diffusion on a vortex core may serve to drive it toward the critical condition. Although v_{max} is decreasing due to diffusion, for a range of swirl the interaction of a negative $\frac{\partial v}{\partial z}$ with w through the pressure may retard w at an even faster rate to allow the effective swirl parameter in the core to increase.

Whether viewed as an instability, a large amplitude wave disturbance, or as separation, breakdown appears to represent the leading edge of a transition from a vortex with a monotonic axial velocity to one with a reversal in w as observed by Harvey (1962) and So (1967) and others. This may be observed in Fig. 3.11, where the swirling jet emanating from the end-wall boundary layer adjusts to a vortex core with reversed flow. The bubble observed in Fig. 5.10, although probably best analyzed as a solitary wave, represents the case when the deceleration in the flow is not adequate to support complete transition to a two cell flow.

The separation model of breakdown also provides some insight into the difference between an axisymmetric mode of breakdown and the spiral mode. In order for a smooth axisymmetric breakdown to occur it is necessary for the total pressure in the center of the stagnation bubble to equal the total pressure on the axis just upstream of breakdown. But, for an open-ended bubble, the total pressure at the stagnation point of the bubble must be less than the total pressure at the point where the reverse flow streamlines originate. Thus a necessary condtion for an axisymmetric breakdown should be that the centerline total pressure be less than the ambient pressure to which the vortex flow is exhausting. If the centerline total pressure is greater than the downstream ambient pressure the centerline streamline can not be stagnated. However, it is still possible for the spiral mode separation to occur since in this case the point of separation from the axis is not a stagnation point for the flow originating from upstream of this point.

As seen above, the theories all pretty well agree on the critical value of swirl, particularly in the case of the Rankine vortex for which the equations remain linear. For the more general case, it is not possible to say how much the nonlinearity in Eq. 5.6-1 may reduce the critical value of swirl required for breakdown, i.e. how supercritical the flow may be and still undergo breakdown.

Aside from the visual pictures, little information is available in the literature on the flow changes across the breakdown transition. The free vortex often degenerates to general turbulence a few core diameters downstream of the breakdown, but may remain organized as a vortex with a core of reversed flow. In the case of a flow in a tube, the vortex is most likely to remain organized, even if highly turbulent. It is interesting to speculate on the size of the reversed flow core downstream of the breakdown. When the core radius is defined as the radius of the dividing streamline between the flow originating from upstream and that from downstream then it is analogous to r_c utilized in Chapter II. If the assumption is made that r_c may still be determined by the same extremum problem, then it is equivalent to assuming that breakdown supports the maximum possible pressure jump consistent with conservation relations across the transition. Hawkes (1969) has worked out jump conditions for some flow models based on this assumption. For the Rankine vortex model used in determining the critical conditons in Eq. 5.6-6, he found $r_c/r^* \simeq 0.3$ and $\Delta p(0)/(\rho v^2_{max}/2)$ equal to 0.22 and 0.75 for r^*/r_w equal to 1 and 0 respectively.

It should be noted that in setting the conservation relations across the breakdown it is not possible to conserve both axial momentum and total pressure. As shown by Benjamin (1962), if total pressure is conserved the integrated value of axial momentum is greater for the subcritical flow with a core than for the initial supercritical flow ahead of the breakdown. This difference is balanced by the momentum associated with the waves in the subcritical flow. Conversely, if these waves are assumed to breakup into turbulence it would lead to a loss in total pressure with axial momentum conserved. There is almost no difference in the above quoted values of r_c and $\Delta p(0)$ between the case where axial momentum is conserved and that in which total pressure is conserved.

In summary, the conditions leading to breakdown may be fairly well determined from available theories, but the structure of the flow following breakdown is subject to considerable speculation. In a confined vortex, breakdown may be expected to occur at varying positions along the axis as a function of swirl. For small values of swirl breakdown will not occur anywhere. For moderate values of swirl which permit the flow at the minimum exhaust cross

section to still be slightly supercritical, breakdown should occur downstream of this cross section as flow expands, and becomes less supercritical (increases its maximum swirl angle). As the swirl is increased, breakdown will move upstream towards the minimum exhaust cross section. When the swirl is sufficiently large for the breakdown to move upstream of the exhaust the flow becomes subcritical all along the axis and the breakdown must jump to the wall opposite the exhaust where it is associated with the eruption of the end wall boundary layer as in Fig. 3.12.

It can now be seen that Mager's swirl dominated solution for viscous exhaust flow in Section 3.6 is incompatible with the present model of breakdown. The transition from uniform axial velocity to a reverse-flow core should not occur in the accelerating portion of the nozzle.

It is interesting to note that the present model of breakdown implies that in order for tangential velocity to be much larger than the maximum axial velocity anywhere in the neighborhood of the vortex exhaust the flow must be subcritical. For subcritical flow, the core size is determined by the extremum condition that mass flow be a maximum for a given pressure drop. Section 6.5 contains an argument that this leads to a chamber instability when the angular momentum flux per unit mass flow exceeds a certain bound so that even in subcritical flow v_{max} can not greatly exceed w_{max}.

VI. TURBULENT VORTICES

6.1 Introduction

For the vast majority of applications of confined vortex flows, Reynolds numbers of practical interest to engineers exceed those required for transition to turbulence, at least, in some region of the flow. The formal turbulent equations of motion can be obtained by decomposing the fluid velocity, as well as the pressure, density, and enthalpy at any point, into an average, mean part and a small perturbation that fluctuates irregularly with time. The Navier-Stokes equations of motion may then be averaged over a time interval that is long compared with the time scale of turbulent fluctuations but short compared with the time scale of the mean motion. The averages of different fluctuation products then form Reynold's stresses which must be added to molecular stresses in determining the stress tensor τ that should be used in Eqs. 1.1-1.3. For example, for incompressible, steady mean flow the Reynold's stress tensor in Cartesian coordinates may be written as

$$\tau_T = -\rho \begin{bmatrix} \overline{q_x'^2} & \overline{q_x'q_y'} & \overline{q_x'q_z'} \\ \overline{q_y'q_x'} & \overline{q_y'^2} & \overline{q_y'q_z'} \\ \overline{q_z'q_x'} & \overline{q_z'q_y'} & \overline{q_z'^2} \end{bmatrix} \tag{6.1-1}$$

where the prime denotes the fluctuating part and the subscript denotes velocity component direction and the bar denotes the time average. Little success has been achieved in dealing with the general turbulent equations of motion since the general dependence of the Reynold's stresses on the mean velocity components and their gradients must be determined before the system of equations is complete.

Even in turbulent flow, strong vortices can be divided into two regimes depending upon whether axial or radial shear stresses are more important. As seen in Chapter III, axial shear may be expected to be important only in the boundary layers imposed by axial boundary conditions which force a strong axial gradient on the flow, e.g. in the end-wall boundary layers. Outside of these layers, which can best be treated by boundary-layer methods a quasi-cylindrical approximation is appropriate for the equations of motion. That is, it is appropriate to assume that variations of mean values in the axial

direction are small compared with the corresponding variations in the radial direction. It follows from the continuity equation that the mean radial velocity must be small.

The quasi-cylindrical equations for compressible, turbulent flow as given by Hall (1966) are:

Continuity equation,

$$\frac{\partial \rho}{\partial t} + \frac{1}{r}\frac{\partial r\rho u}{\partial r} + \frac{1}{r}\frac{\partial (r\overline{\rho' u'})}{\partial r} + \frac{\partial \rho w}{\partial z} = 0 \tag{6.1-2}$$

Momentum equations,

$$\frac{\rho v^2}{r} = \frac{\partial p}{\partial r} \tag{6.1-3}$$

$$\rho\left(\frac{\partial v}{\partial t} + u\frac{\partial v}{\partial r} + w\frac{\partial v}{\partial z} + \frac{uv}{r}\right) = \frac{1}{r^2}\frac{\partial}{\partial r}\left[r^2\mu\left(\frac{\partial v}{\partial r} - \frac{v}{r}\right)\right] \tag{6.1-4}$$
$$- \frac{1}{r^2}\frac{\partial}{\partial r}\left(r^2\rho\overline{u'v'}\right) - \overline{\rho' u'}\left(\frac{\partial v}{\partial r} + \frac{v}{r}\right)$$

$$\rho\left(\frac{\partial w}{\partial t} + u\frac{\partial w}{\partial r} + w\frac{\partial w}{\partial z}\right) = -\frac{\partial p}{\partial z} + \frac{1}{r}\frac{\partial}{\partial r}\left(r\mu\frac{\partial w}{\partial r}\right) \tag{6.1-5}$$
$$- \frac{1}{r}\frac{\partial}{\partial r}\left(r\rho\overline{u'w'}\right) - \overline{\rho' u'}\frac{\partial w}{\partial r}$$

and the energy equation

$$\begin{aligned}\rho\left(\frac{\partial H}{\partial t} + u\frac{\partial H}{\partial r} + w\frac{\partial H}{\partial z}\right) - \frac{\partial p}{\partial t} \\ = \frac{1}{r}\frac{\partial}{\partial r}\left[\frac{\mu}{Pr}\, r\frac{\partial H}{\partial r} + \frac{\mu}{Pr}(Pr-1)r\left(v\frac{\partial v}{\partial r} + w\frac{\partial w}{\partial r}\right) - \mu v^2\right] \\ - \frac{1}{r}\frac{\partial}{\partial r}\left(r\rho\overline{u'H'}\right) - \overline{\rho' u'}\frac{\partial H}{\partial r} + \frac{5}{3}\frac{1}{r}\frac{\partial}{\partial r}\left[\mu r\left(\overline{\frac{v'}{r}\frac{\partial u'}{\partial \theta}} + \overline{w'\frac{\partial u'}{\partial z}}\right)\right]\end{aligned} \tag{6.1-6}$$

where

$$H = h + \frac{1}{2}\left(u^2 + v^2 + w^2\right) + \frac{1}{2}\left(\overline{u'^2} + \overline{v'^2} + \overline{w'^2}\right)$$

$$H' = h' + uu' + vv' + ww'$$

and $Pr = \mu c_p/k$ is the Prandtl number which is assumed not to fluctuate. Even though mean values with respect to time have been taken in the derivation of the above equations, the time variations of the mean quantities have been retained, to admit mean motions which vary slowly with time compared with the fluctuating components.

For incompressible flow, the energy equation may be decoupled from Eqs. 6.1-2 to 6.1-5 and the terms involving $\overline{\rho' u'}$ and $\partial\rho/\partial t$ dropped. The

tangential component of the vorticity equation, analogous to Eq. 3.1-7, may be formed by cross differentiating Eqs. 6.1-3 and 6.1-5 to give

$$\frac{1}{r}\frac{\partial v^2}{\partial z} = -\frac{\partial}{\partial r}\left[\frac{\partial w}{\partial t} + u\frac{\partial w}{\partial r} + w\frac{\partial w}{\partial z}\right] + \frac{\partial}{\partial r}\frac{1}{r}\frac{\partial}{\partial r}\left[r\nu\frac{\partial w}{\partial r} - r\overline{u'w'}\right] \qquad (6.1\text{-}7)$$

Thus the arguments of Section 3.1 deducing that the tangential velocity tends to be independent of z when $S^2 >> 1$ still hold for turbulent flow. Under these conditions the tangential momentum equation leads to

$$\frac{\partial v}{\partial t} + u\frac{\partial v}{\partial r} + \frac{uv}{r} = \frac{1}{r^2}\frac{\partial}{\partial r}r^2\left[\nu\left(\frac{\partial v}{\partial r} - \frac{v}{r}\right) - \overline{u'v'}\right] \qquad (6.1\text{-}8)$$

Before Eq. 6.1-8 can be solved it is necessary to relate $\overline{u'v'}$ in some manner to the mean motion. Ragsdale (1961), Donaldson and Snedeker (1962) and Kinney (1966) have attempted to do this with a mixing length approach. However, most attempts at analyzing turbulent vortices have used an "eddy" viscosity approach. That is, an eddy viscosity is defined such that

$$\overline{u'v'} \equiv -\varepsilon_T\left(\frac{\partial v}{\partial r} - \frac{v}{r}\right) \qquad (6.1\text{-}9)$$

The sole justification for this approach is that it reduces the turbulent equation to an equivalent laminar problem. This appears to be adequate justification until some other dependency of $\overline{u'v'}$ is more firmly established. With the eddy viscosity approach it is still necessary to determine ε_T as a function of time and space.

Numerous attempts to relate ε_T to tangential Reynolds number have been made. Figure 6.1 is a summary of some of these attempts. The standard procedure is to compare theory and experiment and determine the value of ε_T which results in the best agreement. Part of the scatter of correlations in Fig. 6.1 may be attributed to differences in the theories to which the experiments were compared. The correlations of Keyes (1960), Ragsdale (1961) and Donaldson and Snedeker (1962) compare experiments with Eq. (3.3-17) without considering boundary-layer influences. Therefore they should be expected to yield values of ε_T/ν which are high. The line marked Modified Ragsdale shows the adjustment which including the effect of the boundary layer makes in reducing the same data. Thus even when allowances are made for such differences, it seems clear that such a simple dependency for ε_T is inadequate.

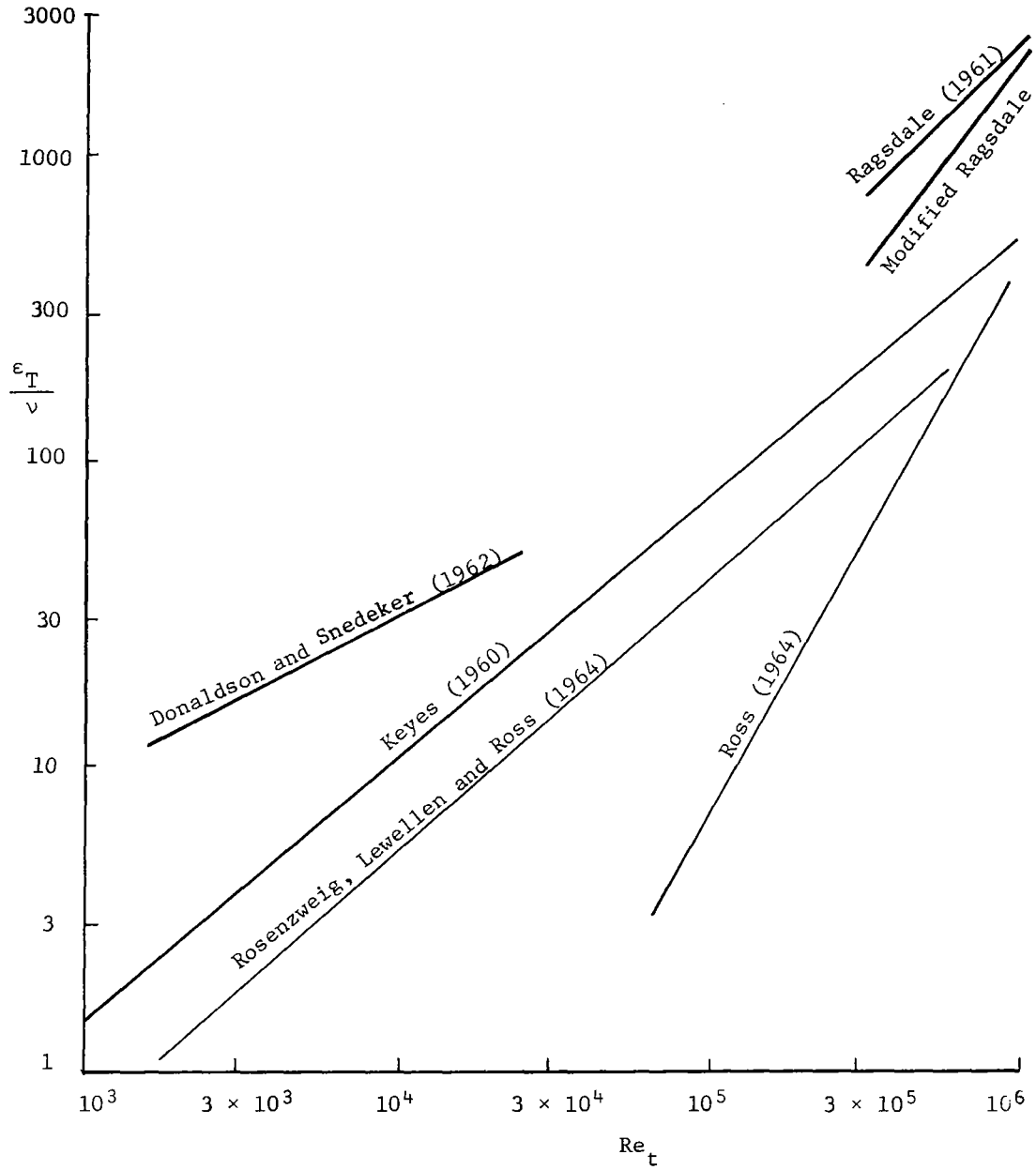

Fig. 6.1 The ratio of laminar radial Reynolds Number to "effective" radial Reynolds Number as a function of tangential Reynolds Number. The modified Ragsdale curve shows the influence of boundary-layer interaction. (Newton, 1968)

Rodoni (1969) has developed a 3 parameter correlation for ε_T/ν. With the theory of Rosenzweig, Lewellen and Ross (1964) used to compare with data obtained from a number of investigators, values of effective ε_T/ν were determined. A computer program was then written to determine what values of x, y, z would result in the least sum of the squares of the differences between the data points and a straight line curve fit for $\ln \varepsilon_T/\nu$ vs $\ln [Re_r(\ell/D)^x Re_t^y]^z$. (Here Re_r is defined the same as N in Chapter III.) The resulting correlation is given in Fig. 6.2 Although this correlation results in a modest scatter it cannot be considered particularly useful. As pointed out by Rodoni (1969) it may be interpreted as simply indicating that the effective radial Reynolds number $Re_r\nu/\varepsilon_T$ can essentially be considered to fall between 1 and 10 because this is the range of radial Reynolds number where most of the variation in velocity distribution occurs (see Fig. 3.10, for example).

The quasi-cylindrical equations have also been used to analyze the decay of a trailing vortex. Owen (1970) argues that existing wind tunnel and full scale flight data are consistent with taking

$$\frac{\varepsilon_T}{\nu} \approx 1.4 \left(Re_{t_{max}}\right)^{1/2} \qquad (6.1\text{-}10)$$

provided that the turbulence has had time to reach a fully developed state. This is a somewhat simpler problem with fewer dimensionless parameters to affect the flow than in the confined vortex. Still it appears that the flow should depend strongly on the ratio of convective velocity to maximum tangential velocity, w/v_{max}. Owen accounts for this by considering the "age" of the vortex, with Eq. 6.1-10 only applicable asymptotically. This corresponds to requiring that v_{max}/w be much less than one.

6.2 Turbulent Shear Measurements

Kendall (1962) made direct measurements of turbulent fluctuations in a jet-driven vortex for various flow rates at Re_t from 10^5 - 10^6 using a hot-wire anemometer. He found u' to be of the same order as v' and to vary from 2 to 10% of v. His measured values of $\overline{u'v'}/v^2$ correspond to ε_T/ν variations from 25 to 300. These fluctuating levels are about a factor of 3 below earlier measurements of Schowalter and Johnstone (1960) for a vortex

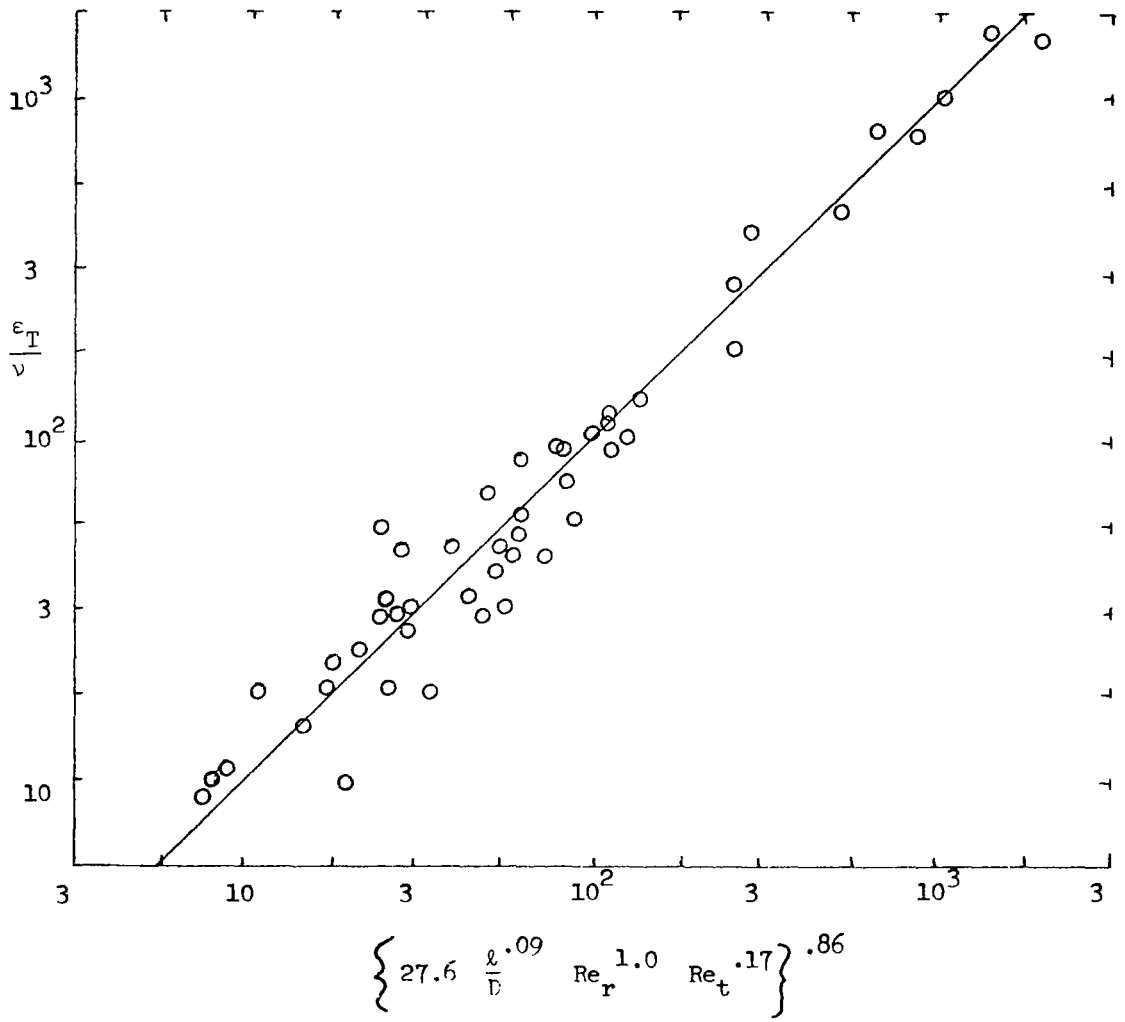

Fig. 6.2 The ratio of the turbulent "eddy" viscosity to the molecular viscosity as a function of ℓ/D, Re_r, Re_t. (Rodoni, 1969)

driven by a single large jet. Also Kendall found that using a rotating porous wall the turbulent shear stress could be reduced to the same order of magnitude as the laminar stress.

Ross (1964), in an attempt to measure turbulent shear without introducing probes into the flow, developed a vortex chamber with which it was possible to measure the angular momentum exhausting from the chamber by measuring the torque exerted on a central porous tube that extracted the angular momentum from the exit flow. Determination of the radial tangential velocity distribution thru differentiation of end wall pressure measurements then made it

possible to estimate the turbulent tangential shear stress on any cylindrical surface in the flow by applying an angular momentum balance to the control volume defined by this cylindrical surface, the two end walls and the central porous tube. The influence of the end wall boundary layers was included in this balance. Values of $\overline{u'v'}/v^2$ determined in this way were of the same order of magnitude as those measured by Kendall at similar tangential Reynolds numbers. The value of ε_T/ν evaluated by Ross in the region of the vortex where Γ is most nearly constant is included in Fig. 6.1.

These reports of large turbulent fluctuations tend to conflict with observations of apparently laminar dye fronts in some vortices as seen in Fig. 6.3 from Clark, Johnson, Kendall, Mensing and Travers (1967). These apparent contradictions can probably best be interpreted as evidence of the complex nature of turbulence in confined vortices. Regions of sharp positive radial gradients of circulation should have a strong damping effect (see Eq. 5.3-5) and thus ε_T/ν should be expected to be a strong function of radius in general.

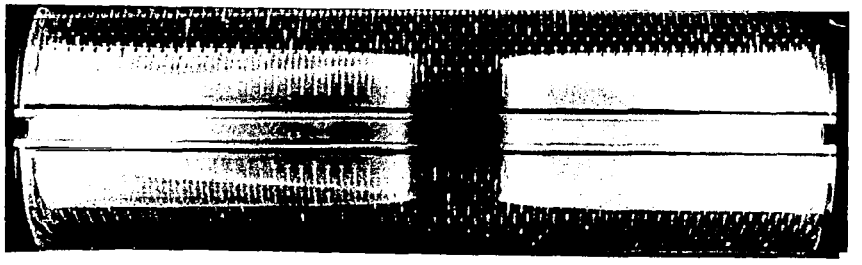

$Re_{t,j} = 120{,}000,\ Re_r = 100$

Fig. 6.3 Typical dye patterns in water vortex tubes with radial inflow. The large number of tangential jets used to drive the flow are visible. Photograph was taken approximately 5 minutes after pulses of dye were injected at the end walls. (Clark, et al 1967)

Direct turbulent shear measurements in confined vortices do not appear adequate at the present time to support a detailed correlation of turbulence with position in a confined vortex. It appears more useful to investigate the nature of turbulence near the walls in the chamber to see to what extent the wall shear may be decoupled from the general turbulence in the vortex core.

6.3 End-Wall Boundary Layer

The simplified momentum integral method outlined in Section 3.4 for the solution of the laminar end-wall boundary-layer problem was also applied to turbulent flow by Rott and Lewellen (1966). The wall shear laws assumed for this purpose were

$$\tau_\theta = C_1 \frac{\rho\Gamma^2}{r^2} \left(\frac{\nu r}{\Gamma\delta}\right)^{\bar{\mu}} \tag{6.3-1}$$

and

$$\tau_s = C_2 \rho \frac{\tilde{Q}\Gamma}{r^2\delta} \left(\frac{\nu r}{\Gamma\delta}\right)^{\bar{\mu}} \tag{6.3-2}$$

This reduces to the laminar form when $\bar{\mu} = 1$. For the turbulent case $\bar{\mu}$ may be expected to lie between 1/4, the value for the Blasius shear law (Schlichting, 1968), and $\bar{\mu} = 0$, the appropriate value for a rough surface. The only other change necessary for Eqs. (3.4-11) and (3.4-12) to apply for turbulent flow is to make appropriate changes in the velocity profile shape constants. If the velocity profiles near the wall are assumed to vary as the 1/7th power of the distance from the wall, the appropriate values to replace those given in Eq. 3.4-18 are

$$\lambda_1 = 4.9,\ \lambda_2 = 1.6 \text{ and } \lambda_3 = 0.22 \tag{6.3-3}$$

A comparison between the 1/7th power law and some measured radial velocity profiles of Owen, Hale, Johnson, and Travers (1961) are given in Fig. 6.4.

Following the procedure outlined in Section 3.4, the generalized shear laws, Eqs. 6.3-1 and 6.3-2, lead to the following generalization of Eq. 3.4-22

$$\tilde{Q} = K_2\, \nu^{2(1-\sigma)} \Gamma^{\lambda_1 - 1} \left[\int_0^s \Gamma^{2-\lambda_1/\sigma} [r(-dr/ds)]^{\frac{(1-\sigma)}{\sigma}}\, ds \right]^{\sigma} \tag{6.3-4}$$

with

$$\sigma = \frac{2+\bar{\mu}}{2(1+\bar{\mu})} \tag{6.3-5}$$

and

$$K_2 = \sigma^{-\sigma} (C_1\lambda_1)^{2\sigma-1} \left[\frac{3+2\bar{\mu}}{2+\bar{\mu}} \frac{\lambda_2}{\lambda_3} + \frac{2}{C_1} \frac{1}{\lambda_1\lambda_3}\right]^{\sigma-1} \tag{6.3-6}$$

For a potential vortex, Γ = const, over a flat disk, $dr/ds = -1$, Eq. 6.3-4 reduces to

$$\tilde{Q} = \sigma^{\sigma} K_2\, \nu^{2(1-\sigma)} \Gamma^{2\sigma-1} r_o [1 - (r/r_o)^{1/\sigma}]^{\sigma} \tag{6.3-7}$$

SYMBOL	Re_{to}	$\overline{Re}_r$	r/R	δ_θ - IN.	PROBE
□	0.90×10^5	114	0.425	0.224	PRESSURE
◇	0.90×10^5	114	0.200	0.180	HOT WIRE
▽	1.03×10^5	317	0.425	0.214	PRESSURE
△	1.03×10^5	317	0.200	0.275	HOT WIRE

— — — Profile assumed for profile constants of Eq. 6.3-3

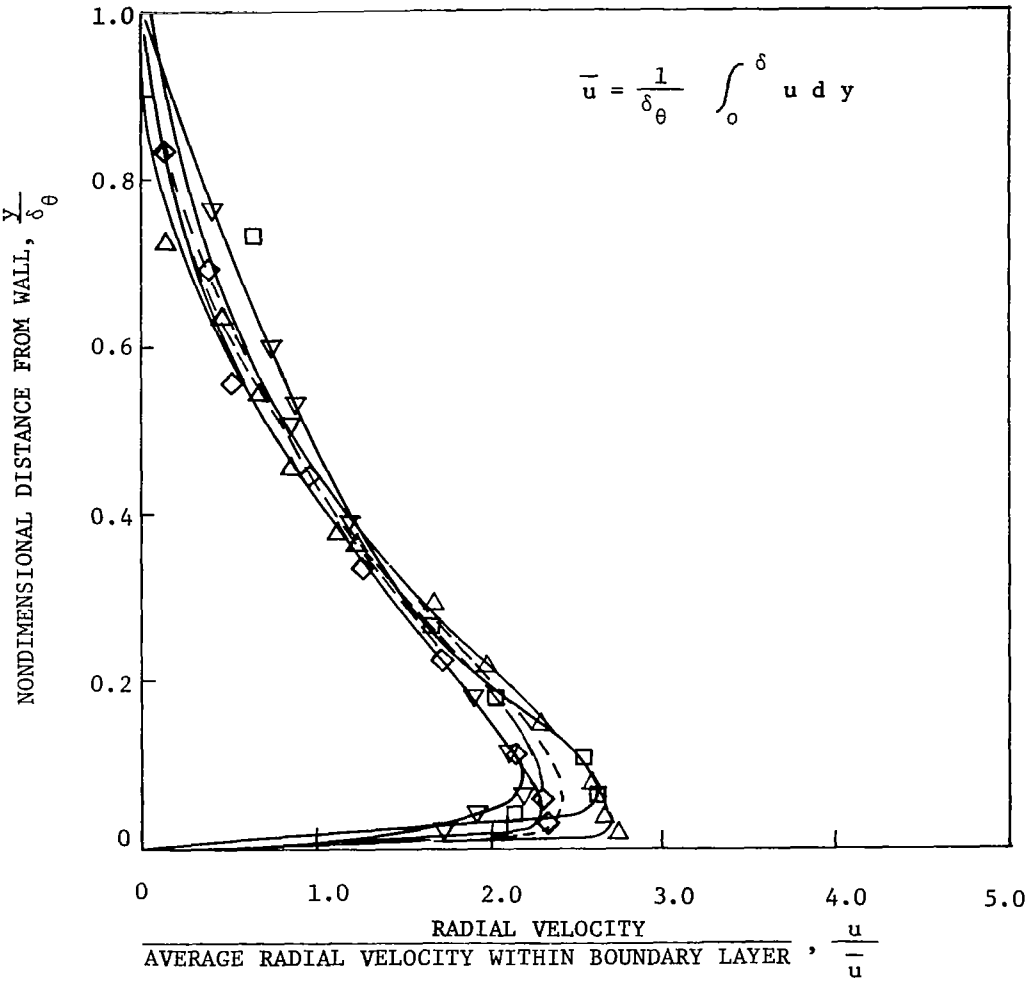

Fig. 6.4 Radial velocity profiles measured in a turbulent boundary layer. (Owen, et. al. 1961)

and the definition of the boundary-layer interaction parameter may be generalized to

$$B = 2\sigma^{\sigma} K_2 \frac{Re_t^{2\sigma-1}}{Re_r} \frac{r_o}{\ell} \tag{6.3-8}$$

As discussed in Section 3.5, a radial stagnation surface, $\hat{r}$, can occur when all of the flow passing thru a vortex chamber reaches the end-wall boundary layers. For a chamber with 2 equal, end-wall boundary layers this can occur when

$$\tilde{Q}(\hat{r}) = \frac{1}{2} \frac{\dot{m}}{2\pi\rho} \tag{6.3-9}$$

Equation 6.3-7 may be combined with Eq. 6.3-9 to give

$$\frac{\hat{r}}{r_o} = [1 - B^{-1/\sigma}]^{\sigma} \tag{6.3-10}$$

The experiments of Travers (1967) discussed in Section 5.5 provide a convenient check on this turbulent boundary-layer theory. Figure 6.5 gives a comparison of Eq. 6.3-10 for $\bar{\mu} = 1/4$ with his observed values of $\hat{r}$. For the case of the rotating peripheral wall where the experimental boundary conditions correspond closely to those assumed at $r = r_o$ in the theory, the agreement is fair. The experiment with the jet-driven vortex involves a coupling between the cylindrical side wall boundary layer and the end wall layer which apparently causes $\hat{r}$ to fall well inside of that predicted.

The uncertainty surrounding the proper constants in the shear law of Eqs. 6.3-1 and 6.3-2 makes it appealing to deal with a simplified coefficient of friction approach, i.e. $\bar{\mu} = 0$ and $C_{\perp} = C_f/2$. This leads to

$$B = \frac{2\pi\lambda_1 C_f \rho \Gamma_o r_o}{\dot{m}} = \lambda_1 C_f \frac{v_o}{u_o} \frac{r_o}{\ell} \tag{6.3-11}$$

and

$$\hat{r} = 1 - 1/B \tag{6.3-12}$$

The solid curve on Fig. 6.5 shows that Eq. 6.3-12 agrees very well with the experiment if C_f is defined so that B remains the same for both curves.

$$C_f = 0.054/Re_t^{1/5} \tag{6.3-13}$$

For $r < \hat{r}$ the boundary layer may be expected to dominate the core flow. Anderson (1961) and Rosenzweig, Lewellen and Ross (1964) have provided numerical solutions of the interaction of the present turbulent boundary-layer flow with a core flow that is assumed laminar. This interaction can be reduced to an analytic solution when $N \to \infty$. In this case the boundary-layer

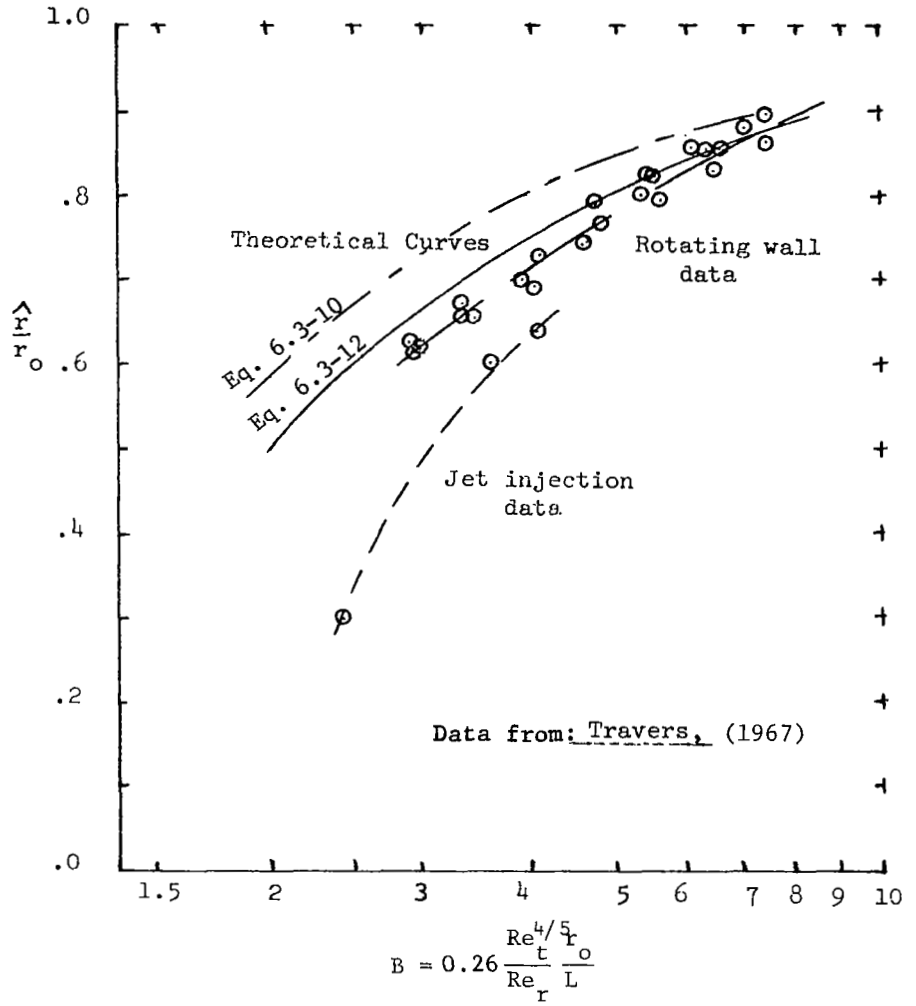

Fig. 6.5 The normalized radius of stagnation as a function of the boundary-layer interaction parameter (B).

flux must remain essentially constant for $r < \hat{r}$ and the tangential momentum equation for the boundary layer can be inverted to solve for $\Gamma(r)$. For $\tau_\theta = \frac{C_f}{2} \rho \frac{\Gamma^2}{r^2}$ and $\tilde{Q}$ = constant, Eq. 3.4-11 reduces to

$$\frac{1}{\Gamma^2} \frac{d\Gamma}{dr} = \frac{\lambda_1 C_f}{2\tilde{Q}(\lambda_1 - 1)} = \frac{2\pi\lambda C_f \rho}{\dot{m}(1-\lambda_1)} \tag{6.3-14}$$

In terms of B, this can be integrated to give

$$1/\Gamma^* = \frac{B}{1-\lambda_1} \frac{r}{r_o} + \text{const} \tag{6.3-15}$$

With $\Gamma^{\flat} = 1$ at $r = \hat{r}$ this constant can be evaluated to give

$$\Gamma^{\flat} = \frac{\lambda_1 - 1}{\lambda_1 - 2 + B(1 - \frac{r}{r_o})} \quad \text{for } r < \hat{r} = 1 - 1/B \tag{6.3-16}$$

Equation 6.3-16 is compared with the numerical solutions in Fig. 6.6. It indicates that the result expressed by Eq. 6.3-16 should suffice for $Re_r \gtrsim 10$.

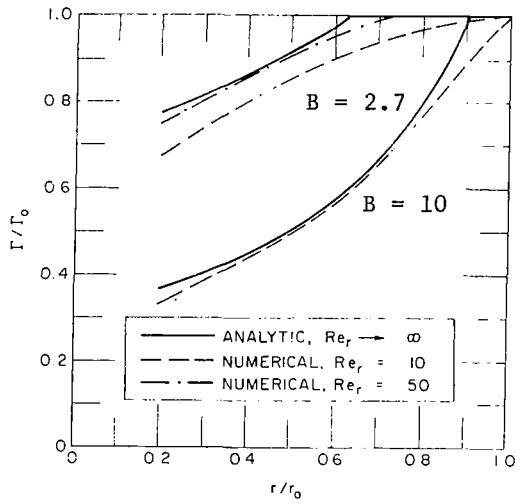

Fig. 6.6 The circulation distribution Γ in a driven vortex as a function of the radius, for two different cases of strong boundary-layer interaction (characterized by the parameter B). Numerical solutions are taken from Rosenzweig, Lewellen and Ross (1964).

Anderson (1961) worked out the turbulent boundary-layer interaction in terms of a parameter, β_T, which is directly proportional to B,

$$B = 0.13\ \beta_T \tag{6.3-17}$$

The solutions of Anderson and that of Rosenzweig, Lewellen and Ross are essentially similar. The major difference is the treatment of the boundary conditions at the exhaust. Rosenzweig, Lewellen and Ross permitted an arbitrary fraction of the flow in the end-wall boundary layer at the edge of the exhaust to be returned to the core flow before exhausting from the chamber, while Anderson assumed all of the boundary-layer flow exhausted directly thru the exhaust hole. This difference does not affect the large Reynolds number solution given by Eq. 6.3-16.

Wormley (1967) also has obtained numerical solutions for the interaction problem. Based on observations in a small L/D chamber, he postulated a model with the circulation constant outside of a stagnation radius and all of the radial flow restricted to the boundary layers for $r < \hat{r}$. His solutions are given in terms of a parameter BLC* which is closely related to B.

$$BLC^* = \frac{2r_o}{\ell} \frac{v_o}{u_o} \frac{f}{\left(\frac{u_o \ell}{2\nu}\right)} 1/4 \qquad (6.3\text{-}18)$$

with f equal to the friction factor which would be .0225 for the Blasius shear law. His results for Γ agree with Eq. (6.3-16) with the relationship between B and BLC* having a slight dependency on u_o/v_o.

Somewhat more approximate treatments of the turbulent end-wall, boundary-layer problem have been made by Schultz-Grunow (1935), Bauer (1968) and Bichara and Orner (1969). These approaches are essentially equivalent to a quasi-one-dimensional analysis in which the losses caused by shear to the end walls are averaged over the total flow at each radial station. The angular momentum equation may be written in this approximation as

$$\frac{d\Gamma}{dr} = \frac{4\pi\rho}{\dot{m}} \frac{C_f}{2} \Gamma^2 \qquad (6.3\text{-}19)$$

In general this can be expected to give a good approximation for the radial variation of Γ when appropriate choices of C_f are made since it only varies by a proportionality constant from Eq. 6.3-14. Consequently these approaches should be valid for determining the radial pressure distribution across the vortex but give no indication of the strong effect of secondary flows on the streamline patterns within the vortex.

Figure 6.5 can be taken as support for the C_f variation in Eq. 6.3-13 when the circulation remains constant. Determination of an appropriate C_f for the more general case is still uncertain. Figure 6.7 is a comparison of Eq. 6.3-13 with integrated torque measurements by Ross (1964). It indicates that a stronger dependence on Re_t would be required to agree with his measurements. A stronger dependence was also indicated by the correlation obtained by Rodoni (1969) by comparing the circulation ratio between the edge of the exhaust and that near the outer radius of the chamber,

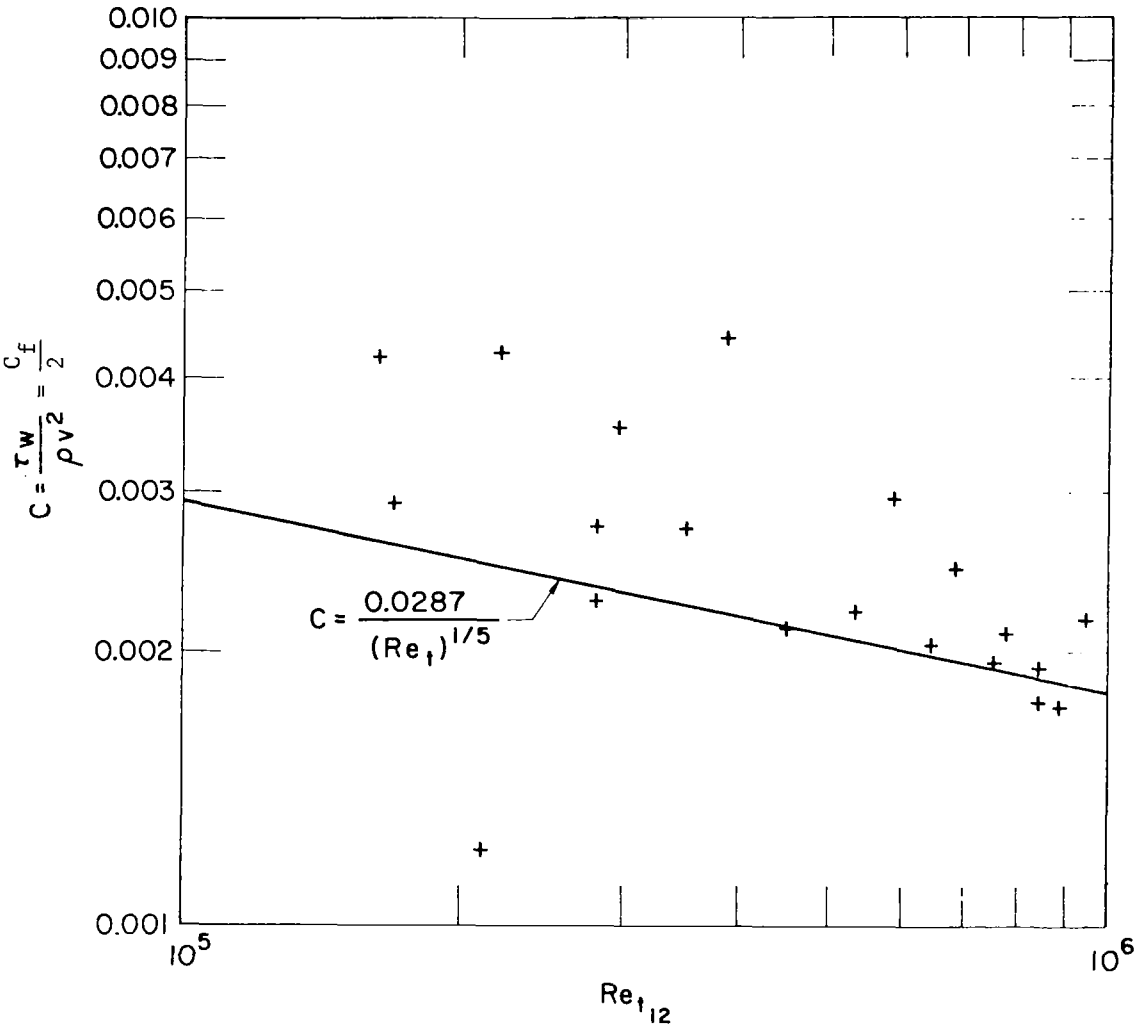

Fig. 6.7 End-wall shear stress coefficient, c, vs tangential Reynolds number Re_t based on the principal circulation in the chamber. (Ross, 1964)

Γ_e/Γ_o, reported by a number of investigators with that obtained by integrating Eq. 6.3-19. His correlation is given in Fig. 6.8. A rather unexpected strong dependence on L/D is indicated.

An even stronger Reynolds number dependence was needed by Bichara and Orner (1969) to make their numerical results agree with experiments. They used

$$C_f = 2.9/(Re_{t_i})^{.405} \qquad (6.3\text{-}20)$$

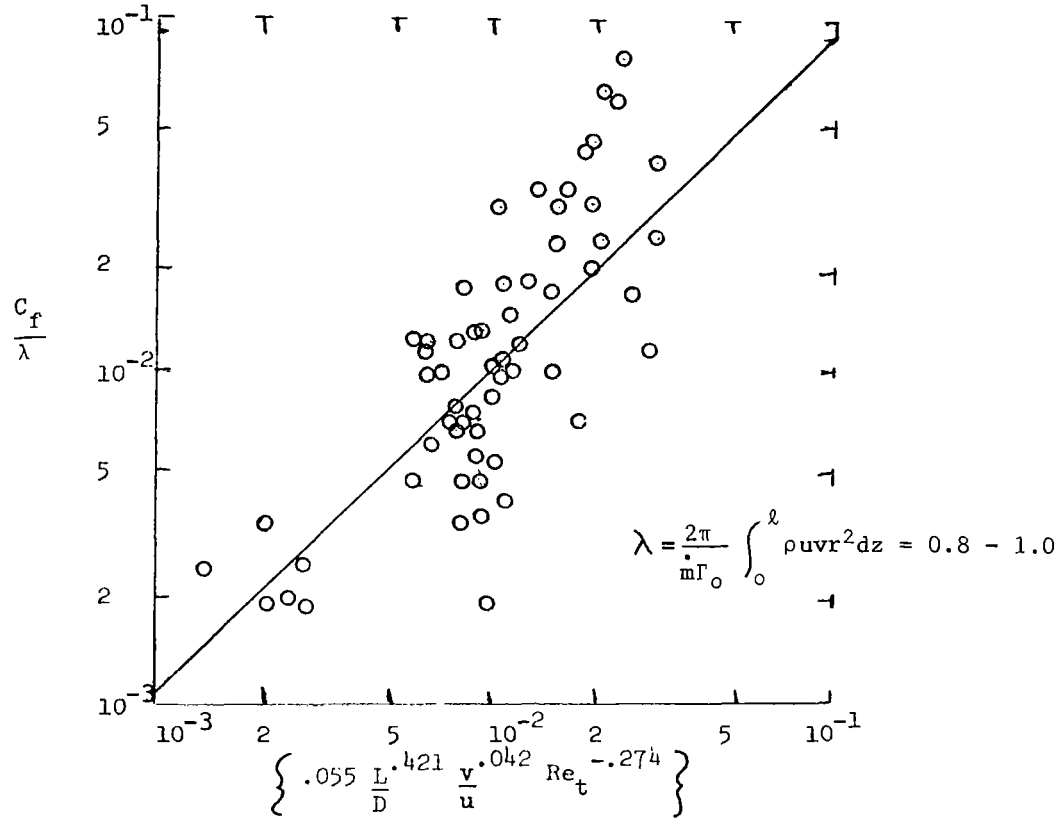

Fig. 6.8 The variation of the effective end-wall skin friction coefficient with L/D, v/u, and Re_t. (Rodoni, 1969)

Another view of the L/D dependence observed by Rodoni is given in Fig. 6.9 which compares Eq. 6.3-16 with experimental values of Γ_e/Γ_o. The theory indicates that the only dependence of Γ_e/Γ_o on L/D should be accounted for in the linear variation of B with D/L, but the experimental variation is a much weaker dependence of Γ_e/Γ_o on L/D. In Fig. 6.8 this shows up as a variation of C_f with L/D. Perhaps the most appropriate interpretation is that there is a coupling between the shear losses on the wall and the general turbulence in the chamber.

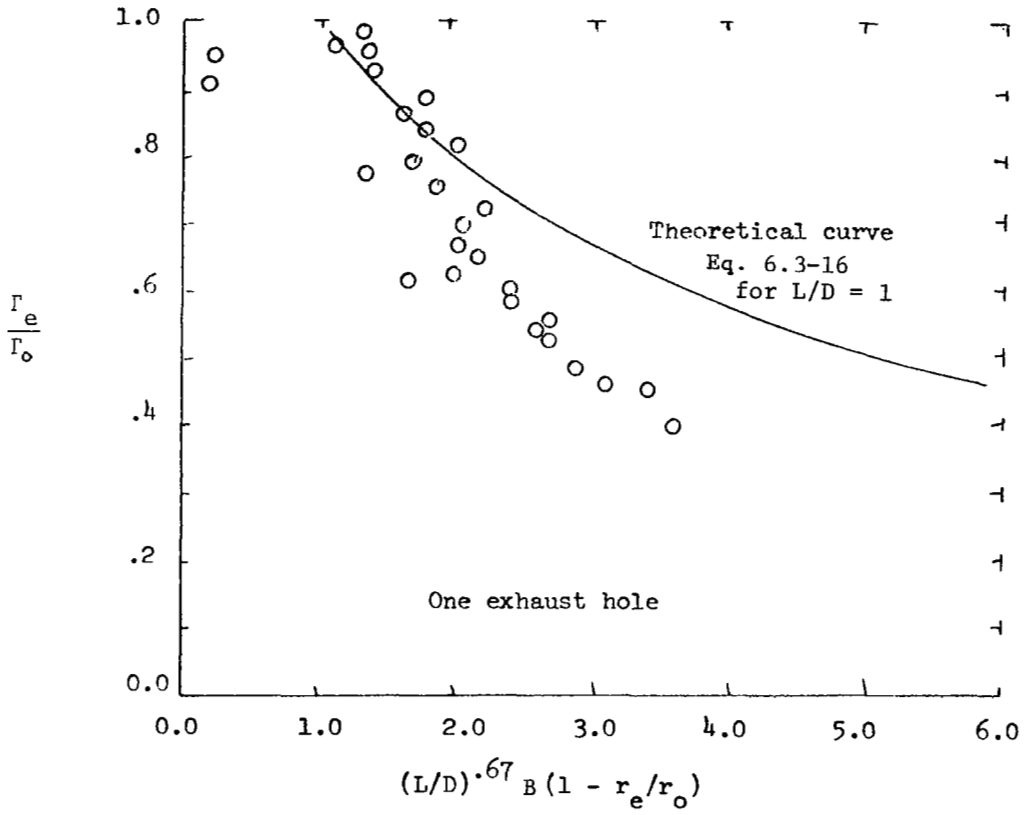

Fig. 6.9 The circulation ratio as a function of L/D, r_e/r_o, and the boundary layer interaction parameter for incompressible flows.

6.4 Cylindrical Wall Boundary Layer

Since the confined vortex is usually driven by tangential injection of fluid near the outer wall it is necessary to consider losses that occur due to shear on the cylindrical wall. This problem was considered for laminar flow in Section 3.8. Equation 3.8-1 may be applied to turbulent flow if τ_w is interpreted as the turbulent wall shear and μ in the last term is replaced by ε_T.

$$\dot{m}\,\Gamma_i = \dot{m}\,\Gamma_o + 2\pi r_o^2 \ell \tau_w - 2\pi r_o \ell \varepsilon_T \frac{2\Gamma_o}{r_o} \qquad (6.4\text{-}1)$$

The difficulty in applying this equation, of course, is involved in the uncertainty in these two parameters τ_w and ε_T. Most attempts at semi-empirically determining the jet recovery factor, Γ_o/Γ_i, have neglected the last term involving ε_T. Thus implying that the wall boundary layer can be decoupled from the vortex core.

Kendall (1962) estimated values of Γ_o from end wall pressure distributions and used Eq. 6.4-1 with the last term neglected to determine τ_w. On this basis he found τ_w to be only about 10% above that which would be predicted for turbulent flow over a flat plate at the same Reynolds number based on the peripheral path length, $2\pi r_o$, and the wall velocity, Γ_o/r_o.

With $\tau_w = \frac{C_f}{2} \rho_o v_o^2$ and the last term neglected, Eq. 6.4-1 may be written as

$$\frac{\Gamma_o}{\Gamma_i} = \frac{1}{1 + \frac{C_f}{2} \frac{v_o}{u_o}} \tag{6.4-2}$$

Alternatively when all of the flow is introduced tangentially, with no compressibility effects

$$\frac{v_o}{u_o} = \frac{2\pi r_o \ell}{A_i} \quad \frac{\Gamma_o}{\Gamma_i} = \frac{A_w}{A_i} \frac{\Gamma_o}{\Gamma_i} \tag{6.4-3}$$

and Eq. 6.4-2 may be written in the form given by Roschke (1966)

$$\frac{\Gamma_o}{\Gamma_i} = \frac{[(2\ C_f\ A_w/A_i) + 1]^{1/2} - 1}{C_f\ A_w/A_i} \tag{6.4-4}$$

Equation 6.4-4 is plotted in Fig. 6.10 with a number of experimental points from various investigators reviewed by Rodoni (1969). The general trend of the curve is supported but a wide variation in C_f is required to explain the scatter in the curve. A correlation of C_f as a function of tangential Reynolds number based on a comparison between this figure and Eq. 6.4-4 shows that it is equivalent to setting

$$C_f = \frac{0.29}{Re_t^{0.275}} \tag{6.4-5}$$

This is substantially different than that which would be predicted by the Blasius expression for a flat plate of length $2\pi r_o$, i.e.

$$C_f = \frac{0.052}{Re_t^{.2}} \tag{6.4-6}$$

The large values of C_f obtained cannot be explained in terms of the ε_T term which was neglected in reducing Eq. 6.4-1 to 6.4-4. Including this term would only serve to increase the empirical values of C_f since it represents angular momentum which is transmitted by shear in the fluid radially outward to the cylindrical wall layer. One reason for the higher values of C_f is that local jet velocities may be much higher than the v_o which is used in the

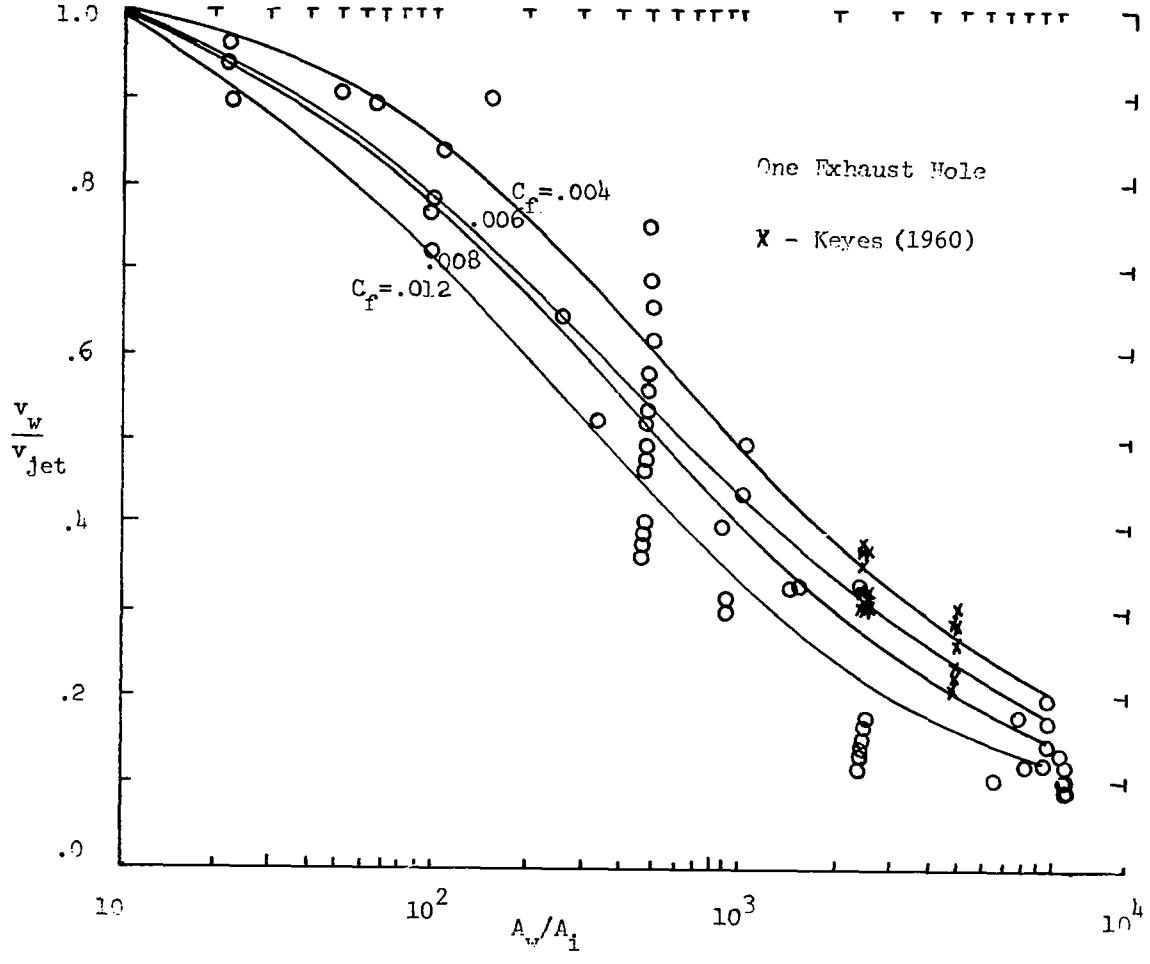

Fig. 6.10 The recovery factor as a function of A_w/A_i with C_f as a parameter. (Rodoni, 1969)

definition of C_f. A better correlation is obtained if the wall velocity is assumed to vary from v_i to v_o in one pass around the periphery. In this case (Felsing, Mockenhaupt, and Lewellen, 1970)

$$\dot{m}dv = \frac{-C_f}{2} \rho_o v^2 \, 2\pi \ell dr \tag{6.4-7}$$

which may be integrated to give

$$\frac{\Gamma_o}{\Gamma_i} = [1 + \frac{C_f}{2} \frac{v_i}{u_o}]^{-1} = [1 + \frac{C_f A_w}{2 A_i}]^{-1} \tag{6.4-8}$$

This is equivalent to setting $\tau_w = \frac{C_f}{2} \rho_o v_o v_i$ in Eq. 6.4-1. Equation 6.4-8

is compared with some experimental points in Fig. 6.11. The scatter is reduced from that in Fig. 6.10. A value of C_f given by Eq. (6.4-6) may be used in conjunction with Eq. 6.4-8 to give a reasonable estimate of Γ_o/Γ_i, particularly at moderate values of A_w/A_i.

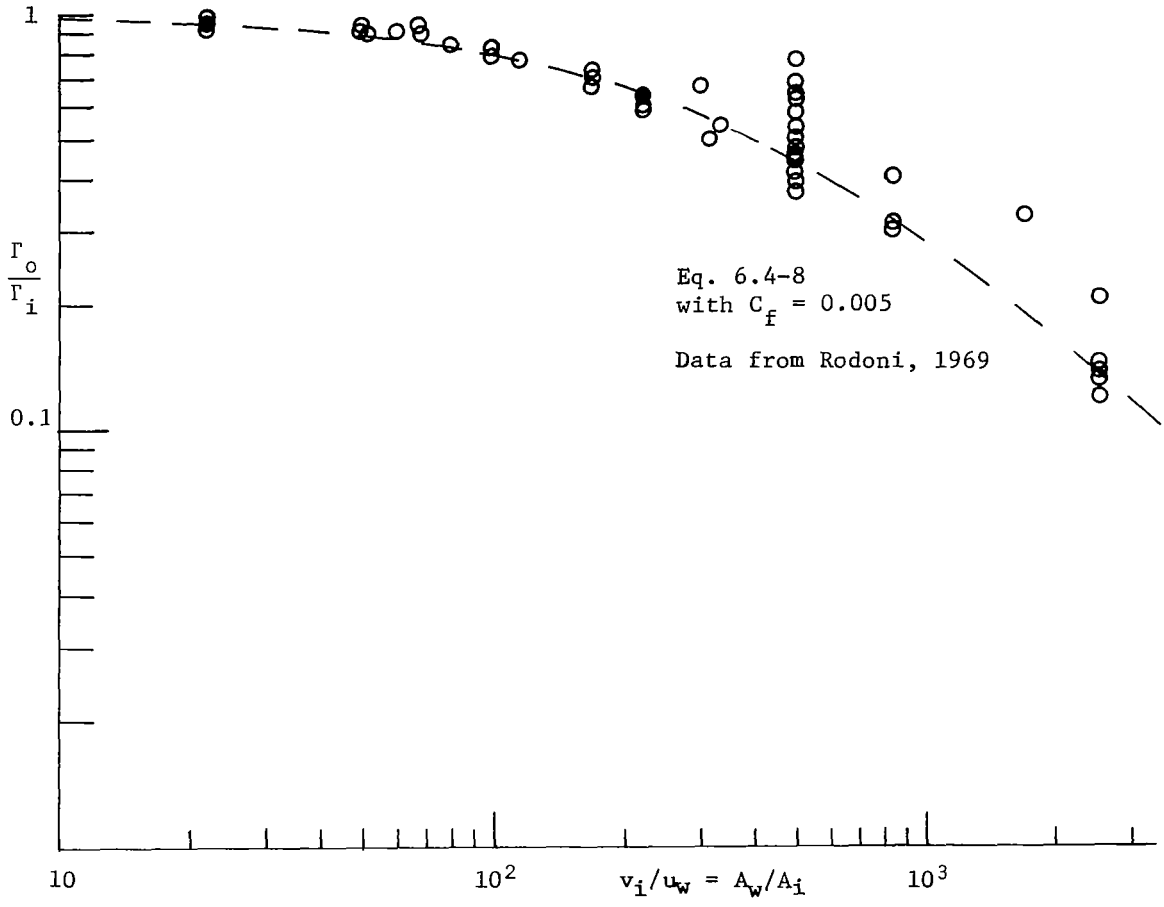

Fig. 6.11 Jet recovery factor as a function of velocity ratio, or equivalently the ratio of wall area to jet injection area.

A strictly empirical correlation for the recovery factor obtained by Rodoni (1969) is given in Fig. 6.12. The data scatter shows little improvement over that in Fig. 6.11 considering the large number of exponents which were allowed to vary in obtaining the correlation. It does have about the same relationship between A_w/A_i and Re_t which would be predicted by the preceeding angular momentum balance. In addition it shows a dependence on overall chamber geometry including the exhaust geometry.

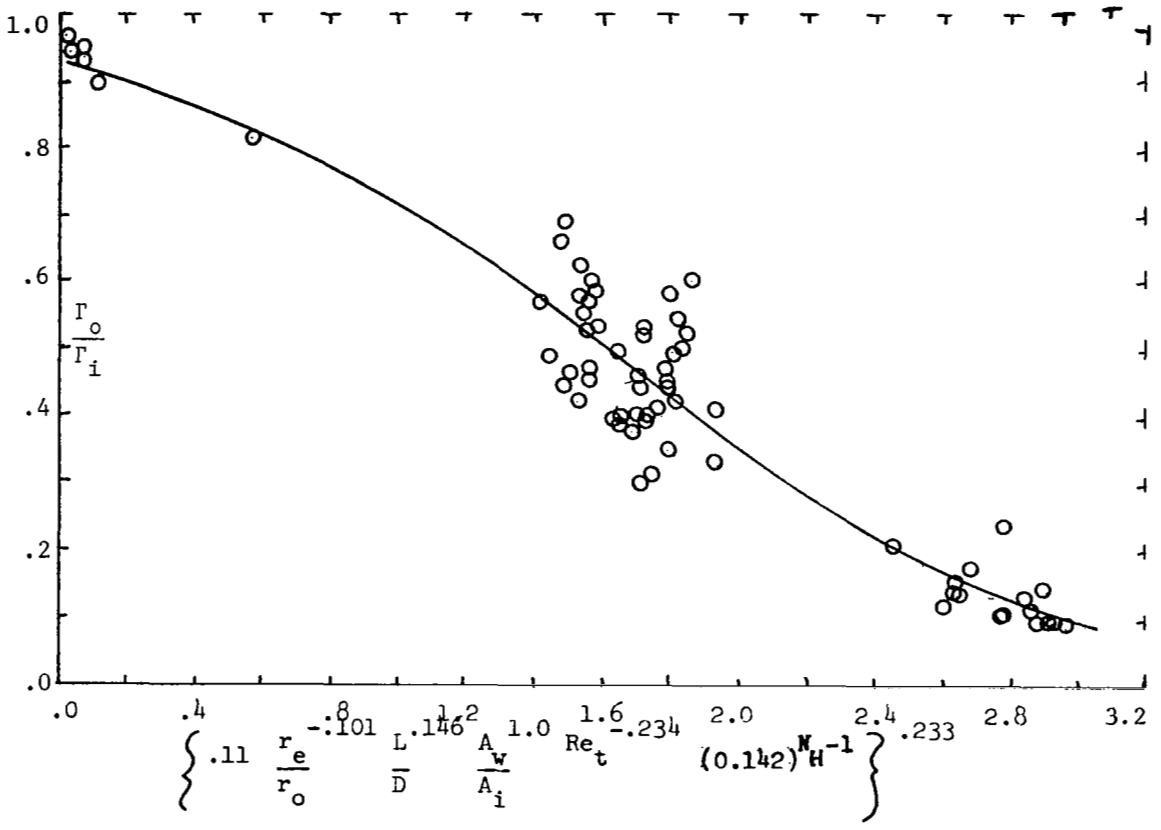

Fig. 6.12 The recovery factor as a function of r_e/r_o, L/D, A_w/A_i, N_H, and Re_t (Rodoni, 1969).

The dependency on exhaust geometry can best be interpreted in light of the argument of Section 6.5. If the angular momentum per unit mass flow is bounded by the exhaust constraint, then an injection arrangement which introduces angular momentum per unit mass flow larger than this bound must necessarily result in large dissipation on some of the walls within the chamber. The ratio of cylindrical-wall losses to flat-end-wall losses is determined by the injection geometry and the L/D of the chamber.

Little is known about the influence of compressibility on the recovery factor. Keyes (1960) indicated that the recovery factor was a strong function of injection Mach number as seen in Fig. 6.13. However, in his experiments Keyes held the product of the mass flow times the square of the injection Mach number to be constant by changing the injection area, such

that the velocity ratio v/u is being varied. Thus Keyes variation with M is quite consistent with Eq. 6.4-8 and no direct conclusions regarding injection Mach number dependence can be drawn.

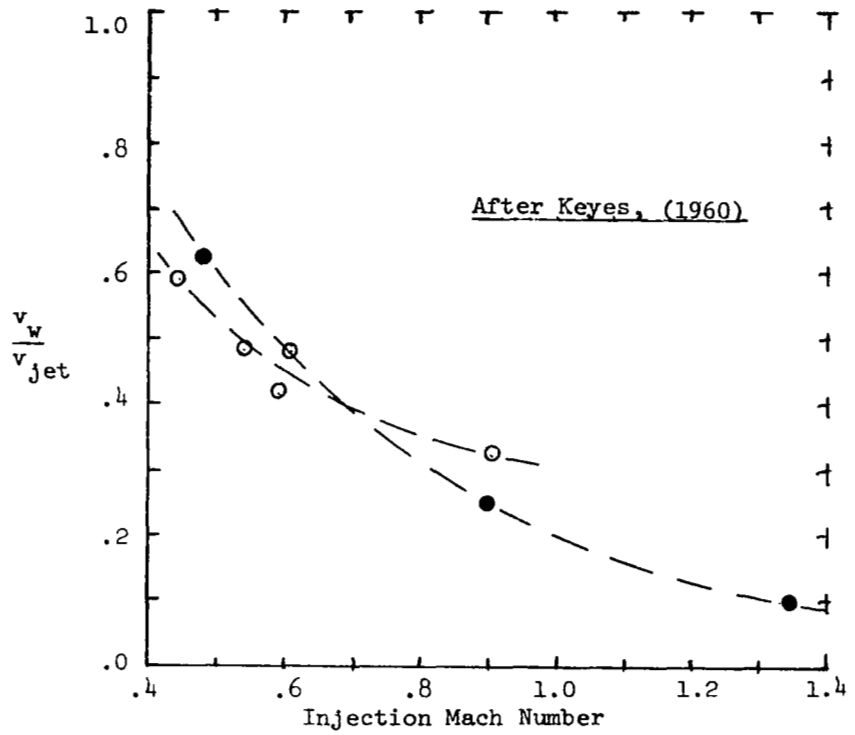

Fig. 6.13 The recovery factor as a function of the Mach number of injection with $\dot{m}\, M_j^2$ fixed.

6.5 Exhaust Constraint

In Chapters 2 and 3 the strong influence of swirl on the relationship between flow and pressure drop for a given exhaust geometry was discussed. To see how this relationship may be coupled with turbulence in the chamber it is useful to replot Fig. 2.3 to present mass flow as a function of angular momentum as given in Fig. 6.14. It may be observed that angular momentum flux is a maximum for intermediate values of swirl. The shape of this curve suggests (Lewellen, Burns and Strickland, 1969) that it may be impossible to

operate the exhaust flow stabily at values of the swirl parameter $\alpha > \hat{\alpha}$ with $\hat{\alpha}$ defined as that value which corresponds to the maximum value of angular momentum. This speculation is supported by the following stability argument which shows that a vortex chamber will have an inviscid instability when α is slightly larger than $\hat{\alpha}$.

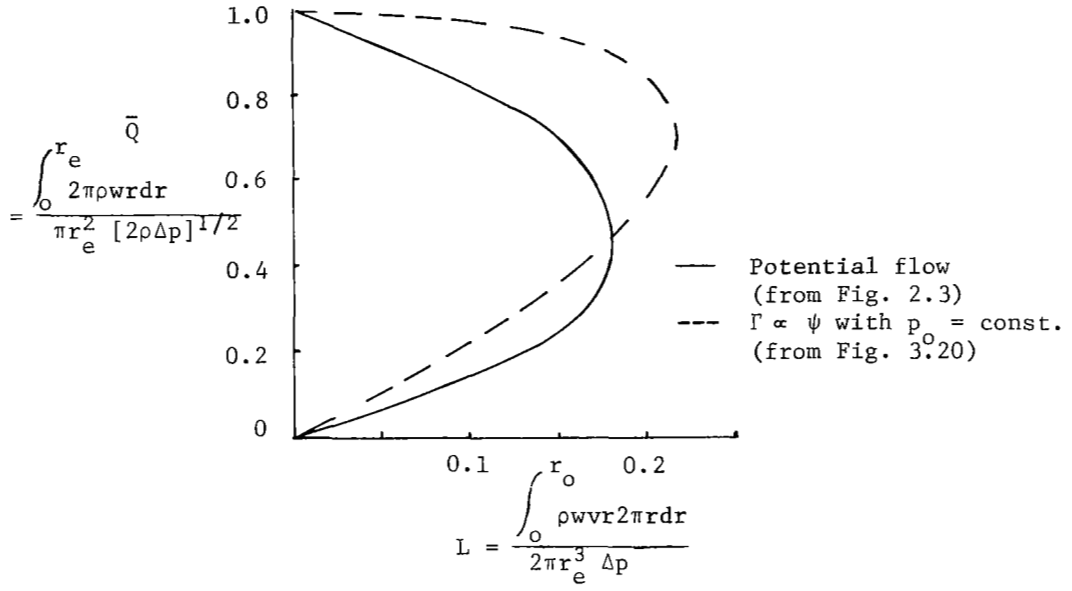

Fig. 6.14 Dimensionless exhaust flow as a function of angular momentum flux

A necessary condition for inviscid stability can be obtained by considering the dependence of chamber flow on wall pressure. For small disturbances from an equilibrium operating point the instantaneous rate of change of wall pressure with time should be proportional to the difference between the mass flow into the chamber and the mass flow out, i.e.,

$$\frac{\partial p_w}{\partial t} = C\ (\dot{m}_{in} - \dot{m}_{out}) \tag{6.5-1}$$

where C is a positive constant which would be a function of geometry and the equation of state of the fluid. For small changes $\dot{m}_{in}$ and $\dot{m}_{out}$ may be approximated as

$$\dot{m}_{in} = \dot{m}(0) + \frac{\partial \dot{m}_{in}}{\partial p_w} [p_w - p_w(0)] \tag{6.5-2}$$

and

$$\dot{m}_{out} = \dot{m}(0) + \frac{\partial \dot{m}_{out}}{\partial p_w} [p_w - p_w(0)] \tag{6.5-3}$$

Equations 6.5-1 thru 3 may be combined to give

$$\frac{\partial p_w}{\partial t} = C \left[\frac{\partial \dot{m}_{in}}{\partial p_w} - \frac{\partial \dot{m}_{out}}{\partial p_w}\right] \left[p_w - p_w(0)\right] \tag{6.5-4}$$

If a perturbation in p_w is to damp out and the flow be stable, it may be seen from Eq. 6.5-4 that it is necessary to have

$$\frac{\partial \dot{m}_{out}}{\partial p_w} > \frac{\partial \dot{m}_{in}}{\partial p_w} \tag{6.5-5}$$

The stability criterion given in Eq. 6.5-5 may be related to the $\bar{Q}(L)$ curve of Fig. 6.15 by first normalizing with respect to the mass flow thru the chamber which would exist at the same wall pressure, ambient exhaust pressure, density and exit area if there were no swirl, i.e.

$$\bar{Q}_{out} = \frac{\dot{m}_{out}}{\dot{m}(p_w, p_a, \rho, A_e)_{\text{no swirl}}} \tag{6.5-6}$$

and

$$\bar{Q}_{in} = \frac{\dot{m}_{in}}{\dot{m}(p_w, p_a, \rho, A_e)_{\text{no swirl}},} \tag{6.5-7}$$

then by noting that for inviscid flow with no dissipation within the chamber

$$L = \left[\frac{\rho_e}{\rho_i} \frac{A_e}{A_i} \frac{r_w}{r_e}\right] \bar{Q}_{in}^2 \tag{6.5-8}$$

when all of the flow is injected tangentially into the chamber at radius r_w at a density ρ_i thru an injection area A_i. At the equilibrium point Eq. 6.5-5 may now be written as

$$\frac{\partial \bar{Q}_{out}}{\partial p_w} > \frac{\partial \bar{Q}_{in}}{\partial p_w} \tag{6.5-9}$$

For a given vorticity distribution in the exhaust, $\bar{Q}_{out}$ is a function only of L, thus Eq. 6.5-9 may be written with the aid of Eq. 6.5-8 as

$$\frac{d\bar{Q}_{out}}{dL} \frac{\partial L}{\partial p_w} > \frac{\bar{Q}_{in}}{2L} \frac{\partial L}{\partial p_w} + \bar{Q}_{in} \frac{\partial (\ln \rho_i/\rho_e)}{\partial p_w} \tag{6.5-10}$$

All of the derivatives with respect to p_w in Eq. 6.5-10 should be negative, so that it is equivalent to

$$\frac{d\bar{Q}}{dL} < \frac{\bar{Q}_{in}}{2L} + \bar{Q}_{in} \left(\frac{\partial (\ln \rho_i/\rho_e)}{\partial p_w} \Big/ \frac{\partial L}{\partial p_w}\right) \tag{6.5-11}$$

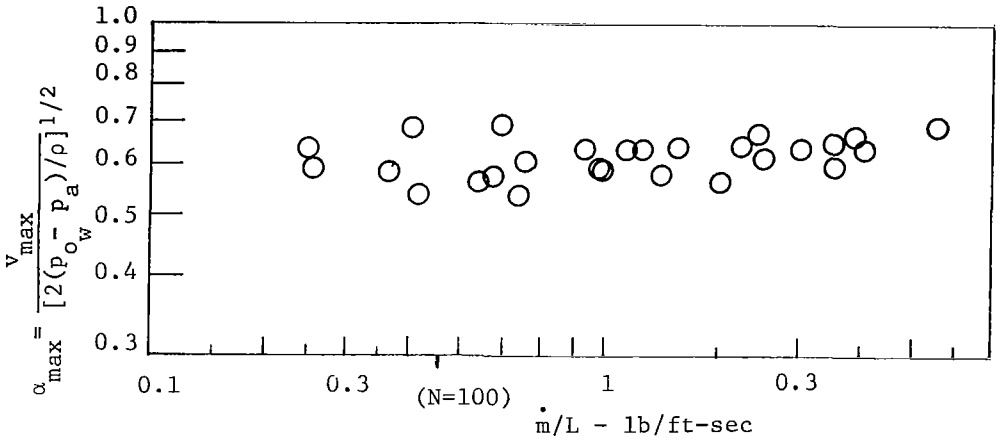

Fig. 6.15 A plot of v_{max} as a function of mass flow (or N) for different values of L/D and r_e/r_w (Data taken from Roschke, 1966).

From Fig. 6.14 it may be observed that $d\bar{Q}/dL > 0$ for $\alpha > \hat{\alpha}$ and in fact $d\bar{Q}/dL \to +\infty$ as α is decreased towards $\hat{\alpha}$. Thus there will always be a region of $\alpha > \hat{\alpha}$ in which the condition given in Eq. 6.5-11 is not satisfied. For incompressible flow with no dissipation of angular momentum within the chamber, the criterion given in Eq. 6.5-11 reduces to

$$\frac{L}{\bar{Q}} \frac{d\bar{Q}}{dL} < \frac{1}{2} \tag{6.5-12}$$

It is not possible to say that all operating points on Fig. 6.14 with $\alpha > \hat{\alpha}$ are necessarily unstable but there must be a region of $\alpha > \hat{\alpha}$ which corresponds to unstable operating points. A bound on α imposes a bound on v_{max}/w_{max} as elluded to in Section 5.6.

Roschke (1966) has carefully documented flow distributions in an incompressible vortex for a number of different values of r_e/r_w, L/D, and N. The value of α, based on the maximum value of v and the difference between the total pressure at the wall and atmospheric pressure to which the flow is exhausting, is plotted in Fig. 6.15 as a function of N. Although there is some scatter to the data, a constant value of $\alpha_{max} \approx 0.6$ is indicated. If constant total pressure is assumed, this corresponds to $v/w = \frac{3}{2}$ at this point.

Kolf (1956) developed an empirical relationship for the effect of swirl on the discharge coefficient, C_D, for free-surface flow of a liquid thru a thin-plate orifice. He found

$$C_D = 0.686 - 0.218\ V' \tag{6.5-13}$$

where V' is defined as the ratio of the circulation ($2\pi rv$) at twice the orifice radius divided by the product of the orifice diameter and the average thru flow velocity thru the exhaust. In terms of the notation of Eq. 6.5-13 this parameter which has been referred to by some of his colleagues as the Kolf number may be written as

$$V' = \frac{\pi \Gamma_{2r_e}}{\Gamma_e} \frac{\alpha}{\bar{Q}} \tag{6.5-14}$$

A plot of a large number of data points from Zielinski and Villemonte (1968) is given in Fig. 6.16. Since Γ_{2r_e}/Γ_e must always be greater than or equal to 1, it may be seen that $\alpha/\bar{Q}$ was always less than 1 for the wide variety geometries and fluids tested. Although unrelated to the present argument it is also interesting to note the departure of the data from the correlation for small swirl. This is probably a result of the low C_D for the no swirl condition. Initially the swirl can reduce the separation of the flow from the thin orifice enough to counterbalance the effect of reducing the center pressure.

A limit on swirl angle in the exhaust should also show up as a constraint on core radius r_c/r_e. The core present in our idealized inviscid exhaust model is highly distorted by momentum diffusion. The readily observable experimental parameter which is more closely related to r_c is the radial position of the maximum tangential velocity, $r_{v_{max}}$. For short chambers, $\ell/r_e = 0(1)$ these two should be closely related while at large values of ℓ/r_e, momentum diffusion should permit the angular momentum to penetrate to smaller radii at the chamber wall opposite the exhaust. Figure 6.17 is a plot of $r_e/r_{v_{max}}$ as a function of ℓ/r_e for available incompressible data ($M_{t_{max}} \lesssim 0.6$). The correlation is quite reasonable when allowances are made for the difficulties in obtaining accurate experiment values of $r_{v_{max}}$. Note that $r_{v_{max}}$ is determined from end wall pressure distributions and thus is being measured at the wall opposite the exhaust.

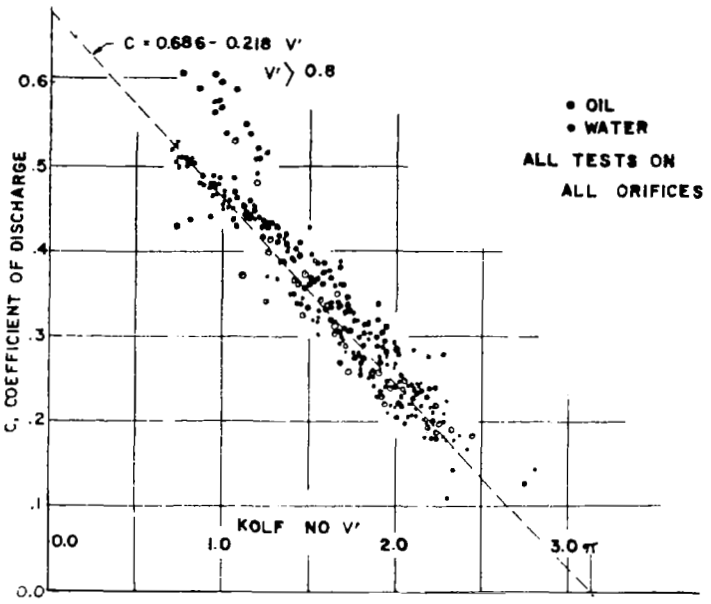

Fig. 6.16 Coefficient of discharge versus Kolf number (Zielinski and Villemonte, 1968).

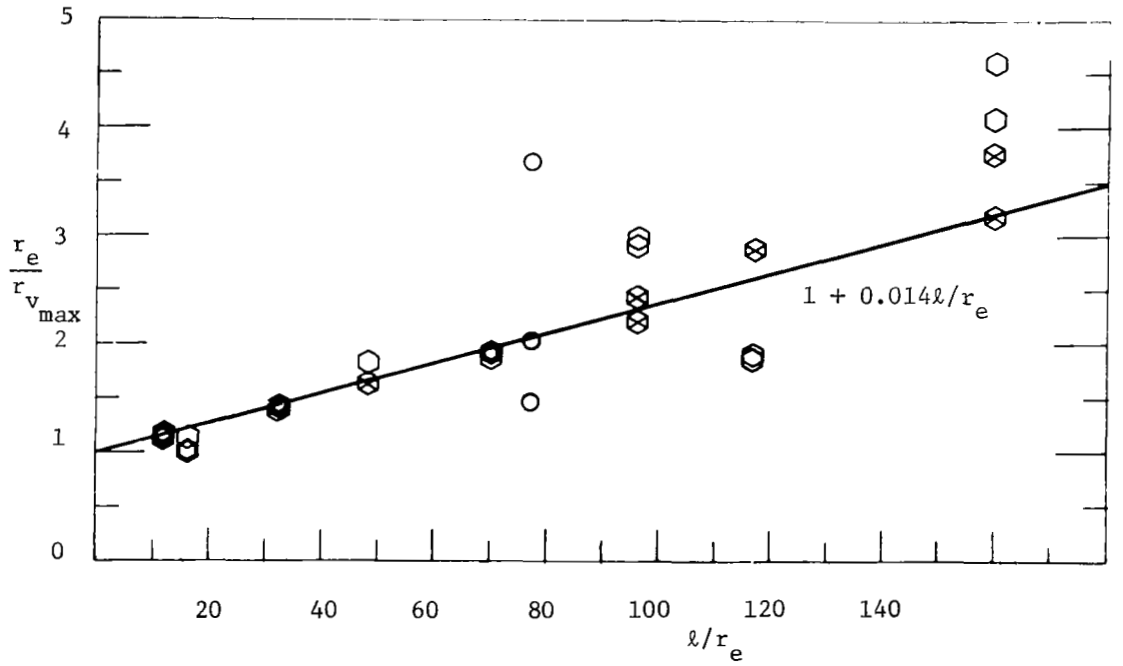

Fig. 6.17 Radial position of the maximum tangential velocity as a function of ℓ/r_e for various values of N and r_e/r_w. Data taken from Roschke, 1966.

The experimental evidence for a stability limit on swirl in the exhaust also is evident for compressible flow. In this case, a bound on the swirl angle in the exhaust implies a bound on tangential Mach number, M_t. Lewellen, Burns and Strickland (1969) predicted a maximum M_t of 1.2 for $\gamma = 1.4$. Several investigators have found experimentally that M_t reaches a limit as the pressure ratio across a vortex chamber is increased as illustrated in Fig. 6.18. Roschke and Pivirotto (1965) reported an $M_{t\ max} = 1.05$, Toomre (1963) a value of 1.03 and Pinchak and Poplawski (1965) reported an $M_{t\ max} = 1.18$ in a vortex chamber designed especially to circumvent the difficulties of end-wall dissipation. There are two reported cases in the literature of M_t exceeding the value of 1.2. Keyes (1960) shows a tangential Mach number distribution obtained in a 1-inch-diameter tube that reaches a value of 1.4 near the center and Gyarmathy (1969) reports a value of 1.6 for essentially the same set up as used by Pinchak and Poplawski. With these notable exceptions the experimental evidence tends to confirm the speculation that flows with $M_t \gtrsim 1.2$ would be unstable.

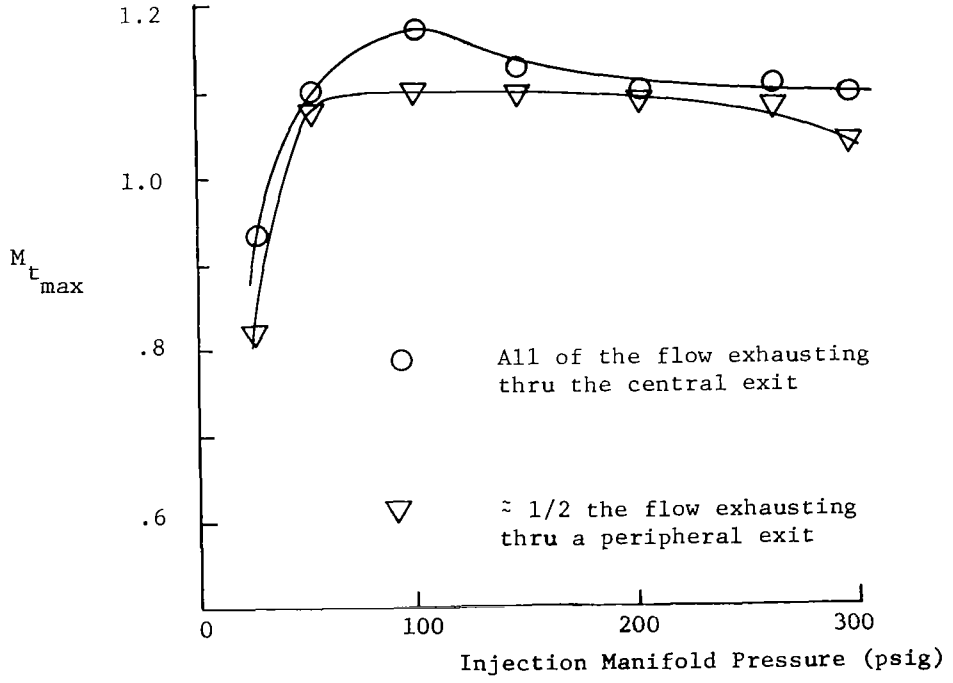

Fig. 6.18 The variation of the maximum Mach number with the injection manifold pressure [Poplawski and Pinchak, (1965)].

How does this bound on angular momentum flux thru the exhaust affect the turbulence generated within the chamber? The complete relationship is unclear at the present time. However, a recent paper by Cassidy and Falvey (1970) contains a possible clue. They found that the vortex becomes unsteady with the vortex core moving in a helical pattern when the angular momentum flux is sufficiently large relative to the flux of linear momentum. Figure 6.19 is a plot of their observed frequency as a function of the momentum parameter. The pressure flucuations were felt throughout the flow, even in the upstream plenum. The frequency falls off to zero somewhere around $L/\pi\bar{Q}^2 \simeq 0.2$. The profiles used in obtaining Fig. 6.14 lead to maximum values of $L/\pi\bar{Q}^2 = 0.14$ and 0.23 for $\Gamma \propto \psi$ and for potential flow, respectively. Thus it appears that when the maximum values of L indicated in Fig. 6.14 are exceeded the flow becomes unsteady. Additional angular momentum can then be carried by the vortex core spiraling around the axis of the flow. It is clear that all of the angular momentum which enters the chamber must either be dissipated as torque on the internal surfaces of the chamber or flow thru the exhaust. Any upper bound on the fraction of angular momentum flux passing thru the exhaust then must imply a lower bound on the fraction of angular momentum dissipated by torque on the wall. If the torque on the walls which would be obtained with local wall induced turbulence is below this lower bound, then the unsteadiness induced by the exhaust constraint may act to increase the general intensity of turbulence within the chamber to result in an increase in wall torque.

If the dissipation in a vortex chamber is to be completely controlled by the exhaust constraint, then the combination of Eqs. 6.5-13 and 6.4-3 would give the ratio of the circulation of the edge of the exhaust to the ideal injected circulation as a function of geometry only.

$$\frac{\Gamma_e}{\Gamma_i} = \frac{\alpha}{\bar{Q}} \frac{A_i}{\pi r_w r_e} \tag{6.5-15}$$

Figure 6.20 gives a correlation obtained by Rodoni (1969) for Γ_e/Γ_i. Although this correlation does retain a rather strong dependence on Re_t it does indicate that there is a flow mechanism coupling the interior flow with the flow near the walls. It also indicates that it would be an over simplification to say that the exhaust completely controls the dissipation within the chamber.

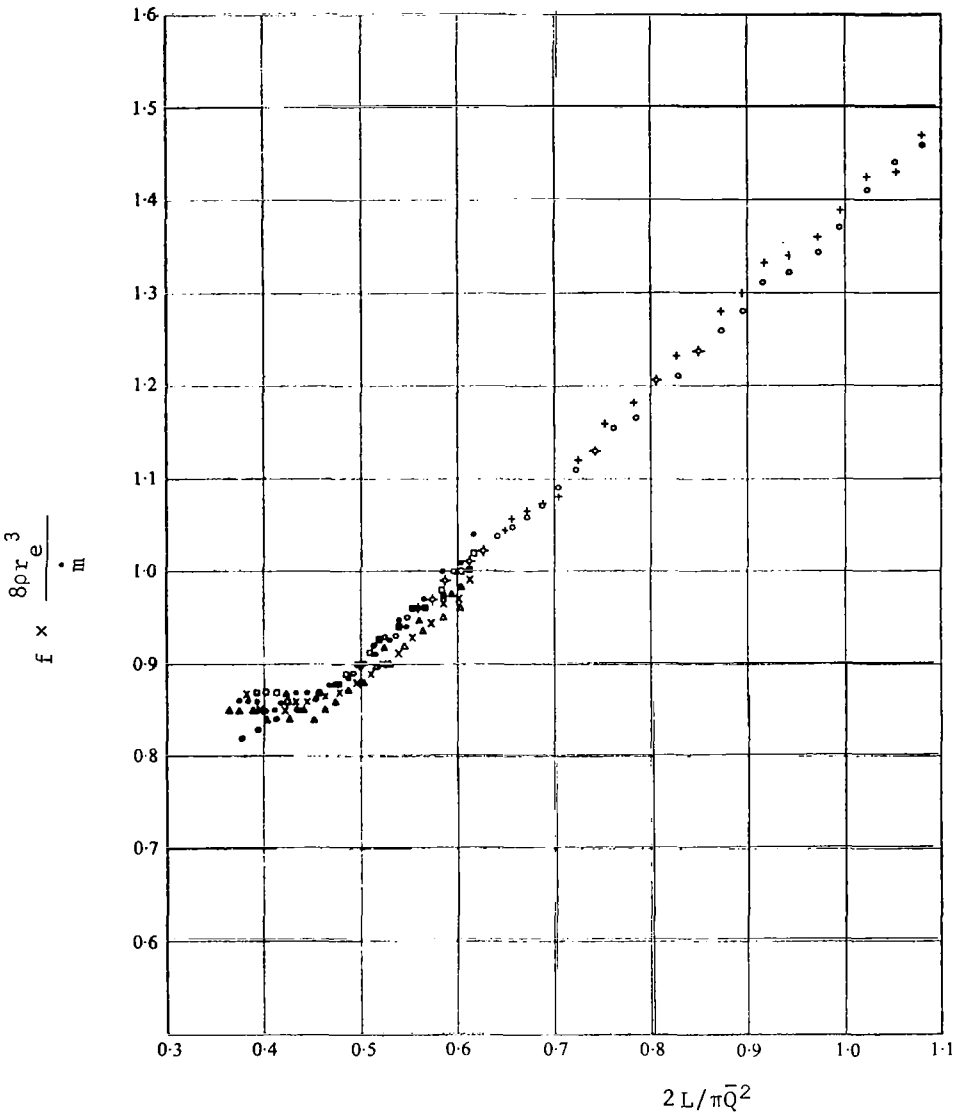

Fig. 6.19 Frequency, f, as a function of angular momentum. (Cassidy and Falvey, 1970)

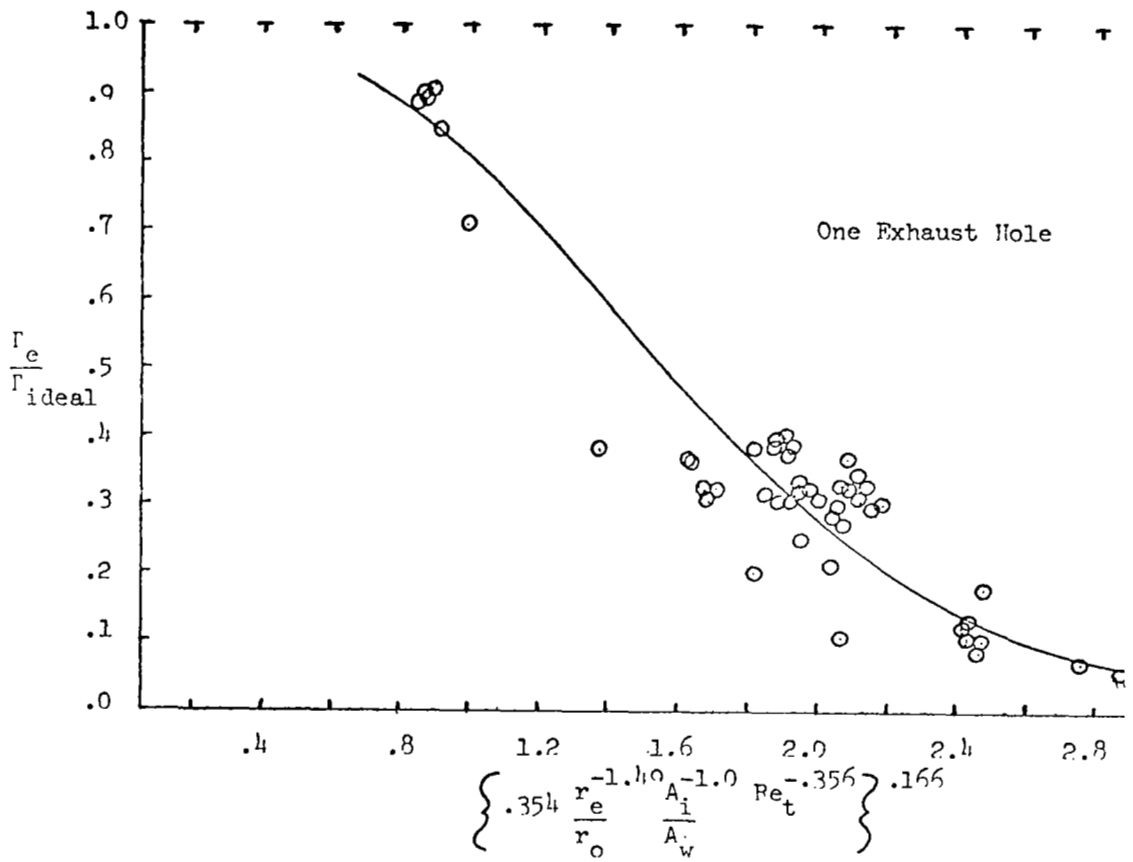

Fig. 6.20 The ideal circulation ratio as a function of the radius ratio, the wall area ratio, and the tangential Reynolds number.

6.6 Empirical Correlations

Since an adequate knowledge of turbulence in a confined vortex is not currently available to theoretically predict all the flow parameters it appears useful to determine what correlations may be obtained by empirical methods to predict turbulent results. Such a study has been carried out by Newton (1968) and Rodoni (1969). Data from some 29 different reports in the literature were used. A computer program was written to find optimum groupings of independent flow parameters which would best fit certain dependent parameters to a given curve.

Using this curve fitting method, empirical correlations were attempted for the ratio of the tangential velocity at the peripheral wall to the jet

injection velocity (v_w/v_{jet}), the ratio of the tangential to radial velocities (v/u), the ratio of the circulation ($\Gamma = vr$) at the radius of the exhaust hole to the circulation just outside of the peripheral wall boundary layer (Γ_e/Γ_o), the ratio of the circulation at the radius of the exhaust hole to the maximum achievable circulation(Γ_e/Γ_{ideal}), the ratio of the mass flow through the vortex to the "no-swirl" mass flow ($\bar{W}_o$), and the maximum tangential Mach number in the vortex ($M_{t_{max}}$). Several of these correlations have already been presented in Figs.6.2, 6.8, 6.9, 6.10, 6.12 and 6.20

One of the best correlations achieved in this work was for the normalized mass flow ratio ($\bar{W}_o$). The empirical correlation shown in Fig. 6.21 allows the prediction of the mass flow ratio $\bar{W}_o$ for a vortex in terms of the parameters r_e/r_o, the ratio of the exhaust hole radius to the outer wall radius; A_i/A_e, the ratio of inlet area to the exhaust area; ℓ/D, the length-to-diameter ratio of the chamber; and N_H, the number of exhausts. It was found that $\bar{W}_o$ was primarily a function of r_e/r_o and ℓ/D for $L/D > 2$ and primarily a function of r_e/r_o, only when $\ell/D < 2$.

The correlations shown in Figs. 6.22 and 6.23 show that the velocity ratio $(v/u)_o$ is a function of the parameters r_e/r_o and L/D as well as the area ratio A_i/A_w predicted by the momentum balance theory. The presence of these geometrical terms not predicted by the momentum balance theory tends to indicate the coupling of the exhaust constraint to the wall shear as discussed in the last section. Note that thru Eq. 6.4-3 these two correlations for $(v/u)_o$ may also be used to estimate recovery factor, Γ_o/Γ_i.

No satisfactory correlation for the maximum tangential Mach number was achieved. This failure was primarily due to the scarcity of data points available, but may also be partially explained by the argument of the last section that M_t can reach an absolute maximum which is a function of γ only. Most of the data points available operated well below this upper bound and thus would be expected to show a geometry and pressure ratio dependence incompatible with those few data points which were operating near the maximum M_t.

These empirical correlations should prove helpful to anyone designing a vortex tube for a particular purpose but they appear inadequate to provide

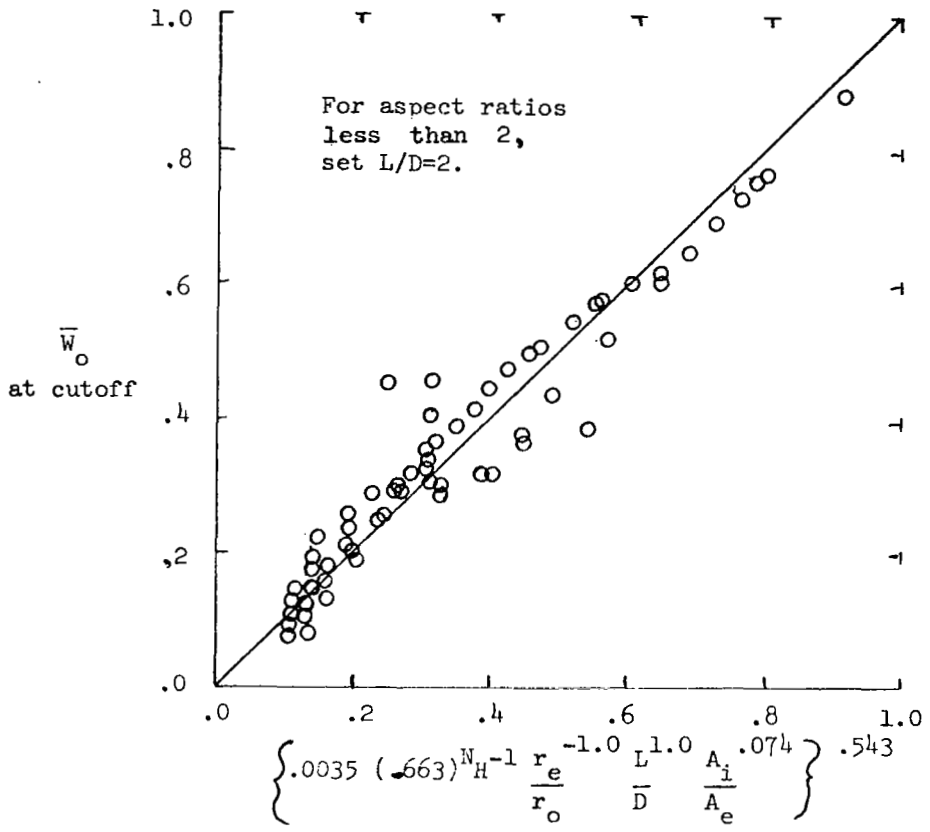

Fig. 6.21 The ratio of the mass flow through the vortex chamber to the "no-swirl" mass flow as a function of r_e/r_o, the ratio of the exhaust hole radius to the outer wall radius; A_i/A_e, the ratio of the inlet area to the exhaust area; L/D, the length-to-diameter ratio of the chamber and N_H, the number of exhausts. (Rodoni, 1969)

the basis for a general theory of turbulence in a confined vortex flow. An attempt to determine a natural Reynolds number for confined vortices has lead R. N. Kumar to the correlation given in Fig. 6.24. The parameter most closely related to dissipation in the chamber which is readily available is the ratio of the circulation at the edge of the exhaust to that imparted to the flow by the inlet tangential jets. Plots of Γ_e/Γ_o vs. a Reynolds number based on $r_{v_{max}}$ (note that the unknown $r_{v_{max}}$ may be determined in terms of geometrical parameters from Fig. 6.17) demonstrated that the data fell in a number of bands. It was then possible to collapse these into one band

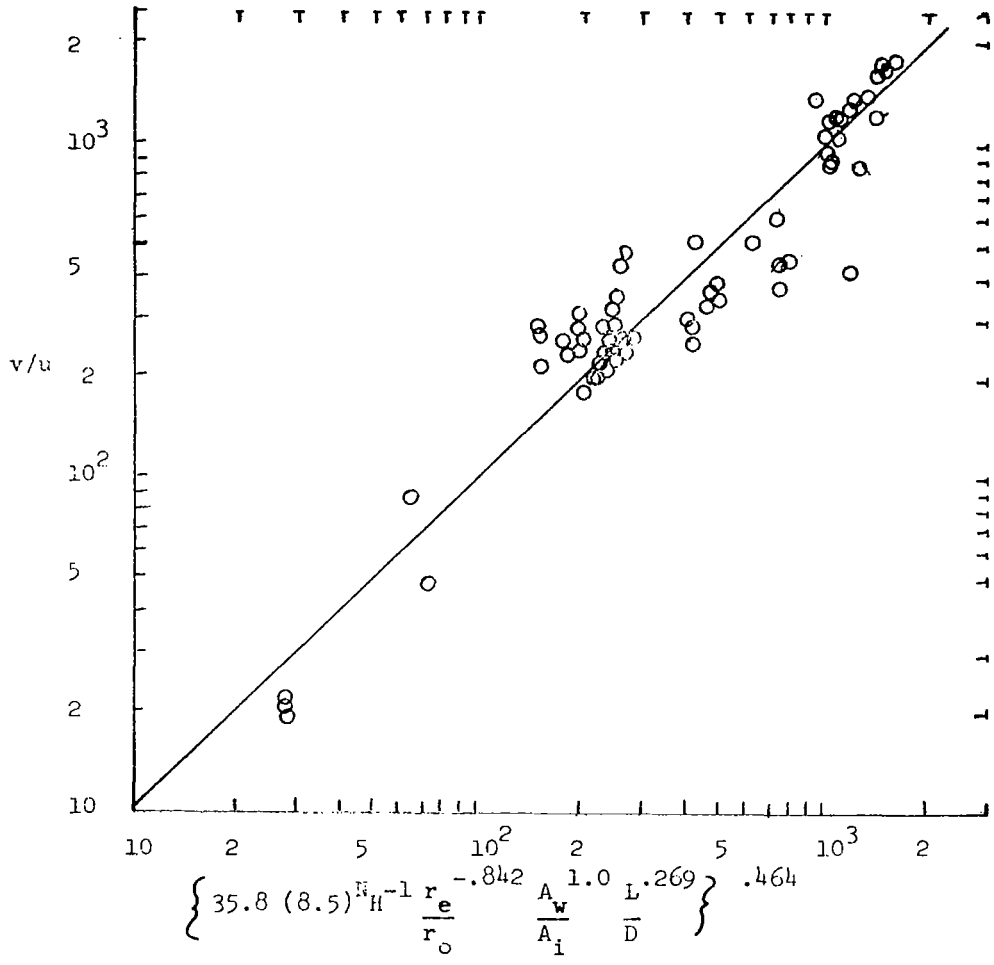

Fig. 6.22 The velocity ratio as a function of r_e/r_o, A_w/A_i, L/D, and N_H (Rodoni, 1969).

with the combination given in Fig. 6.24. The abscissa is the product of the inlet tangential Reynolds number, $Re_i = \rho_i\ v_i\ r_w/\mu$, and $r_{v_{max}}/r_e$. The square root of A_e/A_i enters the ordinate. This correlation should prove more useful to anyone designing a vortex tube than that given in Fig. 6.20. However a great deal of work remains before a general turbulent theory can be achieved.

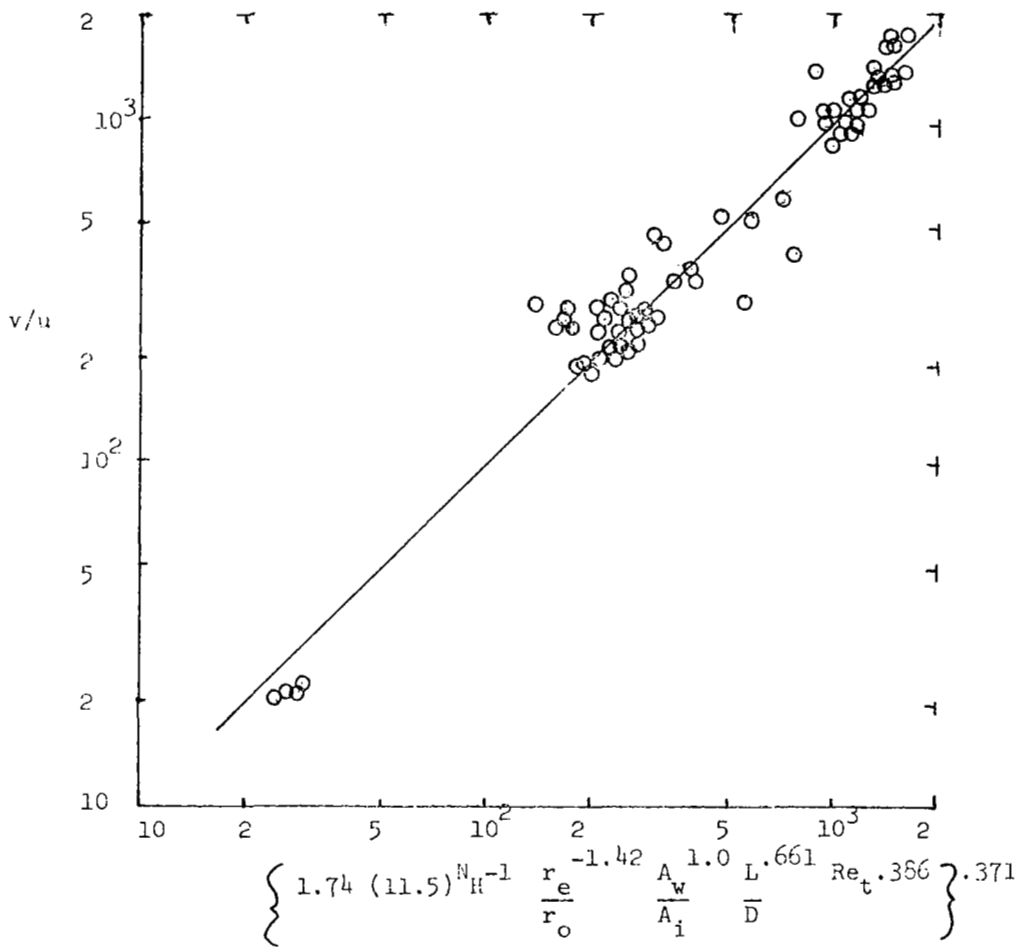

Fig. 6.23 The velocity ratio as a function of r_e/r_o, A_w/A_i, L/D, N_H, and Re_t (Rodoni, 1969).

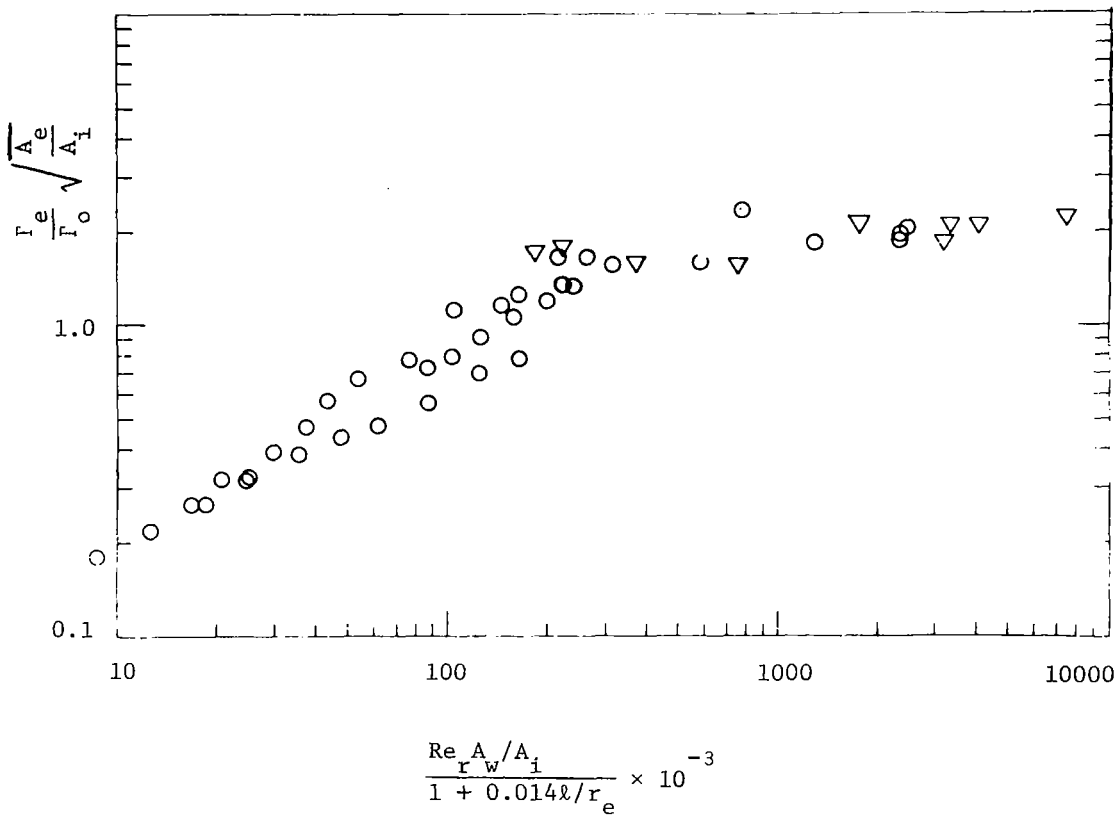

Fig. 6.24 Correlation of dissipation in a vortex chamber as a function geometry and inlet Reynolds number. Data taken from literature survey of Rodoni (1969). Points marked by ∇ have high enough Mach numbers for compressibility to be important.

VII. THE VORTEX AS A FLUIDIC DEVICE

7.1 Introduction

The technology of controlling fluid flow without using mechanically moving parts has come to be known as fluidics. The use of a small control flow to introduce swirl into the flow which one desires to control is one popular way of achieving this. Vortex devices may be used in a number of different ways (Mayer and Taplin, 1965) but the most basic of these is as a flow modulator. The resistance for flow thru an orifice can be increased by introducing swirl into the flow. The effect of a small swirl can be greatly amplified by allowing the flow to converge radially before passing thru the orifice.

In previous chapters, the influence of swirl on the relationship between pressure drop across an orifice and the mass flow thru it has been analyzed in terms of a swirl parameter α. This parameter defined as the ratio of the swirl velocity at the edge of the exhaust to the square root of twice the energy available to the flow, must be related to valve characteristics and geometry in order to predict valve performance. A typical valve geometry is shown in Fig. 1.2. It is characterized by its small length-to-diameter ratio (to minimize internal surface area for a given radius ratio) and the two types of inlets; one which introduces the flow into the chamber with no angular momentum, typically the supply port; and one which introduces angular momentum into the chamber, typically the control port.

The outline of this chapter will be to first analyze valve performance for the simplest possible mode of operation, incompressible flow with the supply pressure and the outlet pressure held constant. Then other modes of operation will be discussed.

7.2 Incompressible Valve with Supply and Outlet Pressures Held Constant

The results of Section 2.2 may be used to determine flow thru the valve as a function of control flow or control pressure for the valve geometry given in Fig. 1.2. From Eq. (2.2-8) the swirl parameter α was defined as

$$\alpha \equiv \frac{\Gamma_e}{r_e[2(p_s - p_a)/\rho]^{1/2}} \qquad (7.2\text{-}1)$$

and the dimensionless flow thru the chamber from Eq. (2.2-9) as

$$\bar{Q} \equiv \frac{\dot{m}}{\pi r_e^2 [2\rho(p_s - p_a)]^{1/2}} \tag{7.2-2}$$

Vortex valve performance may be conveniently given in terms of the dimensionless flow thru the valve $W_o = \dot{m}_o/\dot{m}_{o\ max}$ and the dimensionless control flow $W_c = \dot{m}_c/\dot{m}_{o\ max}$. It can be readily seen that

$$W_o = \bar{Q} \tag{7.2-3}$$

The average tangential velocity, v_w, at the inlet of the valve, assuming conservation of angular momentum in the mixing process, may be written as

$$v_w = \frac{\dot{m}_c v_c}{\dot{m}_o} = \frac{\dot{m}_c^2}{\rho_c A_c \dot{m}_o} \tag{7.2-4}$$

where the subscript c denotes the value associated with the control flow and A_c is the control port area. This permits the swirl parameter α to be written as

$$\alpha = \frac{\Gamma_e r_w W_c^2 A_o}{\Gamma_w r_e W_o A_c} \tag{7.2-5}$$

with A_o the outlet port area. For the ideal case of no dissipation within the valve $\Gamma_e/\Gamma_w = 1$ and Eq. (7.2-5) may be rearranged to give

$$W_c \left[\frac{r_w}{r_e} \frac{A_o}{A_c}\right]^{1/2} = [\alpha \bar{Q}]^{1/2} \tag{7.2-6}$$

The transformation given by Eqs. (7.2-3) and (7.2-6) may be used to transform Fig. 2.3 into a plot of W_o vs. W_c. Such a curve is given in Fig. 7.1 from Strickland (1968) labeled as $K = \infty$. A typical experimental curve from Wormley (1967) also is included for comparison. The agreement between theory and experiment is poor. The comparison for part of the curve can be improved by including the effects of vorticity in the outlet flow as was done in Section 3.6. The curve for circulation proportional to the stream function with constant total pressure transformed from Fig. 3.20 is given here as $K = 0$.

The two basic requirements for this simple theory to be valid are (a) that the valve outlet is the major obstruction to the flow and (b) that dissipation by shearing losses on the walls be negligible. The first of these is satisfied if $\ell/r_e \geq 2$ and the ratio of the supply port to the outlet is ≥ 4. As long as $\ell/D \ll 1$, shear losses on the flat end walls may be expected

to be more important than that on the cylindrical side wall. Losses on these end walls may be conveniently measured in terms of the boundary-layer interaction parameter B, defined in Eq. 3.5-3 for laminar flow and Eq. 6.3-11 for turbulent boundary layers. In terms of the vortex valve notation this parameter may be written as

$$B = \frac{1}{N_H} \frac{A_o}{A_c} \left[\frac{r_w}{r_e} \frac{W_c}{W_o}\right]^2 \times \begin{cases} 5.04/Re_t^{1/2} - \text{Laminar} \\ 10\ c_f - \text{Turbulent} \end{cases} \tag{7.2-7}$$

with N_H = 1 or 2 depending upon whether the valve has a single exhaust or dual exhaust. For the boundary-layer effect to be negligible, B should be less than approximately 1/2. It is clear that as $W_o \to 0$, B will exceed 1, and the boundary-layer effect will become dominant.

Since flow in the valve is usually turbulent the point on the curve in Fig. 7.1 at which the boundary-layer effects become important will be determined principally by the radius ratio. If the radius ratio is sufficiently large the slope of the curve ($\partial W_o / \partial W_c$) remains negative and the operation of the valve is termed "proportional". On the other hand for more modest values of r_w/r_e there is a portion of the curve where $\partial W_o / \partial W_c > 0$ as seen in Fig. 7.2. From Section 6.5 it may be deduced that the flow is statically unstable at the points where $\partial W_o / \partial W_c \to \infty$. When the valve is being turned down the flow jumps along the dotted line (1) and as it is turned up along the dotted line (2). A valve with this type of performance curve is termed "bistable" due to the two potentially stable operating points for a single value of W_c over a portion of the curve.

The performance curve is terminated at the point where the supply flow is shut off and $W_c = W_o$. The reciprocal of W_o at cutoff is termed the turndown ratio, TDR. Theoretical prediction of the turndown ratio calls for a solution to the turbulent exhaust problem for conditions under which the flow in the chamber is completely dominated by the end wall boundary layers. Before considering this, it is desirable to look at some experimental results. As long as the valve is properly designed and the Reynolds number is sufficiently large, TDR should be a function of r_w/r_e and A_o/A_c only. Note, in particular, that neither the inviscid curve nor the boundary-layer interaction parameter depends on the length of the chamber. Since only two principal

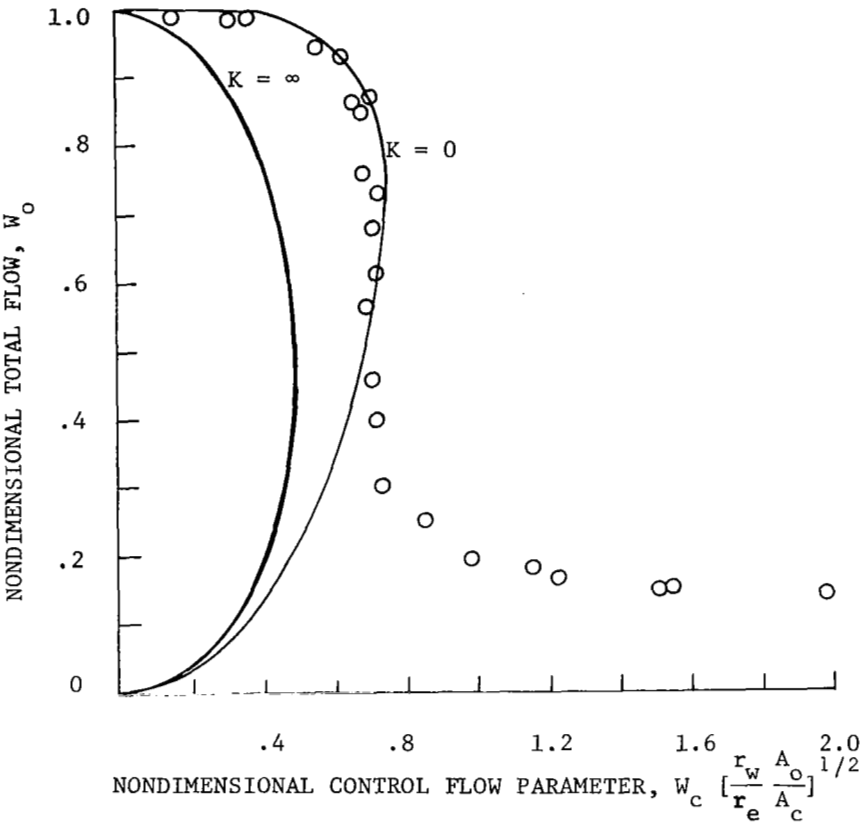

Fig. 7.1 Vortex valve output flow as a function of control flow and geometry. o o experimental points from Fig. 4.5 of Wormley, 1967(C_{D_e} = .8).

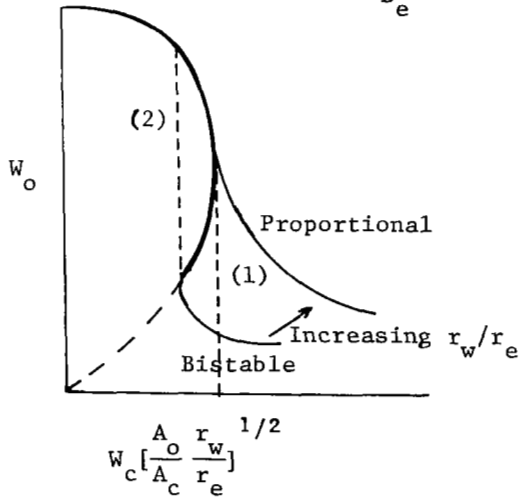

Fig. 7.2 Vortex valve characteristics showing the difference between "Proportional" and "bistable" operation.

parameters are involved, a fairly straightforward empirical correlation for TDR as a function of r_w/r_e and A_o/A_c should be possible. Such a correlation is given in Fig. 7.3 from Wormley and Richardson (1969). This figure also includes two other important characteristics for the valve. One is the control pressure required to cutoff the supply flow. This is given in terms of the ratio of the control pressure at cutoff to the supply pressure, P_{cc}, with both pressures measured relative to the exhaust pressure. The other feature indicated is the line along which the valve's outlet flow may be multiple valued. Although not indicated in the figure, the lines for constant TDR = $1/W_{cc}$ should drop off at large r_e/r_w so that for any given A_c/A_o there is a r_e/r_w which maximizes TDR as seen by Gebben (1967). They also should become vertical at small r_e/r_w so that TDR is essentially independent of A_o/A_c in this regime.

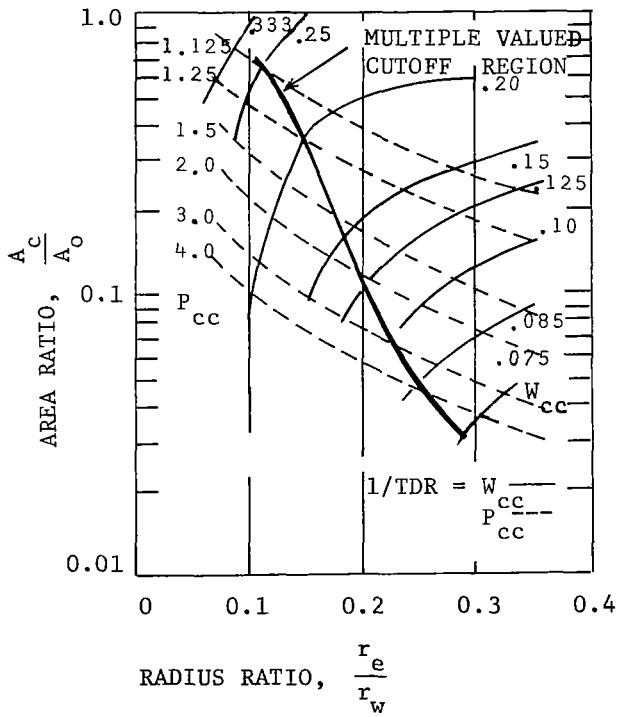

Fig. 7.3 Vortex amplifier cutoff flow characteristics (Single exhaust). (Wormley and Richardson, 1969)

A different empirical approach was used by Mayer (1967, 1969). He plotted W_o as a function of the angle between the flow velocity vector and the wall at the valve entrance, i.e.

$$\tan^{-1}(u/v)_w = \tan^{-1}\left[\left(\frac{W_o}{W_c}\right)^2 \frac{A_c}{2\pi r_w \ell}\right] \tag{7.2-8}$$

From Eq. 7.2-8, it may be seen that the assumption that $W_o = W_o[\tan^{-1}(u/v)_w]$ is equivalent to assuming that $W_o = F[W_c(r_w \ell/A_c)^{1/2}]$. It is not too surprising then that Mayer found the resulting curve to be independent of A_c for numerous control port configurations as shown in Fig. 7.4. The inviscid curve for K = 0 from Fig. 7.1 also is included for comparison. Mayer also found his W_o curve to be approximately independent of size, temperature, and exhaust pressure, but it varied with r_w/r_e, ℓ and the number of outlets.

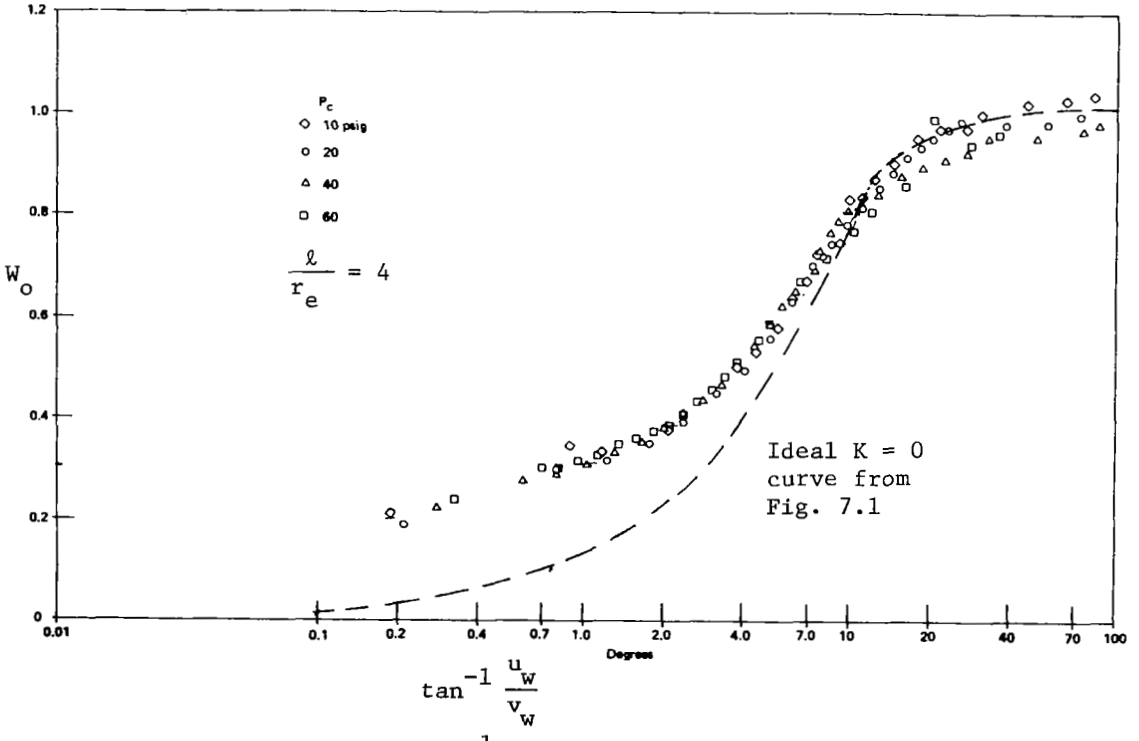

Fig. 7.4 Plot of W_o vs. $\tan^{-1} u_w/v_w$ for a particular valve following Mayer (1967).

Theoretical analyses of the operation of a vortex valve, e.g. Taplin (1965), Wormley (1967) and Mayer (1967, 1969), have usually assumed that the exhaust flow can be adequately described by the difference between the internal static pressure at the exhaust radius and the external exhaust pressure. This is equivalent to assuming that v goes to zero discontinuously at the edge of the exhaust and that w is constant across the exhaust. A comparison with the definitions of $\bar{Q}$ and α reveals that this corresponds to setting

$$\bar{Q} = [1 - \alpha^2]^{1/2} \tag{7.2-9}$$

Comparison with Fig. 3.20 shows that this falls only a little to the right of the curve for Γ proportional to Ψ with constant total pressure. Therefore, Eq. 7.2-9 is more valid than the physical assumptions leading to it might indicate. If Eq. (7.2-9) is used the equation for inviscid valve performance corresponding to the curves in Fig. 7.2 is given by

$$W_c^2 [\frac{r_w}{r_e} \frac{A_e}{A_c}] = W_o [1 - W_o^2]^{1/2} \tag{7.2-10}$$

as given by Wormley (1967).

The W_o vs. W_c curve sometimes shows an increase in W_o as the control flow is turned on. (See Fig. 7.5 from Taplin, 1965). This occurs when the initial discharge coefficient of the outlet is significantly less than 1 due to convergence of the streamlines to a cross sectional area less than the physical orifice. In this case the addition of swirl to the flow can encourage the flow to remain attached to the walls and increase the discharge coefficient to initially over compensate for the loss in effective pressure. (Effect also observed in Fig. 6.16).

7.3 Theoretical Predictions of Turndown Ratio

As seen in the last section, chamber flow will be dominated by end-wall boundary-layer effects when the supply flow is shut off. Thus it should be possible to use the analysis of Section 6.3 to predict the pressure drop across the chamber near turndown and obtain an estimate of minimum flow.

Near turndown the tangential velocity component is much larger than either the radial or axial components within the main part of the chamber flow. Therefore the radial momentum equation may be written approximately as

$$\frac{\partial p}{\partial r} = \frac{\rho v^2}{r} \tag{7.3-1}$$

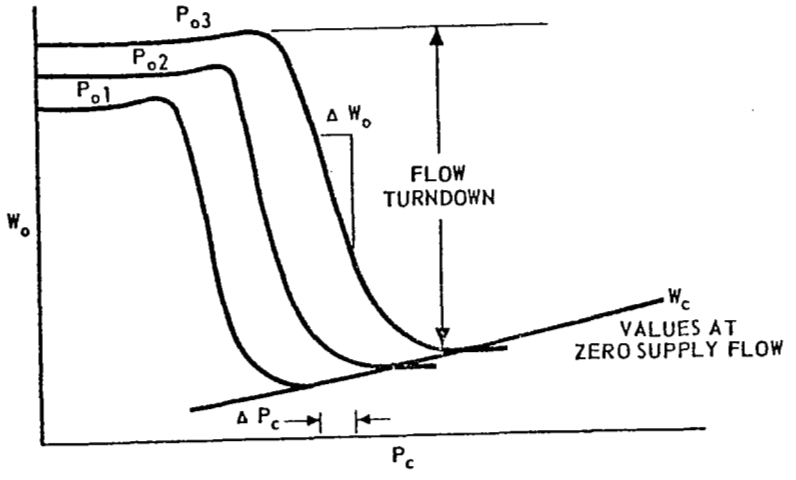

Fig. 7.5 Vortex valve performance curve showing an increase in discharge coefficient with increasing swirl.

With the circulation assumed constant for $r > \hat{r}$ and given by Eq. 6.3-16 for $r < \hat{r}$, Eq. 7.3-1 may be integrated between the exhaust and the cylindrical wall to give

$$p_w - p_e = \int_{\hat{r}}^{r_w} \frac{\rho \Gamma_o^2}{r^3}\, dr + \int_{r_e}^{\hat{r}} \rho \Gamma_o^2 [1 + A_1(1 - \frac{r}{\hat{r}})]^{-2} \frac{dr}{r^3} \tag{7.3-2}$$

with $A_1 = (B - 1)/(\lambda_1 - 1)$, and $\hat{r} = 1 - 1/B$. After integration Eq. 7.3-2 yields

$$\frac{(p_w - p_e) r_w^2}{\rho \Gamma_o^2} = F\ (B, \frac{r_e}{r_w}) \tag{7.3-3}$$

with

$$F(B, \frac{r_e}{r_w}) = \frac{1}{2}[(\frac{r_w}{\hat{r}})^2 - 1] + \frac{r_w^2}{\hat{r}^2 (1+A_1)^4} \left[\frac{1}{2}(1+A_1)^2 [(\frac{\hat{r}}{r_e})^2 - 1] \right.$$

$$+ 2A_1(1 + A_1)[\frac{\hat{r}}{r_e} - 1] + 3A_1^2 \ln [A_1(\frac{\hat{r}}{r_e} - 1) \tag{7.3-4}$$

$$\left. + \frac{\hat{r}}{r_e}] + A_1^3 \left(1 - [A_1(\frac{\hat{r}}{r_e} - 1) + \frac{\hat{r}}{r_e}]^{-1}\right) \right]$$

Consistent with the approximation which lead to Eq. 7.2-9, the normalized output flow may be approximated as

$$W_o = \left(\frac{p_e - p_a}{p_w - p_a}\right)^{1/2} \tag{7.3-5}$$

With the aid of Eq. 7.2-4 the ideal circulation introduced into the valve may be written as

$$\Gamma_i = \frac{W_c^2 \, r_w A_o [2\rho(p_w - p_a)]^{1/2}}{\rho_c \, A_c \, W_o} \tag{7.3-6}$$

Since the ℓ/D of the valve chamber is small it should be possible to neglect shear losses on the cylindrical wall in comparison to those on the flat end walls, so that it is consistent to assume that

$$\Gamma_o = \Gamma_i \tag{7.3-7}$$

At turndown $W_{o_{min}} = W_{cc}$ and Eqs. 7.3-3 thru 7.3-7 may be combined for $p_s = p_c$ to give

$$W_{cc} = \frac{1}{TDR} = [1 + 2 \, A_o^2 F / A_c^2]^{-1/2} \tag{7.3-8}$$

This theoretical prediction of turndown ratio is plotted in Fig. 7.6. It gives a turndown ratio which increases as radius ratio decreases. However, if the control flow required at cutoff is less than the maximum W_c in the inviscid curve the turndown point will be an unstable point (Fig. 7.2). With the aid of Eq. 7.2-10, this value is given by

$$W_{c_{max}} = 0.595 \left[\frac{r_e}{r_w} \frac{A_c}{A_o}\right]^{1/2} \tag{7.3-9}$$

which gives a bound for stable TDR

$$TDR_{max} = 1.68 \left[\frac{r_w}{r_e} \frac{A_o}{A_c}\right]^{1/2} \tag{7.3-10}$$

This line is included on Fig. 7.6. The achievable TDR is governed by Eq. 7.3-10 for low r_w/r_e and by Eq. 7.3-8 for large r_w/r_e with the maximum value of TDR occurring at the intersection of the two curves.

Within the uncertainty surrounding the proper value of c_f discussed in Section 6.3, these theoretical predictions agree with experiments. The optimum radius ratios for maximum turndown are indicated as is the significant gain in turndown ratio achieved by using a dual exhaust rather than a single exhaust. From Eq. 7.2-7, it may be seen that going to a dual exhaust is like cutting c_f in half. This is easily understood by recognizing that the minimum flow condition is set by the mass flow supported by the end wall

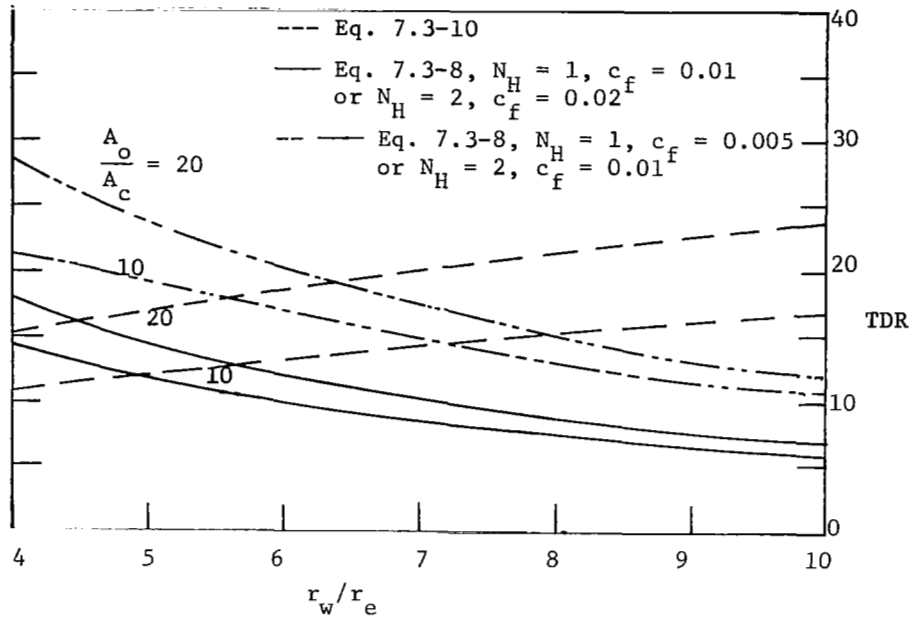

Fig. 7.6 Theoretical prediction of TDR as a function of radius ratio. Achievable TDR governed by the lower of the two curves.

boundary layer. For a given exhaust radius it is independent of whether the chamber has a dual or a single exhaust. However the maximum flow for a given exhaust radius is double for dual exhaust of that for a single exhaust. Thus the ratio of maximum flow to minimum flow which is the turndown ratio should be approximately twice as much for a dual exhaust valve.

Computer programs have been written to predict incompressible valve performance by Bichara and Orner (1969) and for either compressible or incompressible by Felsing, Mockenhaupt and Lewellen (1970). Bauer (1968) has programmed the case of a choked outlet. The boundary-layer treatment for all of these analyses is essentially similar to that given herein and thus also suffers from incomplete knowledge of the dependence of c_f on Re_t and geometry.

7.4 Other Modes of Operation for a Fluidic Vortex

The basic features of the vortex valve can be used in several ways to suit different purposes other than the primary purpose of flow modulation. An indication of the possible variation is given by the following list.

a) Signal Amplifier

Figure 7.7 is a schematic of a five port vortex amplifier developed by Bendix Research Laboratories, Taplin (1969). One mode of operation is to amplify a control pressure change by connecting the external port as the signal receiver with the exhaust port acting as a vent and the internal port blocked. Large changes in P_o can be obtained with small changes in p_c. With this arrangement it is even possible to reverse the flow in the external port.

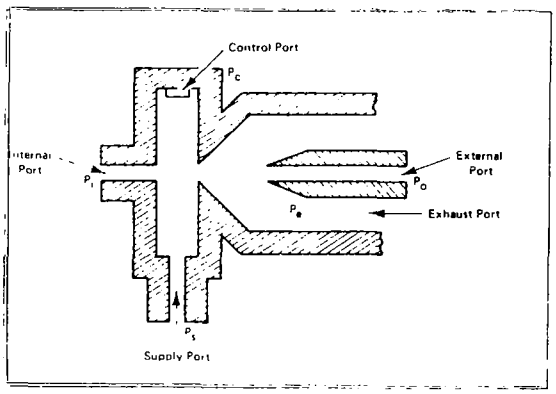

Fig. 7.7 Five port vortex amplifier (Taplin, 1969).

If it is desired to amplify the absolute pressure rather than the pressure change, the internal port may be used as the signal input with the supply port as the signal output.

b) Pressure Regulator with Variable Flow Rate

If the control pressure is held constant, the supply pressure is essentially constant over a range of output flow as shown in Fig. 7.8.

c) Diode

A two port valve, as sketched in Fig. 7.9 may be used to provide a much higher resistance to flow in one direction than the other. For an incompressible diode the ratio of pressure drop required for flow in the reverse direction to that required for the same flow in the forward direction is equal to the square of the turndown ratio of the equivalent vortex valve. Thus with proper design this can be of the order of 100 to 1, which is a much higher ratio than can be obtained with any other type fluid diode (Paul, 1968).

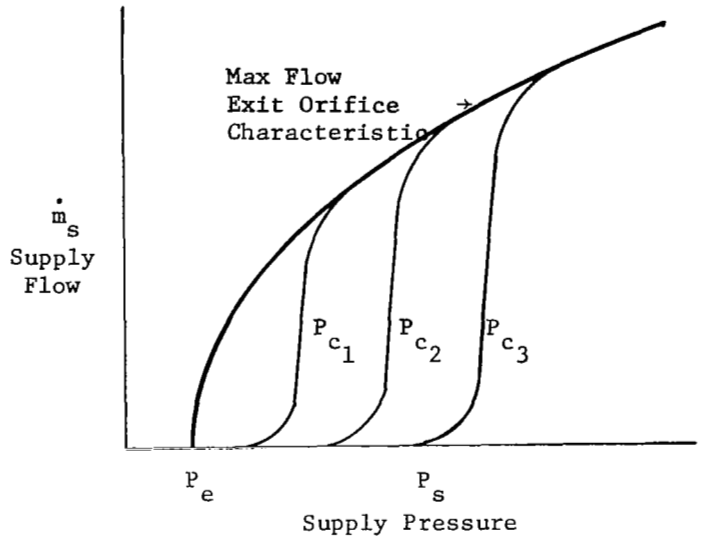

Fig. 7.8 Vortex chamber characteristic curves with regulated control.

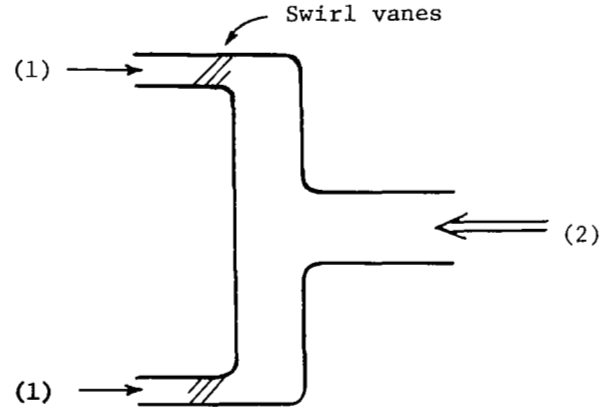

Fig. 7.9 Schematic of vortex diode. There is a large pressure drop required for flow in direction (1) and a low drop for flow in direction (2).

d) Signal Summation

By using a number of control ports around the periphery signals may be added or, using opposing control ports, subtracted. Bendix (Taplin and Mc Fall, 1969) has demonstrated the processing of as many as 16 separate control ports on a single 1 inch diameter amplifier.

e) Oscillator

As demonstrated in Section 7.2 a vortex valve can be made to operate in regions where it behaves as if to provide negative resistance to the flow thru it. This provides the possibility of operating the vortex as an oscillator. An arrangement which is particularly conducive to a smooth oscillator is sketched in Fig. 7.10(a). A reservoir is added to the supply inlet to act as a capacitor. The quasi-steady operating curve for such a valve is sketched in Fig. 7.10(b) for the control pressure held constant. The frequency of oscillation may be set by varying the volume of the capacitors. The range of oscillation may be improved by biasing the supply flow to introduce swirl into the vortex in a direction opposite to the control. Such an oscillator provides the promise of becoming an accurate temperature sensor. (Bell, 1966; Hart, 1969).

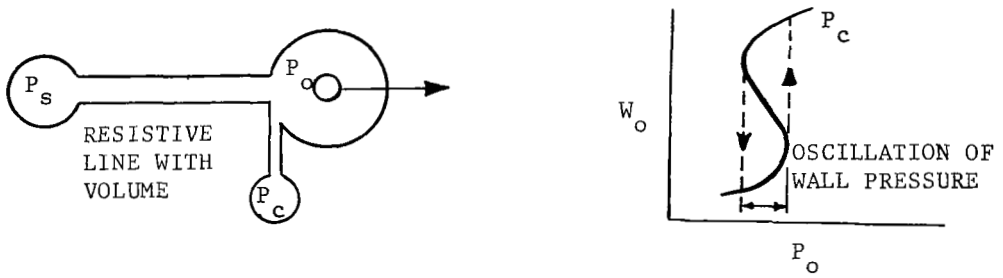

(a) SCHEMATIC (b) OPERATING RANGE

Fig. 7.10 Negative resistance oscillator (Taplin, 1965).

f) Flow Meter

If the radius ratio between the annular inlet and the center outlet in Fig. 7.9 is reduced to approach 1 so there is little dissipation within the valve, there will be an oscillation associated with the outlet. When the normalized angular momentum flux is greater than that which can pass thru the exhaust in steady flow (see Section 6.5) the flow thru the exhaust is

unsteady. For a fixed geometry the frequency of this oscillation varies linearly with flow rate (Ryan, 1969) to provide the basis for a flowmeter with a digital readout.

g) Fluid Gyroscope

For large radius ratios, and low values of swirl, small angular velocities may be greatly amplified as the flow converges to the exhaust. Thus a pressure measurement near the axis of the chamber in Fig. 1.2 would be sensitive to small rotations of the porous ring. Fiebig (1966) and Sarpkaya (1968) show that such a device can be a sensitive angular-rate sensor over a wide frequency band.

h) Vorticity Meter

If an independent measurement of thru flow is available the pressure drop required to drive a swirling flow thru an orifice may be used to determine the vorticity flowing into the orifice. Possible arrangements for such a fluidic vorticity meter have been analyzed by Guenette (1970).

VIII. ADVANCED NUCLEAR ROCKET CONCEPTS EMPLOYING VORTEX CONTAINMENT

8.1 Introduction

Since the advent of the space program many concepts have been proposed for utilizing nuclear energy for space propulsion. The high energy density of nuclear fuel (2×10^7 kcal/gm for the fission reaction compared with 3 kcal/gm for a typical chemical reaction) makes nuclear energy very attractive as an energy source for space systems. However, nuclear fuel is both expensive and has a high molecular weight, hence it is necessary to transfer a large portion of the energy generated in the nuclear fuel to a gas which is more suitable for use as a propellant. The easiest way of achieving this appears to be by containing the nuclear fuel in a solid core heat exchanger and allowing the propellant gas to flow thru the heat exchanger to receive energy from the hot nuclear fuel rods before the propellant is expanded thru the rocket nozzle. This is the basis for the NERVA nuclear rocket. Such a rocket has been successfully designed, built, and ground tested and has proven that it is possible for a nuclear rocket to achieve a propellant exhaust velocity which is about twice that which can be achieved by any chemical rocket. This means twice as much total impulse can be delivered to a space vehicle from the same amount of propellant.

The performance of the NERVA nuclear rocket is limited by material constraints on the temperature. The performance can be increased in 3 general ways. (1) It may be possible to obtain better materials which are capable of operating at higher temperatures. (2) It may be possible to accelerate the propellant to higher exhaust velocities without increasing its static temperature. (3) It may be possible to contain the nuclear fuel in the gaseous phase to circumvent the temperature limit on the nuclear fuel. All three approaches are being pursued. The most promising approach to the second method is to first convert the thermal energy from the nuclear reaction into electrical energy and then to use some type of electric thruster to accelerate the propellant. The major disadvantage of such nuclear-electric propulsion systems is the large mass of the electric power generator which forces the system to have a relatively low thrust-to-weight ratio. McLafferty (1967) and Ragsdale (1968) have reviewed some of the concepts proposed following the third approach.

In this review we are primarily interested in considering to what extent

vortex flows may be useful in realizing more of the potential of nuclear propulsion systems. Kerrebrock and Meghreblian (1961) proposed vortex containment for a gaseous fission rocket in a classified report in 1958. Grey (1959) published the same idea in the unclassified literature. The idea is to suspend an annulus of fissioning fuel by maintaining an equilibrium between the centrifugal force on the rotating fuel and the hydrodynamic force of hydrogen flowing radially inward thru the fissioning fuel. Analysis indicated promising possibilities. This led to a number of experimental and theoretical investigations of vortex containment and to a general evolution of other ways of utilizing vortex flows for containment. Rather than follow a historical approach to these investigations, let us first look at the general requirements of a gaseous core nuclear rocket and then determine to what extent these requirements can be met with vortex containment.

8.2 Design Requirements for a Gaseous Nuclear Rocket

To maintain the stable, continuous fission reaction needed for a nuclear reactor it is necessary to have a critical mass of fuel. This critical mass depends strongly on geometry and on the other materials present in the reactor. The smallest values are achieved when materials are present to moderate the high speed neutrons generated by the fission reaction without absorbing them. In the case of a gaseous nuclear rocket almost all of the moderating material will be located around the cavity containing the fuel as seen in Fig. (8.1) Critical experiments on such a cavity reactor have been run by Pincock and Kunze (1967 - 1969). Most of their experiments have used strips of metal foil to simulate a gaseous fuel but a check has been made using UF_6 gas to ascertain that the foil strips do adequately simulate the gas conditions to a 10% accuracy. Figure (8.2) shows some of their results both in terms of the critical mass and the concentration of Uranium - 235 required as a function of the fraction of the radius to which the fuel is restricted. The value of 9 kg for the U^{235} distributed over the whole cavity is about the minimum that can be achieved for any geometry. The actual critical mass required in a gaseous core rocket may be from 2 to 5 times greater than this due to such effects as the restriction of the fuel away from the walls, leakage of neutrons out the rocket nozzle, and neutron absorption in the structural members of the rocket.

It is possible to reduce the amount of fuel required in the gaseous state if some solid fuel is included in the moderator but this degrades the performance

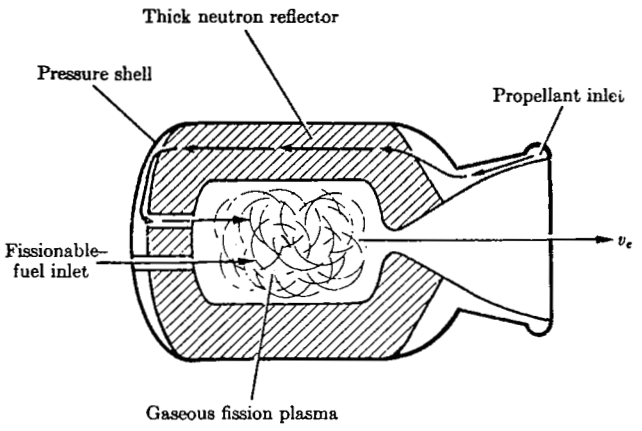

Fig. 8.1 Direct gaseous-heater rocket reactor——basic concept.

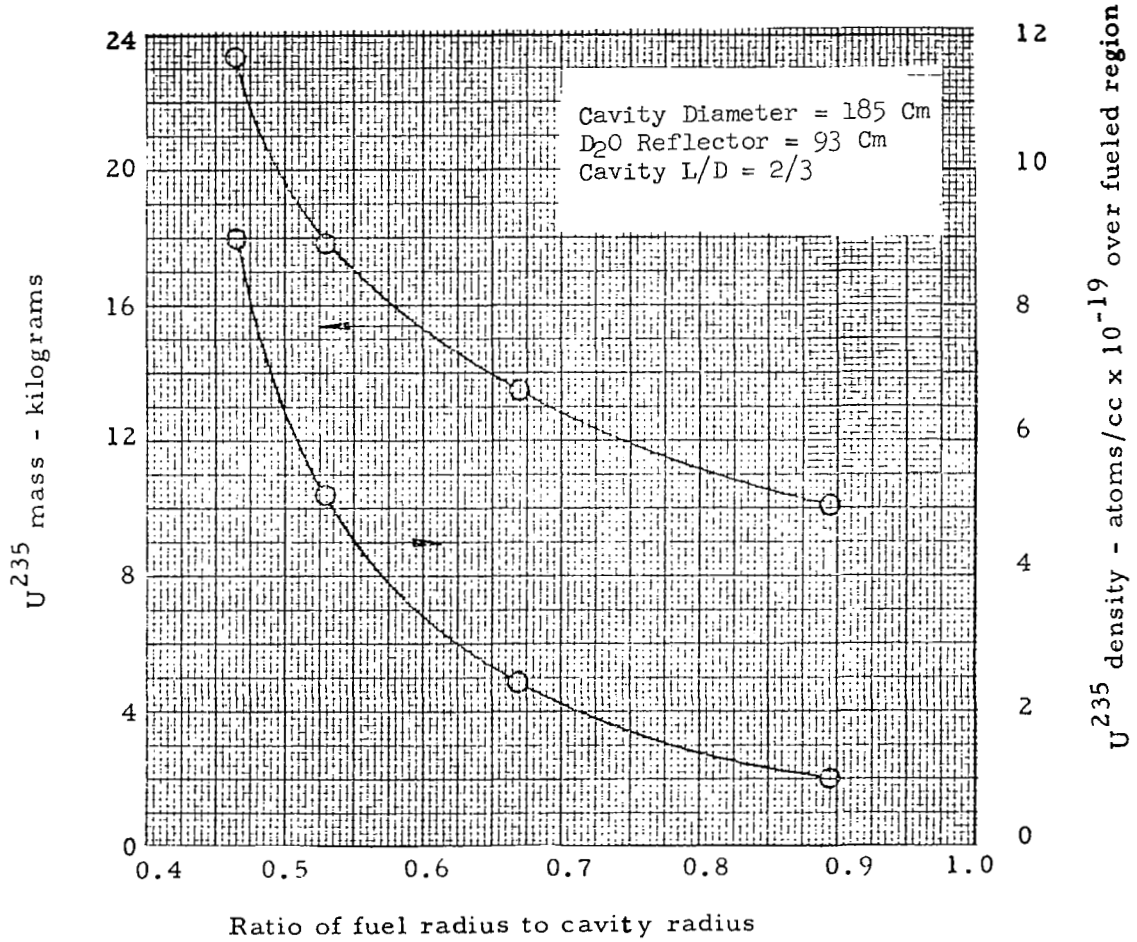

Fig. 8.2 Effect of ratio of fuel radius to cavity radius on critical mass and U^{235} density (Pincock and Kunze, 1967-69).

potential of the system. This can be demonstrated by an energy balance of the system which also gives an idea of design temperatures. Even in a gaseous core system there is still a temperature limit imposed on the solid components of the rocket. If these solid components are to be cooled by the propellant flow before it enters the cavity, an energy balance for the propellant shows that

$$h_g/h_s = 1 + (1 - \kappa)\ (1 - \chi)/[\kappa + \chi(1 - \kappa)] \qquad (8.2\text{-}1)$$

where h_g is the final enthalpy of the propellant after passing thru the cavity, h_s is the enthalpy of the propellant leaving the solid components, κ is the fraction of the total energy which is generated by fuel in the solid components and χ is the fraction of the energy generated in the gas which is deposited in the walls. The ratio of propellant exhaust velocity obtainable in a gaseous core nuclear rocket to that in a solid core limited to the same maximum temperature in the solid components is given by

$$\frac{v_{e_g}}{v_{e_s}} \simeq \left[\frac{h_g}{h_s}\right]^{1/2} = \left[1 + \frac{(1-\kappa)(1-\chi)}{\kappa + \chi(1 - \kappa)}\right]^{1/2} \qquad (8.2\text{-}2)$$

About 12% of the energy available from the fission of U^{235} is invested in γ and β rays and in high energy neutrons. Energy of this form cannot be efficiently transferred directly to the gas, instead it will be deposited in the solid components of the reactor. Thus a lower bound on χ is approximately 0.1. This would be increased by any convective or radiative heat transfer from the gas to the solid components and by any secondary nuclear reactions. The upper bound on the exhaust velocity corresponding to $\chi = 0.1$ and $\kappa = 0$ in Eq. (8.2-2) is

$$v_{e_g}/v_{e_s} \leq [10]^{1/2} \qquad (8.2\text{-}3)$$

This bound on performance is rapidly decreased as κ increases. If 1/2 the fuel is placed in the solid components than this potential boost in exhaust velocity is cut to ≤ 1.35.

The limits on the performance of a gaseous core nuclear rocket imposed by the above energy considerations can, of course, be circumvented by using a radiator to provide additional cooling. This in turn forces a trade off between increasing exhaust velocity and decreasing thrust-to-weight ratio which

makes it difficult to improve overall performance in this manner.

A plot of ideal exhaust velocity versus chamber temperature is plotted in Figure (8.3) for hydrogen at various pressures. These curves assume that essentially all the thermal energy of the propellant is converted into directed kinetic energy by the rocket nozzle. The NERVA engine is designed for $\approx$ 2500°K. Figure (8.3) and Equation (8.2-3) show that the average stagnation temperature of the hydrogen propellant in a gaseous core system will be $\lesssim$ 10,000°K.

The fuel pressure required for criticality can be determined from the density in Fig. (8.2) when the temperature is specified. A concentration of 10^{19} atoms/cm^3 at a temperature of 10,000°K would yield a uranium pressure of

$$\text{i.e.,} \quad p_u = nkT \approx \frac{(10^{19}\ \text{atoms/cm}^3)(1.38\times10^{-23}\ \text{Kg-m}^2/\text{sec}^2\text{-°K})(10{,}000\text{°K})}{(10^{-6}\ \text{m}^3/\text{cm}^3)(1.013\times10^{5}\ \text{Kg m/sec}^2\ \text{atm.})}$$

$$p_u \approx 14\ \text{atm.} \qquad (8.2\text{-}4)$$

The pressure of the uranium gas just computed should not be confused with the chamber pressure. Most of the fission energy must be transferred to a light propellant gas such as hydrogen if a high exhaust velocity is to be achieved. The degradation in performance due to the increase in molecular weight, $\tilde{M}$, of an exhaust mixture at a fixed stagnation temperature is given by

$$\frac{v_{e_{mixture}}}{v_{e_{H_2}}} \approx \left[\tilde{M}_{H_2}/\tilde{M}_{mixture}\right]^{1/2} \qquad (8.2\text{-}5)$$

This may be written as

$$\frac{v_{e_{mixture}}}{v_{e_{H_2}}} \approx \left[\frac{p_{H_2}}{p_{total}} + \frac{p_u}{p_{total}}\frac{\tilde{M}_u}{\tilde{M}_{H_2}}\right]^{-1/2} \qquad (8.2\text{-}6)$$

and when $p_u << p_{H_2}$

$$\frac{v_{e_{mixture}}}{v_{e_{H_2}}} \approx \left[1 + \frac{\dot{m}_u}{\dot{m}_{H_2}}\right]^{-1/2} \qquad (8.2\text{-}7)$$

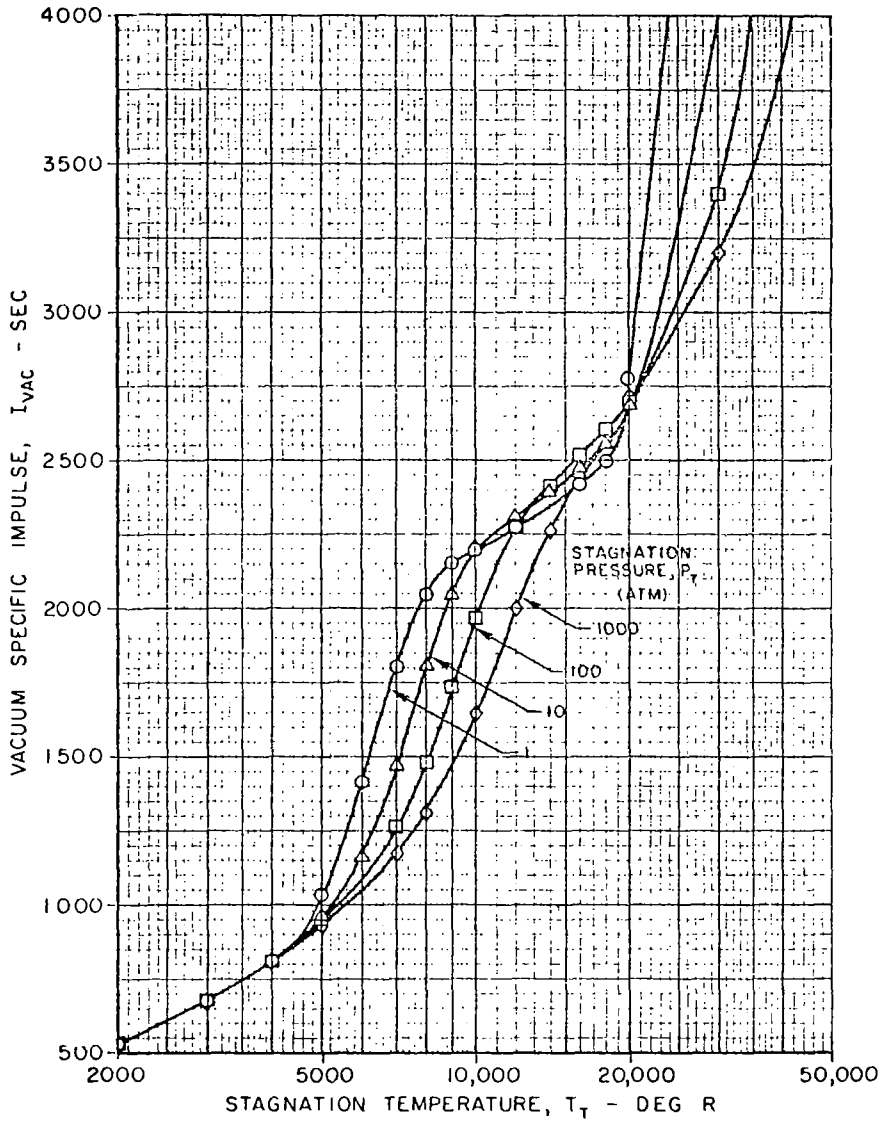

Fig. 8.3 Effect of stagnation temperature and pressure on vacuum specific impulse achieved by an equilibrium expansion of Hydrogen thru a pressure ratio of 10^5. (Roback, 1966)

From Equation 8.2-7, it may be seen that 90% of the ideal hydrogen exhaust velocity may be achievable if $\dot{m}_u/\dot{m}_{H_2} < 0.2$.

The mass flow ratio of fuel to propellant arrived at in the last paragraph can be used to determine a pressure for the hydrogen if a gaseous core system is to operate with a uniform mixture, i.e. with no separation between fuel and propellant.

$$p_{H_2} \approx \frac{\dot{m}_{H_2}}{\dot{m}_u} \left(\frac{\tilde{M}_u}{\tilde{M}_{H_2}}\right) p_u \tag{8.2-8}$$

so that

$$p_{H_2} \gtrsim (5)\left(\frac{235}{2}\right) 14 \text{ atm} \simeq 8 \times 10^3 \text{ atm} \tag{8.2-9}$$

The propellant would have to be injected into the chamber at some still higher pressure. This appears to be beyond the current state of the art of pump design.

Even if it were possible to operate at the high pressures just arrived at, the rocket would prove uneconomical for all but a few very ambitious missions, since nuclear fuel costs in the neighborhood of $14,000 per kilogram. Some mission analysis must be performed to arrive at a mass flow ratio of $\dot{m}_{H_2}/\dot{m}_{U^{235}}$ that will give the gaseous core system a significant improvement over a solid core nuclear rocket. Ragsdale (1963) proposed that this may be as low as $\dot{m}_{H_2}/\dot{m}_{U^{235}} \gtrsim 35$ based on the assumption that the higher exhaust velocity of the gaseous nuclear rocket will give it an advantage as long as the total fuel cost is less than the cost of the propellant. The figure of 35 is based on a propellant cost of $400/kg, the approximate cost of placing anything in earth orbit with Saturn V rocket. If the current plan for an earth-orbit shuttle system proves successful in its goal of reducing orbit cost an order of magnitude (Chako, 1969) this will also increase the required $\dot{m}_{H_2}/\dot{m}_{U^{235}}$ for an economical rocket an order of magnitude to something between 10^2 amd 10^3. Although the exact mass flow ratio limit is unclear it is evident that some degree of separation between the fuel and propellant must be achieved rather than depending upon increasing pressure to increase $\dot{m}_{H_2}/\dot{m}_{U^{235}}$.

One way of expressing the separation between fuel and propellant is in

terms of a "containment time", τ_c , defined as a ratio of the dwell time of fuel in the cavity to the dwell time of the propellant, i.e.,

$$\tau_c = \left(\frac{\rho_u}{\rho_{H_2}}\right)_{\text{average}} \frac{\dot{m}_{H_2}}{\dot{m}_{U^{235}}} \tag{8.2-10}$$

This containment time may be expressed in terms of cavity pressure as

$$\tau_c \approx \frac{\dot{m}_{H_2}}{\dot{m}_{U^{235}}} \frac{\rho_{crit}}{p} \frac{\mathcal{R}}{\tilde{M}_{H_2}} T_{H_2} \tag{8.2-11}$$

With ρ_{crit} specified by the criticality condition as approximately 0.005 gm/cm^3, $\dot{m}_{H_2}/\dot{m}_{U^{235}}$ set at approximately 10^2 as demanded by economics, T_{H_2} set at 10,000°K to achieve an Isp of $\approx$ 2500 seconds, and p set at 1,000 atmospheres (a pressure that appears within the state of the art of pump design Duke and Houghton, 1966), and $\tilde{M}_{H_2} = 1$ since hydrogen is dissociated at this temperature and pressure, then

$$\tau_c \gtrsim 400 \tag{8.2-12}$$

In summary, a successful flow containment scheme for a gaseous nuclear rocket calls for hydrogen to flow thru the cavity at least 400 times the rate at which U^{235} flows thru the cavity.

8.3 Containment by Pressure Diffusion

Pressure diffusion in a binary gas mixture within a vortex flow has been considered by many authors. No attempt is made here to give a historical review of this work. Rather, the intention is to review the pertinent facts and to see what conclusions can be drawn.

Based on a one-dimensional, inviscid model, Kerrebrock and Meghreblian (1961) have shown that in order to have significant containment it is necessary to have

$$\Theta \equiv \frac{\left(\frac{\tilde{M}_2}{\tilde{M}_1} - 1\right)\gamma_1 M^2_{t_1 \max}}{\dot{m}/2\pi\rho_1 D_{12} L} > 1 \tag{8.3-1}$$

within the vortex. In Equation (8.3-1) the subscripts 1 and 2 refer to the light and heavy gas respectively, $\tilde{M}$ is the molecular weight, γ the ratio of specific heats, M_t the tangential Mach number, and D_{12} the binary diffusion coefficient.

Essentially the same conclusion was also reached by Lewellen, Ross, and Rosenzweig (1966) using a quite different three-dimensional, viscous model for the vortex flow. The 3-dimensional model they assumed is given in Fig. (8.4). It calls for nullifying the secondary flow on the end wall through

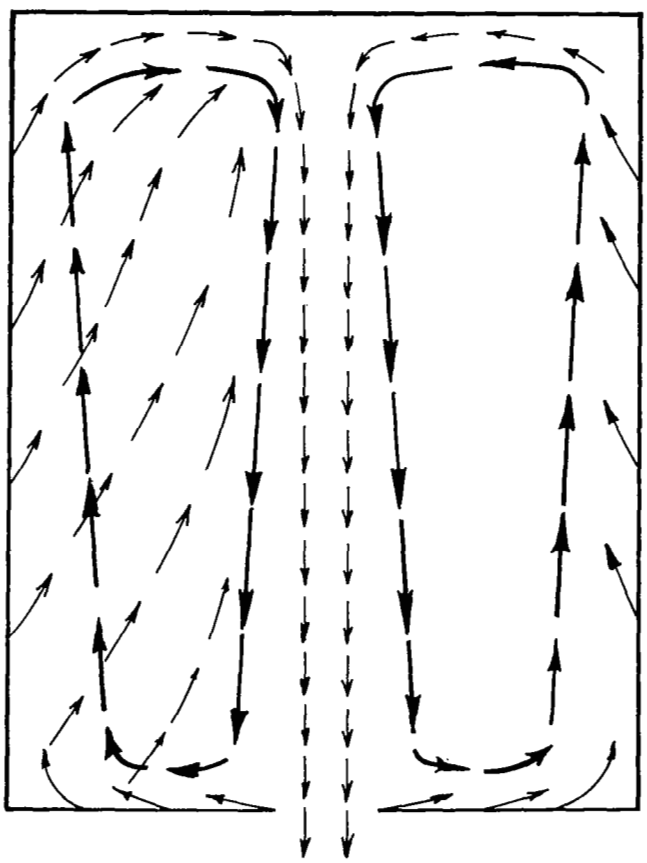

Fig. 8.4 Secondary flow pattern modified to control boundary-layer flow and thus enhance separation.

which the flow will finally exhaust. Pinchak and Poplawski (1965) and Ross (1964) have shown that this is possible by tangential blowing in the end wall. The model also calls for the radial stagnation surface, $\hat{r}$, discussed in earlier chapters to occur slightly outside the radius of the exhaust. If the flow across the chamber from the end wall boundary layer out the exhaust is modelled as a flow with uniform axial velocity, with the M_t proportional to r and the concentration ratio of light to heavy species assumed a function of z only, then it is possible to show that

$$\frac{\rho_2}{\rho_1+\rho_2} = \left(\frac{\rho_2}{\rho_1+\rho_2}\right)_{z=0} \exp(-\Theta z/L) \tag{8.3-2}$$

As discussed in the last section, the ratio of uranium density to hydrogen density in the exhaust should be less than 10^{-2} to have an economical rocket. But, the density ratio must be of the order of 1 in the main part of the chamber to achieve criticality while holding the chamber pressure to less than 1000 atmospheres. These two conditions can be satisfied if

$$\Theta \geq 5 \tag{8.3-3}$$

Equation (8.3-3 or Equation (8.3-1) as observed by Kerrebrock and Meghreblian (1961), imposes a severe restriction on the mass flow per unit length of the vortex and leads to the concept of a large number of small diameter vortices to form a matrix reactor. For example, with $\tilde{M}_2/\tilde{M}_1 = 235$, corresponding to U_{235} and dissociated H_2; with $M_{t1\ max} \simeq 1$, with $\gamma_1 \simeq 1.3$; and with $\rho_1 D_{12} \approx 10^{-3}$ gm/cm - sec as estimated by Schneiderman (1964); the mass flow per unit length is limited to

$$\dot{m}/L \leq 0.5 \text{ gm/cm - sec} \tag{8.3-4}$$

For a rocket thrust of 50,000 kg at an Isp = 2500 sec, it would be necessary to have $\dot{m} \simeq$ 20 kg/sec which implies a total vortex length of $\simeq$ 400 m.

An estimate of the required vortex tube radius can be obtained from criticality conditions. Total reactor volume for a minimum critical mass reactor should be of the order of 1 m^3. This can be achieved over a total

length of 400 m, if $r_o \approx 1$ cm. A possible reactor geometry would appear to be a matrix of 400 tubes with $L \approx 1$ m and $r_o \approx 1$ cm packed to form a cylindrical reactor.

The critical question is whether such high tangential Mach numbers can be achieved at the low mass flow rates available to drive the vortices. Assuming a Schmidt number of order 1 ($Sc = \mu/\rho_1 D_{12}$), Equation 8.3-3 implies

$$M^2_{t_{1\ max}}/N \geq 0.02 \tag{8.3-5}$$

Table (8.1) summarizes the results of various attempts that have been made to maximize M_t^2/N in vortex chambers. The maximum value that has been obtained was a value of 0.01 by Lewellen, Ross, Rosenzweig (1966). Although this later value appears close to that required, it should be noted that it was obtained at $Re_t \approx 5{,}000$ which is at least two orders of magnitude smaller Reynolds number than what would be expected for design conditions.

Table 8.1

Values of $M^2_{t\ max}/N$ obtained in various experiments

	$M_{t\ max}$	N	$M^2_{t}\ max/N$
Ragsdale (1960)	.6	4000	10^{-4}
Keyes (1961)	.7	75	.007
Poplawski and Pinchak (1965)	1.2	4700	3×10^{-4}
Roschke and Pivirrotto (1965)	1.0	330	.003
Pivirrotto (1966)	.7	240	.002
Lewellen, Ross and Rosenzweig (1966)	.45	20	.01
Nakamura (1966)	.75	200	.003

The principal obstacle to obtaining large values of M_t^2/N in a jet-driven vortex is the angular momentum losses due to shear on the inner surfaces of the chamber wall. An upper bound on the Mach number at the edge of the exhaust may be given as

$$M_{t_e} < \frac{\Gamma_o}{\Gamma_i} M_{t_i} \frac{a_i}{a_e} \frac{r_i}{r_e} \tag{8.3-6}$$

where the subscript i denotes the value at injection, e the value at the edge of the exhaust, Γ_o is the core value of circulation, and a is the local speed of sound. The speed of sound ratio a_e/a_i corresponds to the desired increase in Isp for the rocket, i.e. $a_e/a_i \simeq 3$. The injection Mach number cannot be much greater than 1 without imposing large pressure drops and shock losses. The circulation ratio Γ_o/Γ_i can be estimated from an angular momentum balance as given in Equation (6.4-8)

$$\frac{\Gamma_i}{\Gamma_o} = \left(1 + \frac{c_f}{2}\frac{v_i}{u_w}\right)^{-1} \tag{8.3-7}$$

which leads to

$$\frac{\Gamma_o}{\Gamma_i} = \left[1 + c_f \frac{\rho_w v_i \pi r_w}{\dot{m}/\ell}\right]^{-1} \tag{8.3-8}$$

With $\dot{m}/L$ given from Equation (8.3-4), a sonic injection velocity of approximately 4×10^3 m/sec (corresponding to hydrogen at 2500°K), ρ_o of approximately 0.005 gm/cm^3 to meet the criticality condition, and r_i of approximately 1 cm this leads to

$$\frac{\Gamma_o}{\Gamma_i} \approx \frac{1}{1 + 4\pi \times 10^3 c_f} \tag{8.3-9}$$

As seen from Chapter VI, C_f is rather uncertain, but for Re_t between 10^5 and 10^7 it is not likely to be less than 0.002. Thus

$$\frac{\Gamma_o}{\Gamma_i} \leq 0.04 \tag{8.3-10}$$

Under these circumstances a radius ratio, r_w/r_e, of the order of 75 would be required according to Equation (8.3-6) before there is any possibility of reaching $M_{te} = 1$.

The radius ratio is limited by the requirement that all of the flow must flow thru the exhaust. The larger the radius ratio, the smaller the exhaust and the smaller the total flow thru the chamber. This in turn fixes the length of the chamber according to Equation 8.3-4. But shortening the length of the chamber can force the losses in the end-wall boundary layers to also become more

important. The length-to-diameter ratio can be estimated by another consideration. If $\hat{r}$ is to occur in the position indicated in Fig. (8.4), it is necessary to have $B \approx 1$. From Equation 6.3-11, this leads to

$$B \approx \frac{2\pi c_f \lambda \rho \Gamma_o r_w}{\ell(\dot{m}/\ell)} \approx 1 \tag{8.3-11}$$

Which for small values of Γ_o/Γ_i leads in combination with Equation (8.3-8) to

$$\ell \approx 2\lambda r_w \approx 10 \text{ cm}$$

which is the same order of magnitude as the 1 m length assumed earlier for the reactor matrix geometry. This means that the mass flow per tube must be of the order of 5 gm/sec. If the effective total pressure driving the flow out the exhaust is of the order of 200 atmospheres after considering the swirl, then Roback (1967) shows that

$$\frac{\dot{m}}{A^*} \approx 75 \frac{\text{gm}}{\text{cm}^2\text{-sec}} \tag{8.3-12}$$

which calls for

$$\pi r_e^2 \approx .07 \text{ cm}^2 \tag{8.3-13}$$

or

$$r_e \approx 0.15 \text{ cm} \tag{8.3-14}$$

This corresponds to $r_w/r_e \approx 7$, over an order of magnitude lower than the required value of 75 obtained earlier. Or viewed from another prospective, an $r_w/r_e \approx 75$ would lead to large values of B and consequently intolerable end wall shear losses.

The conclusion is that in order to make this type of reactor work it is necessary to either find some method of adding angular momentum to the vortex or some way of cutting wall shear losses. Both methods have been tried in the literature. Methods of driving the vortex using electromagnetic body forces have been analyzed by Lewellen (1960), Gross and Kessey (1964), Romero (1964) and Johnson (1964). There still remains the possibility that enough angular momentum can be added to the flow to make such a system work. However, such a magnetohydrodynamically driven vortex would still be subject to

the limit on mass flow given in Equation (8.3-4). Thus it would still call for a large number of vortices packed in some type of matrix arrangement. No analysis of a reactor based on a matrix of magnetohydrodynamically driven vortices is available in the literature.

Rosenzweig (1961) presented an idea of forming a vortex matrix without the intervening walls to reduce wall shear losses. An end view schematic of such an arrangement is given in Fig. (8.5). Subsequent experimental tests have shown that approximately 1/2 of the internal wall structure is needed to stabilize the vortex arrangement given here (Rosenzweig and Lewellen, in Cooper 1965). Thus the maximum possible increase in $M^2_{t\ max}/N$ using this approach as opposed to the individual vortex tubes would be approximately 2 which would still not be adequate. To make this matrix approach workable for a reactor, it appears necessary to find some vortex arrangement that is inherently stable so that the internal surfaces between the vortices could be nearly completely removed. (A recent numerical study by Murty and Rao (1970) indicates that a large array of parallel line vortices may be stabilized by allowing them to rotate uniformly about the centroid of the array.)

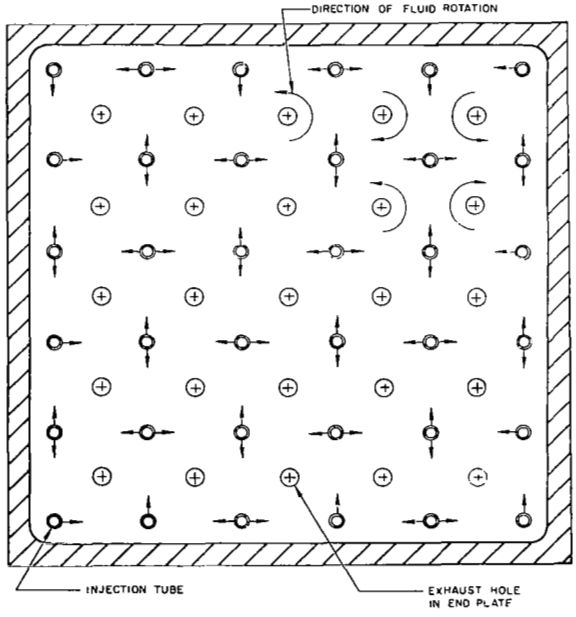

Fig. 8.5 Cross-section of vortex matrix designed to support a large number of vortices without intervening walls (Rosenzweig, 1961)

8.4 Containment by Secondary Flows

The closed cells evident in Figs. (3.13 and 3.14) provide another means of containment. One fluid may be contained in the closed cells while the other fluid remains separate from it and passes thru the boundary layers. The only losses of the contained fluid would be due to diffusion at the boundaries between the two fluids. This type of containment has been intensively studied at United Aircraft Research Laboratories and to a lesser extent at Aerospace Corporation and at Catholic University of America. A nuclear rocket based on this type containment is sketched in Fig. (8.6). In this concept, axial flow has been added to enhance the mass flow ratio of propellant to fuel. Since successful containment of this type requires that the fuel and propellant never mix it is necessary to rely on thermal radiation to transfer energy from the fissioning fuel to the hydrogen propellant. A small amount of seed material such as submicron-size tungsten particles would be added to the hydrogen to increase its absorptivity at low temperatures and complete the effective transfer of energy.

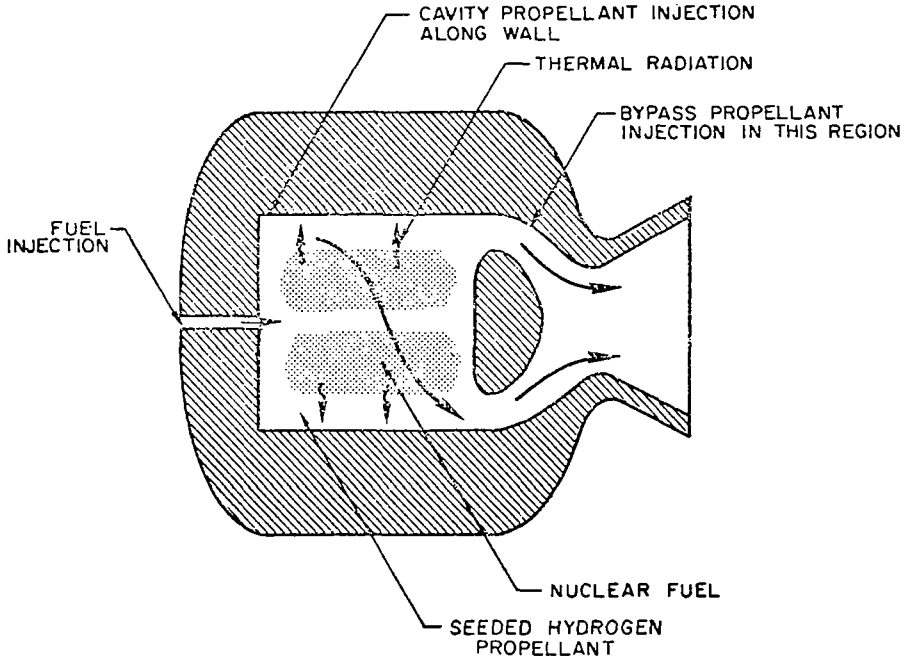

Fig. 8.6 Open cycle vortex stabilized gaseous nuclear rocket engine concept (McLafferty, 1961)

A demonstration of significant containment is shown in Fig. (8.7) which is a plot of the radial distribution of the density ratio of two different gases. The configuration used to obtain this result is shown in Fig. (8.8). Annular exhausts were provided to permit axial bypass flow. The radial distribution of the contained species was determined optically through windows in the end walls. The "simulated buffer gas" was injected thru the wall jets distributed around the periphery of the chamber. The contained "fuel" was

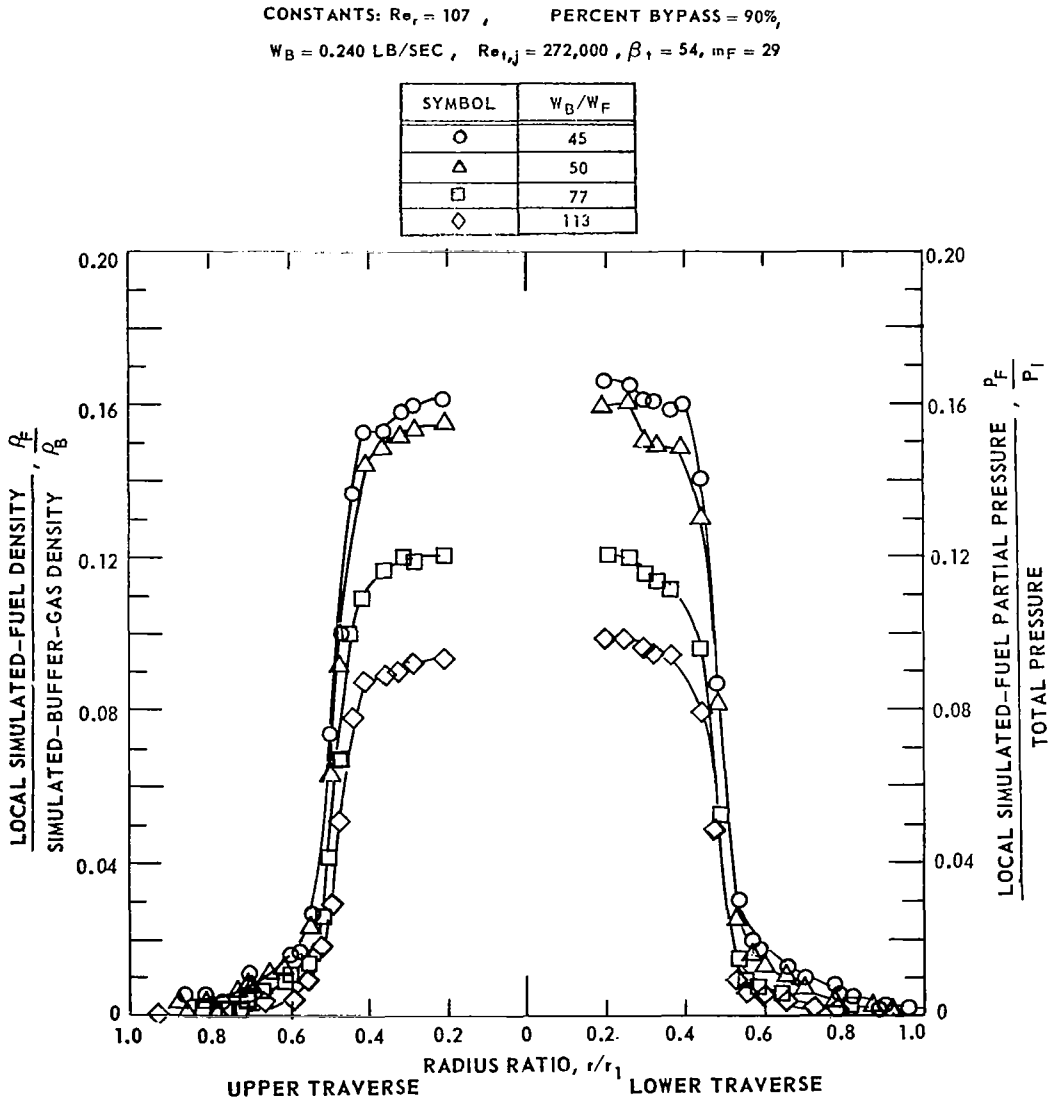

Fig. 8.7 Radial distributions of simulated fuel obtained with nitrogen/iodine mixture as simulated fuel in an air vortex. Air is denoted as the buffer gas. (Kendall, 1967)

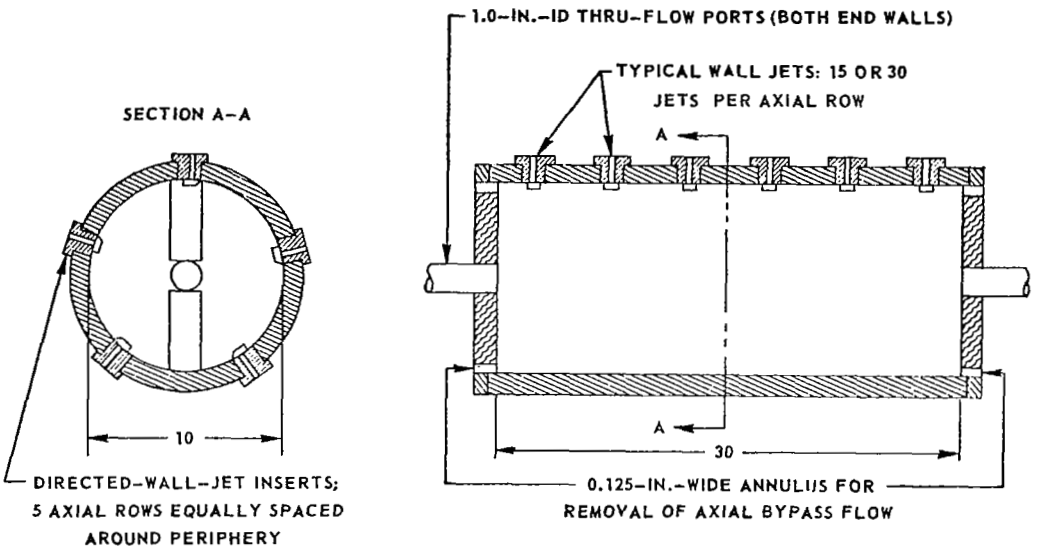

Fig. 8.8 Directed-wall-jet vortex tube with axial bypass in which the distributions of Fig. 8.7 were obtained.

injected axially thru one of the end walls. In spite of the rather distinct interface between the two species evident in Fig. (8.7), the containment as measured by the containment time τ_c, defined in Equation 8.2-10 is disappointingly low, approximately 2 for this particular set of experiments. Two different mechanisms appear responsible for this relatively poor containment. There is the problem of turbulence at the interface of the two gases, particularly in the end wall boundary layer, and second the problem of disruption of the closed cell by the continuous injection of the "contained" gas.

In a low Reynolds number, transient experiment, which eliminates both of the above fundamental problems, Chang, Chi, and Chen (1968) achieved containment times approaching those required by Equation 8.2-12. A summary of their results is given in Fig. (8.9) as a function of the average density ratio of contained "heavy" gas to the light gas passing thru the chamber. It may be

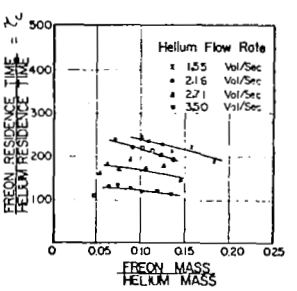

Fig. 8.9 Residence time ratio at various concentration ratio and helium flow rates, helium flow rates are given in cavity volume per second. Chang, Chi and Chen, 1968.

possible to overcome the problem of replenishing the slow losses of contained gas without unduly disturbing the closed cells with clever injection schemes, but there is no apparent way of circumventing the turbulent diffusion at the interface of the two gases at the large Reynolds numbers which would be required in a full scale reactor. Compounding the difficulty of stabilizing the interface is the fact that the average density of the fuel, $\bar{\rho}_f$ divided by the propellant density at the periphery of the chamber, ρ_{p1}, would have to be greater than 1 to achieve criticality. The negative $\partial\rho/\partial r$ required for this will have a destabilizing influence according to Section 5.3. Some results of United Aircraft Corporation [Clark, et al (1968)] show that containment is sharply reduced when $\bar{\rho}_f/\rho_{p_1}$ is increased above $\simeq 0.2$. Typical results are shown in Fig. 8.10. Over two thousand different flow conditions have been

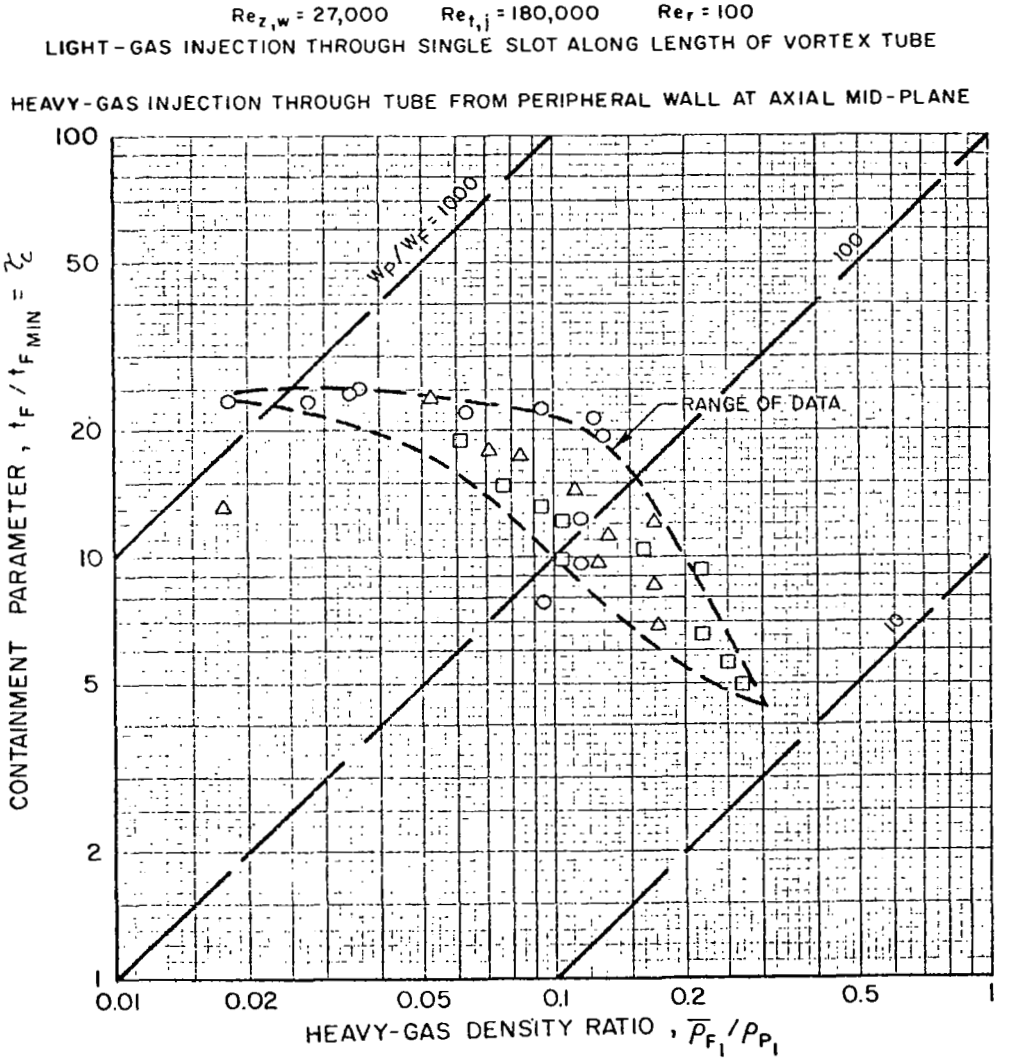

Fig. 8.10 Typical results of containment tests for basic vortex tube with radial inflow [Clark, Johnson, Kendall, and Mensing, 1967]

tried (See the work of Clark, Johnson, Kendall, Mensing and Travers) in attempts to increase both τ_c and $\bar{\rho}_f/\rho_{p_1}$. Since their work on stability (see Chapter V) indicated that larger negative density gradients should be stable with the large circulation gradients predicted for vortices with radial outflow then for radial inflow, much of their work has concentrated on this configuration [Johnson (1967) and Kendall, Mensing and Johnson (1967)]. A summary of their results for radial outflow is given in Fig. 8.11. Although there is a slight gain in τ_c at the larger values of density ratio, the best

AXIAL-FLOW REYNOLDS NUMBER , $Re_{z,w}$ = 46,000 TO 481,000
HEAVY-GAS INJECTION AT CENTER OF NONAXIAL-FLOW END WALL

Kendall, Mensing and Johnson, 1967

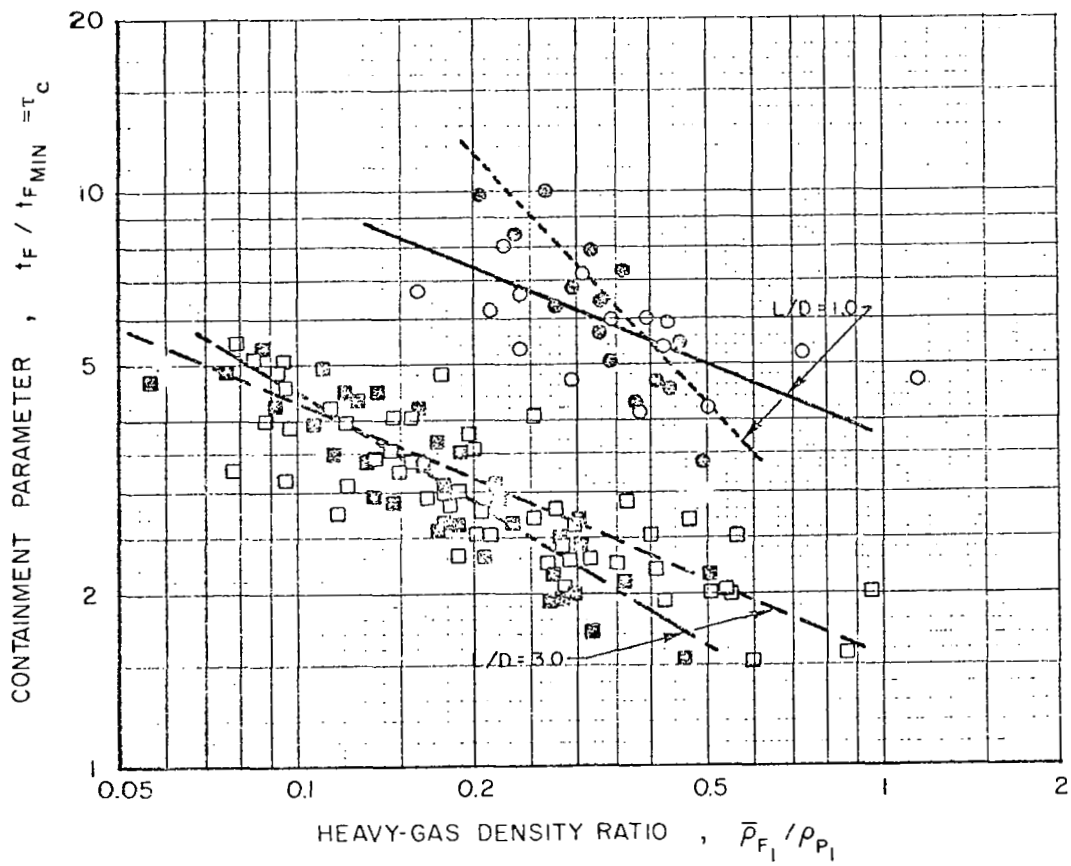

Fig. 8.11 Summary of principal results of containment tests for axial-flow vortex tubes with radial outflow.

combination of τ_c and $\bar{\rho}_f/\rho_{p_1}$ falls far short of the conditions necessary for open cycle containment. As previously noted in Section 5.7 radial outflow does not stabilize the flow. This type of containment for the gaseous nuclear rocket must apparently be abandoned unless some way of stabilizing the negative radial density gradient can be discovered.

The relatively poor containment achieved has lead UAC to direct its attention toward the closed cycle "Nuclear Light Bulb" concept shown in Fig. 8.12. In the nuclear light bulb engine an internally cooled transparent wall

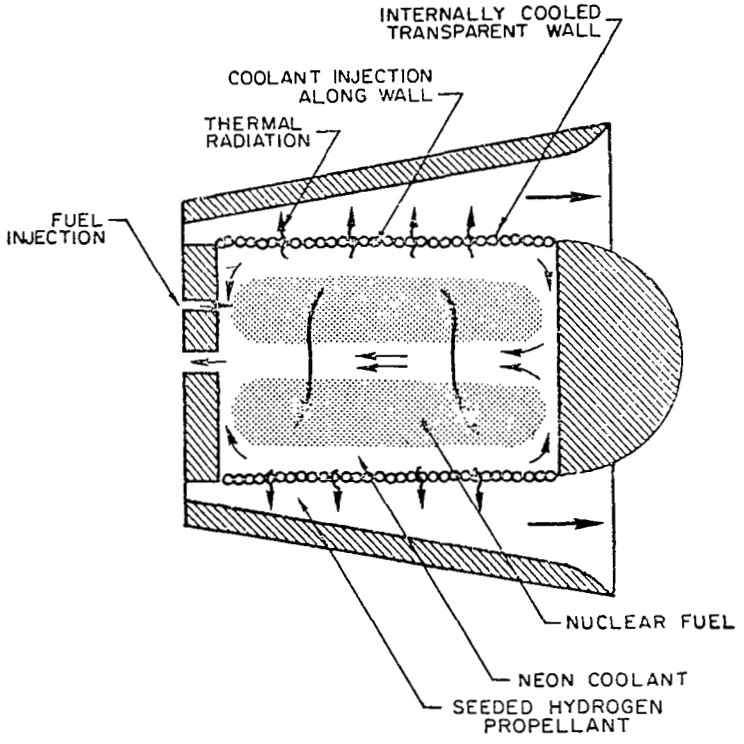

Fig. 8.12 Nuclear light bulb concept (McLafferty, 1967).

(made of fused silica or beryllium oxide) is used to separate the fuel and the propellant while allowing thermal radiation to pass thru it. Neon coolant gas is injected tangent to the inner surface of the transparent wall to drive the vortex which is used to isolate the gaseous nuclear fuel from the transparent wall. The major fluid dynamic advantage of this concept is that the cool neon has a much higher density than the propellant hydrogen and positive

radial density gradients can be maintained throughout the vortex to provide a strong stabilizing influence. A density discontinuity (but no pressure discontinuity) is maintained across the transparent wall between the outer, low density hydrogen and the inner, high density neon. McLafferty (1967) estimates that the energy deposited in the transparent wall by small, but finite thermal radiation and by convection, can be removed by the coolant flow provided the walls are sufficiently thin (on the order of 0.005 in.). The only strength requirement on the wall is that it be capable of stabilizing the boundary. A preliminary analysis by Tam, Goracke, and Lewellen (1970) indicates that such thin walls are, at least, capable of stabilizing the elementary Kelvin-Helmbotz instability at the interface.

The requirements on the vortex are quite different for this closed cycle system than for the previous open cycle system. A large value of τ_c is no longer required since what uranium flows thru the vortex can be cooled, separated from the neon, and recycled to the reactor. The containment requirement is replaced by the condition that the partial pressure of uranium at the inner surface of the transparent wall must be low to prevent condensation on the wall. Condensation of uranium on the transparent wall would block the transmission of thermal radiation and greatly increase the energy deposited in the wall. The conceptual design given by McLafferty (1969) calls for a transparent wall temperature of the order of 1000°K. The vapor pressure of U^{235} at this temperature according to the extrapolation of the curves given by Ragsdale, Kascak and Donovan (1967) is of the order of 10^{-15} atmospheres. When it is noted that the center line U^{235} pressure must be of the order of 100 atm., this implies that an extremely low value of the ratio of the partial pressure at the wall to the average partial pressure ($p_{f_w}/\bar{p}_f$) must be maintained. However, it appears probable that a uranium vapor pressure far above equilibrium pressure can be maintained in the presence of the very large thermal radiation flux associated with the concept. It then becomes a question of determining how large the partial pressure of uranium at the wall can become without unduly increasing the energy transfer to the wall. This does not appear to have been firmly established. Values of $p_{f\ wall}/\bar{p}_f$ as low as 0.04 have been achieved in an unheated vortex (McLafferty, 1970). Tests (Mensing and Jaminet, 1969) have also been conducted with r - f heated vortices to simulate the radial temperature

gradients expected near the outer periphery. This has a strong stabilizing effect and results in a strong decrease in simulated fuel partial pressure near the wall. Whether this degree of containment is adequate for the nuclear light bulb or not cannot be answered until a better estimate of the allowable partial pressure of uranium at the inner surface of the transparent wall is obtained.

8.5 Other Types of Containment

Other arrangements of closed streamline patterns may be imagined such as a two-dimensional forced vortex of the type which may be found in the separated wake of a bluff body (Evvard, 1965). However all of these configurations which consist of a heavy rotating fluid contained inside a lighter one are plagued with stability problems. The nature of the stability problem associated with Evvards proposal is discussed by Reshotko and Monnin (1965).

A somewhat different approach is taken by Moore and Leibovich (1970). They considered flows with closed bubbles which could have zero velocity inside the contained bubble with the expectation that such a constant pressure bubble would be more stable. They have shown that such flows can be theoretically obtained in at least two ways either by producing a special type of vortex breakdown (see Section 5.6) in a swirling flow or by using tangential vorticity without any swirling velocity. Perhaps the simplest way of viewing both flows is as a separation bubble. If an axisymmetric flow with a sufficiently strong, positive, radial gradient in total pressure is decelerated it will separate from its axis. Subsequent reacceleration will force the separation bubble to close. The radial gradient in total pressure for an axisymmetric flow may be caused by either axial vorticity (a swirling flow) or tangential vorticity (a bundle of coaxial "smoke-rings" in axial motion). Although the closed bubble (see Fig. 5.10) may be formed by a wide class of flows, only very special conditions may be expected to lead to the condition of zero velocity, constant pressure, within the separated bubble. The question of the stability of such a bubble filled with a heavier fluid is still a matter for speculation.

8.6 Particle or Droplet Containment

Since containment for a gaseous core nuclear rocket has proven so elusive, it appears useful to reexamine the liquid core concept. The

temperature limit of such a concept is imposed by fuel vaporization. Nelson, Grey, and Williams (1965) argue that specific impulses as high as 1500 seconds may be achieved if the uranium fuel is highly diluted with a low vapor pressure moderator such as zirconium carbide. This is not far below the 1800 seconds estimated by McLafferty (1970) for the nuclear light bulb concept. Is the possibility of containing a liquid fuel sufficiently closer to the state of the art than that of containing a gaseous fuel to more than compensate for the poorer performance?

The problem of particle or droplet containment is very close to that of centrifugally separating particles from a particle laden fluid. The engineering art of cyclone separators used for this purpose is well developed (see Section 9.1). Equation 9.1-13 may be used to estimate the lower bound on particle size which may be readily separated from a hot hydrogen flow. For a ZrC particle in a hydrogen stream at 100 atm. pressure and 5,000°K, $\rho_p/\rho \simeq 10^4$, $\nu \simeq 1$ cm^2/sec and $a_e \simeq 3 \times 10^5$ cm/sec. For criticality ℓ needs to be of the order of 1 m and r_e, the throat radius, is determined by the thrust level; $r_e \simeq 4$ cm corresponds to roughly 10,000 lb. thrust. When these values are used in Eq. 9.1-13 it shows that particles with a diameter larger than $\simeq 0.1$ microns should be readily separated from the flow. Thus containment for a liquid core rocket should be within the state of the art.

Perhaps a more difficult problem for any liquid core concept is the liquid-solid boundary. If swirl is provided by a rotating porous cylinder as in the Nelson, Grey and Williams concept, flow thru the cylinder, with a heavy fluid on the inside of the cylinder and a light fluid on the outside, leads to a Rayleigh-Taylor type instability. This has been experimentally demonstrated by McQuirk and Parks (1969). If swirl is provided by tangential jets as in a cyclone separator, the problem reduces to minimizing the interaction between the liquid and the wall. This problem has two facets: first the shear between the fluid mixture and the wall will reduce the swirl injected into the chamber and ultimately limit the density ratio of contained fluid mixture to thru flow; and second the heat transfer to the wall must not exceed 1/4 to 1/2 of the energy generated in the liquid or the Isp of the system will be compromised (see Eq. 8.2-2) by the energy balance in the wall.

Using the double cylinder arrangement shown in Fig. 8.13, experiments at the Aerospace Research Laboratories of Wright-Patterson Air Force Base

(Jackomis and von Ohain, 1970) have been able to achieve extremely high particle concentrations within the chamber without particle deposition at the cavity walls. Ratios of particle mass to the mass of the carrier gas (corresponding to $\bar{\rho}_f/\rho_{p_1}$) of the order of 100 have been demonstrated. This provides adequate containment for an attractive reactor concept (Tang, Stefanko, Dickson and Drawbaugh, 1970). A schematic of the reactor is given in Fig. 8.13. The question of whether the interactions between the carrier gas, the contained particles and the wall are adequate for proper heat transfer is yet to be determined.

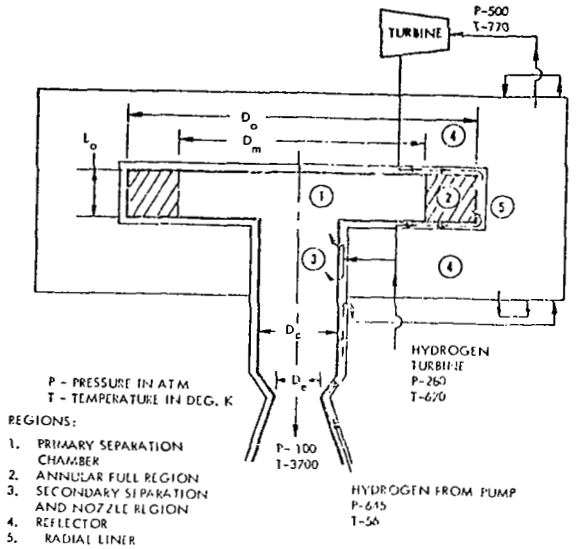

Fig. 8.13 Schematic of a colloid fueled, cavity reactor configuration [Tang, et al (1970)].

IX. OTHER VORTEX TUBES

9.1 Cyclone Separator

The most wide spread application of a confined vortex flow is that of a cyclone separator. The popular arrangement shown in Fig. 1.4 is only slightly different from that given in a German patent granted in 1855. Design modifications over the last century have proceeded on an empirical basis. Two books, one edited by Rietema and Verver (1961) and another written by Bradley (1965), give detailed information on dimensions and performance of cyclones for different applications. What is intended in this chapter is to present a simple theory for this standard cyclone and then to compare the results of the theory with some of the empirical design parameters.

The flow pattern sketched in Fig. 1.4 implies that the radial velocity thru the main part of the chamber is essentially zero with all of the thru flow passing thru the boundary layer. The conical shape of the cyclone insures that the boundary-layer flow towards the tip with its attached collector will be much larger than the boundary layer flow on the flat end of the chamber. The extension of the exhaust pipe into the chamber to form a so-called "vortex finder" ensures that even the small boundary-layer flow on the flat end wall will be forced to negotiate an extremely sharp turn and have most of the particles that are carried thru it separated from the exhaust flow. Most of the separation takes place as the majority of the flow passes from the tip of the cone, across the chamber, to the exhaust.

To analyze this model of a cyclone separator, it is convenient to first consider a much simpler ideal problem of centrifugal separation. Consider the uniform rotation of a one-dimensional flow of a fluid laden with particles of a uniform diameter d and density ρ_p. Assume the fluid velocity to be a constant w in the axial direction x with a uniform angular rotation Ω about the z axis. The radial velocity of the particles, u_p may be obtained from a balance between drag forces on the particle and centrifugal forces, with the inertia of the particles assumed negligible. For Stokes drag law this gives

$$u_p = \frac{d^2}{18} (\rho_p - \rho) \frac{\Omega^2 r}{\mu} \qquad (9.1\text{-}1)$$

The distribution of particles in the z direction n(z) may be obtained from the continuity equation for the particles

$$\frac{\partial nwr}{\partial z} + \frac{\partial nur}{\partial z} = 0 \qquad (9.1\text{-}2)$$

If the particles are assumed to be removed from the flow when they reach some radius r_o then it is consistent with Eqs. 9.1-1 and 9.1-2 to assume that n is a function of z only. Substitution of Eq. 9.1-1 into 9.1-2 gives

$$\frac{1}{n}\frac{dn}{dz} = -\frac{1}{w}\left[\frac{d}{9}^2 (\rho_p - \rho) \frac{\Omega^2}{\mu}\right] \qquad (9.1\text{-}3)$$

which can be integrated to give

$$n(z) = n(0) \exp - \left[\frac{1}{9}\left(\frac{\rho_p}{\rho} - 1\right) \frac{\Omega d^2}{\nu} \frac{\Omega z}{w}\right] \qquad (9.1\text{-}4)$$

This simple model of separation can be used to estimate the separation obtained in the cyclone model given in Fig. 1.4. The flow from the tip of the cone to the exhaust is not much different from that assumed in this simple model. The primary requirement in relating Eq. 9.1-4 to cyclone performance is to relate Ω and w to pressure drop and flow capacity since these are the quantities most conveniently measured. If essentially all of the flow passes thru the conical boundary layer and then across the chamber

$$w \simeq \dot{m}/\pi r_e^2 \rho \qquad (9.1\text{-}5)$$

and the relationship between pressure drop Δp and rotation Ω is given by the swirl parameter α from Eq. 2.2-8

$$\Omega = \frac{\alpha}{r_e}\left[\frac{2\Delta p}{\rho}\right]^{1/2} \qquad (9.1\text{-}6)$$

Eqs. 9.1-5 and 9.1-6 may be used to reduce Eq. 9.1-4 to

$$n(e) = n(0) \exp - \left[\frac{1}{9}\left(\frac{\rho_p}{\rho} - 1\right)\frac{d^2 2\Delta p \pi L \alpha^2}{\dot{m}\nu}\right] \qquad (9.1\text{-}7)$$

or, rearranging

$$\left(\frac{\rho_p}{\rho} - 1\right) d^2 \frac{\Delta p}{\nu} \frac{L}{\dot{m}} = \frac{9}{2\pi} \frac{1}{\alpha^2} \ell n \frac{n(0)}{n(\ell)} \qquad (9.1\text{-}8)$$

In order to optimize separation, it is clear from Eq. 9.1-8 that α should be maximized. In Section 6.5 it was argued that the maximum stable

value of α corresponds to the value of α that maximizes the flow of angular momentum. This occurs for $\alpha \approx 0.5$. Thus for a properly designed cyclone it should be possible to have

$$\left(\frac{\rho_p}{\rho} - 1\right) \frac{d^2 \Delta p}{\nu} \frac{L}{\dot{m}} \simeq 6 \ln \frac{n(0)}{n(L)} \tag{9.1-9}$$

A convenient measure of a cyclone's performance is to determine the particle size which is only 50% separated out. If this size particle is denoted by d_{50} then Eq. 9.1-9 gives

$$\left(\frac{\rho_p}{\rho} - 1\right) \frac{d_{50}^2 \Delta p}{\nu} \frac{L}{\dot{m}} \simeq 4 \tag{9.1-10}$$

Figure 9.1 is a plot of the dimensionless grouping given in Eq. 9.1-10 for various values of the dimensional quantities for what Rietema and Verver (1961) refer to as "well designed" cyclones. The agreement with Eq. 9.1-10 is even better then the simple theory would appear to warrant.

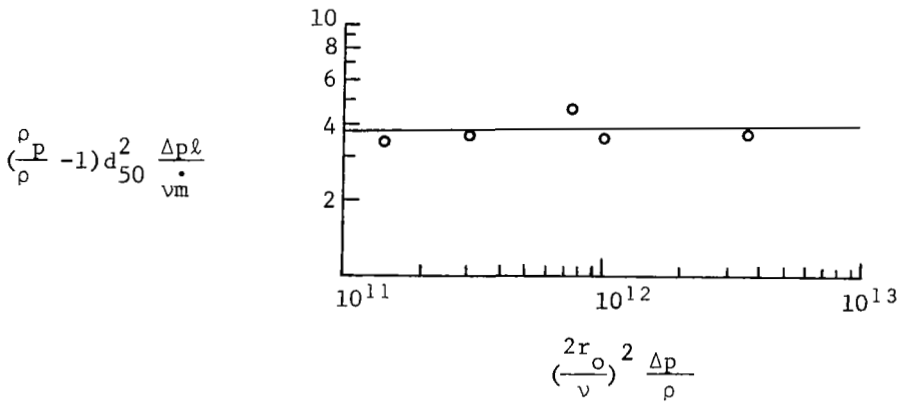

Fig. 9.1 Correlation of particle size separated out at different pressure drops for different fluids. (Rietema and Verver, p. 53).

Why isn't it necessary to include any influence of turbulence in determining the concentration distribtuion of particles? The distribution given in Eq. 9.1-4 is not influenced by any concentration diffusion. Small random velocity fluctuations should average out and leave this distribution unaffected.

Equation 9.1-10 should not be expected to remain valid as large pressure drops are applied across the chamber and the flow chokes sonically. To determine the lower bound on particle size that may be expected to be separated out in a cyclone it is more convenient to work in terms of w and Ω. The maximum

value of Ω can be estimated from the upper bound on tangential Mach number given in Section 6.5

$$\Omega_{max} \approx M_{t_{max}} \frac{a_e}{r_e} \approx 1.2 \frac{a_e}{r_e} \tag{9.1-11}$$

The average value of w_e is given approximately by

$$w_e \approx \psi^*(1,\alpha)\ a_e \approx a_e/2 \tag{9.1-12}$$

When Eqs. 9.1-11 and 9.1-12 are substituted into Eq. 9.1-4 it leads to

$$d_{50}^2 \approx \frac{2}{\frac{\rho_p}{\rho} - 1)} \frac{\nu}{a_e} \frac{r_e^2}{\ell} \tag{9.1-13}$$

For dirt in air $\rho_p/\rho \approx 2 \times 10^3$, $\nu \approx 0.2$ cm^2/sec and $a_e \approx 3 \times 10^4$ cm/sec and for Rietema and Verver's "well designed" cyclone $r_e/\ell \approx 0.03$. This gives

$$d_{50} \approx 1.4 \times 10^{-5}\ r_e^{1/2} \tag{9.1-14}$$

with both d_{50} and r_e in cm. Or for d_{50} in microns and r_e in cm.

$$d_{50} \approx 0.1\ r_e^{1/2} \tag{9.1-15}$$

Thus particles of the order of 0.1 μ can be separated out in a small cyclone separator.

It is evident from both Eqs. 9.1-10 and 9.1-15 that the smaller the cyclone the better it will perform as a separator. In designing a separtion system it is well to set the size of the cyclones by the requirement on particle size to be separated out at a given pressure drop, and then determine the number required to obtain the desired flow capacity.

What about the geometrical ratios of a well designed cyclone? If the flow pattern assumed in the separation model is to be achieved with minimum dissipation within the chamber it is desirable to have the radial stagnation surface, $\hat{r}$, occur just outside the radius of the exhaust. The results of Section 6.3 may be applied to estimate the length of the cone required to do this. When both Γ and dr/ds are assumed constant in Eq. 6.3-4 it is possible to generalize the definition of B to include the effect of the conical wall. Assuming all the flow to pass thru the boundary layer on the conical wall the appropriate generalization is

$$B = \frac{2\pi\rho r_o \Gamma_o \lambda_1 C_f}{(-dr/ds)\,\dot{m}} \tag{9.1-16}$$

To have $\hat{r} = r_e$ then Eqs. 6.3-12 and 9.1-16 lead to

$$r_e = 1 - \frac{(-dr/ds)\,\dot{m}}{4.9\ C_f\ 2\pi\rho r_o \Gamma_o} \tag{9.1-17}$$

For a slender cone

$$-\frac{dr}{ds} = \frac{r_o - r_e}{[L^2 + (r_o - r_e)^2]^{1/2}} \approx r_o/L \tag{9.1-18}$$

The ratio $\dot{m}/2\pi\rho r_o \Gamma_o$ may be written in terms of dimensionless exhaust parameters as

$$\frac{\dot{m}}{2\pi\rho r_o \Gamma_o} = \frac{\bar{Q}}{\alpha}\,\frac{r_e}{2r_o} \tag{9.1-19}$$

Equations 9.1-19 and 9.1-18 may now be combined with Eq. 9.1-17 to give

$$\frac{r_e}{L} \approx \left(1 - \frac{r_e}{r_o}\right) \frac{9.8\alpha C_f}{\bar{Q}} \tag{9.1-20}$$

In order to have the pressure drop associated with the inlet small in comparison to the pressure drop across the exit it is desirable to have $(r_e/r_o)^2 << 1$. On the other hand making this radius ratio too small would unduly restrict the flow capacity of a given size device. A good compromise appears to be $r_e/r_o \approx 1/3$.

From Section 6.5 the maximum value of $\alpha/\bar{Q}$ is of the order of 1, so from Eq. 9.1-20

$$\frac{r_e}{L} \approx 7\ C_f \tag{9.1-21}$$

Rietema and Verver give values of $\ell/r_o = 10$ and $r_o/r_e = 3$ as optimum dimensions for a cyclone. Equation 9.1-21 would predict their value of $r_e/\ell = 0.03$ for $C_f = 0.004$, a reasonable value of C_f for Re_t between 10^5 and 10^6. Thus the present model appears consistent with the experimentally observed optimum geometry.

Other arrangements of vortex chambers may be used for particle separation. In particular, the arrangement used by Fletcher, Gyarmathy and Hasinger (1966)

is noteworthy since it completely eliminates any possible particle losses thru the boundary layer on the chamber wall thru which the flow exhausts. This arrangement suggested by H. von Ohain is shown in Fig. 9.2. High momentum fluid is used to reverse the secondary flow patterns. However, since the so called vortex finder works fairly satisfactory in separating particles from the boundary layer by forcing a sharp turn in this flow the sophistication of the reverse flow chamber is not warranted for most applications. More important gains in separation efficiencies are likely to be gained by novel arrangements to use an array of small chambers in place of a single large chamber.

The separation formulae of this section are all based on Stokes drag law. The validity of this drag law is bounded for large particles by the need to keep the particle Reynolds number small and for small particles the need to keep the mean free path of the fluid less than the particle diameter. These limits can be somewhat extended by applying the Oseen correction for the Reynolds number effect and the Cunningham correction for effects of slip flow. In this case

$$\text{Drag} = 3\pi\mu du \; \frac{1 + \frac{3}{16}\frac{\rho u d}{\mu}}{1 + 2.5\lambda/d} \qquad (9.1\text{-}22)$$

where λ is the mean free path of the fluid.

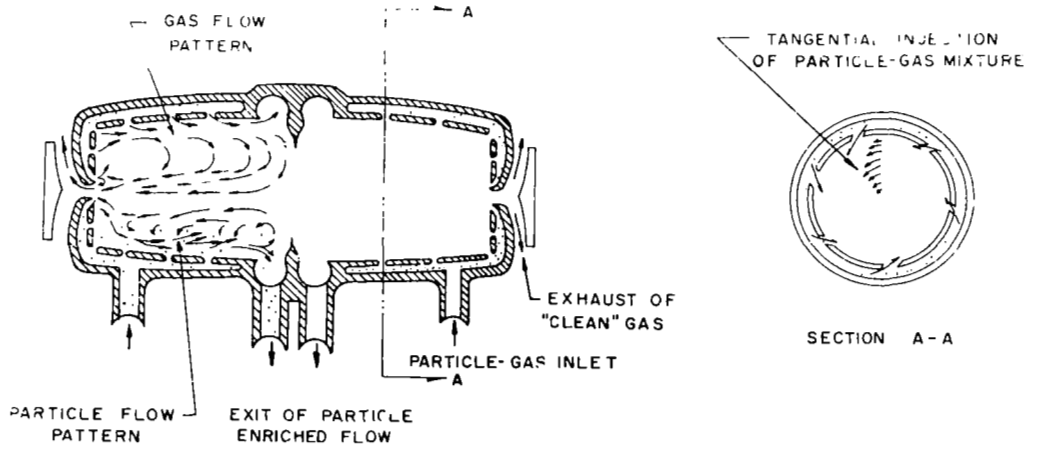

Fig. 9.2 Simplified flow diagram of a swirl chamber with reversed secondary flow (Fletcher, Gyarmathy and Hasinger, 1966).

9.2 Ranque-Hilsch Tube

Ranque applied for a French patent in 1931 for "an apparatus for obtaining from a fluid under pressure two currents of fluids at different temperatures". Ranque's device was similar to that sketched in Fig. 1.3. It received little attention until Hilsch in 1944 tried to develop it to cool underground mines. Hilsch (1947) gave performance data and optimum dimensions for the vortex tube. The possibility of an extremely simple device replacing many of the more complicated refrigeration appliances stimulated a large number of investigations in the next few years. By 1950, it had become clear that the vortex tube made a very inefficient refrigerator. Fulton (1950) quotes an efficiency of the order of 1%. Over the past 20 years the device has remained an intriguing subject for study. Westley (1954) lists 116 references related to the Ranque-Hilsch Tube. The more easily accessible references published in the last 10 years are included in the present bibliography. The purpose of this section is to summarize the experimental performance and give a rough analysis.

One of the best sources of data for determining optimum performance of the tube is Westley (1957). He found that the maximum temperature drop ratio $(T_{o\ in} - T_{o\ cold})/T_{o\ in}$ occurred when the cold outlet radius was approximately 0.4 times that of the tube radius and the ratio of inlet area-to-tube cross sectional area approximately 0.2. No optimum L/D was reported. The only requirement appears to be that L/D exceed approximately 10. The maximum temperature drop occurs for a ratio of cold flow to total flow between 0.15 and 0.35. Figure 9.3 is Westley's curve of maximum temperature drop as a function of pressure ratio for his optimum geometry.

As seen in Chapter 6 the detailed prediction of the three-dimensional flow pattern in a highly turbulent vortex tube is still beyond the state of the art. Since the energy separation depends upon this flow pattern it is to be expected that the numerous attempts to predict the performance of a Ranque-Hilsch tube (e.g. Kassner and Knoernschild, 1947; Fulton, 1950; Deissler and Perlmutter, 1960; Lay, 1959; Sibulkin, 1961; and Linderstrom-Lang, 1970), although each contributing to the understanding of tube, have not met with complete success. Rather than pursue a critique of these papers a semi-quantitative analysis of the mechanism will be given here by circumventing

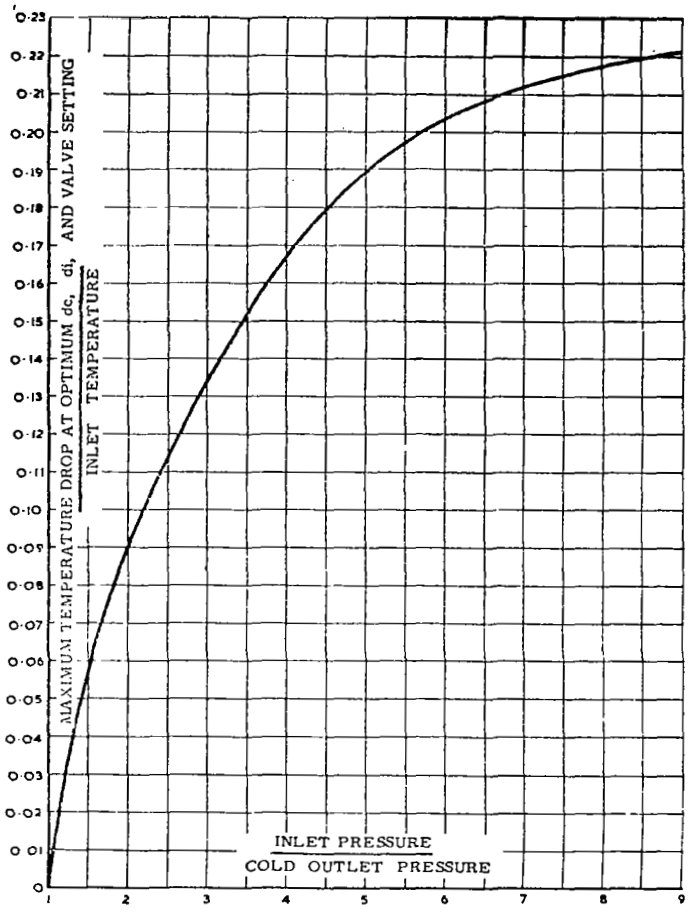

Fig. 9.3 Variation of temperature drop efficiency with pressure ratio at optimum cold outlet size, optimum valve setting and fixed inlet diameter (Westley, 1952).

most of the flow details within the chamber.

First, it is important to note the internal counter flow pattern sketched in Fig. 9.4. As seen in Chapter III this pattern is a consequence of the tendency of the swirling flow towards two-dimensionality. However, the tube is made long enough that two-dimensionality cannot be preserved due to torque on the internal cylindrical wall. If the tube length is extended beyond the counterflow cell the flow pattern in the cold end should be unaffected. Thus as long as the tube wall is insulated the temperature separation

in the tube should be unaffected by L/D as long as some minimum is exceeded. As a consequence of the counterflow pattern the radial velocity is very small within a few diameters of the cold outlet.

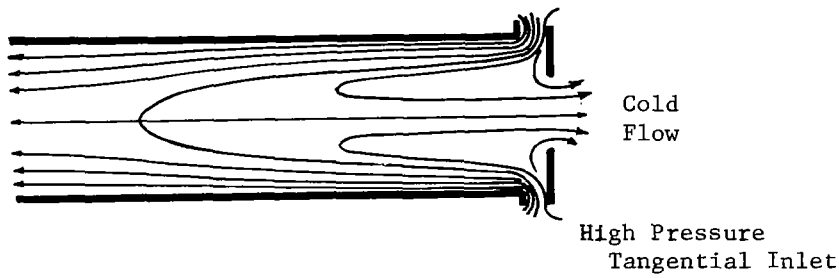

Fig. 9.4 Sketch of flow streamlines near the cold outlet of a Ranque-Hilsch Tube.

Second, the internal torque exerted between concentric rings of fluid produces a radial transport of energy as originally pointed out by Ranque (1933). As long as the angular velocity decreases with increasing radius this transfer of energy due to work done on the fluid will be directed outward. This will be counterbalanced by an energy flow inward due to heat transfer. As pointed out by Fulton (1950) the flow of energy in a laminar irrotational vortex due to the work term should exceed the flow due to heat transfer as long as Pr > 1/2. This can be seen from Mack's solution given in Eq. 4.1-8. In fact, it should be possible to estimate a bound on the energy separation from this expression if the assumption is made that turbulent transport can be related to laminar simply by using a turbulent Prandtl number. (This assumption has as yet not been justified.) The maximum tangential Mach number in the tube may be expected to occur near the dividing line between the counter flows in the vicinity of the cold outlet. If this reverse flow has persisted long enough in the axial direction to permit the radial transfer of energy to reach the same equilibrium it would for w = 0, then Eq. 4.1-8 may be used directly to relate total temperature drop to maximum tangential Mach number.

$$\frac{T_{o_{in}} - T_{o_{cold}}}{T_{o_{in}}} = \frac{(Pr - 1/2)\, M_{t_{max}}^2}{\frac{1}{\gamma - 1} + Pr\, M_{t_{max}}^2} \qquad (9.2\text{-}1)$$

In Section 6.5 it was argued that M_t will increase as the pressure ratio across the vortex tube is increased until an upper bound of approximately 1.2 is reacheddue to an instability in the exhaust flow. A value of $M_{t_{max}} = 1.2$ and an assumed turbulent Prandtl number of 1 in Eq. 9.2-1 gives

$$\frac{T_{o_{in}} - T_{o_{cold}}}{T_{o_{in}}} \simeq 0.185 \qquad (9.2\text{-}2)$$

Although this is somewhat lower than Westley's asymptotic value of 0.22 it is close enough to suggest that the model is basically sound. In fact agreement can be achieved by a 10% change in either $M_{t_{max}}$ or Pr neither of which are known to that accuracy.

The pressure ratio required to reach this maximum separation depends upon dissipation in the tube, and thus would be more difficult to predict, but Fig. 6.18 shows that a pressure ratio of 7 to 8 was required to reach this asymptotic value of M_t. Since the Ranque-Hilsch tube may be expected to have larger wall dissipation than the arrangement used by Poplawski and Pinchak it is expected that a somewhat larger pressure ratio would be required.

9.3 Miscellaneous Vortex Tubes

The applications considered in Chapters VII, VIII, and in Sections 9.1 and 9.2 do not exhaust all the possibilities for confined vortex flows. Many other devices involving such a flow are referred to in the attached bibliography. In compiling the bibliography an attempt was made to include the literature directly concerned with confined vortices which has been published in the last 10 years. Older references were included only when they were deemed important enough to be referred to in the body of the review.

Although somewhat outside the scope of this review of confined vortex devices, it seems useful to refer to two different flows closely related to the vortex tube, gas centrifuges and meteorological vortices. Gas centrifuges share many of the secondary flow features of the vortex tube. They differ in that swirl is supplied by rotating walls and flow patterns which hold radial flow to a minimum are chosen to maximize the diffusion parameter in Eq. 8.3-1. The basic theory of centrifuges as applied to isotope separation was given by Cohen (1951) and reference to more recent literature may be found in Wensel (1967) and Krauze (1970). Meteorological vortices are often modeled in the

laboratory as confined vortices, but the boundary conditions appear to differ in at least two essential ways. The density gradient with altitude plays an important role in the dynamics of both the tornado and the hurricane and the horizontal extent of an atmospheric vortex is set by stability conditions rather than confining walls. A review of meteorological vortices was given by Morton (1966).

References

(References for Chap. VIII only are listed here; other references are included in the bibliography)

Chacko, G. K. (1969), Reducing the Costs of Space Transportation, Space and Technology Series, Vol. 21.

Duke, E. E. and Houghton, W. J. (1966), Gaseous fueled nuclear rocket engine, AIAA Paper No. 66-621 (June).

McQuirk, J. P. and Parks, C. (1969), Hydrodynamic simulation of a rotating liquid core nuclear rocket chamber, unpublished paper.

Nelson, S. T., Grey, J. and Williams, P. M. (1965), Conceptual study of a liquid-core nuclear rocket, J. of Spacecraft and Rockets, 2, 384-391.

Pincock, G. D. and Kunze, J. F. (1967-69), Cavity reactor critical experiment, Vol. I (1967) NASA-CR-72234; Vol. II (1968) NASA-CR-72415; Vol. III (1968) NASA-CR-72384; Vol. IV (1969) NASA-CR-72550.

Ragsdale, R. G. (1963), Outlook for gas-core nuclear rocket, Astronautics and Aeronautics, Vol. 1, 88-91 (August).

Ragsdale, R. G., Kascak, A. F. and Donovan, L. F. (1967), Heat and mass transfer characteristics of an axial-flow liquid-core nuclear rocket employing radiation heat transfer, NASA TND-4127 (August).

Roback, R. (1967), Theoretical performance of rocket engines using gaseous hydrogen in the ideal state at stagnation temperatures up to 200,000°R, NASA-CR-696, (February).

Schneiderman, S. B. (1964), Theoretical viscosities and diffusivities in high temperature mixtures of hydrogen and uranium, NASA-CR-213.

Tam, C. K. W., Goracke, D. B. and Lewellen, W. S. (1970), Stability considerations for a transparent wall in a gaseous nuclear rocket to be published in the Proceedings of the Symposium on Research on Uranium Plasmas and their Technological Application held at University of Florida, January, 1970.

BIBLIOGRAPHY

Confined Vortex Flows

Acharya, Y. V. G., Krishnamurthy, K. and Irani, P. A. (1965), Vortex Flows, (NAL, Bangalore, India), NASA Accn No. N66-24832, Report No. TN-AE-28-65.

Adams, R. G. (1969), An experimental investigation of the inward flow of an incompressible viscous fluid between parallel co-rotating disks, Arizona State Univ. Ph.D. Thesis.

Amber, C. M. (1961), Theory of Centrifugation, Ind. Eng. Chem., 53, 430-3.

Anderson, O. L. (1961), Theoretical solutions for the secondary flow on the end wall of a vortex tube, UARL Report R-2494-1 (November).

Anderson, O. L. (1963), Theoretical effect of Mach number and temperature gradient on primary and secondary flow in a jet-driven vortex, Air Force Systems Command Report RTD-TDR-63-1098 (November).

Anderson, O. L. (1966), Numerical solutions of the compressible boundary layer equations for axisymmetric flows, UARL Report E110266-1 (October). Also Ph.D. Dissertation from Rensselaer Polytechnic Institute.

Andrade, E. N. (1963), Whirlpools, vortices and bath tubs, New Scientist, 17, 302 (December).

Armitage, J. V. (1968), Computation of axial-symmetric transonic swirl flows by the unsteady flow approach, ARL 68-0070 (April).

Arora, C. (1961), Theoretical Analysis of Ranque-Hilsch tube, 7th Congress of Theoretical and Applied Mechanics, Proc. Bombay, India (December).

Astill, K. N., Ganley, J. T., Martin, B. W. (1968), The developing tangential velocity profile for axial flow in an annulus with a rotating inner cylinder, Proc. of the Royal Soc. Series A, 307, 55-69 (October).

Baker, D. W. (1967), Decay of swirling, turbulent flow of incompressible fluids in long pipes, Maryland University Ph.D. Thesis.

Balvev, E. D., and Troyankin, Yu. V. (1967), The aerodynamic structure of gas flow in a cyclone chamber, Teploenergetika, 14(1), 63-5, (in Russian).

Barber, E. (1960), Vortex tubes, Jet Propulsion Laboratory, Vortex Literature Search No. 56 (October).

Barcilon, A. I. (1967), Vortex decay above a stationary boundary, J. Fluid Mech., 27, 155-175.

Batchelor, G. K. (1951), Note on a class of solutions of the Navier-Stokes Equations representing steady rotationally-symmetric flow, Quart. J. Mech. and Appl. Math., 4, 29-41 (March).

Batchelor, G. K. (1964), Axial flow in trailing line vortices, J. Fluid Mech., 20, 645.

Batchelor, G. K. (1967), An Introduction to Fluid Dynamics, Cambridge University Press.

Batson, J. L. and Sforzini, R. H. (1970), Swirling flow through a nozzle, Journal of Spacecraft and Rockets, 7, No. 2, 159-163 (February).

Bauer, A. B. (1968), Vortex valve operation in a vacuum environment, ASME Paper No. 68-FE-47 (May).

Bell, A. C. (1965), Optimization of a vortex valve, S.M. Thesis, Dept. of Mechanical Engineering, MIT (December).

Bell, A. C. (1967), Multiple inlet vortex valve studies, TR-AFFDL-TR-67-23 (January).

Benjamin, T. B. (1962), Theory of the vortex breakdown phenomenon, Journal of Fluid Mechanics, 14, 593.

Benjamin, T. B. (1965), Significance of the vortex breakdown phenomenon, Journal of Basic Engineering. Trans. of the ASME Series D., 518 (June).

Benjamin, T. B. (1966), Internal waves of finite amplitude and permanent form, J. Fluid Mech., 25, 241.

Benjamin, T. B. (1967), Some developments in the theory of vortex breakdown, J. Fluid Mech., 28, 65-84.

Benjamin, T. B. and Barnard, B. J. S. (1964), A study of the motion of a cavity in a rotating liquid, J. Fluid Mech., 19, Part 2 (June).

Bichara, R. T. and Orner, P. A. (1969), Analysis and modeling of the vortex amplifier, ASME J. of Basic Engineering, 91, Series D., 755-763 (Dec.).

Bien, F. and Penner, S. S. (1970), Velocity profiles in steady and unsteady rotating flows for a cylindrical geometry, The Physics of Fluids, 13, 1665-1671 (July).

Binnie, A. M. (1949), The passage of a perfect fluid through a critical cross section or "throat", Proc. Royal Soc. A, 197, 545.

Binnie, A. M. (1951), The theory of waves traveling on the core of a swirling liquid, Proc. Royal Soc. A, 205, 530-540.

Binnie, A. M. (1957), Experiments on the slow swirling flow of a viscous liquid through a tube, Quart. Journal Mech. and Appl. Math, 10, 276-290 (August).

Binnie, A. M. and Harris, D. P. (1950), The application of boundary-layer theory to swirling liquid flow through a nozzle, Quart. J. Mech. and Applied Math. III, Part 1.

Binnie, A. M. and Hookings, G. A. (1948), Laboratory experiments on whirlpools, Prof. Royal Soc. A, 194, 348-415.

Binnie, A. M., Hookings, G. A. and Kamel, M. Y. M. (1957), The flow of swirling water through a convergent-divergent nozzle, Journal of Fluid Mechanics, 3, No. 3, 261-274 (December).

Binnie, A. M. and Kamel, M. Y. M. (1959), Experiments on the flow of water in a tube at high rates of swirl, Houille Blanche, 14, 348-360 (May/June).

Blatter, A. and Keranen, T. W. (1970), A vortex valve for flow modulation of 5500°F gas, J. of Spacecraft and Rockets, 7, No. 2, 169-174 (February).

Bödewadt, V. T. (1940), Die Drehstromung uber festem Grunde, Zeits. Ang. Math. Mech., 20, 241-253 (October).

Borisenko, A. I., Iakovlev, A. I., and Safonov, V. A. (1968), Increasing the energetic cooling efficiency of vortex tubes used for cooling aircraft components, Samoletostroenie I Tekhnika Vozdushnógo Floato, edited by Alekseev, I. N. (A69-14488).

Bornkessel, V. and Pilot, J. (1962), Zur Gas-und Isotopentrennung im Wirbelrohr, Z. F. Physikalische Chemie, 221, 177-184 (November).

Bossel, H. H. (1967), Inviscid and viscous models for vortex breakdown phenomenon, Ph.D. Dissertation, University of Calif., Berkeley.

Bossel, H. H. (1969), Vortex breakdown flowfield, The Physics of Fluids, 12, 498-508 (March).

Boyd, K. E. and Rice, W. (1968), Laminar inward flow of an incompressible fluid between rotating disks, with full peripheral admission, ASME J. of Appl. Mech., Paper No. 68-APM-12.

Bradley, D. (1965), The hydrocyclone, Pergamon Press.

Brookman, R. S., Phillippi, J. F. and Maisch, C. L. (1963), Small diameter cyclones, Chem. Eng. Prog., 59, 11, 66-69 (November).

Bruun, H. H. (1967), Theoretical and experimental investigation of vortex tubes (in Danish), Dept. of Fluid Mech., Report No. 67-1, Danish Technical University.

Burgers, J. M. (1948), A mathematical model illustrating the theory of turbulence, Advances in Applied Mechanics, Academic Press, 1, 197-199.

Burggraf, O. R. (1968), A linearized analysis of mass transfer effects on confined laminar vortex flows, Ohio State Univ. Research Foundation Project 7116, Report No. ARL 68-0071 (April).

Burton, K. R. (1970), Influence of gravity on the performance of a conical vortex separator, AIAA J., 8, 956-958 (May).

Cassidy, J. J. and Falvey, H. T. (1970), Observations of unsteady flow arising after breakdown, J. Fluid Mech., 41, 727-736.

Catchpole, B. G. (1969), Fluidics - The characteristics of a simple vortex flow modulator, Aeronautical Research Labs, Report ARL/ME-310, Melbourne, Australia (November).

Chanaud, R. C. (1965), Observations of oscillatory motion in certain swirling flows, J. Fluid Mech., 21, Part 1, 111-127.

Chandrasekhar, S. (1961), Hydrodynamic and hydromagnetic stability, Clarendon Press, Oxford.

Chang, C. C., Chi, S. W. and Chen, C. M. (1967), Gas-core nuclear rocket fluid mechanics experiments at Catholic University, AIAA Paper No. 67-502 (July).

Chang, C. C., Chi, S. W. and Chen, C. M. (1968), Experimental exploration of recirculation zone in the gas-core nuclear rocket concept, J. Spacecraft and Rockets, 5, 480-481 (April).

Chang, C. C. and Lundgren, T. S. (1959), Flow of an incompressible fluid in a hydromagnetic capacitor, The Physics of Fluids, 2, 627 (June).

Chang, T. S. (1965), Hydromagnetic stabilization of nondissipative vortex flow, Developments in Theoretical and Applied Mechanics II, Pergamon Press, 261-276.

Chang, T. S. (1965), Exact criterion of hydromagnetic stability of inviscid vortex flow with finite conductivity, AIAA J., 3, 2050 (November).

Chang, T. S. and Sartory, W. K. (1965), Hydromagnetic stability of dissipative vortex flow, The Physics of Fluids, 8, 235-241 (February).

Chang, T. S. and Sartory, W. K. (1965), Hydromagnetic stability of dissipative flow between rotating permeable cylinders, J. Fluid Mech., 27, 65-79.

Chang, T. S. and Sartory, W. K. (1968), Comments on circulatory flow of a conducting liquid about a porous, rotating cylinder in a radial magnetic field, AIAA J., 6, 382-383 (February).

Chervinsky, A. (1968), Similarity of turbulent axisymmetrical swirling jets, AIAA J., 6, 912-914 (May).

Chigier, N. A. and Beer, J. M. (1964), Velocity and static pressure distributions in swirling air jets issuing from annular and divergent nozzles, ASME J. of Basic Engineering, 4, 788.

Chow, C. Y. (1969), Swirling flow in tubes of non-uniform cross-sections, J. Fluid Mechanics, 38, 843-854 (October).

Chow, S. K. (1968), An experimental study on the characteristics of vortex valves, International Federation of Automatic Control, Symposium on Fluidics, London, England (November).

Clark, J. W., Johnson, B. U., Kendall, J. S., Mensing, A. E. and Travers, A. (1968), Open-cycle and light-bulb types of vortex-stabilized gaseous nuclear rockets, J. of Spacecraft and Rockets, 5, 941-947 (August). (Also UAC-RL Report F 910093-13, May, 1967).

Cochran, W. G. (1934), The flow due to a rotating disk, Proc. Cambr. Phil. Soc., 30, 365-375.

Cohen, K. (1951), The Theory of Isotope Separation, McGraw Hill, New York.

Coles, D. (1965), Transition in circular couette flow, J. Fluid Mech., 21, 385-425.

Colgate, S. A. (1964), Vortex gas accelerator, AIAA J., 2, 2138-2141 (December).

Collins, J. C. and Stubbs, T. F. (1964), Qualitative experimental investigations on various vortex tube configurations, University of California, Lawrence Radiation Laboratory, UCRL 12045.

Colquitt, C. W., Jr. (1969), Fluidics for propellant tank pressurization, Journal of Spacecraft and Rockets, 6, 111-116 (February).

Conover, R. A. (1968), Laminar flow between a rotating disk and a parallel stationary wall with and without radial inflow, ASME J. of Basic Engineering, 90, 325-332 (September).

Cooke, J. C. (1952), On Pohlhausen's method with application to a swirl problem of Taylor, J. Aeron. Sci., 19, 486-490.

Cooke, J. C. (1966), Numerical solution of Taylor's swirl atomizer problem, Royal Aircraft Establishment Tech. Report 66128.

Cooper, J. (1964), Vortex motions in ideal Bose superfluid, Phys. Chem., 73A, 309-12 (May).

Cooper, R. S., Editor (1965), Proceedings of an Advanced Nuclear Propulsion Symposium, Los Alamos Scientific Laboratory, LA-3229-MS (January).

Cooper, R. S. (1965), Advanced nuclear propulsion concepts, AIAA Paper No. 65-531, AIAA Second Annual Meeting, San Francisco, California (July).

Datta, S. K. (1965), Stability of spiral flow between concentric circular cylinders at low axial Reynold's number, J. of Fluid Mech., 21, 635 (April).

Davis, W. C. et al (1961), Research and development on a vortex MHD power generator, Final Report No. ER-4737, Tapco Div., TRW, Inc. (December).

Deissler, R. G. (1965), Unsteady viscous vortex with flow toward the center, NASA TN D-3026 (September).

Deissler, R. G. and Perlmutter, M. (1958), An analysis of the energy separation in laminar and turbulent compressible vortex flows, Proc. of Heat Transfer and Fluid Mechanics Institute, Stanford University Press.

Deissler, R. G. and Perlmutter, M. (1960), Analysis of the flow and energy separation in a turbulent vortex, International Journal of Heat and Mass Transfer (August).

Dergarabedian, P. (1960), The behavior of vortex motion in an emptying container, Proceedings of the 1960 Heat Transfer and Fluid Mechanics Institute, Stanford University Press, 47-61 (June).

Dexter, E. M. (1961), No moving parts: a feature of new valves, Journal of the Society of Automotive Engineers, 69, 102 (September).

Dobratz, B. M. (1964), Vortex tubes, a bibliography, University of California, Lawrence Radiation Lab. Report UCRL-7829.

Donaldson, C. DuP. (1956), Solutions of the Navier-Stokes equations for two and three-dimensional vortices, Ph.D. Dissertation, Princeton University (December).

Donaldson, C. DuP. (1961), The magnetohydrodynamic vortex power generator: basic principles and practical problems, Aeronautical Research Associates of Princeton, Report No. 30.

Donaldson, C. DuP. and Snedeker, R. S. (1962), Experimental investigation of the structure of vortices in simple cylindrical vortex chambers, ARAP Report 47.

Donaldson, C. DuP. and Sullivan, R. D. (1960), Examination of the solutions of the Navier-Stokes equations for a class of three-dimensional vortices, Aeronautical Res. Associates of Princeton Inc., AFOSR TN 60-1227 (October).

Donaldson, C. DuP. and Sullivan, R. D. (1960), Behavior of solutions of the Navier-Stokes equations for a complete class of three-dimensional viscous vortices, Proc. of the 1960 Heat Transfer and Fluid Mechs. Inst., Stanford University Press, 16-30.

Donaldson, C. DuP. and Sullivan, R. D. (1962), Examination of the solutions of the Navier-Stokes equations for a class of three-dimensional vortices, Part II Velocity and pressure distributions for unsteady motion, Aero. Res. Assoc. Princeton Rep. 50 (AFOSR TN 60-1227) (1963), Ibid Part III Temperature distributions for steady motion, Aero. Res. Assoc. Princeton Rep. 51 (AFOSR TN 60-1227).

Donaldson, C. DuP. and Williamson, G. G. (1964), An experimental study of turbulence in a driven vortex, ARAP Tech. Memo 64-2.

Dorfman, L. A. and Romanenko, Yu. B., Flow of a viscous fluid in a cylindrical vessel with a rotating cover, Izv. Akad. Nauk. SSSR. Mekh. Zhidk. Gaza. 1966(5) p. 63-69 (in Russian).

Dubinskii, M. G. (1969), On the thermodynamics of the process of separation of a gas into two flows with different energy, Translation into English from Izv. Energ. I Transp. 4, 130-143, (1968) AD-700299.

Duff, J., Foster, K., and Mitchell, D. G. (1965), Some experiments on the vortex valve, in Proceedings of the First International Conference on Fluid Logic and Amplification, Cranfield, England, British Hydromechanics Research Association (September).

Dupree, S. A. (1968), The vortex gas core nuclear rocket, a binary diffusion model, with application, Ph.D. Thesis, Purdue Univ.

Easton, C. R. and Johnson, K. P. (1963), Fluid mechanical studies of fuel containment in a gaseous core reactor, Douglas Aircraft Co. Report SM-44886 (November).

Einstein, H. A. and Huon Li (1951), Steady vortex flow in a real fluid, Proceedings of the 1951 Heat Transfer and Fluid Mechanics Institute.

Eisler, T. J. (1966), Taylor instability in a stratified flow, NASA TN D-2951 (November).

Ekman, V. W. (1905), On the influence of the earth's rotation on ocean currents, Arkiv Mathematik, Astr, och Fysik, Stockholm, 2, 1-52.

Elco, R. A., Hughs, W. F. and Young, F. J. (1962), Theoretical analysis of the radial field vortex magneto-gas dynamic generator, Z. F. Angewandte Mathematik und Physik, 13, 1-12 (January).

Evvard, J. C. (1965), Wheel-flow gaseous-core reactor concept, NASA TN D-2951 (November).

Farris, G. J., Kidd, G. L. Jr., Lick, D. W. and Textor, R. E. (1969), A study of vortex flow, Union Carbide Corp., Nuclear Division, Oak Ridge, Tenn., Report No. CTC-7 (March).

Farris, G. J., Kidd, G. L. Jr., Lick, D. W. and Textor, R. E. (1969), A theoretical and experimental study of confined vortex flow, ASME Journal Applied Mechanics, 36, 687 (December).

Fax, D. H., Daskin, W., et al (1953), Hydrodynamic analysis of flow through spherical vessels, The John Hopkins University, Baltimore, Maryland (June).

Felsing, G. W., Mockenhaupt, J. D. and Lewellen, W. S. (1970), Investigation of a vortex valve to control chamber pressure in the NERVA Engine, AIAA Paper No. 70-658 (June).

Fiebig, M. (1966), Motion within fluid gyroscopes, AIAA J., 4, 667-74 (April).

Fiorino, T. D. and Poplawski, R. (1965), Experimental optimization of the reverse-flow swirl chamber, Aerospace Research Laboratories, Report 65-66 (April).

Fletcher, E. C., Gyarmathy, G. and Hasinger, S. (1966), Separation of submicron condensate particles in a vortex chamber, Aerospace Research Laboratories Report 66-0218 (November).

Foley, W. M. (1965), Comparison of simulated and required flow characteristics for vortex-stabilized gaseous nuclear rocket engine, UARL Report UAR-D46A (May).

Fragoyannis, G. B. (1966), A contribution to the theory of jet-wakes and vortices in free and confined surroundings, Research Report No. 67, Aerophysics Dept., Miss. State Univ. (also AD646656), (November).

Frey, K. P. H., Vasuki, N. C. and Trask, P. (1965), New comprehensive studies on sudden enlargements, Proceedings of the HDL Fluid Amplification Symposium, 1, (October).

Fulton, C. D. (1950), Rangue's tube, Refrigerating Engineering, 58, 473-479 (May).

Gartshore, I. S. (1962), Recent work in swirling incompressible flow, National Aeronautical Establishment, AR-LR-343, Ottawa (June).

Gartshore, I. S. (1963), Some numerical solutions for the viscous core of an irrotational vortex, NAE Aero. Report No. LR-378, NRC (June).

Gebben, V. D. (1967), Vortex valve performance power index, Advances in Fluidics, ASME, N. Y., N. Y.

Giannotti, H. (1966), Air filtration for the gas turbine, ASME Paper No. 66-GT-119.

Ginsberg, T. (1966), Flow distributions in a confined viscous vortex, Penn. State Univ. Ordnance Research Lab. Tm 605-2621-04 (April).

Glick, R. L. and Kilgore, M. S. (1967), Effect of specific heat ratio on mass flow for swirling nozzle flow, J. of Spacecraft and Rockets, 4, 1098.

Gol'dshtik, M. A. (1960), A paradoxical solution of the Navier-Stokes equations, PMM, 24, No. 4, 610-621.

Gol'dshtik, M. A., Leontov, A. K., and Paleev, I. I. (1960), Aerodynamics of a vortex chamber, Leningrad Polytechnic Institute.

Gore, R. W. and Ranz, W. E. (1964), Backflows in rotating fluids moving axially through expanding cross sections, Am. Inst. Chem. Eng. J.,10,(1), p. 83-8.

Gortler, H. (1954), Decay of swirl in an axially symmetrical jet, far from the origin, U. S. Air Force Rept., Contract No. AF-61(514)-625-C.

Gostintsev, Yu. A. and Margolin, A. D. (1966), Boundary layer on the free surface of a hollow vortex, Izv. Akad. Nauk SSSR, Mekh. Zhidk. Gaza, 6, 45-49 (in Russian).

Granger, R. (1966), Steady three-dimensional vortex flow, Journal of Fluid Mechanics, 25, 557-576.

Granger, R. A. (1968), Speed of a surge in a bathtub vortex, J. Fluid Mechanics, 34, 651-656.

Greber, I., Koerper, P. E. and Taft, C. K. (1965), Fluid vortex amplification optimization, Proceedings of the Fluid Amplification Symposium, II, Harry Diamond Laboratories, 223-243 (October).

Greber, I., Taft, C. K. and Abler, J. (1966), Experimental scaling study of fluid amplifier elements, NASA CR-75668 (March).

Greenspan, H. P. (1968), The Theory of Rotating Fluids, Cambridge University Press.

Grey, J. (1959), A gaseous-core nuclear rocket utilizing hydrodynamic containment of fissionable material, ARS Paper No. 848-59 (June).

Grohne, D. (1956), Uber die laminare Stromung in einer Kreiszilindrischen Dose mit rotierendem Deckel, Nachr. Akad, Wiss. Gottingen Math. Phys. K 1.

Groothoff, C. C. (1969), The influence of rotation on the burning rate of a small hybrid rocket motor, National Lucht-en Ruimtevaart Laboratorium, NLR MP 69010 U (A69-41932), (May).

Gross, R. A. and Kessey, K. O. (1964), Magnetohydrodynamic species separation in a gaseous nuclear rocket, AIAA J., 2, 295 (February).

Guenette, G. R. (1970), An evaluation of the vortex valve as a means of measuring vorticity, M. S. Thesis, Dept. of Aero. & Astro., M.I.T., (February).

Gulyaev, A. I. (1966), Vortex tubes and the vortex effect (Ranque effect), Soviet Physics, Techn. Physics, 10, 1441.

Gupta, A. S. (1967), Circulatory flow of a conducting liquid about a porous rotating cylinder in a radial magnetic field, AIAA J., 5(2), 380-2.

Gyarmathy, G. (1967), Optical measurements of radial density distribution in a high-speed confined air vortex, ARL 67-0234 (December). Also AIAA J., 7, 1838-1845 (October, 1969).

Hall, M. G. (1965), A numerical method for solving the equations for a vortex core, Aeronautical Research Council 27150, R & M No. 3467, R.A.E. Dept. 65106.

Hall, M. G. (1966), The structure of concentrated vortex cores, Progress in Aeronautical Sciences, 7, Pergamon Press.

Hall, M. G. (1967), A new approach to vortex breakdown, Proc. 1967 Heat Transfer and Fluid Mech. Inst., Stanford University Press, 319-340.

Hamel, G. (1916), Spiralförmige Bewegung Zäher Flussigkeiten, Jahresber d. Dt. Mathematikev-Vereinigung, 25, 34-60.

Hart, T. J. (1969), The design and application of the vortex valve oscillator as a fluidic temperature sensor, Dept. of Mechanical Engineering, MIT, M. S. Thesis (May).

Hartnett, J. P. and Eckert, E. R. G. (1956), Experimental study of the velocity and temperature distribution in a high-velocity vortex-type flow, Proceedings of the Heat Transfer and Fluid Mechanics Institute, Stanford University Press; also see (1957) Transactions of the ASME.

Harvey, J. K. (1962), Some observations of the vortex breakdown phenomenon, J. Fluid Mech., 14, 585.

Hawkes, J. W. (1969), A simple model of the vortex breakdown phenomenon, M. S. Thesis, Dept. of Aero. & Astro., MIT (August).

Hayes, W. F. and Kwok, C. (1965), Impedance matching in bistable and proportional fluid amplifiers through the use of a vortex vent, HDL Fluid Amp. Symp., 1, (October).

Heim, R. (1929), An investigation of the Thoma counterflow brake, Transactions of the Hydraulic Institute, Munich Technical University Bulletin, 3, 13-28.

Hellbaum, R. F. (1965), Flow studies in a vortex rate sensor, HDL Fluid Amplification Symp., II, (October).

Hester, J. A. (1966), The effect of L/D and mass flow rate on the strength of a confined vortex, S. M. Thesis, MIT, Dept. of Aero. & Astro. (June).

Hide, R. (1968), On source-sink flows in a rotating fluid, J. of Fluid Mech., 32, 737-764.

Hill, C. T., Huppler, J. D. and Bird, R. B. (1966), Secondary flows in a disk and cylinder system, Chem. Eng. Sei., 21, (1966), p. 815.

Hilsch, R. (1947), The use of the expansion of gases in a centrifugal field as cooling process, Rev. Sci. Instr., 18.

Hocking, L. M. (1970), Radial filling of a rotating container, The Quarterly Journal of Mechanics and Applied Mathematics, 23, 101-118 (February).

Holman, J. P. and Moore, G. D. (1961), Experimental study of vortex chamber flow, J. Basic Eng., 83, 632-636.

Hondur, Y. T. (1968), Experimental investigation and modeling of the hydraulic vortex amplifier, Purdue Univ. Ph.D. Thesis.

Hornbeck, R. W. (1969), Viscous flow in a short cylindrical vortex chamber with a finite swirl ratio, NASA TN-D5132 (March).

Howard, L. N. and Gupta, A. S. (1962), Hydrodynamic and hydromagnetic stability of swirling flows, Journal of Fluid Mechanics, 14, 463-476.

Howland, G. R. (1965), Performance characteristics of vortex amplifier, HDL Fluid Amplification Symp., II, (October).

Hummel, D. (1965), Unterseuchungen Uber das Aufplatzen der Wirbel an Schlanken Deltaflugeln, Z. Flugwiss, 13, 158-168.

Iesalnieks, G. A. (1966), A theoretical and experimental investigation of a pneumatic angular rate sensor, University of Nebraska Ph.D. Dissertation, Univ. Microfilms, Inc., Ann Arbor, Michigan.

Jackomis, W. and H. J. P. von Ohain (1970), Comments on the colloid core reactor, in Proceedings of the Symposium on Research on Uranium Plasmas and their Technological Application held at U. of Florida, January, 1970.

Johnson, B. V. (1964), Analysis of secondary-flow control methods for confined vortex flows, UARL Report C-910091-1 (September). Also issued as NASA Report CR-276 (1965).

Johnson, B. V. (1965), Analytical study of propellant flow requirements for reducing heat transfer to the end walls of vortex-stabilized gaseous nuclear rocket engines, UARL Report D-910091-6 (September).

Johnson, B. V. (1967), Exploratory flow and containment experiments in a directed-wall jet vortex tube with radial outflow and moderate superimposed axial flows, UARL Report F-910091-11 (May).

Johnson, B. V. and Travers, A. (1965), Application of flow control to a confined vortex, UARL Report UAR-D 50 (March). Also presented at 4th AIAA Propulsion Conference, Cleveland, Ohio (June, 1968).

Johnson, B. V. and Travers, A. (1965), Analytical and experimental investigation of flow control in a vortex tube by end-wall suction and injection, UARL Report D-910091-8 (September).

Johnson, B. V., Travers, A. and Hale, R. W. (1963), Measurements of flow patterns in a jet-driven vortex, Air Force Systems Commend Report RTD-TDR-63-1094 (November).

Johnson, B. V. and Van Dine, C. P. (1967), Laminar boundary layer similarity solutions for rotating flows with wall suction, Proceedings of the 9th Midwestern Mechanics Conference, Wiley.

Johnson, K. P. (1966), A plasma core nuclear rocket utilizing a magneto-hydrodynamically-driven vortex, AIAA J., 4, 635 (April).

Jones, J. P. (1960), Breakdown of vortices in separated flow, Univ. of Southhampton, Dept. of Aero. & Astro., U.S.A.A. Report 140.

Kalishevskii, L. L. and Ganchev, B. G. (1967), Flow pattern of cyclone process during combustion of a solid fuel, Teploenergetika, 14(2), 46-49.

Kao, T. W. (1966), Concentration profile establishment of binary gas mixture in swirl and dust flows, NASA Report CR-399 (March). The Physics of Fluids, 9, 1216 (1966).

Kao, T. W. (1967), Baro-diffusion effect on diffusion time, The Physics of Fluids, 10, 1814 (August).

Kasselmann, J. T. and Delozier, T. R. (1967), All fluid amplifier development for liquid rocket secondary injection thrust vector control, NASA CR-72145 (November).

Kasselmann, J. T. and Rivard, J. G. (1965), Development of an all-fluid amplifier for liquid rocket applications, NASA CR-544 6 (November).

Kassner, R. and Knoernschild, E. (1947), Friction laws and energy transfer in circular flow, TR F-TR-2198-ND, Wright Patterson Air Force Base.

Kearsey, H. A. and Hibbert, N. S. (1959), The separation of gases from liquids by vortical flow in an cylindrical vessel, The Industrial Chemist, 371-374 (August) and 475-480 (October).

Kelsall, D. G. (1952), A study of the motion of solid particles in a hydraulic cyclone, Trans. Inst. Chem. Engrs., 30, 87-108.

Kendall, J. M. Jr. (1962), Experimental study of a compressible viscous vortex, JPL Tech. Report No. 32-290 (June).

Kendall, J. S. (1967), Experimental investigation of heavy gas containment in constant temperature radial-inflow vortexes, United Aircraft Research Laboratories Report F-910091-15 (September). Also NASA CR-1029.

Kendall, J. S. and Mensing, A. E. (1966), Experimental investigation of the effect of heavy-to-light-gas density ratio on vortex containment characteristics, UARL Report UAR-E54 (April). Also presented at AIAA Propulsion Conference in Colorado Springs, Colorado (June).

Kendall, J. S., Mensing, A. E. and Johnson, B. V. (1967), Containment experiments in vortex tubes with radial outflow and large superimposed axial flows, UARL Report F-910091-12; NASA CR-993 (May).

Kendall, J. S., Roman, W. C. and Vogt, P. G. (1968), Initial radio frequency gas heating experiments to simulate the thermal environment in a nuclear light bulb reactor, United Aircraft Research Lab. Report G-910091-17 (September). Also issued as NASA CR-1311.

Keranen, T. W. and Blatter, A. (1968), Research and development of a vortex valve for flow modulation of a 16% aluminized, 5500°F. Propellant gas, NASA CR-1091 (June).

Kerrebrock, J. L. and Meghreblian, R. V. (1961), Vortex containment for the gaseous fission rocket, J. of the Aerospace Science, 28, 710-724. Also Oak Ridge National Laboratories Report CF 57-11-3 (1958).

Kessey, K. O. (1964), Rotating electrically conducting fluids in a long cylinder, AIAA J., 2, 864-871 (May).

Kessey, K. O. and Gross, R. A. (1964), Gaseous nuclear rocket with MHD vortex fuel containment, AIAA J., 2, 1461-1464 (August).

Keyes, J. J. Jr. (1960), An experimental study of gas dynamics in high velocity vortex flow, Proc. of the 1960 Heat Transfer and Fluid Dynamics Institute, Stanford University Press.

Keyes, J. J. Jr. (1961), An experimental study of flow and separation in vortex tubes with application to gaseous fission heating, ARS J., 31, 1204.

Keyes, J. J. Jr. (1964), An experimental hydromagnetic investigation of jet-driven confined vortex-type flow, Developments in Theoretical and Applied Mechanics, Vol. 2, 2nd Southeastern Conference on Theoretical and Applied Mechanics Proceedings, Georgia Institute of Technology (March).

Keyes, J. J. Jr., Chang, T. S. and Sartory, W. K. (1967), Hydromagnetic stabilization of jet-driven vortex flow, Oak Ridge National Laboratory Report TM-1896 (October).

Keyes, J. J. Jr. and Dial, R. E. (1960), An experimental study of vortex flow for application to gas-phase fission heating, Oak Ridge National Laboratory Report 2837.

Kidd, G. J. Jr. (1966), Confined vortex flow near a stationary disk; theory and experiment, Oak Ridge National Laboratory, ORNL-TM 1387 (April).

Kidd, G. J. Jr. and Farris, G. J. (1968), Potential vortex flow adjacent to a stationary surface, ASME Paper No. 68-APM-15 (June). Also Journal of Applied Mech., 35, 209-215 (June).

King, W. S. (1963), Momentum-integral solutions for the laminar boundary layer on a finite disk in a rotating flow, Aerospace Corp. Report No. ATM-63-(9227)-3 (June). ASME Paper No. 64-FE-14 (1964).

King, W. S. (1967), A theoretical investigation of swirling flows through a nozzle, Ph.D. Thesis, UCLA.

King, W. S. (1967), On swirling nozzle flows, J. Spacecraft and Rockets, 4, 1404 (October).

King, W. S. and Lewellen, W. S. (1963), Boundary-layer similarity solutions for rotating flows with and without magnetic interaction, Aerospace Corp., ATN-63(9227)-6 (July). Physics of Fluids, 7, 1674 (October, 1964).

Kinney, R. B. (1966), Theoretical effect of seed opacity and turbulence on temperature-distributions in the propellant region of a vortex-stabilized gaseous nuclear rocket, UARL Report E-910092-8 (September). NASA Report CR-694.

Kinney, R. B. (1967), Universal velocity similarity in fully developed rotating flows, ASME Trans. Series E. J. Appl. Mech., 34, 437-442 (June).

Kirkpatrick, D. L. I. (1964), Experimental investigation of the breakdown of a vortex in a tube, Great Britain Royal Aircraft Estb. AD 449 461 TN AERO 2963 (May).

Knapp, A. B. (1968), The development and control of a vented vortex amplifier, Paper J4, Proc. 3rd Cranfield Fluidics Conf., British Hydromechanics Res. Ass., Cranfield (May).

Knapp, D. E. (1966), Lecture notes on advanced fluid core nuclear propulsion concepts, AIAA Los Angeles Monographs: Advanced Propulsion, Vol. I, pp. 1-24.

Koerper, P. E. (1965), Design of an optimized vortex amplifier, E.D.C. Report 7-65-6, Control Systems Synthesis Laboratory, Case Inst. of Tech., Cleveland, Ohio.

Kolf, R. C. (1956), Vortex flow from horizontal thin plate orifices, Ph.D. Thesis, University of Wisconsin (July, 1956).

Kolf, R. C. and Zielinski, P. B. (1960), The vortex chamber as an automatic flow-control device, J. of the Hydraulics Division, ASCE, Vol. 86, Proc. Paper 2535 (June).

Kosecky, L. (1966), Longitudinal circulation in a fluid moving spirally in a circular cylinder, Collection Czech. Chem. Commum., 31 (11), 4312-23, (in English).

Krause, E. (1970), 1-D flow of compressible, binary gases in centrifuges, Deutsche Forschung und Versuchsanstalt fuer Luft-und Raumfahrt, Porz/West Germany, (February).

Kreith, F. (1966), Mass and heat transfer in a radial flow between two parallel, stationary or co-rotating disks, Inter-Journal Heat & Mass Transfer, 9(4), p. 265-82.

Kreith, F., Doughman, E. and Kozlowski, H. (1963), Mass and heat transfer from an enclosed rotating disk with and without source flow, J. Heat Transfer, 85, 153-63.

Kreith, F. and Margolis, D. (1959), Heat transfer and friction in turbulent vortex flow (swirling flow in a pipe), Appl, Sci. Res. A8, p. 457-473.

Kriebel, A. R. (1961), Particle trajectories in a gas centrifuge, J. Basic Eng., 83, 333.

Kruegar, E. R. and Di Prima, R. C. (1964), The stability of a viscous fluid between rotating cylinders with an axial flow, J. of Fluid Mech., 19, 528.

Kuchemann, D. (1965), Report on the I.U.T.A.M. Symposium on Concentrated Vortex Motions in Fluids, J. Fluid Mech., 21, Part 1, 1-20.

Kuo, H. L. (1969), Axial symmetric flows in the boundary layer of a maintained vortex, Univ. of Chicago, Dept. of Geophysical Sciences, Planetary Circulation Project Report No. 15, (April).

Kurzweg, U. H. (1967), Criteria for the stability of heterogeneous swirling flows, UARL Report UAR-F96 (May). Also Zeitschrift fuer Angewandte Mathematik und Physik, 20, 141-143 (January, 1969).

Kwok, C. C. K. (1966), Vortex flow in a thin cylindrical chamber and its application in fluid amplifier technology, McGill University (Montreal) Department of Mech. Eng. Report 66-80.

Kwok, C. C. K. (1969), A theoretical study of vortex flow in a thin cylindrical chamber, Bendix Technical Journal, 1, 42-51 (winter).

Lafferty, J. F. and Hammitt, F. G. (1967), Experimental investigation of a two-phase vortex, ANS Trans., 10, 362-363.

Lafferty, J. F. et al (1968), Velocity distributions in two-phase vortex flow, J. Basic Eng., 90, 368-72 (Sept.).

Lagerstrom, P. A. (1964), Laminar flow theory, in Theory of Laminar Flows, edited by Moore, F. K., Princeton University Press.

La Mont, P. E. (1969), Pilot-plant testing of a two-phase vortex fluid amplifier for liquid flow control, Idaho Nuclear Corp., Idaho Falls, IN-1271, (March).

Lance, G. N. and Rogers, M. H. (1962), The axially symmetric flow of a viscous fluid between two infinite rotating disks, Proc. Royal Society, Ser. A., 226, 109-121.

Larson, R. H. (1966), Vortex amplifier parameters, Instruments and Control Systems, 39, 105-110 (October).

Larson, R. H. (1968), The vortex amplifier; its performance and application, Paper J1, Proc. 3rd Cranfield Fluidics Conf., British Hydromechanics Res. Ass., Cranfield (May).

Lavan, Z. (1965), Luminescence in supersonic swirling flows, Illinois Institute of Technology, J. Fluid Mech., 23, Part 1, 173-183.

Lavin, Z. and Fejer, A. A. (1966), Swirling flows in ducts, AD639325, Avail CFSTI.

Lawler, M. T. and Ostrach, S. (1965), A study of cyclonic two-fluid separation, Case Institute of Technology, Report No. FTAS-TR-65-2 (June).

Lay, J. E. (1959), An experimental and analytical study of vortex-flow temperature separation by superposition of spiral and axial flows, Part 1 and 2, Trans. of ASME/J. of Heat Transfer, 202-221 (August).

Leamer, P. C. and Maxwell, R. L. (1969), A qualitative investigation of secondary flows in a confined viscous vortex, AIAA Student Journal, 7, 81-86 (April).

Lee, J. D. (1965), Research on separation of solid particles from a swirling fluid flow, Ohio State University Research Foundation Project 7116, Report No. 13, Air Force Contract AF 33(615)-1063 (March).

Lee, J. D. (1968), An experimental study of the flow in a low pressure swirl chamber, Ohio State University Research Foundation Project 7116, Report No. ARL 68-0072 (April).

Lee, J. D. (1968), Nature of the flow in a swirl chamber having end-wall flow reversal, Ohio State University Research Foundation Project 7116, Report No. ARL 68-D131 (July).

Leibovich, S. (1968), Axially-symmetric eddies embedded in a rotational stream, J. Fluid Mech., 32, 529-548.

Leibovich, S. (1969), Stability of density stratified rotating flows, AIAA J., 7, 177-178 (January).

Leibovich, S. (1970), Weakly non-linear waves in rotating fluids, J. Fluid Mech., 42, 803-822 (August).

Leineweber, L. (1967), Dimensioning of cyclone separators for desired particle size, pressure loss and throughput rates, Staub Reinhaltung Luft, 27 (3), 123-129 (in German).

Lengyel, L. L. and Ostrach, S. (1963), An analysis of a vortex type magneto-hydrodynamic induction generator, NASA TN D-2006.

Letham, D. L. (1966), Fluid system design VIII-vortex amplifiers, Machine Design, 38, 178-181 (July).

Lewellen, W. S. (1960), Magnetohydrodynamically driven vortices, Proc. of the Heat Transfer and Fluid Mechanics Institute, Stanford University Press, 1-15.

Lewellen, W. S. (1962), A solution for three-dimensional vortex flows with strong circulation, J. of Fluid Mech., 14, 420 (November).

Lewellen, W. S. (1962), Comment on flow of an incompressible fluid in a hydromagnetic capacitor, The Physics of Fluids, 5, 1663 (December).

Lewellen, W. S. (1964), Three-dimensional viscous vortices in incompressible flow, Ph.D. Thesis, UCLA.

Lewellen, W. S. (1965), Linearized vortex flows, AIAA J., 3, 91 (January).

Lewellen, W. S. (1969), Discussion of potential vortex flow adjacent to a stationary surface, ASME J. of Applied Mechanics, 36, Series E, 374-375 (June).

Lewellen, W. S., Burns, W. J. and Strickland, H. J. (1969), Transonic swirling flow, AIAA J., 7, 1290 (July).

Lewellen, W. S. and Grabowsky, W. R. (1962), Nuclear space power systems using magnetohydrodynamic vortices, J. Am. Rocket Soc., 32, 693-700 (May).

Lewellen, W. S. and King, W. S. (1965), The boundary layer of a conducting vortex flow over a disk with an axial magnetic field, Developments in Mechanics, Proceedings of the 8th Midwestern Mechanics Conference (April, 1963), in Cleveland, Ohio, Pergamon Press, 108-127.

Lewellen, W. S., Ross, D. H. and Rosenzweig, M. L. (1966), Binary diffusion in a confined vortex, AIAA J., 4, 396-405 (March).

Linderstrom-Lang, C. U. (1967), A model of the gas separation in a Ranque-Hilsch vortex tube, Acta Polytechnica Scandivavica, No. 45, 1-24.

Linderstrom-Lang, C. U. (1970), Vortex tubes with weak radial flow, unpublished report from Research Establishment Riso, Roskilde, Denmark.

Lipatov, N. N. (1963), Some properties of converging flows between centrifuge plates, Iza. Vysshikh Uchebn. Zavedenii, Khim i Khim, Tekhol, 6 (3), 498-503 (1963).

Long, R. R. (1956), Sources and sinks at the axis of a rotating liquid, Quarterly Journal of Mechanics and Applied Math, IX, Part 4, (December).

Long, R. R. (1958), Vortex motion in a viscous fluid, J. of Meteorology, 15, 108-112 (February).

Long, R. R. (1961), A vortex in an infinite viscous fluid, The John Hopkins Univ., Dept. of Mech., 11, (December). Also J. of Fluid Mechanics, 11, 611-624 (December).

Loper, D. E. and Ostrach, S. (1968), Analysis of confined magnetohydrodynamic vortex flows, The Physics of Fluids, 11, 1450-1465 (July).

Lorenz, P. J., Ericson, G. D. and Hayes, J. D. (1961), The Hilsch Tube: low pressure effects, Iowa Academy of Science, Proc., Vol. 68, 443-451.

Ludwieg, H. (1960), Stability of flow in an annular space, Zeitschrift für Flugwissenschaften, 8, 135-140.

Ludwieg, H. (1961), Extension of the work on the stability of flow in an annular space, Zeitschrift für Flugwissenschaften, 9, 359-361.

Ludwieg, H. (1964), Experimentelle Nachprüfung der Stabilitatstheorien für reiburgsfreie Strömungen mit schraubenlinien förmigen Stromlinien, Zeitschrift fur Flugwissenschatten, 12, 304-309.

Lugt, H. J. and Schwiderski, E. W. (1965), On the birth and decay of vortices, U. S. Naval Weapons Laboratory, Dahlgren, Virginia, NWL Report No. 1972 (April).

Mack, L. M. (1960), The compressible viscous heat-conducting vortex, J. Fluid Mech., 8, 284.

Mack, L. M. (1962), Laminar boundary layer on a disk of finite radius in a rotating flow, Part I, JPL Report TR-32-224.

Mack, L. M. (1963), Laminar boundary layer on a disk of finite radius in a rotating flow, Part II, JPL Report TR-32-366.

Mager, A. (1961), Approximate solution of isentropic swirling flow through a nozzle, ARS Journal, 31, 1140-1148 (August).

Mager, A. (1970), Incompressible, viscous, swirling flow through a nozzle, AIAA Paper No. 70-51 (January).

Marris, A. W. (1967), Theory of Bathtub Vortex, J. Appl. Mech., 34, 11-15 (March).

Martynov, A. V. and Bordyanskii, V. M. (1967), Vortex flow parameters inside a Ranque-Hilsch tube, Inzh-Fiz., Zh. 12 (5), 639-644.

Martynovskii, V. S. and Alekseev, V. P. (1956), Investigation of the vortex thermal separation effect for gases and vapors, Soviet Phys.-Tech. Physics, 1, translated from Zhur. Tekh. Fi, 26.

Martynovskii, V. S. and Voytko, A. M., (1961), The efficiency of the Ranque Vortex tube at low pressure, Teploenergetica, 2, 80-85.

Marxman, G. A. and Kerrebrock, J. L. (1960), Heat transfer in a two-dimensional vortex flow of a dissociating gas, STL TR 60-0000-09061 (February).

Massier, P. F. (1963), Axisymmetric steady flow of a swirling compressible fluid through a convergent-divergent nozzle, J.P.L. Space Programs Summary, 4, No. 37-33 (June 30, 1965) 133-141. Also No.'s 37-24, (December 31, 1963) 105-108; No. 37-34 (August 31, 1965) 149-157; No. 37-35 (October 31, 1965) 161-165 and No. 37-36.

Matsch, L. and Rice, W. (1968), An asymptotic solution for laminar flow of an incompressible fluid between rotating disks, ASME J. of Applied Mechanics, Paper No. 68-APM-5.

Maxworthy, T. (1964), The flow between a rotating disk and a co-axial stationary disk, Space Programs Summary 37-27, 4, Sec. 327, Jet Propulsion Laboratory, Pasadena, Calif.

Maxworthy, T. (1967), The flow creating a concentration of vorticity over a stationary plate, J.P.L. Space Programs Summary 37-44, 4, 243.

Maxworthy, T. (1968), A storm in a teacup, ASME J. of Applied Mechanics, 35, 836 (December).

Mayer, E. A. (1965), Photoviscous flow visualization in fluid state devices, Proceedings of the 3rd Fluid Amplification Symposium, Harry Diamond Laboratory, 2, 347-361 (October).

Mayer, E. A. (1967), Large-signal vortex valve analysis, Advances in Fluidics, ASME, N.Y., N.Y.

Mayer, E. A. (1969), Parametric analysis of vortex amplifiers, Bendix Technical Journal, 1, 52-67 (winter).

Mayer, E. A. and Maker, P. (1964), Control characteristics of vortex valves, HDL, 2nd Fluid Amp. Symp. (May).

Mayer, E. A. and Taplin, L. B. (1965), Vortex devices, Fluidics, Fluid Amplifier Associates, Inc., Boston, Mass., 185-200.

McCorquodale, J. A. (1968), Scale effects in swirling flow, Am. Soc. Civil Eng. Proc. (HY) 94: 285-300 (January).

McCune, J. E. and Donaldson, C. DuP. (1960), On the magnetogasdynamics of compressible vortices, American Rocket Society Reprint #1319-60.

McEvan, A. D. (1970), Inertial oscillations in a rotating fluid cylinder, J. Fluid Mechanics, 40, 603-640 (February).

McFall, R. H. and Taplin, L. B. (1969), Vortex amplifiers and circuits, Bendix Technical Journal, 1, 33-41 (winter).

McFarlin, D. J. (1965), Experimental investigation of the effect of peripheral wall injection technique on turbulence in an air vortex tube, UARL Report D-910091-5 (September). NASA Report CR-68867.

McLafferty, G. H. (1961), Investigation of a unique gaseous-core nuclear rocket concept, Summary Report, United Aircraft Research Laboratories Report R-2494-4 (November).

McLafferty, G. H. (1963), Summary of investigations of a vortex-stabilized gaseous nuclear rocket concept, Air Force Systems Command Report RTD-TDR-63-1097 (November).

McLafferty, G. H. (1965), Analytical study of the performance characteristics of vortex-stabilized gaseous nuclear rocket engines, UARL D-910093-20 (September).

McLafferty, G. H. (1967), Survey of advanced concepts in nuclear propulsion, AIAA Paper No. 67-783 (October). J. of Spacecraft and Rockets, 5, 1121 (October, 1968).

McLafferty, G. H. (1969), Investigation of gaseous nuclear rocket technology, Summary Technical Report, UARL Report H-910093-46 (November).

McLafferty, G. H. and Anderson, G. E. (1963), Analytical investigation of diffusive loss rates of gaseous iodine from a helium vortex, Air Force Systems Command Report RTD-TDR-63-1095 (November).

McLafferty, G. H. and Bauer, H. E. (1968), Studies of specific nuclear light bulb and open-cycle vortex-stabilized gaseous nuclear rocket, NASA CR-1030 (April).

McLafferty, G. H., Bauer, H. E. and Sheldon, D. E. (1966), Preliminary conceptual design study of a specific vortex-stabilized gaseous nuclear rocket engine, UARL Report E-910093-29 (September).

Melherbe, C. (1966), A study of combustion in a cyclone furnace, Rev. Gen. Therm., 5 (57), 855-871.

Mensing, A. E. and Jaminet, J. F. (1969), Experimental investigations of heavy gas containment in R-F heated and unheated two-component vortexes, UARL-H-910091-20 (September).

Mensing, A. E. and Kendall, J. S. (1963), Experimental investigation of containment of gaseous iodine in a jet-driven vortex, Air Force Systems Command Report RTD-TDR-63-1093, prepared by UARL (November).

Mensing, A. E. and Kendall, J. S. (1964), Experimental investigation of containment of a heavy gas in a jet-driven light-gas vortex, UARL Report C-910091-3 (September).

Mensing, A. E. and Kendall, J. S. (1965), Experimental investigation of the containment of a heavy gas in a light-gas vortex, UARL D-910091-4 (March). Also presented at the AIAA Propulsion Conference at Colorado Springs, Colorado (June).

Mensing, A. E. and Kendall, J. S. (1965), Experimental investigation of the effect of heavy-to-light gas density ratio on two-component vortex tube containment characteristics, UARL Report D-910091-9 (September). Also NASA CR-68926.

Michelson, J. (1955), Theory of the vortex whistle, Journal of the Acoustical Society of America, 27, 930.

Miller, D. P. (1964), Characteristics of a vortex fluid throttle, HDL 2nd Fluid Amp. Symp. (May).

Miller, D. P. (1965), Experimental investigation of the flow and pressure characteristics of a vortex fluid throttle, UAC Research Lab Dept. D110117-1 (February).

Miller, H. L., Mund, M. G. and Olson, L. J. (1966), New design concepts and materials for engine induction air filters, Final Technical Report Cont. No. DA-11-022-ORD-3101, ORD Project No. TW-609 (TTI-843); Donaldson Co., Inc., (November), DDC No. Ad251003.

Miller, R. A. and Poplawski, R. (1966), The ARL inertial particle separator for military turbine-powered vehicles, Proc. OAR Research Applications Conf., Washington, D.C. (April).

Mironer, A. and Dosanjh, D. S. (1969), Coupled diffusion of heat and vorticity in a gaseous vortex, Int. J. of Heat and Mass Transfer, 12, 1231-1248.

Moore, F. K. and Leibovich, S. (1970), Self-confined rotating flows for containment, in Proceedings of the Symposium on Research on Uranium Plasmas and their Technological Applications held at University of Florida, January.

Povinelli, L. A., Heidmann, M. F. and Feiler, C. E., Experimental investigation of transverse-mode solid-propellant combustion instability in a vortex burner, NASA TN-D-3708.

Prager, S. (1964), Spiral flow in a stationary porous pipe, The Physics of Fluids, 7, 6 (June).

Pritchard, W. G. (1970), Solitary waves in rotating fluids, J. Fluid Mech., 42, 61-84 (June).

Proudman, J. (1916), On the motion of solids in liquids possessing vorticity, Proc. Roy. Soc. A, 92, 408-424.

Ragsdale, R. G. (1960), NASA research on the hydrodynamics of the gaseous vortex reactor, NASA TN D-288.

Ragsdale, R. G. (1961), A mixing length correlation of turbulent vortex data, ASME Paper No. 61-WA-244 (August).

Ragsdale, R. G. (1963), Performance capability of single-cavity vortex gaseous nuclear rockets, NASA TN D-1579 (May).

Ragsdale, R. G. (1963), Outlook for gas-core nuclear rockets, Astronautics & Aerospace Engineering, 1, 88 (August).

Ragsdale, R. G. (1968), Are gas-core nuclear rockets attainable? AIAA Paper No. 68-570 (June).

Ragsdale, R. G. and Lanzo, C. D. (1969), Some recent gaseous reactor fluid mechanic experiments, AIAA Paper No. 69-477 (June). Also NASA TM-X-1847.

Rakowsky, E. L., Galowin, L. S. and DeSantis, M. J. (1967), Vortex phenomena study continuation program, General Precision Systems, Inc., Report No. 1590-6707, Little Falls, N. J. (December).

Ranque, G. J. (1933), Experiences Sur la Dentente Giratoire Avec Productions Simultanees d'un Echappement d'Air Froid, Bull Bi-Mersuel de la Société Francaise de Physique, p. 1125 (June).

Ranque, G. J. (1934), Method and apparatus for obtaining from a fluid under pressure two currents of fluids at different temperatures, U. S. Patent Office No. 1,952,281.

Rashod, C. R. M. (1966), MHD species separation in a gaseous nuclear rocket using a time varying traveling wave electromagnetic field, AIAA Paper No. 66-499.

Rayleigh, L. (1917), On the dynamics of revolving fluids, Proc. Roy. Soc. London A, 93, 148-154.

Reilly, R. J. (1969), Fluidic control system for aerospace propulsion, AGARDograph 135 (September).

Reshotko, E. and Monnin, C. F. (1965), Stability of two-fluid wheel flows, NASA TN D-2696.

Reynolds, A. J. (1961), Energy flows in a vortex tube, ZAMP, XII.

Reynolds, A. J. (1961), On the dynamics of turbulent vortical flow, ZAMP, XII.

Reynolds, A. J. (1962), A note on vortex tube flow, J. Fluid Mech., 14, 18-20 (September).

Rietema, K. and Krajenbrink (1959), Theoretical derivation of tangential velocity profiles in a flat vortex chamber. Influence of turbulence and wall friction, Appl. Sci. Res., Sect. A, Vol. 8.

Rietema, K. and Verver, G. A. (1961), Cyclones in Industry, Elsevier Publishing Co.

Riley, N. (1962), Radial jets with swirl, Part I. Incompressible flow, Quarterly Journal Mech. and Applied Math. XV, Part 4.

Riley, N. (1962), Radial jets with swirl, Part II. Compressible flow, Quarterly Journal Mech. and Applied Math. XV, Part 4.

Ringleb, F. (1963), Vortex motion, Aerophysics, Mississippi State University Research Report 47 (October).

Ringleb, F. O. (1964), Discussion of the problems associated with standing vortices and their applications, ASME.

Rivard, J. G. and Walberen, J. C. (1965), A fluid state vortex hydraulic servovalve, Paper at 21st National Conference on Fluid Power (October).

Rochino, A. P. and Lavan, Z. (1968), Analytical investigation of incompressible turbulent swirling flow in pipes, NASA CR-1169 (September).

Rochino, A. P. and Lavan, Z. (1969), Analytical investigations of incompressible turbulent swirling flow in stationary ducts, ASME J. of Applied Mechs., 36, Series E, 151-158 (June).

Rodoni, C. A. (1969), An investigation of the flow parameters of a confined turbulent vortex, S.M. Thesis, Department of Aeronautics & Astronautics, MIT (August).

Roffman, G. (1963), Absolute pressure ratio measurement for jet engine control, R-RCA-63-17 (April).

Rogers, M. H. and Lance, G. N. (1960), The rotationally symmetric flow of a viscous fluid in the presence of an infinite rotating disk, J. of Fluid Mech., 7, 617-631 (April).

Rogers, M. and Lance, B. (1964), The boundary layer on a disc of finite radius in a rotating fluid, Quart. J. Mech. Appl. Mech., 17, 319-330.

Roman, W. C. and Klein, J. F. (1969), Investigation of high-pressure vortex-stabilized R-F plasma discharge, AIAA Paper No. 69-695 (June).

Roman, W. C., Klein, J. F. and Vogt, P. G. (1969), Experimental investigation to simulate the thermal environment, transparent walls, and propellant heating in a nuclear light bulb engine, UARL Report H-910091-19 (Sept.).

Romero, J. B. (1964), Fuel containment in the gaseous-core nuclear rocket by MHD-driven vortices, AIAA J., 2, 1092 (June).

Roschke, E. J. (1961), Vortex tube flow visualization, CIT, JPL Film No. 641-2. Also water vortex visualization studies workprint film (1963).

Roschke, E. J. (1963), Comments on the stability of curved compressible flows, JPL SPS No. 37-24, Vol. IV.

Roschke, E. J. (1966), Experimental investigation of a confined, jet-driven water vortex, JPL Report 32-982, NASA CR-78550.

Roschke, E. J. (1966), Flow-visualization studies of a confined, jet-driven water vortex, JPL Report 32-1004.

Roschke, E. J. and Pivirotto, T. J. (1965), Similarity in confined vortex flows, JPL TR No. 32-789 (August).

Roschke, E. J. and Pivirotto, T. J. (1967), End wall pressure distributions in a confined vortex, AIAA J., 5, 817-819 (April).

Rosenzweig, M. L. (1961), Velocity and shear reduction in jet-driven vortex tubes, Aerospace Corp. Report TDR-594 (1203-01) TN-1 (March).

Rosenzweig, M. L. (1961), The vortex matrix approach to gaseous nuclear propulsion, Aerospace Corp., American Rocket Society Paper No. 1735-61 (May).

Rosenzweig, M. L., Lewellen, W. S. and Kerrebrock, J. L. (1961), Feasibility of turbulent vortex containment in the gaseous fission rocket, ARS J., 31, 873 (July).

Rosenzweig, M. L., Lewellen, W. S. and Ross, D. H. (1964), Confined vortex flows with boundary layer interaction, AIAA J., 2, 2127 (December).

Rosenzweig, M. L., Ross, D. H. and Lewellen, W. S. (1962), On secondary flows in jet-driven vortex tubes, J. Aerospace Science, 29, 1142 (September).

Ross, D. H. (1964), An experimental study of secondary flow in jet-driven vortex chambers, Aerospace Corp. Report No. ATN-64(9227)-1 (January).

Ross, D. H. (1964), An experimental study of turbulence levels in jet-driven vortex chambers, Aerospace Corp. ATN-64(9227)-5 (October).

Rott, N. (1958), On the viscous core of a line vortex, J. of Applied Math. and Physics, ZAMP, IXb, Fax. 5/6, 543-553.

Rott, N. (1959), On the viscous core of a line vortex, II, J. of Applied Math. and Physics, ZAMP, X, Fasc. 1, 73-81.

Rott, N. (1962), Turbulent boundary layer development on the end wall of a vortex chamber, Aerospace Corp. ATN-62(9202)-1.

Rott, N. and Lewellen, W. S. (1965), Some examples of rotating boundary layers, Recent Developments in Boundary Layer Research, AGARDograph 97 (May).

Rott, N. and Lewellen, W. S. (1966), Boundary layers in rotating flows, Proceedings of the Eleventh International Congress of Applied Mechanics held September, 1964 in Munich, Germany, Springer-Verlag Press, 1030-1036.

Rott, N. and Lewellen, W. S. (1966), Boundary layers and their interactions in rotating flows, Progress in Aeronautical Sciences, 7, Pergamon Press, 111-144.

Rott, N. and Ohrenberger, J. T. (1968), Transformations of the boundary-layer equations for rotating flows, J. Fluid Mech., 33, 113-126 (July).

Royle, J. K. and Hassan, M. A. (1967), Characteristics of vortex devices, Second Cranfield Fluidics Conference, Cambridge (January).

Rumpf, H., Borko, K. and Reickert (1968), Optimum dimensioning of cyclones by means of simplified model calculations, National Lending Library Trans. 68/155 (902204) (October).

Ryan, F. M. (1969), Flowmeter produces pulse output from fluid vortex oscillations, Instrumentation Tech., 16: 14 (September).

Saffman, P. G. (1962), Flow of a dusty gas between rotating cylinders, Nature 193, p. 463-4.

Sarpkaya, T. (1963), A bistable vortex oscillator, ASME Transactions, Series E, J. of Applied Mech., 30, 629-630 (December).

Sarpkaya, T. (1965), A theoretical and experimental investigation of the vortex-swirl angular rate sensor (1965); Characteristics of counter-vortex oscillators (1965); Characteristics of a vortex device and the vortex-breakdown phenomenon. All in HDL Fluid Amp. Symp., II, (October).

Sarpkaya, T. (1966), Forced and periodic vortex breakdown, ASME Paper No. 66-WA/FE-7.

Sarpkaya, T. (1968), The vortex valve and the angular rate sensor, Fluidics Quarterly, 1, No. 3, 1-8 (April).

Sarpkaya, T., Goto, J. M. and Kirshner, J. M. (1967), A theoretical and experimental study of vortex rate gyro, Advances in Fluidics, ASME.

Savino, J. M. and Keshock, E. G. (1965), Experimental profiles of velocity components and radial pressure distributions in a vortex contained in a short cylindrical chamber, NASA TN D-3072 (October).

Savino, J. M. and Ragsdale, R. G. (1960), Some temperature and pressure measurements in confined vortex fields, ASME Paper No. 60-SA-4, (June), also ASME Trans, Series C-J, Heat Transfer, 83, 33-38 (February, 1961).

Shapiro, A. H. (1962), Bathtub vortex, Nature, Vol. 196, 1080-1081, (December).

Scheller, W. A. and Brown, G. M. (1957), The Ranque-Hilsch vortex tube, Industrial Engineering Chemistry, 49, 1013-1016.

Schlichting, H. (1968), Boundary-Layer Theory, McGraw-Hill Book Co., Sixth Ed.

Schowalter, W. R. and Johnston, H. F. (1960), Characteristics of the mean flow patterns and structure of turbulence in spiral gas streams, A.I.C.H.E. E. Journal, 6, 648.

Schulz-Jander, B. (1963), Determination of the flow field in a confined vortex chamber, M.S. Thesis, Rice University.

Schultz-Grunow, F. (1935), Der Reibungswiderstand rotierender Scheiben in Gehausen. ZAMP, 15, No. 4.

Schwiderski, E. W. (1968), On the axisymmetric vortex flow over a flat surface, Naval Weapons Lab. Report TR-2210 (September).

Schwiderski, E. W. and Lugt, H. J. (1963), Vortex flows normal to a flat surface, Tellus, XV, 241, 245 (August).

Schwiderski, E. W. and Lugt, H. J. (1964), Rotating flows of von Karman and Bodewadt, The Physics of Fluids, 7, 6 (June).

Scott, B. F. (1968), Boundary-layer effects in the turbulent spiral vortex flow of a compressible fluid, Inst. Mech. Eng. Proc. 183, No. 9: 179-186.

Sibulkin, M. (1961), Unsteady viscous circular flow, Part 1, J. Fluid Mech., 11, (September).

Sibulkin, M. (1962), Unsteady viscous circular flow, Part 2, J. Fluid Mech., 12, (January).

Sibulkin, M. (1962), Unsteady viscous circular flow, Part 3, Application to the Ranque-Hilsch Vortex Tube, Journal of Fluid Mechanics, 12, 289-293 (February).

Sibulkin, M. (1962), A note on the bathtub vortex, J. Fluid Mech., 14, 21-24 (September).

Smith, J. L. Jr. (1962), An analysis of the vortex flow in the cyclone separator, ASME J. Basic Engin., 84, 602.

Smith, J. L. Jr. (1962), An experimental study of the vortex in the cyclone separator, ASME J. Basic Engin., 84, 609.

So, K. L. (1967), Vortex decay in a conical diffuser, AIAA J., 5, 1072-1078 (June). (Also MIT Gas Turbine Lab Report 75, September, 1964).

Spangler, J. G. (1966), Vortex boundary-layer interactions, NASA-CR-76772.

Squire, H. B. (1960), Analysis of vortex breakdown phenomenon, Part 1, Imperial College of London, Aero. Dept. Report 102.

Steiger, M. H. and Bloom, M. H. (1962), Axially symmetric laminar free mixing with large swirl, Transactions of the ASME, 370 (November).

Stewartson, K. (1953), The flow between two rotating coaxial disks, Proc. of the Cambridge Phil. Soc., 49, 333-341.

Stewartson, K. (1957), Magneto-hydrodynamics of a finite rotating disk, Quarterly Journal of Mechanics and Applied Mathematics, 10, 137-147 (May).

Stewartson, K. (1957), On almost rigid rotations, J. Fluid Mechs., 3, 1 (October).

Stewartson, K. (1958), On rotating laminar boundary layers, Boundary Layer Research Symposium Freiburg, Springer-Verlag, Berlin, 59-71.

Strickland, H. J. (1968), Quasi-one-dimensional acceleration of swirling flow through a minimum cross section, M.S. Thesis, Dept. of Aero. & Astro., MIT (August).

Stuart, J. T. (1954), On the effects of uniform suction on the steady flow due to a rotating disk, Quarterly J. Math. and Appl. Math.

Sullivan, R. D. (1959), A two-cell vortex solution of the Navier-Stokes equations, J. of Aero./Space Science, 11, 767-768 (November).

Sukhovich, E. P. (1969), Vortex Chamber Aerodynamics, Akademiia Nauk Latviiskoi SSR, Izvestiia, Seriia Fizicheskikh I Teknicheskikh Nauk, 4, 78-88.

Suzuki, M. (1960), Theoretical and experimental studies on the vortex tube, Institute of Physical and Chemical Research, Scientific Papers, Tokyo University, Vol. 54, 42-87 (March).

Swithenbank, J. and Sotter, G. (1963), Vortices in solid propellant rocket motors, AIAA J., 1, 1682-1684 (July).

Syred, N., Royle, J. K. and Tippetts, J. R. (1968), Optimization of high gain vortex devices, Third Cranfield Fluidics Conference, J3-37-48 (May).

Takahama, H. (1965), Studies on vortex tubes, Bulletin of J.S.M.E., 8, 433.

Takahama, H. and Soga, N. (1966), Studies on vortex tubes, Bulletin of J.S.M.E., 9, 33, 121-130 (February).

Talbot, L. (1954), Laminar swirling pipe flow, J. of Applied Mechanics, 21, No. 1, 1-7.

Tan, H. S. and Ling, S. C. (1963), Final-stage decay of a single line vortex, AIAA J., 1, 1193-1194 (May).

Tang, Y. S., Stefanko, J. S., Dickson and Drawbaugh, D. W. (1970), An engineering study of the colloid fueled reactor concept, AIAA Paper No. 70-688.

Taplin, L. B. (1965), Phenomenology of vortex flow and its application to signal amplification, Bendix Corp. RLDP-65-14 (October), presented at Penn. State Univ. (July). Also in Fluidics Quarterly, 1, No. 2 (Jan., 1968).

Taplin, L. B. (1968), Small signal analysis of vortex amplifiers, AGARDograph-118, Fluid Control-Components and Systems, (December).

Taplin, L. B. (1969), Multiport vortex amplifiers, Bendix Research Laboratories Report 69-6, (Prepared for AGARD Lecture Series on Fluidic Control Systems for Aerospace Propulsion) (August).

Taplin, L. B. and McFall, R. H. (1969), Vortex amplifiers and circuits, Bendix Technical Journal, 1, No. 4 (winter).

Tatro, P. R. and Mollö-Christensen, E. L. (1967), Experiments on Ekman layer instability, J. Fluid Mechs., 28, 531-544.

Taylor, G. I. (1921), Experiments with rotating fluids, Proc. Roy. Soc. A, 100, 114-121.

Taylor, G. I. (1950), The boundary layer in the converging nozzle of a swirl atomizer, Quarterly J. Mechs. and Applied Math., 3, 129-139 (June).

Templemeyer, K. E. (1964), Vortex flow in air heaters, AIAA J., 2, No. 4, 766-767 (April).

Ter Linden, A. J. (1953), Cyclone dust collectors for boilers, Transactions of the A.S.M.E., 75, 433-440.

Textor, R. E. (1968), A numerical investigation of a confined vortex problem, Oak Ridge National Laboratory, Computing Technology Center USAEC Report K-1732.

Thoma, D. (1928), Fluid lines, U. S. Patent 1,839,616 (June).

Thompson, J. F. Jr. (1963), The structure of free and confined turbulent vortices, Miss. State Univ., Research Note No. 44 (May).

Timm, G. K. (1967), Survey of experimental velocity distributions in vortex flows with bibliography, Boeing Scientific Research Laboratories Document DI-82-0683 (November).

Toomre, J. (1963), Highly swirling flows through a converging-diverging nozzle, S.M. Thesis, MIT Dept. of Aero. and Astro. (June).

Travers, A. (1965), Experimental investigation of peripheral-wall injection techniques in a water vortex tube, United Aircraft Research Laboratories Report D-910091-7 (September).

Travers, A. (1967), Experimental investigation of flow patterns in radial-outflow vortices using a rotating peripheral-wall water vortex tube, UARL Report F-910091-10 (May).

Travers, A. (1967), Experimental investigation of radial-inflow vortexes in jet-injection and rotating-peripheral-wall water vortex tubes, United Aircraft Research Laboratories Report F-910091-14 (September). Also issued as NASA CR-1028.

Travers, A. and Clark, J. W. (1968), Experimental investigation of flow stability and flow patterns in radial-outflow vortexes, AIAA Paper No. 68-695 (June).

Travers, A. and Johnson, B. V. (1965), Measurements of flow characteristics in a basic vortex tube, NASA CR-278 (January).

Travers, A. and Johnson, B. V. (1965), Measurements of flow characteristics in an axial-flow vortex tube, NASA CR-277 (August).

Truesdell, C. (1954), The kinematics of vorticity, Indiana Univ. Press.

Tsai, D. H. (1964), Flow field in a swirl chamber, AIAA J., 2, 1504-5 (Aug.).

Tumm, G. W. (1966), Vergleichande analyse von gaskern-reaktoren für Antriebe von raumfhrzengen, Dissertation Technical University of Berlin (Nov.).

Tumm, G. W. (1966), Critical mass calculations for coaxial and vortex flow gaseous core reactor, Columbia University, Plasma Report No. 26.

Turner, J. S. (1965), The constraints imposed on a class of strong vortices by an axial boundary, J. of Fluid Mechs., 25, Part 2, 377-400.

Van Atta, C. (1965), Exploratory measurements in spiral turbulence, NASA CR-64421.

Van Deemter, J. J. (1952), On the theory of the Ranque-Hilsch cooling effect, Applied Scientific Research, 3, 174-196.

Van Dongen, J. R. J. and Ter Linden, A. J. (1958), The application of gas/liquid cyclones in oil refining, Trans. ASME, 245-251 (January).

Vasilev, O. F. (1958), The fundamentals of the mechanics of spiraling and circulating flows, Moscow-Leningrad, English translation (1964) by Trirogoff, K. N. and Lewellen, W. S., Aerospace Corp. Report LR-64-T-20 (September).

Vivian, C. H. (1968), Ranque-Hilsch tube, Compr. Air Mag., 68, 26-28 (May).

von Kármán, T. (1921), Uber laminare und turbulente Reibung, Zeits. Ang. Math. Mech., 1, 233-252 (August).

Vonnegut, B. (1950), Vortex thermometer for measuring true air temperature and true air speeds in flight, Rev. Sci. Instr., 21, No. 2 (February).

Walsh, R. F., Lewellen, W. S. and Stickler, D. B. (1970), Investigation of a solid-propellant rocket motor modulated by a fluid vortex valve, AIAA Paper No. 70-643 (June).

Weber, H. E. (1956), Boundary layer inside a conical surface due to swirl, ASME J. of Applied Mechanics, 23-E.

Weber, H. E. and Keenan, J. H. (1956), Head loss in flow through a cyclone dust separator or vortex chamber, ASME Paper 56-A-8.

Wenzel, I. (1967), Literaturzusammenstellung über Isotopensentrifugen, Frankfurt: Sentralstelle für Atomenergie-Dokumertation beim Guelin-Institut, 17.2.

Weske, J. R. and Rankine, T. M. (1963), On the generation of secondary motions in the field of a vortex, Univ. of Maryland Tech. Note BN-313 (March).

Wesseling, P. (1967), The driving mechanism of strongly developed Taylor vortex flow, California Inst. of Tech., Ph.D. Thesis.

Westley, R. (1954), A bibliography and survey of the vortex tube, The College of Aeronautics, Cranfield, Note No. 9.

Westley, R. (1955), Optimum design of a vortex tube for achieving large temperature drop ratios, College of Aeronautics, Cranfield, Note No. 30.

Westley, R. (1957), Vortex tube performance data sheets, College of Aeronautics, Cranfield, Note No. 67.

Wilks, G. (1968), Swirling flow through a convergent funnel, J. Fluid Mech., 34, 575-593.

Williamson, G. G. and McCune, J. E. (1961), A preliminary study of the structure of turbulent vortices, ARAP Report No. 32.

Wilson, J. F. (1967), Swirling laminar flow between parallel plates and concentric cylinders, Ohio State University Ph.D. Dissertation, University Microfilms, Inc., Ann Arbor, Michigan.

Wolf, L. Jr., Lavan, Z., and Fejer, A. A. (1969), Measurements of the decay of swirl in turbulent flow, AIAA J., 7, 971-972 (May).

Wormley, D. N. (1967), An analytical model for the incompressible and experimental investigation of vortex-type fluid modulator, Ph.D. Dissertation, MIT, Cambridge, Mass.

Wormley, D. N. (1968), An analytical model for the incompressible flow in short vortex chambers, ASME J. of Basic Engineering, 91D, 264-276 (June).

Wormley, D. N. and Richardson, H. H. (1969), A design basis for vortex-type fluid amplifiers operating in the incompressible flow regime, Proceedings of the Joint Automatic Control Conference, Boulder, Colorado (August). To appear in the ASME Journal of Basic Engineering.

Yeptov, V. M., Kalashnikov, V. N. and Rayskiy, Y. D. (1967), On parameters which determine the vortex effect, Investiya. Mekhanika shidkosti i gaza, 3.

Yuan, S. W. and Finkelstein, A. B. (1956), Laminar pipe flow with injection and suction through a porous wall, Transactions of the ASME, 28, 719-724 (May).

Zappanti, C. J. (1964), Gas separation in a vortex, DDC Report AS-604 832, Air Force Inst. of Tech., Wright-Patterson Air Force Base, Ohio (May).

Zaroodny, S. J. (1966), Revised theory of vortex rings - a simplified review of the state-of-the-art, U.S. Army Limited War Laboratory Technical Memorandum No. 66-01 (April).

Zielinski, P. B. and Villemonte, J. R. (1968), Effect of viscosity on vortex-orifice flow, Journal of the Hydraulics Division, Proc. of the American Society of Civil Engineers, Vol. 94, p. 745 (May).